UNIVERSITY OF SOUTHAMPTON

The Transport of Mediterranean Water in the North Atlantic Ocean

DEBORAH RUTH SLATER

A thesis submitted for the degree of Doctor of Philosophy
School of Ocean and Earth Science

January 2003

UNIVERSITY OF SOUTHAMPTON

ABSTRACT

FACULTY OF SCIENCE
SCHOOL OF OCEAN AND EARTH SCIENCES

Doctor of Philosophy

THE TRANSPORT OF MEDITERRANEAN WATER IN THE NORTH ATLANTIC OCEAN

Deborah Ruth Slater

Ocean circulation is a fundamental component of the Earth's climate system. The Atlantic thermohaline circulation, driven by deep convection at high latitudes, has a central role in regulating European climate through its transport and redistribution of heat. Either directly or indirectly, Mediterranean Water (MW) provides the high salinities found in the Nordic Seas which are required to precondition for deep convection. The precise mechanisms and pathways remain undetermined and yet are fundamental to understanding the effect that any change in the Mediterranean Outflow may have on circulation and ultimately on climate.

This thesis investigates the transport of MW in the North Atlantic Ocean using hydrographic and model data. The primary objective is to quantify how much MW flows northwards and how much flows westwards from its source in the Gulf of Cadiz. Two boxes (Med Boxes) were constructed using hydrographic sections in the eastern North Atlantic enclosing the Strait of Gibraltar and Mediterranean Outflow. Inverse methods were used to determine the velocity field from which volume transports and salt fluxes were calculated. The main northward flow of MW across 41°N occurs east of 12°W, at depths of 500 to 1500 m, and transports 50 to 75% of the MW. An advective westward pathway across 20°W transports MW at similar depths into the ocean interior between 35°N and 40°N. Insignificant salt fluxes across the southern section (24°N) at MW depths confirm that no MW crosses the southern Med Box boundary.

The net overturning circulation of the Med Box, with inflowing surface waters and outflowing intermediate waters, is attributed both to the exchange at the Strait of Gibraltar and also to water mass transformation associated with entrainment of North Atlantic Water into the Mediterranean Outflow. The magnitude of the circulation provides an estimate of this entrainment of 1.6 ± 0.6 Sv, within the Med Box boundaries.

For comparison with these observational estimates, the model used is OCCAM, a $\frac{1}{4}^{\circ}$ level model from the Ocean Circulation and Climate Advance Modelling Project. The primary reason for choosing this model is that experiments have been undertaken with the Strait of Gibraltar both open and closed, enabling a new approach to the investigation of MW transport. MW is identified using the salinity difference between the two model experiments. Although the model circulation (in the open-Strait run) has a similar net overturning to the hydrography, different MW transport pathways are observed. A weak and variable northward pathway along the Iberian Peninsula and a strong southwestward flow from the Gulf of Cadiz result in a higher proportion of MW flowing westwards (61%) than northwards (39%). Seasonal variability is observed, with maximum westward flow in Autumn (70%) and minimum in Spring (50%). There is no evidence in the model that the northward boundary current provides a direct route for Mediterranean salt to reach the Nordic Seas.

To Mum, Dad and Dean, with love always.

CONTENTS

1	**Introduction**	**1**
2	**Background**	**4**
2.1	INTRODUCTION	5
2.2	THE NORTH ATLANTIC OCEAN	5
	2.2.1 Topography	6
	2.2.2 Water Masses and Circulation	7
2.3	THE MEDITERRANEAN OUTFLOW	11
	2.3.1 Discovery of the Mediterranean Outflow	11
	2.3.2 The Origin of Mediterranean Outflow Water	12
	2.3.3 Exchange at the Strait of Gibraltar	12
2.4	MEDITERRANEAN WATER IN THE ATLANTIC OCEAN	15
	2.4.1 Observations in the Gulf of Cadiz	15
	2.4.2 The Spreading of the Mediterranean Water Tongue	16
	2.4.3 Meddies	17
	2.4.4 Northward Flow of Mediterranean Water	19
	2.4.5 Westward Flow of Mediterranean Water	22
	2.4.6 Input of Mediterranean Water to the Nordic Seas	22
2.5	SUMMARY	24
3	**Data**	**26**
3.1	INTRODUCTION	27
3.2	HYDROGRAPHY	28
	3.2.1 Med Box 88 Datasets	28
	3.2.2 Med Box 98 Datasets	29
3.3	HYDROGRAPHIC SECTION PROPERTIES	31
	3.3.1 Northern Section: Med Box 98	31
	3.3.2 Western Section: Med Boxes 88 and 98	31
	3.3.3 Southern Section: Med Box 88	33
3.4	DATA QUALITY CONTROL	34
	3.4.1 Calibration Corrections	34
	3.4.2 Temperature Scales, Salinity and Standard Seawater	35
	3.4.3 Salinity Biases	36
	3.4.4 Note On Deep Water Potential Density	38
	3.4.5 WOCE Section AR16	39
3.5	LEVITUS CLIMATOLOGY	40
3.6	OCCAM DATA	41
4	**Methods**	**43**
4.1	INTRODUCTION	44
4.2	DATA MANIPULATION	44
4.3	JOINING SECTIONS	45
4.4	EKMAN TRANSPORT	52
4.5	BOTTOM TRIANGLES	53
4.6	HEAT & SALT FLUX CALCULATIONS	54
4.7	NET EVAPORATION	55
4.8	THE BOX INVERSE METHOD	57

5	**Hydrography: Circulation and Fluxes in the Med Box**	**60**
5.1	INTRODUCTION	61
5.2	DETERMINATION OF THE VELOCITY FIELD	61
	5.2.1 Initial Reference Level	61
	5.2.2 Inverse Model Constraints	62
	5.2.3 Selection of Solution	64
	5.2.4 Assumptions and Limitations	67
5.3	CIRCULATION	68
	5.3.1 Overturning Circulation	68
	5.3.2 Evaporation	70
	5.3.3 The Circulation in Med Box 98	73
	5.3.4 Hydrographic Variability – Med Box 88	77
	5.3.5 Seasonal Variability – Levitus Med Boxes	81
5.4	SALT FLUXES	87
	5.4.1 Med Box Fluxes	87
	5.4.2 Med Water Fluxes	90
5.5	SUMMARY	93
6	**OCCAM: Analysis of a Global Ocean Model**	**96**
6.1	INTRODUCTION	97
6.2	OCCAM DATA	97
	6.2.1 Model Experiments	97
	6.2.2 Model Set-up	98
6.3	DEFINING MEDITERRANEAN WATER	104
6.4	THE MEDITERRANEAN OUTFLOW	106
	6.4.1 Exchange at the Strait of Gibraltar	106
	6.4.2 Model Stability	108
6.5	CIRCULATION	112
	6.5.1 Initial Mediterranean Water Spreading	112
	6.5.2 Annual Average Med Box Circulation	114
	6.5.3 Variability of the Circulation	115
	6.5.4 Effects of the Mediterranean Outflow	122
	6.5.5 Extent of the Mediterranean Water in OCCAM	129
6.6	MED BOX FLUXES	131
	6.6.1 Net Fluxes and Evaporation	131
	6.6.2 Mediterranean Water Fluxes	134
6.7	SUMMARY	139
7	**Conclusions**	**143**
7.1	INTRODUCTION	144
7.2	DATA AND METHODS	145
7.3	HYDROGRAPHIC DATA ANALYSIS	145
7.4	RESULTS FROM A GLOBAL OCEAN MODEL	146
7.5	SUMMARY	147
7.6	FUTURE WORK	148
	References	**149**

ACKNOWLEDGEMENTS

I would like to thank my supervisor, Harry Bryden, for his encouragement, patience and unwavering positive outlook and support. Thanks also to my thesis panel, Peter Killworth and Neil Wells, for fruitful discussions and general encouragement along the way, and to Phil Richardson and Amy Bower at WHOI for broadening my oceanographic horizons.

Particular thanks to my friends; Zoe, for keeping me company in SOC's darkest hours and truly understanding... Liz, for continual encouragement and supportive friendship; Cesar and James, for being true friends and not forgetting about me after relocation to the basement; and Emma and David, for providing me with a home from home.

To my family; Mum and Dad for your unconditional encouragement and belief in me; Keith, for always having the quiet faith that I'd get there; Nanna, for your constant support; and most importantly Dean, my love and gratitude are not something I can put into words, but I wouldn't have made it without you.

If we knew what it was we were doing, it wouldn't be called research, would it?

Albert Einstein 1879-1955

Chapter One

Introduction

How inappropriate to call this planet Earth when clearly it is Ocean

Arthur C. Clarke 1917-, (Nature 1990, **344**, 102)

Ocean circulation is a fundamental component of the Earth's climate system. The climate is driven by solar energy received in the form of shortwave radiation which has its greatest intensity at low latitudes. The cooling of the Earth by outgoing longwave radiation is more globally uniform, resulting in an energy imbalance which is redressed by a redistribution of approximately 5.5×10^{15} W towards the poles by the ocean and atmosphere (Bryden and Imawaki, 2001).

The oceans play a central role in regulating our climate, having considerable capacity to store and transport heat, fresh water and carbon (Clarke et al., 2001). In the Atlantic Ocean, the meridional overturning circulation is responsible for the majority of the heat and property transport (Hall and Bryden, 1982). The principal component is the thermohaline circulation which is driven by deep water formation at high latitudes. This circulation system transports large amounts of heat northwards, releasing vast quantities to the atmosphere and thus providing Europe with a relatively mild climate compared to similar latitudes elsewhere. The northern North Atlantic is a site of deep convection due partly to the high salinity in the Nordic Seas. The products of this convection contribute to the formation of North Atlantic Deep Water which flows southwards towards the Antarctic in the cool lower limb of the thermohaline circulation, leading to the formation of Antarctic Bottom Water. This pathway intimately links the circulation of the Atlantic Ocean with climate.

It has been suggested that Mediterranean Water (MW) reaches the Nordic Seas (Reid 1979, 1994), providing the high salinities required to precondition for deep convection. This would give MW a significant role in maintaining our present climate through its influence on the thermohaline circulation. Although there is general agreement that the influence of MW can be seen in the Nordic Seas, it is controversial whether this is by a direct or an indirect route. One explanation is that there is a direct northward flow of MW from the Gulf of Cadiz at mid-depth as an eastern boundary undercurrent into the Rockall Trough where it rises sufficiently to cross the shallow ridges and flow into the Nordic Seas (Reid 1979). An alternative suggestion is that the MW reaches these latitudes indirectly by contributing to the characteristics of the North Atlantic Current Waters which feed the Nordic Seas (McCartney and Mauritzen, 2001). Whichever hypothesis is correct, MW is an important water mass in the context of the Atlantic thermohaline circulation and climate.

Mediterranean Water can be observed spreading northwards and westwards in the Atlantic Ocean as an intermediate tongue of high salinity waters. It remains unknown how much of the MW flows northwards and how much flows westwards from its source in the Gulf of Cadiz, although this is fundamental to understanding the importance of MW in the Atlantic. The primary purpose of this thesis is to quantify the northwards and westwards transports of MW in the eastern North Atlantic,

using both hydrographic and model data. A detailed description of the current state of knowledge of MW, for both the outflow itself and its spreading in the North Atlantic, is described in Chapter 2 which puts this work in the context of the wider North Atlantic circulation. The impetus for this Ph.D. is revealed in the outstanding questions concerning Mediterranean Water.

Three forms of data are used in this work and are described in Chapter 3: WOCE hydrographic sections; the Levitus climatology; and a fine resolution ocean general circulation model, OCCAM. The chapter principally concentrates on the hydrography, outlining the cruises from which the data are taken, considering issues of data quality control, and describing the main temperature and salinity characteristics of the sections. A brief outline of the model is given, which is later expanded in Chapter 6. The methods used to analyse the observations are presented in Chapter 4, concentrating mainly on the hydrography and Levitus data sets as these require more analysis than the model data in which all variables are specified. Particular attention is paid to the inverse method used to calculate the absolute velocities.

The use of both hydrographic and model data gives alternative, complementary perspectives of oceanic circulation, each having advantages and limitations. The results of the hydrographic and Levitus data analyses are presented in Chapter 5. A detailed explanation of the velocity field determination is given first, followed by a discussion of the circulation fields. Salt fluxes are then calculated and used to investigate and quantify the MW transport.

The OCCAM experiments and setup are explained in Chapter 6, highlighting the reasons behind the choice of this particular model. This is supported by a description of how the MW was defined and an examination of the outflow. The model allows investigation of temporal variability, and also of the effects and extent of the MW in the North Atlantic. A detailed study of the circulation and fluxes in the eastern basin is made, concluding with a quantification of the MW transport. The thesis is concluded in Chapter 7 with a summary of the work presented and a look to the future.

Chapter Two

Background

2.1	INTRODUCTION	5
2.2	THE NORTH ATLANTIC OCEAN	5
	2.2.1 Topography	6
	2.2.2 Water Masses and Circulation	7
2.3	THE MEDITERRANEAN OUTFLOW	11
	2.3.1 Discovery of the Mediterranean Outflow	11
	2.3.2 The Origin of Mediterranean Outflow Water	12
	2.3.3 Exchange at the Strait of Gibraltar	12
	i Quantifying the Exchange	13
	ii Controls on the Exchange	14
2.4	MEDITERRANEAN WATER IN THE ATLANTIC OCEAN	15
	2.4.1 Observations in the Gulf of Cadiz	15
	2.4.2 The Spreading of the Mediterranean Water Tongue	16
	2.4.3 Meddies	17
	2.4.4 Northward Flow of Mediterranean Water	19
	2.4.5 Westward Flow of Mediterranean Water	22
	2.4.6 Input of Mediterranean Water to the Nordic Seas	22
2.5	SUMMARY	24

2.1 INTRODUCTION

The principal endeavour of this thesis, as its title suggests, is to investigate the transport of Mediterranean Water in the North Atlantic Ocean. In order to accomplish (or even start) this task it is necessary to have an understanding of the general circulation of the North Atlantic Ocean and the current state of knowledge of Mediterranean Water.

To that end, this chapter starts with a description of the North Atlantic Ocean; its topography, principal water masses, and circulation. The second half of the chapter is concerned with Mediterranean Water; the outflow, and its spreading in the North Atlantic. Detail of the outflow is included as it determines the way in which Mediterranean Water mixes with Atlantic waters and thus is fundamental to the overall understanding of the Atlantic circulation. The chapter ends with a summary of the key issues and outlines the main outstanding questions concerning Mediterranean Water, revealing the impetus for this work.

2.2 THE NORTH ATLANTIC OCEAN

The North Atlantic Ocean is the smallest of the world's oceans, containing just 10% of their total volume (Worthington, 1976, 1981). It is also the warmest and most saline ocean, due to both the positive net evaporation and the inflow of water from marginal seas. A comparison of the mean properties of each ocean is shown in Table 2.1, highlighting these differences.

	Volume (10^6 km^3)	Mean θ (°C)	Mean Salinity
World Ocean	1320	3.51	34.72
Pacific Ocean	712	3.14	34.60
Indian Ocean	283	3.88	34.78
Atlantic Ocean	326	3.99	34.92
North Atlantic Ocean	137	5.08	35.09

Table 2.1 Volume, mean potential temperature (θ) and mean salinity of the oceans (Worthington, 1981).

2.2.1 Topography

Oceanic topography has a great impact on circulation, in places constraining flow, and in others, steering. Figure 2.1 illustrates the North Atlantic topography. The Atlantic Ocean is essentially split into two halves due to the presence of the Mid Atlantic Ridge running roughly down the central axis of the ocean. The depth of the ridge varies between 1500 and 2000 m, although in some places it does break the surface, forming islands such as Iceland and the Azores. The ridge abounds with fracture zones, some creating gaps connecting the deep basins of the western and eastern North Atlantic; the Charlie Gibbs, Vema and Romanche fracture zone sills are all at depths greater than 4000 m.

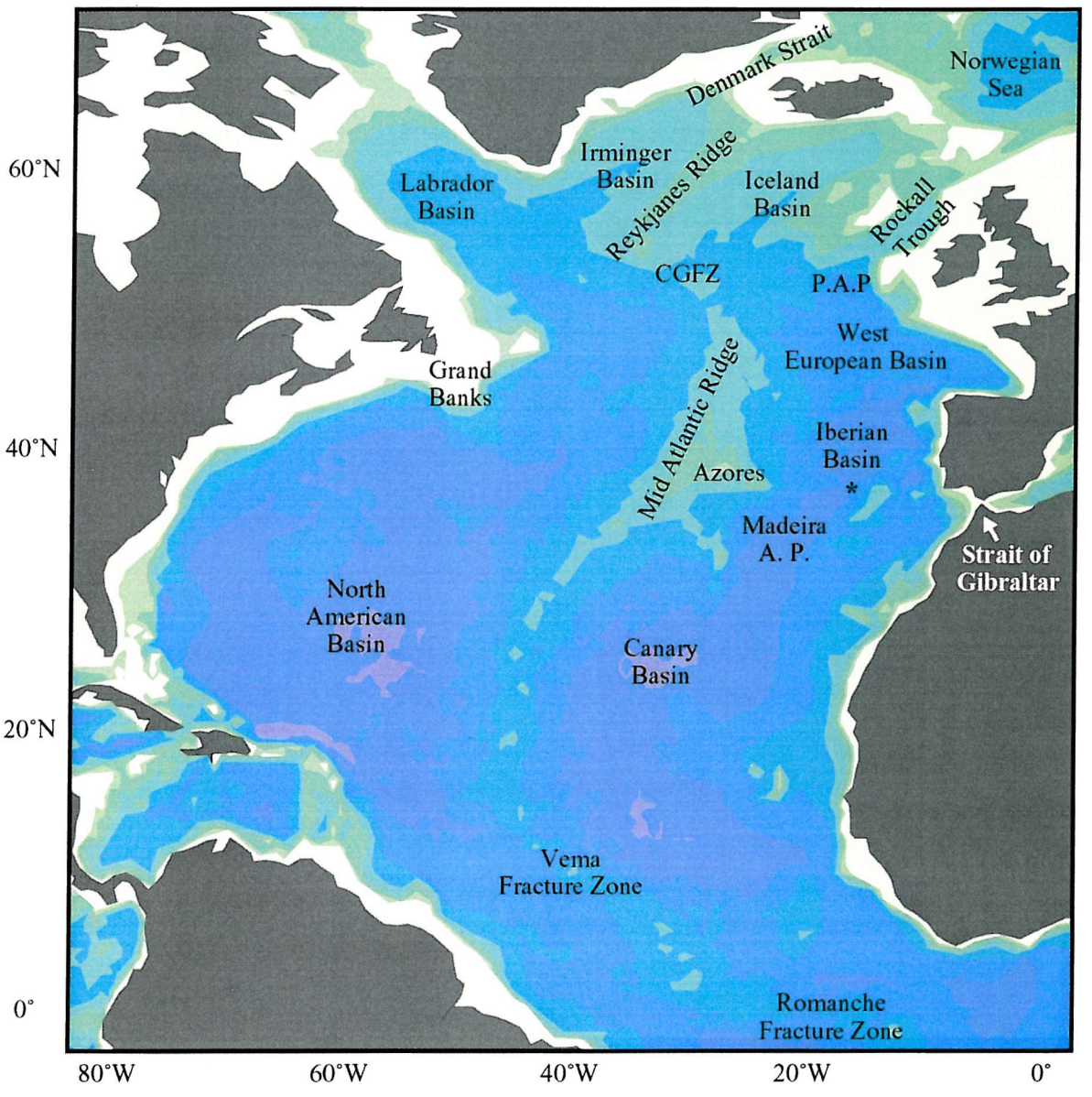

Figure 2.1 *North Atlantic Topographic Features (CGFZ = Charlie Gibbs Fracture Zone, A.P. = Abyssal Plain, P.A.P. = Porcupine Abyssal Plain, * = Discovery Gap).*

Each main basin is divided into smaller basins. Figure 2.1 identifies the Labrador, Irminger and North American Basins in the western North Atlantic, and the Iceland, West European, Iberian and Canary basins in the eastern North Atlantic. The Reykjanes Ridge (part of the Mid Atlantic Ridge) separates the Irminger and Iceland Basins, and the Rockall Plateau separates the Iceland Basin from the Rockall Trough. Some of the ridge systems between these smaller basins also contain deep gaps. In the eastern basin for example, an east-west ridge runs along 37°N, separating the deep basins of the Madeira and Iberian Abyssal Plains. Its crest is at 4000 to 4500 m depth, with two low points, one at 19.5°W and the other, known as Discovery Gap, at 16°W (Saunders, 1987).

In the northern North Atlantic, a number of ridges separate the Nordic Seas from the basins to their south; the Denmark Strait between Greenland and Iceland, with a sill depth of 600 m; the Iceland-Faroe Ridge between Iceland and the Faroe Islands; and the Wyville-Thomson Ridge to the northwest of Scotland. The deepest connection is the 850 m sill of the Faroe Bank Channel.

2.2.2 Water Masses and Circulation

The water mass structure of the North Atlantic Ocean is highly complex, due largely to the inputs of deep and intermediate waters formed in marginal seas. Water mass formation and circulation are directly driven by atmospheric action on the sea surface (Worthington, 1976). The circulation in the North Atlantic can be divided into two segments; the thermohaline overturning circulation, involving the warm to cold water mass transformation at high latitudes; and the wind driven circulation associated with geostrophic and Ekman layer dynamics, involving the horizontal surface gyres. It is difficult to discuss these two types of circulation separately as they are interlinked and each affects the other to a certain extent; however, a brief description of each will be given, leading on to a description of the water masses encountered in the eastern North Atlantic.

The wind field over the North Atlantic and the associated Ekman convergence and divergence force the subtropical and subpolar gyres respectively, each showing westward intensification in the form of western boundary currents. The subtropical gyre is anticyclonic, lies roughly between 10°N and 40°N, and has the Gulf Stream at its western edge. The Gulf Stream circulation is enhanced by smaller scale recirculations that return water to the northward flowing boundary current. The subpolar gyre, north of 40°N, is cyclonic and has the East Greenland and Labrador Currents as its western boundary currents.

The Gulf Stream originates from the ~30 Sv Florida Current which flows through the Straits of Florida, ~45% of which comes from the South Atlantic (Schmitz and McCartney, 1993). It heads eastward into the North Atlantic at about 40°N, and then to the southeast of the Grand Banks at

about 45°W where it bifurcates, with one branch turning north as the North Atlantic Current and making its way around the subpolar gyre, and the other branch continuing eastwards. This branch of the Gulf Stream heads towards the Azores and then due east towards the Gulf of Cadiz at a latitude of about 35°N as the Azores Current. The Azores Current is a shallow, narrow (~60 km wide), highly energetic flow, transporting approximately 10 Sv eastwards (Käse and Siedler, 1982).

An explanation has recently been put forward for the presence of this zonal flow at mid-latitudes, far to the south of the mean zero wind stress curl. The water mass transformation associated with the entrainment of North Atlantic Central Water into the Mediterranean Outflow Water introduces a sink to the upper ocean layer at the eastern boundary of the North Atlantic. Using a model both with and without representation of the Mediterranean Outflow, Jia (2000) suggests that this sink (along with the inflow to the Mediterranean) induces the Azores Current. This neat explanation is further supported by earlier laboratory experiments and theory (for example, Pedlosky 1996, Webb 1993, Stommel et al., 1958).

The Gulf Stream and North Atlantic Current are parts of the Atlantic thermohaline circulation, which involves the northward flow of 'warm' water (~14 Sv; McCartney and Talley, 1984) and its transformation to southward flowing 'cold' water. This system transports large amounts of heat northwards, giving up vast quantities to the atmosphere en route, and consequently provides Europe with a relatively mild climate compared with similar latitudes elsewhere. The thermohaline circulation is driven by deep water formation at high latitudes, North Atlantic Deep Water (NADW) in the north, and Antarctic Bottom Water (AABW) and Antarctic Intermediate Water (AAIW) in the south.

Antarctic Bottom Water is the densest water mass in the global ocean, and is formed by deep convection in the Weddell Sea at the continental shelf of Antarctica (Warren, 1981). It mixes with water masses of North Atlantic origin and spreads northwards, confined primarily to the western basin. At the equator some AABW passes into the eastern basin through the Romanche Fracture Zone, and at 11°N half of its roughly 4 Sv flow turns eastward and passes through the Vema Fracture Zone into the eastern basin (McCartney and Curry, 1993), then continues its northward passage. By the time it reaches the Canary Basin, the AABW has a temperature of 1.95°C and a salinity of 34.88 due to mixing with overlying NADW (Tsuchiya et al., 1992). Its temperature and salinity continues to increase as it progresses further north.

The North West Atlantic, north of about 40°N is the only region of the World Ocean containing abyssal water derived from a source other than AABW (Mantyla and Reid, 1983). Here, the source is the overflow water from the Nordic Seas, comprising Denmark Strait Overflow Water (DSOW)

and Iceland-Scotland Overflow Water (ISOW), which result from wintertime convection and escape southwards through the Denmark Strait and Faroe Bank Channel, and over the Wyville-Thompson Ridge. The Nordic Seas are preconditioned for deep convection by the inflow of relatively high salinity water from the North Atlantic (Reid, 1994; McCartney and Mauritzen 2001). South of 40°N, these water masses overlie the deep water of southern origin. ISOW is found at depth in the Iceland Basin, although in the southern part of the basin it has a significant component of deep water from the south (Tsuchiya et al., 1992). The deep layer formed in the western North Atlantic by DSOW and ISOW, that has made its way through the CGFZ, has been traced through the South Atlantic, South Indian and South Pacific oceans, and is thus a major source of salt to the deep water of the World Ocean.

North Atlantic Deep Water is formed in the northern North Atlantic. It penetrates into the South Atlantic and the Antarctic Circumpolar Current and has an influence on the Pacific and Indian Oceans. It is split into two layers: upper NADW (at temperatures between 3° and 4°C) originates from the Labrador Sea and contains a component of MW; whilst lower NADW (at 1.8° to 3°C) originates from the Nordic Sea overflows (ISOW and DSOW). NADW formation is estimated to be around 20 Sv (Lavin et al., 1998), which is almost equal in magnitude to the cross-equatorial contribution to the Florida Current transport (Schmitz and McCartney, 1993), the 'warm' water pathway of the thermohaline circulation.

Above the deep waters of the North Atlantic lie intermediate waters. In the eastern basin there are three primary intermediate water masses; Labrador Sea Water, Mediterranean Water, and Antarctic Intermediate Water.

Labrador Sea Water (LSW) is the coldest and densest mode water found in the Atlantic Ocean (Talley and McCartney, 1982), and contributes to the thermohaline circulation as a major component of NADW (~8.5 Sv; McCartney and Talley, 1984). It is formed by deep convection in the Labrador Basin, which is estimated to reach depths of around 1500 m (Reid, 1994). Due to its formation mechanism, LSW is characterised by low potential vorticity and high oxygen. In fact, LSW has the highest oxygen concentration of all the world oceans below 500 m (Reid, 1994). It is also characterised by a salinity minimum due to the excess of freshwater input over evaporative loss in the Labrador Sea, and because it is the final product of Subpolar Mode Water (SPMW) which has been freshening as it circulates in the subpolar gyre (McCartney and Talley, 1982).

All these characteristics have been successfully used as tracers to identify LSW in the North Atlantic (for example, Talley and McCartney, 1982; Paillet et al., 1998). Rhein et al. (2002) have recently used CFC (chlorofluorocarbon) data to elucidate the pathways of LSW in the North

Atlantic, as shown in Figure 2.2. LSW is exported northeastward into the Irminger Sea north of 56°N, and southwards in the Deep Western Boundary Current to about 18°N. It also spreads eastwards at mid-depths into the North Atlantic, north of 40°N (McCartney and Talley, 1982). From the Porcupine Abyssal Plain, the LSW enters the subtropical gyre in a narrow region close to the continental slope (Rhein et al., 2002).

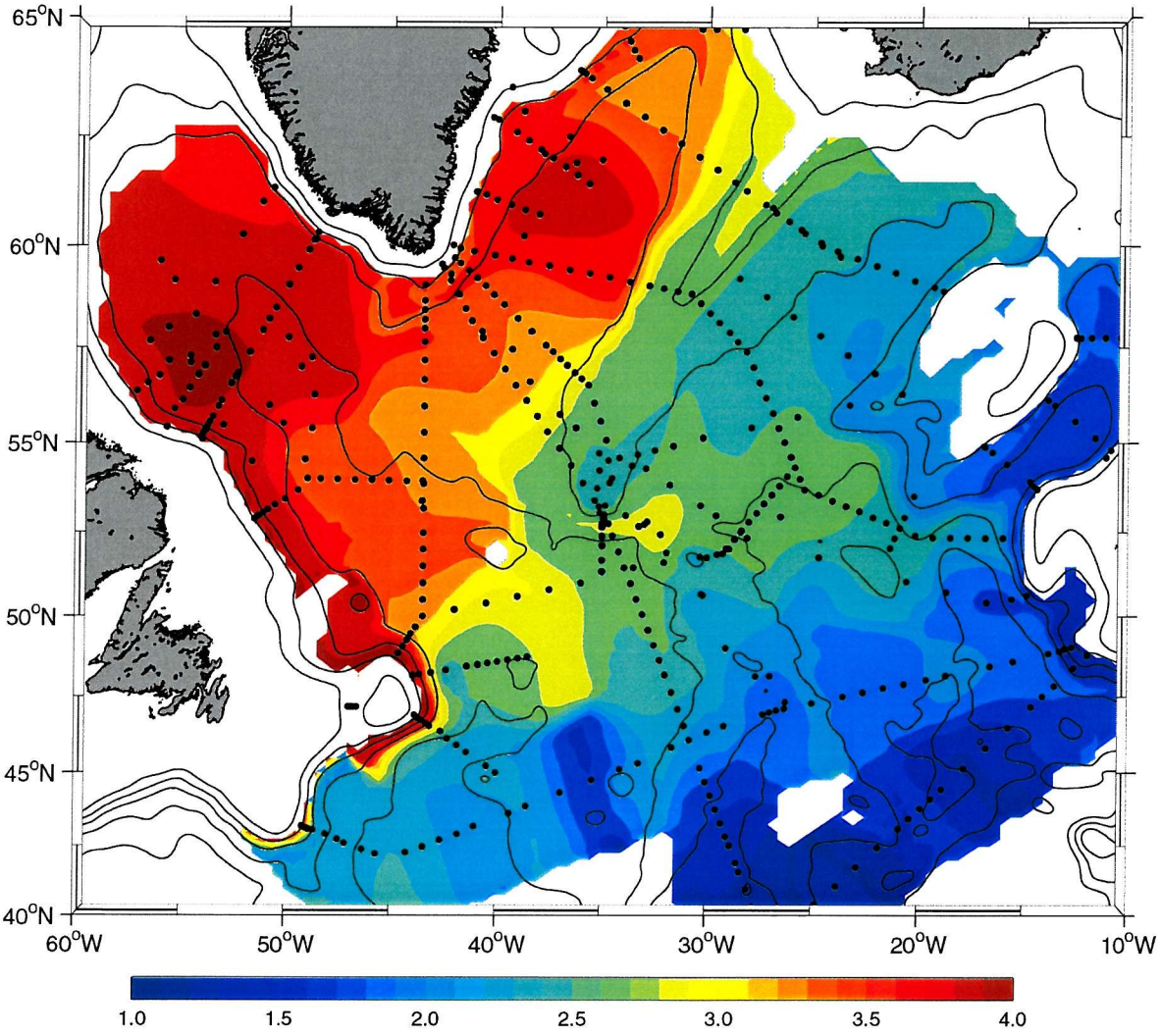

Figure 2.2 *Chlorofluorocarbon (pmolkg^{-1}) distribution of Labrador Sea Water (σ_θ = 27.74 - 27.80), interpolated from mean CFC-11 concentration at individual stations (Rhein et al., 2002).*

Mediterranean Water (discussed fully in Section 2.4) lies roughly between 800 and 1300 m in the eastern North Atlantic, is traced principally by its high salinity and temperature characteristics, and encounters the southward flowing LSW near the Azores. The so-called Deep Mediterranean Water (Harvey and Arhan, 1988) is thought to result from double diffusive mixing in the eastern basin between LSW and the overlying MW (Paillet et al., 1998).

Antarctic Intermediate Water is traced by virtue of its low salinity and oxygen to around 30°N in the eastern North Atlantic. Here it is found at depths of 600 to 800 m (Tsuchiya et al., 1992). It is encountered farther north in the eastern basin due to its rapid mixing through the western Atlantic in the Gulf Stream - North Atlantic Current system.

Above these intermediate water masses lies North Atlantic Central Water (NACW), formed from Mode Waters, the principal components being Sargasso Sea and Madeira Mode Waters. Mode Waters are annually persistent pycnostads[1] formed by wintertime convection (McCartney and Talley, 1982). At any particular depth or density surface, NACW is saltier in the eastern North Atlantic than in the western North Atlantic. Mauritzen et al. (2001) find that the salinity of the Central Water is influenced by the saline Mediterranean Outflow in the eastern Gulf of Cadiz where the two water masses are in physical contact. There is a cross-isopycnal flux from the MW to the Central Water, and recirculation of the Central Water in the Gulf of Cadiz allows the now higher salinity Central Water to spread into the North Atlantic. This is backed up by laboratory experiments and direct current observations, and indicates another far-reaching effect of the outflow from the Mediterranean.

2.3 THE MEDITERRANEAN OUTFLOW

2.3.1 Discovery of the Mediterranean Outflow

The Strait of Gibraltar connects the Mediterranean Sea, a semi-enclosed basin, with the North Atlantic Ocean. It was recognised centuries ago that the inflow of Atlantic Water into the Mediterranean, along with riverine inputs and precipitation, was far larger than could be balanced by evaporation (Deacon, 1971). This problem stimulated many of the early advances in oceanography.

When Marsigli (1681) was studying the flow of Black Sea Water through the Bosporus, he devised a clever laboratory experiment in which he separated water of two different densities by a vertical partition in a box. When he opened holes at the top and bottom of the partition the denser water was observed to flow through the hole at the bottom and a compensating flow of less dense water through the hole at the top. He then went out into the Bosporus and demonstrated that there was a deep counter-current by lowering a drogued line and observing the deviation of the line from the vertical.

[1] Pycnostads have increased vertical separation between isopycnals.

It was nearly two centuries later that Carpenter and Jeffreys (1870) made a similar observation in the Strait of Gibraltar. They lowered a drogue from a small rowing boat, and when the drogue was at 350 m, the boat drifted westward, in opposition to both the eastward surface current and the wind.

2.3.2 The Origin of Mediterranean Outflow Water

The two characteristic Mediterranean subsurface water masses are the Levantine Intermediate Water (LIW) and Western Mediterranean Deep Water (WMDW), both of which are formed by wintertime deep convection (Pickard and Emery, 1990). Deep convection occurs over very limited 'patches', where the combination of surface cooling and strong mixing due to the late-winter winds causes the density of the surface layer to reach that of the layers beneath (Sankey, 1973). This surface water then mixes rapidly downwards, completely destroying the intermediate layer and incorporating much of the deep water. The resulting column of dense water spreads laterally in the deeper layers where its density matches that of the surrounding waters.

Levantine Intermediate Water is formed off the south coast of Turkey with a temperature of 15°C and a salinity of 39.1 (Pickard and Emery, 1990). It is characterised by intermediate maxima in both temperature and salinity, but as it flows westward, it mixes with WMDW formed south of France in the Gulf of Lions, and its maxima become much diminished. The WMDW is typically homogeneous, having a range of potential temperature of approximately 12.7 to 13.0°C and a salinity range of 38.40 to 38.46. Bryden and Stommel (1982) found that WMDW flows toward Gibraltar along the Moroccan continental slope but does not recirculate back into the Mediterranean, and hence must flow over the sill at Gibraltar into the Atlantic. This was first shown to be possible by Stommel et al. (1973) using Bernoulli theory, and has been backed up by observations which have shown pure WMDW on the Atlantic side of the Gibraltar sill during both spring and neap tides (Kinder and Parrilla, 1987). However, WMDW makes only a small contribution to the outflow, with most of the outflow (90%) consisting of LIW (Bryden and Stommel, 1984).

2.3.3 Exchange at the Strait of Gibraltar

The net evaporation over the Mediterranean Basin leads to a water deficit which is balanced by a net inflow of fresher water through the Strait of Gibraltar. The net evaporation also increases the salinity of the Mediterranean, and therefore the outflow must have proportionately higher salinity to provide a balance (Candela et al., 1989).

i *Quantifying the Exchange*

The classical method for determining the flow through the Strait of Gibraltar uses the Knudsen relations, derived from mass and salt conservation considerations for the Mediterranean Sea. Assuming constant volume and salinity for the Basin:

Mass conservation: $Q_A + Q_M = E$

Salt conservation: $Q_A S_A + Q_M S_M = 0$

where Q_A, Q_M, S_A and S_M are the mass transports and salinities of the Atlantic Water inflow and Mediterranean Water outflow through the Strait of Gibraltar, and E is the net evaporation over the Mediterranean, shown schematically in Figure 2.3. Solving these equations reveals the Knudsen relations:

Atlantic Water inflow: $$Q_A = \frac{S_M E}{(S_M - S_A)}$$

Med Water outflow: $$Q_M = -\frac{S_A E}{(S_M - S_A)}$$

Nielson (1912) was the first to use these relations for the Strait of Gibraltar along with measurements of the salinities and an estimate of the net evaporation to determine an inflow of 1.88 Sv and an outflow of 1.78 Sv. Since then, estimates of the inflow and outflow using this method have varied from 0.9 to 1.8 Sv (Bryden et al., 1989)

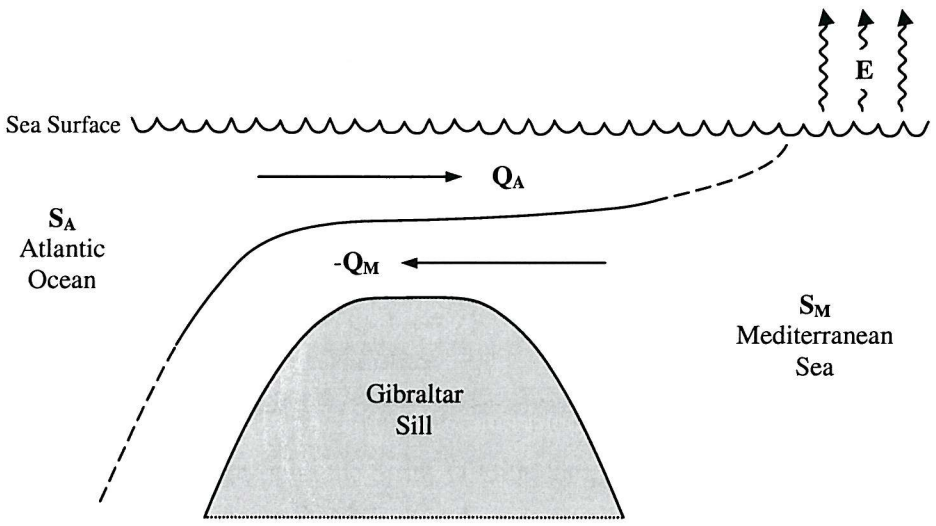

Figure 2.3 *Schematic of the two-layer flow over the Gibraltar sill. Q_A, Q_M and S_A, S_M are the transports and salinities of the inflowing Atlantic Water and outflowing Mediterranean Water and E is the net evaporation (evaporation minus precipitation minus river run-off) over the Mediterranean Basin (Bryden and Kinder, 1991b).*

In 1994, Bryden et al. examined the data from the Gibraltar Experiment[2] and realised the importance of time-series salinity measurements for defining the exchange across the sill. From the current meter measurements, they estimated the time-averaged outflow to be -0.68 Sv and the outflow salinity transport to be –1.5 Sv ppt, which is equivalent to a net evaporation over the Mediterranean basin of 52 cm yr^{-1} (giving a net inflow of 0.04 Sv). Subsurface current meter measurements extrapolated up to the surface gave a time-averaged inflow of 0.93 Sv, which was deemed to be unreasonably large, and redefined to be 0.72 Sv (the sum of the more realistic time-averaged inflow and the net evaporation). It is interesting to note that the outflow salinity transport gives an indirect estimate of the net evaporation over the Mediterranean Basin (Bryden et al., 1989).

ii Controls on the Exchange

The exchange at the Strait of Gibraltar is controlled by the depth of the sills and the width of the Tarifa Narrows (Bryden & Kinder, 1991a). Tides & mean currents contribute approximately equally to the exchange at Gibraltar, and the tides are actually strong enough to reverse the mean flow in each layer for part of the tidal cycle (Bryden & Kinder, 1991b).

There are various constituents of the flow through the Strait of Gibraltar. There is barotropic subinertial flow reaching values up to I Sv, which is mainly meteorologically forced[3]; there is also a baroclinic mode, modulated by the spring-neap tidal cycle (where there is a significant correlation between strong outflow and a shallow interface between the Atlantic and Mediterranean Waters at tidal frequencies), stronger inflow and outflow are found at neap tides and the amplitude of these fortnightly variations in transport are of order 0.1 Sv; these contribute for 84% and 12% of the variance observed at these frequencies respectively (Candela et al., 1989). Seasonal and longer term flow fluctuations are also baroclinic.

There are three internal hydraulic control points along the Strait acting as controls on the flow; the Spartel and Camarinal sills act on the Mediterranean outflow (although the Camarinal sill control is subject to strong time dependence); and the Tarifa Narrows controls the Atlantic Water inflow (Armi and Farmer, 1985).

There is clear evidence of the Coriolis effect in the Strait of Gibraltar, principally at the sill, with the Atlantic Water inflowing on the south side of the Strait and the Mediterranean Water tending to exit deeper on the northern side (Canavate et al., 1988).

---

[2] The Gibraltar Experiment was a year-long field experiment (1985-1986) designed to study the dynamics and kinematics of the exchange between the Atlantic and Mediterranean through the Strait of Gibraltar (Bryden and Kinder, 1986).

[3] When pressure over the Mediterranean is low, the sea level in the Mediterranean rises; when the atmospheric pressure is high, the sea level falls. This "inverse barometer" effect causes fluctuations in the net inflow/outflow through the Strait over 5 day time scales (Candela et al., 1989)

2.4 MEDITERRANEAN WATER IN THE ATLANTIC OCEAN

Mediterranean Water has been found as far west as the Bermuda Rise (Armi and Bray, 1982) and as far north as the Rockall Trough (Reid, 1979), but knowledge of the actual pathways the MW takes in the North Atlantic, and where it ends up, is limited. Reid (1979, 1994) hypothesised that the MW provides the source for the relatively high salinity waters found in the Nordic Seas, being transported northwards in an eastern boundary undercurrent. If the MW does flow into the Nordic Seas, it could be a very important element in the Atlantic thermohaline circulation, and as such, hold consequences for climate. This direct advection of MW into the Nordic Seas by an eastern boundary undercurrent is a very controversial theory however, and will be explored later in Section 2.4.6.

2.4.1 Observations in the Gulf of Cadiz

As the water spills over the sill at the Strait of Gibraltar and flows down into the Gulf of Cadiz as a bottom boundary current, it accelerates to 1.3 ms^{-1} and the flow is highly turbulent, entraining large amounts of North Atlantic Central Water (salinity > 36.0; Price et al., 1993). The outflow is strongly affected by bottom topography, and its acceleration as it descends the continental slope is limited by three factors (Johnson et al., 1994):

1. turbulent stresses arising from bottom friction and entrainment which produce large dissipation throughout the entire plume;
2. the decreasing density anomaly (due to turbulent entrainment), which reduces the pressure force (due to the steep bottom slope) on the outflow;
3. the effect of the Coriolis force in turning the current to the right (looking in a downstream direction) and therefore along the slope, rather than directly down it.

Entrainment increases the volume (width) of the outflow from about 1 Sv (10 km) at the Strait of Gibraltar to 3 Sv (80 km) by the time it reaches Cape St Vincent (Ambar and Howe, 1979; Ochoa and Bray, 1991; Baringer and Price, 1997a). The northern edge of the outflow descends only a few hundred metres and therefore entrains shallower NACW than the southern edge of the outflow which descends approximately 1000 m. This asymmetry causes horizontal θ/S variability across the outflow, the temperature part of which exceeds 2°C by the time the plume has travelled 140 km downstream.

In the western Gulf of Cadiz, as a result of the asymmetrical spreading and varying entrainment across the outflow, there are two distinct cores of mixed Mediterranean Outflow Water (MW). The deep offshore core has a density of $\sigma_\theta = 27.8\ kg\,m^{-3}$ and the shallower near-shore core, which is still in contact with the sea bed, has $\sigma_\theta = 27.5\ kg\,m^{-3}$. The flow follows the topography at a speed of about 0.3 ms^{-1} (greatly reduced from the 1 ms^{-1} descent rate) along to Cape St Vincent, where the upper core now separates from the sea bed (Baringer and Price, 1997b), and the two cores come back into contact with each other as a consequence of the convergence of isobaths at this location. The MW rounds Cape St Vincent and spreads westward and northward in the Atlantic Ocean, conspicuous on hydrographic maps of the lower thermocline as an anomalously warm and salty water mass (Figure 2.4; Worthington, 1976).

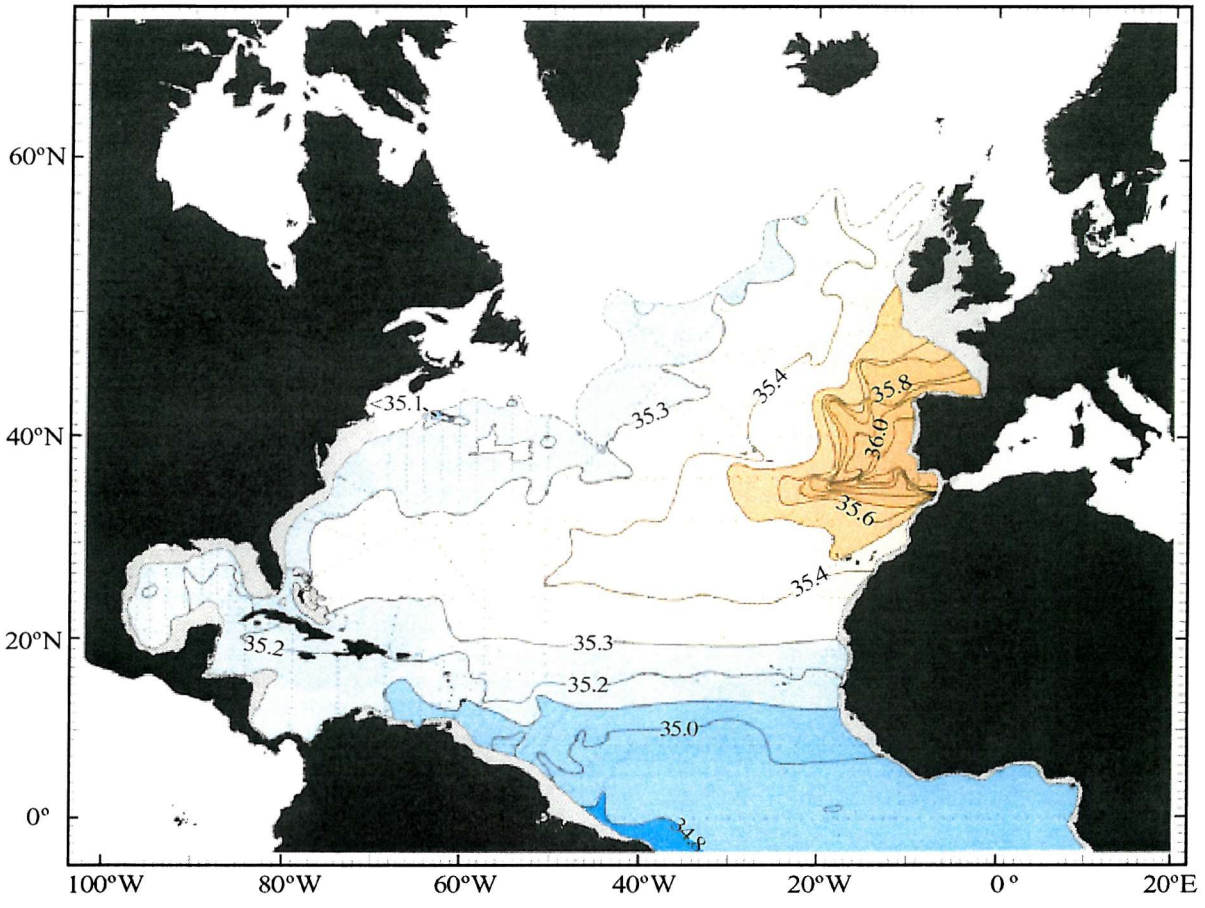

Figure 2.4 Salinity at the 10°C surface in the North Atlantic (Worthington, 1976)

2.4.2 The Spreading of the Mediterranean Water Tongue

The salinity anomaly due to the outflow of MW is found as deep as 3000 m in the North Atlantic. This is most likely to be due to the vertical transport of salt by double diffusive processes (Stephens and Marshall, 1999). Washburn and Kase (1987) studied a 500 km by 500 km grid southeast of the

Azores and found that salt fingering is an important diapycnal mixing process in much of the region. Daniault et al. (1994) calculated that 22% of the Mediterranean salt is brought downward to depths below 1500 m by diffusion.

It is unclear whether the MW tongue is primarily an advective or diffusive feature. Gerdes et al. (1999) and Stephens and Marshall (1999) investigated the spreading of MW in models of the North Atlantic and found that the most important process was the volume flux associated with the exchange at Gibraltar; the occurrence of a mean transport of MW away from the eastern boundary is crucial in obtaining a realistic salinity tongue. Richardson and Mooney (1975) using a simple advection-diffusion model, found that the salinity distribution depended on the value of the Peclet number[4] used, but for any realistic oceanic Peclet number, it is the subtropical gyre passing through the MW tongue that advects it towards the south and west.

2.4.3 Meddies

Traditionally, the MW salt tongue has been interpreted to be the result of an advective-diffusive balance from its source in the Gulf of Cadiz (for example, Needler and Heath, 1975). This view was challenged by the detection of Mediterranean salt lenses – coherent eddies containing warm, salty Mediterranean Water in their cores. It was McDowell and Rossby (1978) who first came across such a lens whilst undertaking a hydrographic survey in the Sargasso Sea. By investigating its temperature and salinity characteristics, they deduced that it was an eddy of Mediterranean origin, for which they coined the term 'meddy'. Although the interpretation of this observation is presently under debate (Prater and Rossby, 1999), the term has endured.

Numerous meddies have since been observed, mainly in the Iberian and Canary basins, recognisable by their large salinity and temperature anomalies, approximately 0.8 and 2.5°C respectively (Armi and Zenk, 1984; Armi et al., 1988; Schultz Tokos et al., 1994). Centred at around 1100 m, with a typical radius of 50 km and vertical extent of 1000 m (Armi et al., 1988; Richardson et al., 1989), they were classified by McWilliams (1985) as "submesoscale coherent vortices". They have been observed to travel with mean velocities of 1 to 2 cms^{-1} in a south to southwest direction and they generally occur in an elliptical region extending 3000 km southwest from the coast of Portugal (Richardson et al., 1989, 1991).

[4] The Peclet number, P = VL/K, where V is velocity, L is length scale and K is the diffusion coefficient, is a measure of the relative effects of advection to diffusion. A value of zero therefore gives pure diffusion.

Meddies decay either slowly due to mixing processes such as thermohaline intrusions and salt fingers (Armi et al., 1988, 1989), or suddenly due to collision with seamounts (Richardson et al., 1989, Richardson et al., 2000, Schultz Tokos et al., 1994). They act as a distributed source of MW in the North Atlantic, providing a new agent for salt transport which is likely to be important in determining the shape and location of the Mediterranean salt tongue.

In numerical experiments, Käse et al. (1989) showed that meddies can be produced by instability of a northward undercurrent; however, actual observations of the process were lacking. A Mediterranean Undercurrent Seeding Experiment (AMUSE; Bower et al., 1997) gave valuable insights into the formation rates and sites of meddies from RAFOS[5] floats seeded into the Mediterranean Undercurrent. Nine meddy formation events were observed at two sites, both where the flow turns sharply to the right (looking downstream) following the topography. This lends credence to the theory that topography plays a key role in meddy formation. The first formation site is in the Portimão Canyon near Cape St Vincent, at the southwest corner of the Iberian Peninsula, the second is near the Estremadura Promontory, along the western Portuguese continental slope (see Figure 2.5). The data suggests that meddies form at Cape St Vincent when the undercurrent speed is greater than 12 cms^{-1} westward.

Estimates of meddy formation rates vary. Richardson et al. (1989) estimated that 8-12 meddies form each year based on an estimate of 24 coexisting meddies with life expectancies of 2-3 years, and that their contribution to the mid-depth salt flux is 25%. From the AMUSE program Bower et al. (1997) made an estimate of a formation rate of 15-20 meddies per year, with each meddy taking approximately 3-7 days to form. These meddies are smaller than the Canary Basin meddies observed by Richardson et al. (1989), which could explain the difference in formation rates and numbers formed per year. Arhan et al. (1994) observed three meddies on their meridional hydrographic section[6] and calculated that they were carrying 18% of the Mediterranean salt, and contributing up to 55% of the zonal salt transport. Armi and Stommel (1983) deduced that the salt flux divergence in an area of the eastern North Atlantic could be balanced by decay of just three meddies per year. However, Armi et al. (1989) calculated that it would take 40 meddies per year to balance the total salt flux through the Strait of Gibraltar, and concluded that there must be other major contributing factors such as mean flows.

---

[5] RAFOS is the reverse spelling of SOFAR (which stands for SOund Fixing And Ranging), referring to the fact that RAFOS floats work in the opposite sense to SOFAR floats; they pick up signals from moored transmitting beacons and track themselves (Bower, 1994).

[6] The Bord-Est hydrographic section runs from 20°N to 60°N at an average distance of 200 nautical miles from the continental slopes (Arhan et al., 1994).

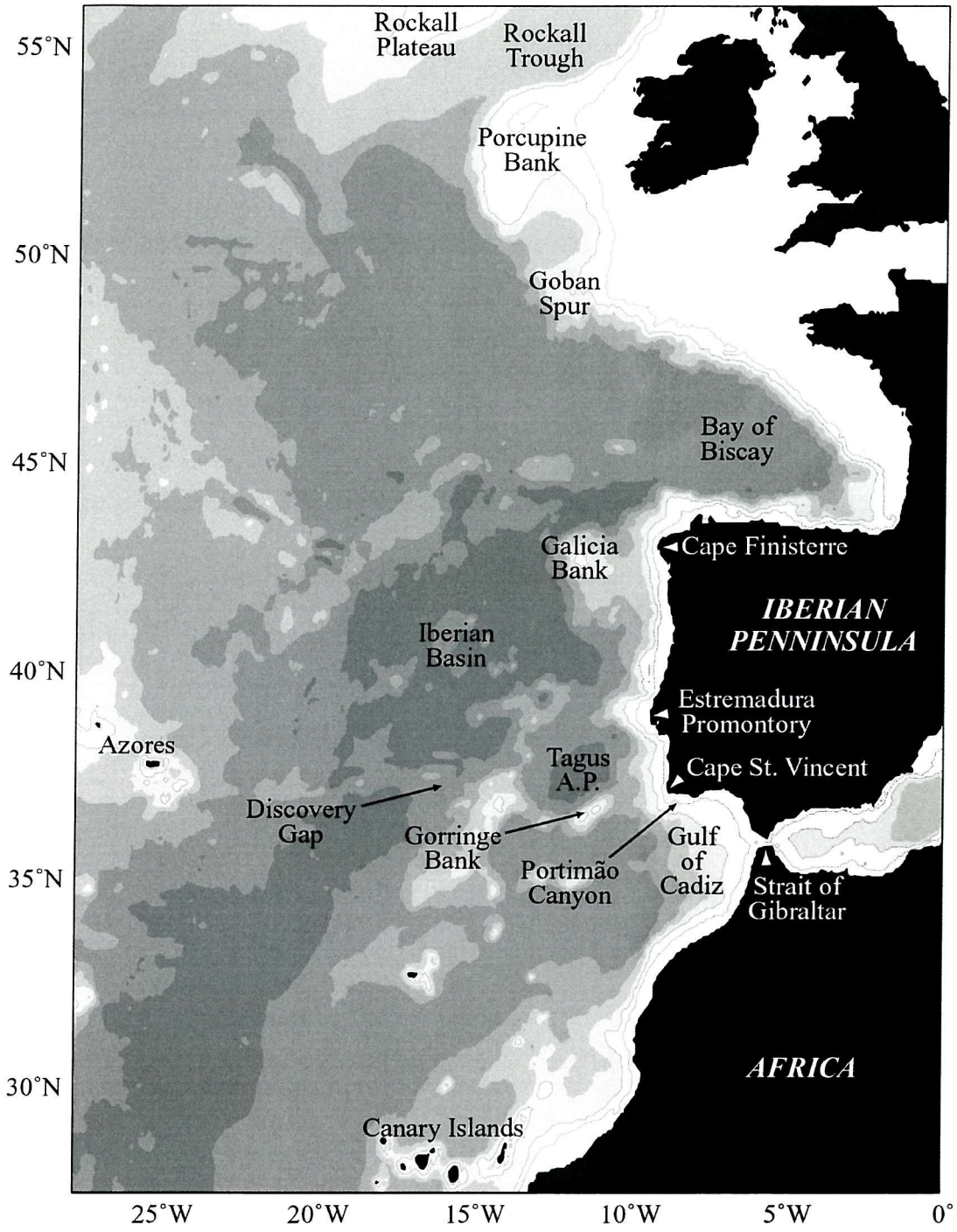

Figure 2.5 Topographic features in the eastern North Atlantic

2.4.4 Northward Flow of Mediterranean Water

The northward progression of MW has been well documented. Zenk and Armi (1990) observed the two aforementioned cores of MW, the upper of which progressed northwards (attaining speeds over 25 cms^{-1}) along the Iberian continental slope to at least 42°N, just above part of the lower core (which reached maximum speeds of 9 cms^{-1}). The remainder of the lower core was observed flowing westward into the Iberian basin, and was a source of meddy formation.

A third well-defined core, at depths between 400 and 600 m, has been detected near 6.7°W in the Gulf of Cadiz to about 38.5°N off western Portugal (Ambar 1983). This shallow vein of MW with a thickness of 50 to 100 m, is distinct from the two main cores and is found at density levels between 27.25 and 27.45 $kg\,m^{-3}$ following a path along the upper continental slope of the Iberian Peninsula. It was suggested by Ambar and Howe (1979) that this core may result from a subdivision of the upper core, probably due to the influence of bottom topography in the Gulf of Cadiz. Fiuza et al. (1998) undertook a detailed study off the west coast of the Iberian Peninsula in May 1993, which included a grid of CTD (conductivity-temperature-depth) stations between 40° and 43°N, from the coast out to 11°W. They did not find any trace of this shallow MW vein, indicating that it is probably restricted to the region south of 40°N.

Fiuza et al. (1998) found that the flow of MW was towards the north throughout their study region, clearly related to the Portugal Slope Undercurrent. They observed that both cores of MW decreased in salinity northwards at an average rate of 0.06 per 100 km. The temperature of the cores also decreased northwards, the upper more markedly (0.24°C per 100 km) than the lower (0.05°C per 100 km). This difference, possibly due to the dominant mixing processes being upward temperature diffusion for the upper core, and salt fingering below the lower core, means that the upper core density and depth hardly change within the study region (average depth ~780 m), whereas the lower core density decreases northwards, so that the lower core rises from an average of 1200 m depth at 40°N to 1000 m at 43°N.

The upper core is clearly marked by its high salinity against the continental slope. It occupies a relatively thin layer of about 100 m and undergoes strong dilution. The lower core, on the other hand, is thicker (400-500 m) and spreads more evenly. It suffers less dilution than the upper core, only about 20% from the south to the north in the study region. Strong gradients west of 10°W at 43°N show the MW being constrained by the influence of colder Atlantic waters. LSW is encountered north of 42.5°N in the vicinity of the Galicia Bank and at 43°N a narrow vein of the lower core (with over 55% of the MW concentration it had at Cape St Vincent) extends northwards against the continental slope.

Iorga and Lozier (1999a, 1999b) used historical hydrographic data along with stream function and velocity fields computed from a diagnostic model to detail the climatological signature of the MW in the eastern North Atlantic. A particular advantage is the spatially continuous picture it gives. They describe a cyclonic recirculation in the western Gulf of Cadiz which acts to spread the salinity signal south of 34°N (Figure 2.6). The rest of the MW turns northwards after Cape St Vincent and enters the Tagus Basin where it diverges, with part of it flowing northwards along the Iberian continental slope and the rest flowing westwards (refer to Figure 2.5 for topographic features). The westward branch is split north and south of the Gorringe Bank, but reconvenes and flows

anticyclonically to meet up with the northward flowing branch just off the Estremadura promontory, creating a 'reservoir' of MW. The MW continues northwards, flowing both east and west of the Galicia Bank, and then following the continental slope around Cape Finisterre into the Bay of Biscay. It recirculates within the Bay of Biscay and then flows in a poleward slope current up to the Porcupine Bank. At about 48°N 10°W, an eastward moving branch of the North Atlantic Current (NAC) converges with the northwestward flowing MW, reducing the salinity signal of the MW. Just west of the Goban Spur some of the MW turns westwards and meets another branch of the NAC, while the remainder continues as a slope current into the Rockall Channel. Its salinity signal, however, is only confirmed as far as 50.3°N. From an analysis of the pressure fields and isopycnal surfaces of the MW, they confirm the possibility that the MW could flow over the Wyville-Thomson Ridge.

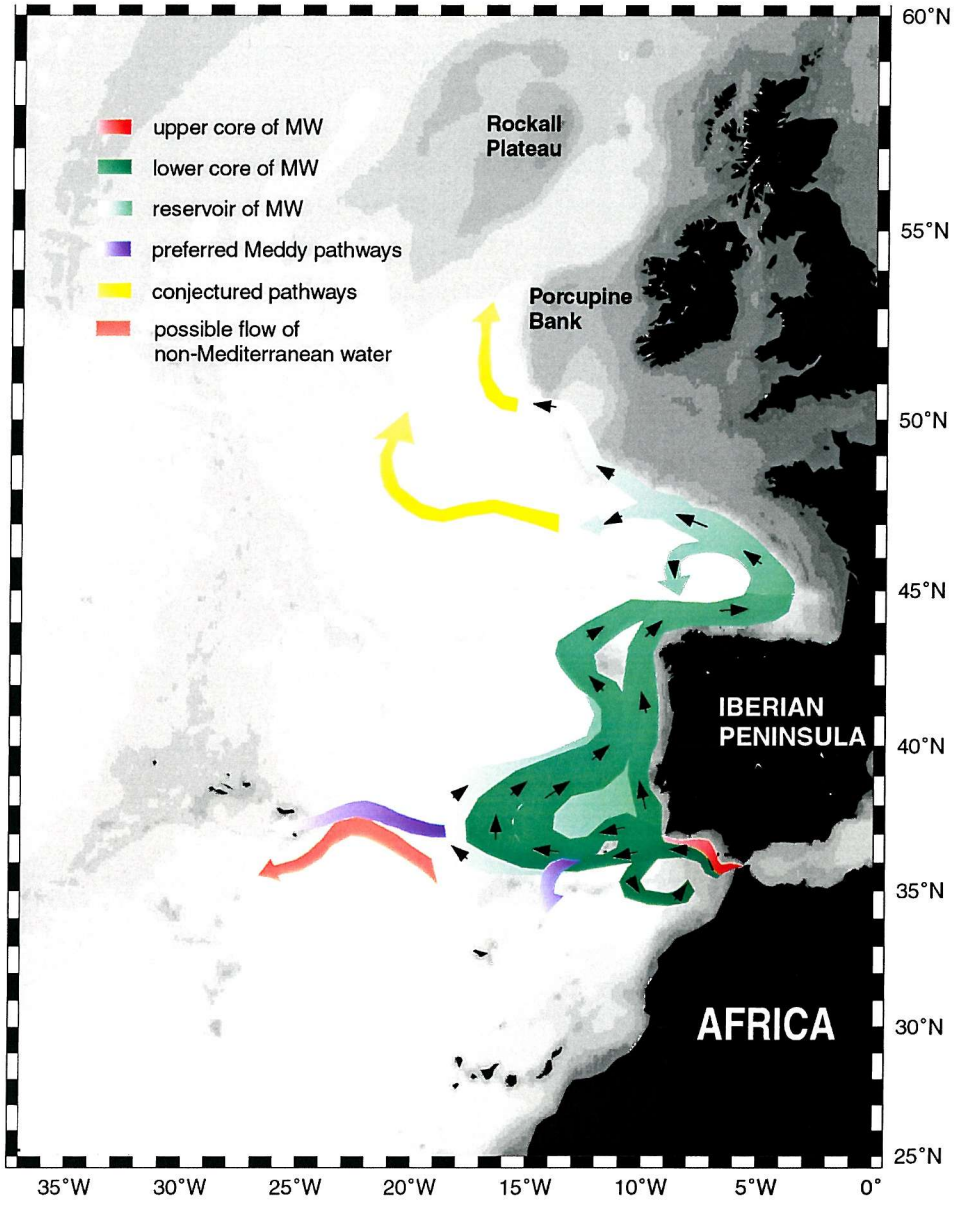

Figure 2.6 *Composite summary of the Mediterranean Water pathways in the eastern North Atlantic basin (Iorga and Lozier, 1999a).*

2.4.5 Westward Flow of Mediterranean Water

Whilst most studies agree that a more or less persistent northward current of MW flows along the Portuguese continental slope, there is no such agreement as to the mechanism of westward spreading of this water mass. Maze et al. (1997) examined data from the Bord-Est 3 experiment and found the meridionally averaged zonal transport of the MW to be eastward. They therefore argued that at Iberian latitudes a direct entry of MW into the ocean interior can occur only through westward meddy propagation. Model results by Paillet and Mercier (1996) support this hypothesis. Shapiro and Meschanov (1996) also deduced from historical hydrographic data that west of 15°W in the Iberian Basin all branches of MW spread in the form of meddies.

Iorga and Lozier's (1999b) model shows westward advection occurring only within the Tagus Basin, recirculating before reaching 20°W, with no significant advection into the subtropical gyre. They suggest that on climatological timescales, the westward penetration of MW is principally diffusive and although their model contains a westward current at ~35°N, they argue that it is not derived from the Mediterranean Outflow (as other authors have found), but from the poleward-flowing, eastern boundary current off Africa which picks up the MW signal as it flows. Ultimately there is little difference between the MW current advecting its signal westward into the North Atlantic or the signal being advected by another current. The result in both cases is the westward transport, by advection, of high salinity originating from the Mediterranean.

In contrast, an advective pathway has been suggested between 35°N and 40°N by analysis of observations (Reid, 1994; Daniault et al., 1994) and model results (Bogden et al., 1993). The maximum Mediterranean salt content is found between 36°N and 40°N (Arhan et al., 1994), the minimum zonal salinity gradient within the MW is found at ~41°N (Fiuza et al., 1998), and these distributions combined with mainly westward velocities observed around 1000 db at these latitudes (Arhan et al., 1994) point to an advective pathway for MW westwards.

2.4.6 Input of Mediterranean Water to the Nordic Seas

The distinct silicate signature of the MW indicates its presence as far north as the Norwegian Sea, and as already mentioned, this has provided the impetus to hypothesise that MW could be important to the Atlantic thermohaline circulation. Northward penetration of MW as far as the Porcupine Bank (~50°N) is generally accepted, however, its transport further northward is strongly disputed.

One of the drawbacks with Reid's (1979) conclusions is that they were based on a data set that was sparse, particularly in the Rockall Trough region, which has since been found to be a critical and dynamic area. New et al. (2001) used three high-resolution ocean circulation models to investigate the supply of saline water masses to the Nordic Seas. They found that the inflows are derived from shallow sources, comprising waters of western subtropical origin and saline eastern North Atlantic Water, transported northwards in a Shelf-Edge Current. None of the models allowed the MW to extend as far as the Nordic Seas; in two, the MW reached the Porcupine Bank (53°N) and in the other, it got as far as the Rockall Trough (to 60°N). Ellett et al. (1986) showed that the flow of water masses on density surfaces appropriate to the MW is typically southwestwards over the Wyville-Thomson Ridge, which argues against the northward progression of the MW into the Nordic Seas. This is confirmed by all three models used by New et al. (2001).

Hydrographic data have shown that limited amounts of MW exist at depths of 800-1200 m against the continental slope at 53.5°N, being transported in a northward slope current (Huthnance, 1986). This could provide the input of MW to the Rockall Channel. McCartney and Mauritzen (2001) argued that MW could not rise up and over the Wyville-Thompson Ridge, preferring to explain the input of saline waters to the Nordic Seas as originating from a shallow source, a northward flowing branch of the NAC, which flows through the Rockall Trough. However, they do point out that MW is certainly a constituent of the NAC, being one of the dominant water masses throughout much of the intermediate North Atlantic. It has also been noted in observations and models that the NAC (with its near-surface salinity maximum due to the net annual evaporation in the subtropical North Atlantic) merges with the MW salinity maximum by a latitude of about 50°N (Price et al., 1993).

In light of recent observations it now seems more of a remote possibility that MW reaches the Nordic Seas directly. However, whether one believes that the route is direct or indirect, the fact that it does influence the high salinity signal found there confirms its importance in the North Atlantic Ocean circulation and climate.

2.5 SUMMARY

The North Atlantic Ocean is the most saline of the world's oceans due at least partially to the inflow of water from the Mediterranean Sea. The high salinity in the Nordic Seas leads to the formation of North Atlantic Deep Water, which by way of the Deep Western Boundary Current reaches the Antarctic and leads to the formation of Antarctic Bottom Water. Reid (1979, 1994) argued that Mediterranean Water is the source for the high salinity found in the northern North Atlantic, and that as such, has a profound influence on the global ocean circulation and hence on climate. MW is certainly implicated in the Atlantic thermohaline circulation, either directly, by its arrival in the Nordic Seas via an eastern boundary undercurrent, or indirectly, by supplying the interior Atlantic with high salinity water (McCartney and Mauritzen, 2001).

A direct effect of the Mediterranean Outflow is to provide heat and salt to the intermediate layers of the North Atlantic gyres. In fact, it is the only source for the maxima in heat and salt content found beneath the thermocline. The westward component of the outflow provides the high heat and salt content of the deep Gulf Stream and of the southward flow along the western boundary (Reid, 1994).

It has also been demonstrated that the Mediterranean Water influences the central waters of the North Atlantic (Mauritzen et al., 2001). Observations, laboratory experiments and direct current measurements show that in the eastern Gulf of Cadiz there occurs a cross-isopycnal flux of salinity from the Mediterranean Outflow Water towards the low-density Central Water where the two water masses are in physical contact. This is hypothesised to be the reason for the difference in salinity between eastern and western varieties of NACW (seen in the salinity section at 36°N, Figure 2.7).

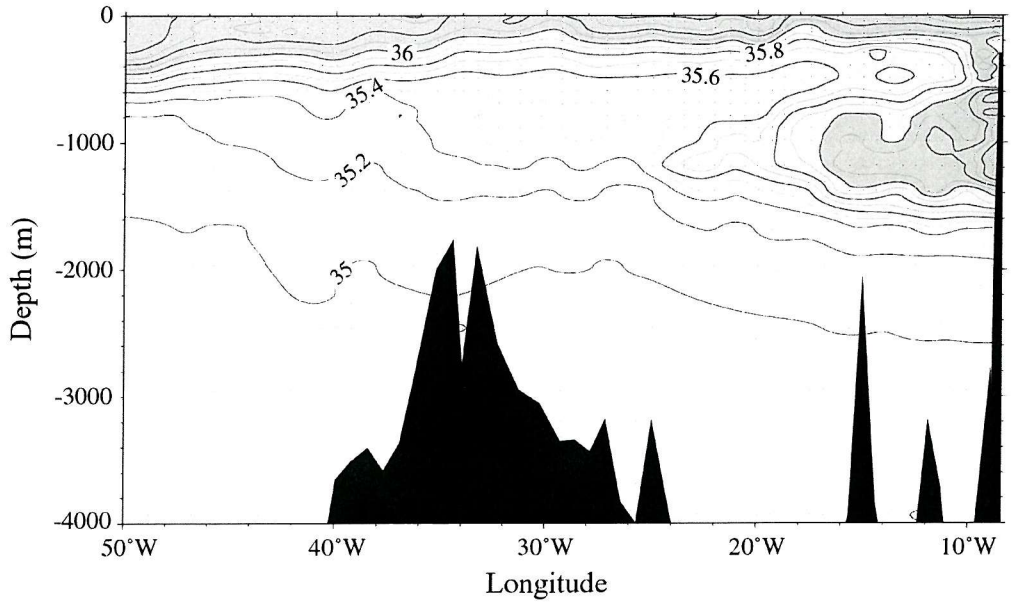

Figure 2.7 Salinity section at 36°N from R/V Atlantis, June-July 1981 (Mauritzen et al., 2001).

As well as having an obvious impact on water properties in the North Atlantic Ocean, the Mediterranean Outflow has a strong dynamical impact on both the upper layer and mid-depth circulation of the eastern basin. The sink introduced in the Gulf of Cadiz by entrainment of NACW into the outflow is thought to induce the Azores Current (Jia, 2000). It is also thought that the buoyancy flux associated with the outflow may generate large-scale baroclinic circulation in the eastern North Atlantic (Bryden and Kinder, 1991a).

The Mediterranean Sea is becoming saltier due to the diversion of fresh riverine inputs, which effectively increases the net evaporation over the Mediterranean Basin (Bryden and Boscolo, 2002). Johnson (1997) argued for a controlling dam at the Strait of Gibraltar to minimise the effect of the increasing Mediterranean Water salinity. He warned that an ice age could be triggered by an increase in Mediterranean Outflow intensity, assuming its high salinity is rapidly conveyed to the Nordic Seas via the eastern boundary undercurrent. It has been pointed out (Bryden and Webb, 1998) that the models on which Johnson (1997) based his theory were too simplistic to resolve all the detail and that he had several factual errors in initial assumptions. They also observed that in order to be able to predict the effect of a higher salinity or higher intensity Mediterranean Outflow, knowledge of, among other things, the ultimate pathways of Mediterranean water in the North Atlantic is needed, including the division between how much proceeds northwards along the Iberian continental slope and how much flows westward into the Atlantic interior.

Candela (2001) in his chapter in the WOCE book (Siedler et al., 2001), which is the definitive reference for large scale ocean circulation at this point in time, states "*With regard to the observational basis for the pathways of the Mediterranean outflow, we do not yet know how much of the outflow proceeds north along the Iberian continental slope and how much flows or circulates slowly westward from the Strait ... quantifying and understanding these details are at the heart of being able to answer with certainty the role played by the Mediterranean outflow on the North Atlantic circulation*".

Although the North Atlantic is the most studied of the world's oceans, it still resists thorough description (Schmitz and McCartney, 1993), and one of the most interesting aspects (partly from the controversy surrounding it) is the transport of Mediterranean Water in the North Atlantic Ocean.

Chapter Three

Data

3.1 INTRODUCTION 27

3.2 HYDROGRAPHY 28
- 3.2.1 Med Box 88 Datasets 28
  - *i Northern Section: Discovery Cruise 189, 1990* 28
  - *ii Western Section: Oceanus Cruise 202, 1988* 29
  - *iii Southern Section: Hesperides Cruise 6, 1992* 29
- 3.2.2 Med Box 98 Datasets 29
  - *i Northern Section: Fourex - Discovery Cruise 230, 1997* 29
  - *ii Western Section: CHAOS - Discovery Cruise 233, 1998* 30
  - *iii Southern Section: Ronald H. Brown Cruise, 1998* 30

3.3 HYDROGRAPHIC SECTION PROPERTIES 31
- 3.3.1 Northern Section: Med Box 98 31
- 3.3.2 Western Section: Med Boxes 88 and 98 31
- 3.3.3 Southern Section: Med Box 88 33

3.4 DATA QUALITY CONTROL 34
- 3.4.1 Calibration Corrections 34
- 3.4.2 Temperature Scales, Salinity and Standard Seawater 35
- 3.4.3 Salinity Biases 36
- 3.4.4 Note on Deep Water Potential Density 38
- 3.4.5 WOCE Section AR16 39

3.5 LEVITUS CLIMATOLOGY 40

3.6 OCCAM DATA 41

3.1 INTRODUCTION

To investigate the transport of Mediterranean Water (MW) in the eastern North Atlantic, three-sided boxes were created around the Strait of Gibraltar, encompassing the Mediterranean Outflow. These are referred to as Med Boxes, and are illustrated in Figure 3.1. The datasets used are described in this chapter and include: hydrographic sections from the World Ocean Circulation Experiment (WOCE); the Levitus climatology; and a fine resolution ocean general circulation model from the Ocean Circulation and Climate Advanced Modelling project, OCCAM. The main hydrographic (temperature and salinity) characteristics and data quality control are also discussed here.

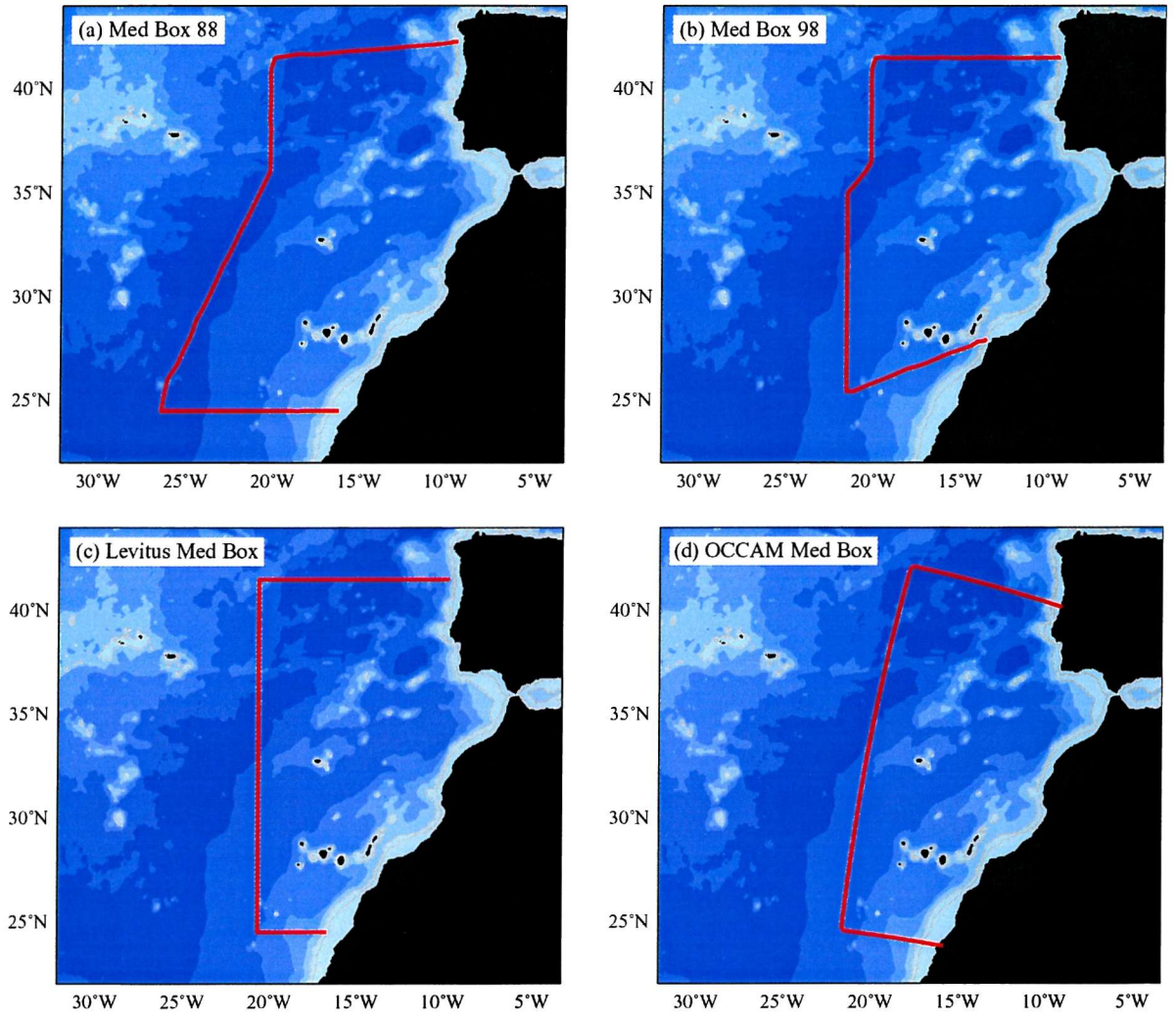

Figure 3.1 Maps of (a) Med Box 88, (b) Med Box 98, (c) Levitus Med Box, (d) OCCAM Med Box.

3.2 HYDROGRAPHY

Data from six cruises were used to create two hydrographic Med Boxes, one for the late 1980's and one for the late 1990's, referred to as Med Box 88 and Med Box 98 respectively. Figure 3.2 shows these two Med Boxes and the cruise station positions.

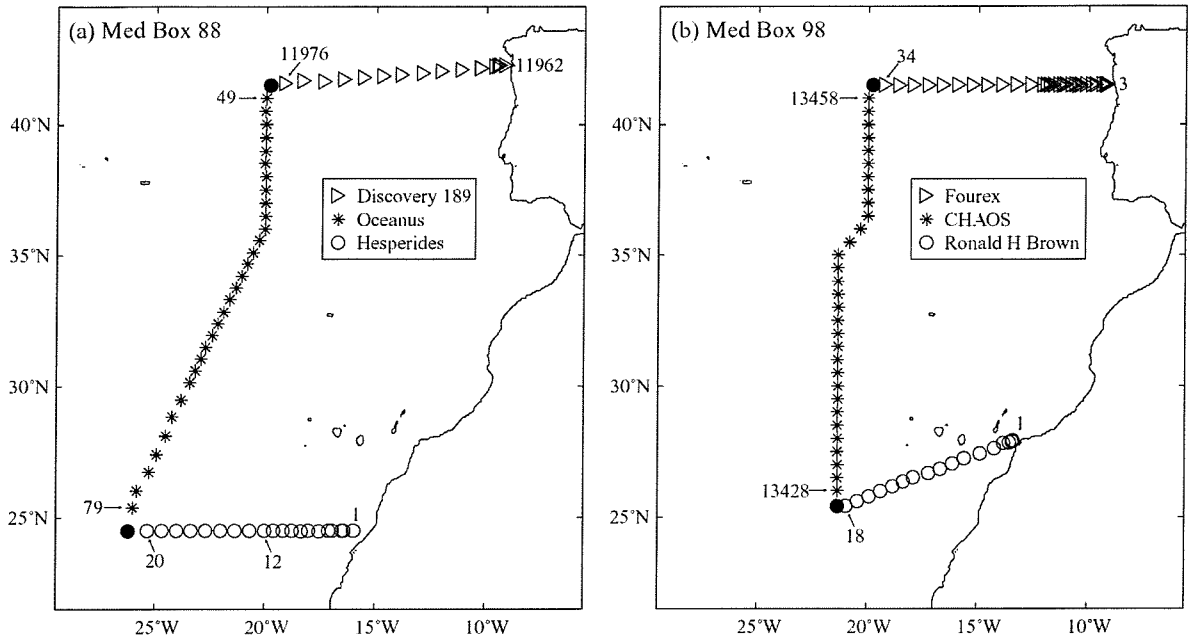

Figure 3.2 Stations used to create (a) Med Box 88 and (b) Med Box 98

3.2.1 Med Box 88 Datasets

i Northern Section: Discovery Cruise 189, 1990

Discovery Cruise 189 was the second of two cruises undertaken to investigate the interannual variability of the ventilating North Atlantic Mode Water northeast of the Azores (King, 1990). A region enclosed by 42°N, 20°W, 53°N and the continental shelf of northwest Europe was surveyed in March 1990 with full depth CTD[1] stations. The stations used to create the northern edge of Med Box 88 include those from stations 11962 at 42.2°N, 9.2°W (170 m depth), to station 11976 at 41.6°N, 19.2°W. The station spacing was approximately 20 km close to the shelf edge and 75 km further offshore.

[1] conductivity-temperature-depth

ii Western Section: Oceanus Cruise 202, 1988

WOCE transect A16 was a quasi-meridional transect extending from Iceland (63°N) to South Georgia (54°S) along a nominal longitude of 20°W (Tsuchiya et al., 1992). Due to the extreme length of the transect, the fieldwork was divided into two: the North Atlantic section was surveyed in July to August 1988 by *RV Oceanus* (the data used in this study); the South Atlantic section was surveyed in 1989. The main objective of Oceanus Cruise 202 was to investigate the mid-ocean zonal circulation at all depths of the eastern Atlantic Ocean. The survey began at the shelf break immediately south of Iceland and continued along 20°W southward to 36°N, where it turned to the west toward 20°N, 29°W, following the deepest portion of the eastern basin. To the north of 30°N the station spacing was generally 56 km, and to the south it was generally 83 km. The western side of Med Box 88 comprises Oceanus stations 49 (at 41°N, 20°W) to 79 (at 25.39°N, 26.0°W).

iii Southern Section: Hesperides Cruise 6, 1992

In July and August 1992, the Spanish Naval Vessel *Hesperides* undertook a transatlantic hydrographic section along 24.5°N to mark the quincentenary of Columbus's historic voyage of 1492 (Parilla et al., 1994a). According to the WOCE implementation plan this transect, named WOCE section A5, was originally located at 24°N. However, as two oceanographic sections were surveyed at 24.5°N in 1957 and 1981, A5 was moved to this latitude (Parilla et al., 1994b), making it one of the best surveyed of all oceanographic sections (Bryden et al., 1996).

Stations 1 to 20 make up the southern edge of Med Box 88. The first station was at the 50 m isobath off the coast of Africa at 24.5°N, 16.0°W. The ship then proceeded westward, with a station made approximately every 33 km at the 100, 150, 1500, 2000 and 2500 m isobaths, after which the station separation was approximately 43 km until the 4000 m isobath (station 12). From station 12 to the eastern limits of the Mid-Atlantic Ridge the stations were separated by 67 km (Parrilla et al., 1994b).

3.2.2 Med Box 98 Datasets

i Northern Section: Fourex - Discovery Cruise 230, 1997

The northern edge of Med Box 98, between 9°W and 20°W along 41.5°N, is the initial part of a WOCE section undertaken by *RRS Discovery* in August 1997 (Bacon, 1997). This survey was designed as a repeat of the International Geophysical Year survey section 4 (first surveyed in 1957), roughly from Cape Finisterre, Spain to Cape Farewell, Greenland, and aimed to investigate decadal variability in the North Atlantic.

The section began with station 3 (the first 2 stations being test stations) on the 200 m contour at 9.2°W. Station 35 was the last of the transect along 41.5°N, after which the ship turned northwest for the rest of the section to Cape Farewell. A brief halt was called after station 21 due to LADCP problems, station 22 was a cast to 2000 m to ensure watertight integrity of the LADCP pressure case, and station 23 was an overlap station, repeating 21. The stations used for the northern edge of Med Box 98 are therefore 3 to 21 and 24 to 34. Stations 21 to 34 cross the bottom of the Iberian Abyssal Plain and station 35 is over a seamount of the Azores-Biscay Rise (Bacon, 1997). The station separation varied from about 15 km near the coast to 56 km further offshore.

ii Western Section: CHAOS - Discovery Cruise 233, 1998

A Chemical and Hydrographic Atlantic Ocean Survey (CHAOS) was undertaken in May and June 1998 aboard *RRS Discovery* (Smythe-Wright, 1999). The cruise was a joint effort between the George Deacon Division and the James Rennell Division at Southampton Oceanography Centre. The data were requested by the WOCE international community to contribute to the WOCE baseline survey of the North Atlantic, and were therefore made to the same high standards. From 20°N up to Iceland, the cruise was along a nominal longitude of 20°W, with a station spacing of 55 km. Various zonal sections were also surveyed for a detailed study of the Rockall Trough. CHAOS stations 13428 (at 26.0°N, 21.3°W) to 13458 (at 41.0°N, 20.0°W) contribute to Med Box 98, forming the western edge of the box.

iii Southern Section: Ronald H. Brown Cruise, 1998

A WOCE repeat cruise (AR01) along 24.5°N aboard the NOAA ship *R/V Ronald H. Brown* was undertaken in January and February 1998. The objectives were to quantify the water masses and determine the meridional overturning circulation responsible for the redistribution of heat, fresh water and carbon in the centre of the subtropical gyre (McTaggart et al., 1999). Although this section ostensibly ran along 24.5°N, it began with a northeast-southwest track off the coast of Africa, and this is the data used for the southern edge of Med Box 98; stations 1 (at 27.9°N, 13.4°W in a depth of 130 m) to 18 (at 25.4°N, 20.9°W in 4600 m depth). The station separation varied from about 40 km near the coast to 70 km further offshore.

3.3 HYDROGRAPHIC SECTION PROPERTIES

This section provides an overview of the main hydrographic characteristics of the region, describing temperature and salinity properties of the Med Box sections (shown in Figure 3.3).

3.3.1 Northern Section: Med Box 98

The most striking features of the northern Med Box 98 section are the salinity and temperature maxima, associated with MW. These can be seen throughout the entire section centred at approximately 1000m depth (Figure 3.3a). The MW signal is much stronger towards the east of the section, and the two regions of greatest salinity and temperature anomalies are between 10.5°W and 12°W and east of 9.5°W, and here they have a vertical scale greater than 1000 m. There are two discernible vertically separate cores of MW at both these positions. The upper core, centred on 800 m depth, is characterised by a temperature maximum (>11.5°C). The lower core, centred on 1200 m depth, is characterised by a salinity maximum (>36.2). The northern section of Med Box 88 (not illustrated) shows similar features and will be described in Chapter 5.

3.3.2 Western Section: Med Boxes 88 and 98

Figure 3.3b shows the vertical sections of temperature and salinity for the Oceanus data (west side of Med Box 88). Once again, the most distinctive features of this section are the maxima in salinity and temperature centred at approximately 1000 m depth between 35°N and 40°N. From the temperature and salinity characteristics (which at the core are > 11.5°C and > 36.1 respectively) these waters are identifiable as MW, which has a vertical extent greater than 800 m. The MW signature is further emphasised by the minimum in salinity lying between 400 m and 700 m, sandwiched between the MW and the higher salinity surface waters. This minimum is particularly strong between 33°N and 35°N. The surface water salinities increase southwards and attain maximum values of more than 37.0 around 24°N, which is a region of excess evaporation (Schmitt et al., 1989).

The two distinctive features are meddies, which are the much smaller isolated cores of highly saline and warm water at the southern end of the section. The meddy at ~25°N has a vertical extent of approximately 300 m, is centred around 800 m and has temperature and salinity values at its centre in excess of 12.0°C and 36.2. The meddy at 27°N is not as anomalous; centred on 900 m, it has a vertical extent of approximately 500 m.

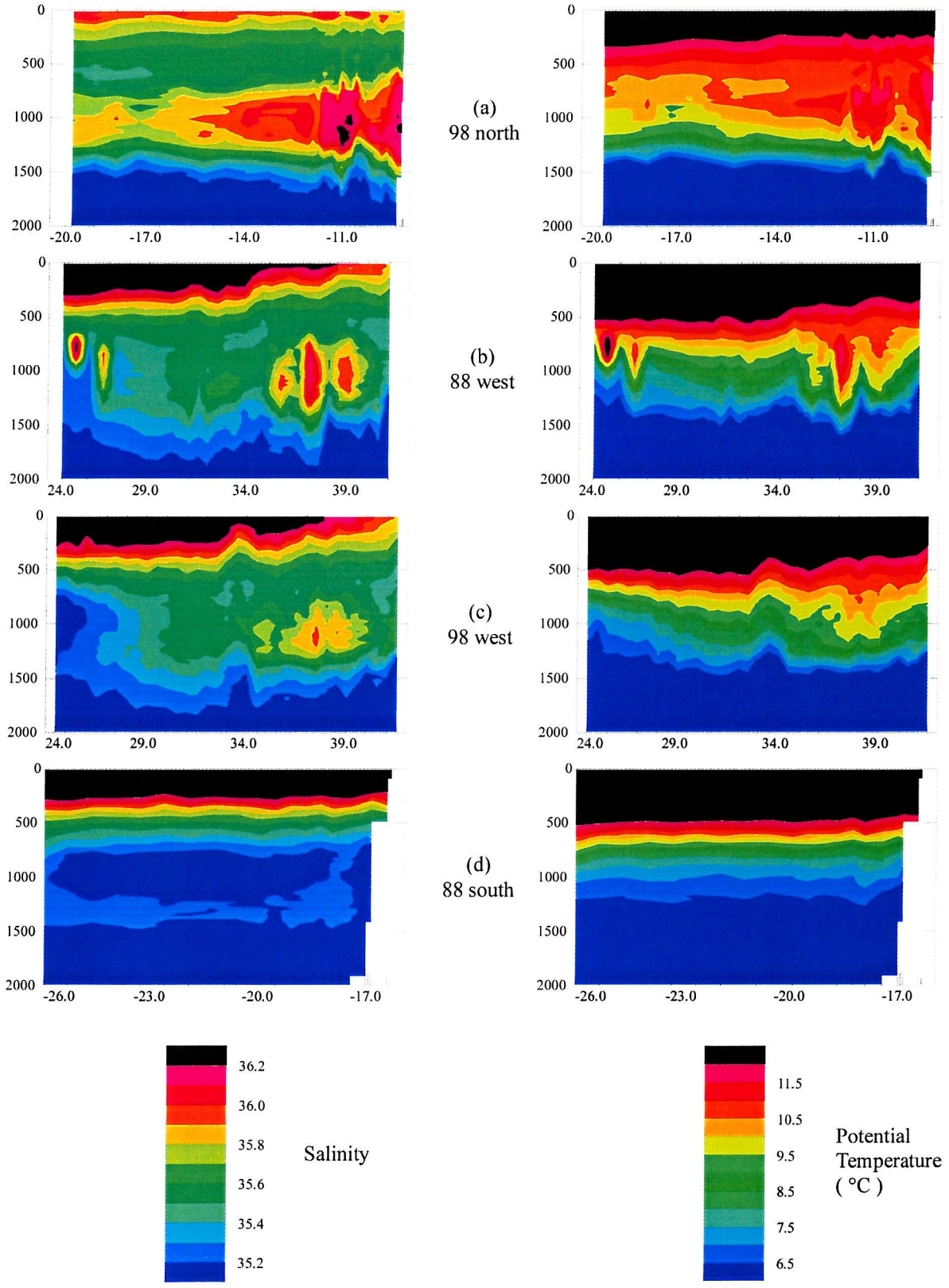

Figure 3.3 *Salinity and potential temperature contour plots of the upper 2000 m for Med Box sections (a) 98 north, (b) 88 west, (c) 98 west, and (d) 88 south.*

The CHAOS section (west side of Med Box 98; Figure 3.3c), along the same meridian as the Oceanus section but taken 10 years later, shows very similar characteristics. The warm and saline MW can again be seen centred at approximately 1000 m depth between 35°N and 40°N, however, the anomalies are weaker, with the core of the MW reaching only 10.6°C and 35.93 in salinity (Figure 3.4 shows the θ/S profiles for the stations containing these maxima). Again there is a minimum in salinity lying between 400 m and 700 m at latitudes 33°N to 35°N. It appears that there were no meddies crossing the 20°W boundary at the time this survey was taken.

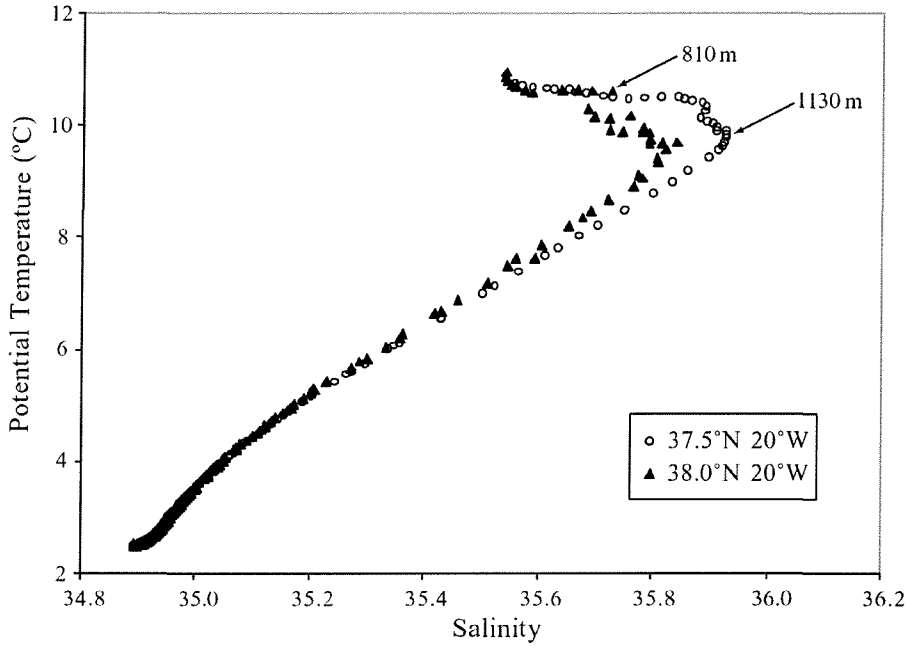

Figure 3.4 θ/S curves of CHAOS stations (data below 600 m) at 37.5°N, 20°W and 38°N, 20°W.

3.3.3 Southern Section: Med Box 88

The southern sections, unlike the other sections, show little variability in temperature and salinity. The temperature decreases with depth throughout the section, and the isotherms are more or less horizontal. The isotherms become slightly deeper at the western end of the section, and slightly shallower at the eastern end, but in each case by only about 50 m. The salinity contours show similar features, however, there is a minimum in salinity centred on 1000 m, which is a large pycnostad[2] of water with a salinity of 35.1, a thickness of 400 m, and temperatures of 6.5°C to 8.5°C. This pycnostad is present throughout most of the section, from 18°W to 25°W, and is bounded on all sides by higher salinity water. The southern section of Med Box 98 (not shown) is similar.

[2] A pycnostad is a layer where the vertical change of density is very small and displays a local minimum.

3.4 DATA QUALITY CONTROL

When using hydrographic data, care must be taken to ensure that the data are carefully examined and quality controlled. Calibrations may have been applied incorrectly, and errors may have occurred during the data processing stage, and it is therefore worthwhile checking the data for obvious errors. Comparison of the data with an independent dataset can reveal errors in individual stations as well as systematic errors which may occur throughout an entire dataset.

3.4.1 Calibration Corrections

Study of the Discovery Cruise 189 data (for the north side of Med Box 88) showed two stations to be slightly offset from the others; stations 11972 and 11979 were 0.003 saltier than other stations as seen in the deep θ/S properties (Figure 3.5a). The bottle data for these stations, however, are within the range of all the other station data (Figure 3.5b). It would therefore seem that a small error was made during the calibration of these two stations. After discussions with the cruise Principal Scientist, Brian King, it was decided that for the purpose of this work a value of 0.003 should be subtracted from the salinity data of stations 11972 and 11979 to correct this calibration error.

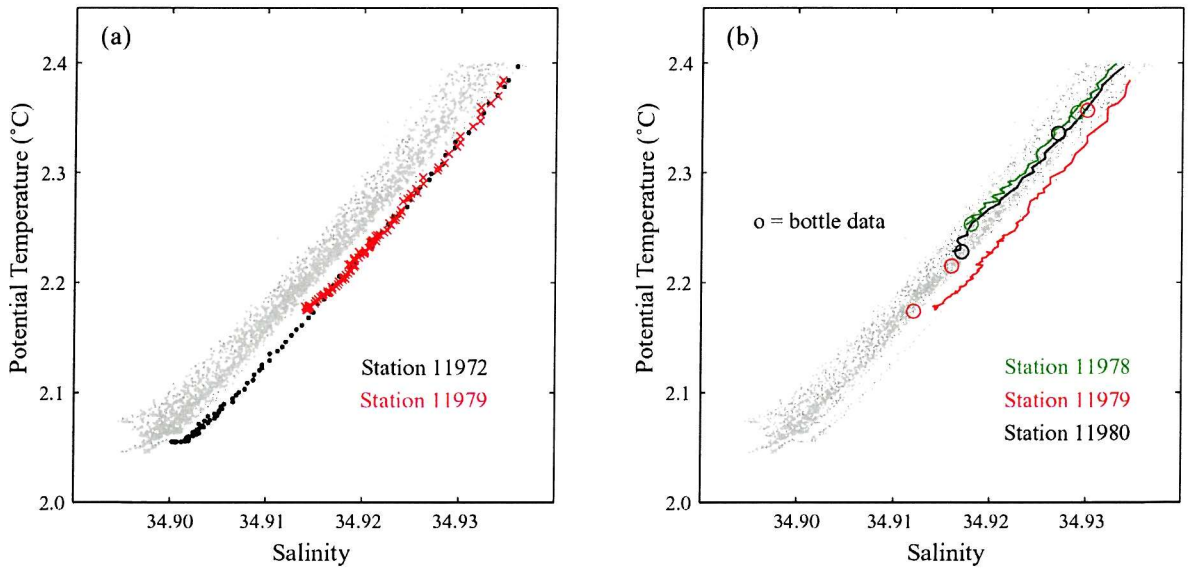

Figure 3.5 *Discovery 189 deep θ/S plots showing (a) the offset of stations 11972 and 11979 from the rest of the data, and (b) the offset of station 11979 from its own bottle data and the stations next to it, where the bottle data are represented by open circles.*

3.4.2 Temperature Scales, Salinity and Standard Seawater

In September 1989, the International Committee for Weights and Measures approved the International Temperature Scale of 1990 (ITS90) to replace the International Practical Temperature Scale of 1968 (IPTS68), as it more closely approximates the thermodynamic temperature scale (Saunders, 1990). The word 'practical' was dropped from the title because no further changes appeared to be needed in the foreseeable future (McGee, 1988). The data used in this thesis were collected both before and after 1990, it was therefore necessary to ensure that all temperatures were reported on the same scale (Table 3.1). Although there is relatively little difference between temperature measurements on the two scales within the range of normal oceanographic values (-2°C to +35°C), the impact of that difference on derived quantities, where temperature is used in their determination, is non-negligible. All temperatures reported in this thesis are on the ITS90 scale, but are converted to IPTS68 for computing derived quantities using the formula suggested by Saunders (1990), $T_{68} = 1.00024 \times T_{90}$.

Cruise	Section	Year	Month	Temperature Scale	Standard Seawater
Hesperides	24.5°N	1992	Jul-Aug	IPTS68	P120, P117
Oceanus	~20°W	1988	Jul-Aug	IPTS68	P108
Discovery 189	41.5°N	1990	Mar-Apr	ITS90	
Baringer	~24°N	1998	Jan-Feb	ITS90	P133
CHAOS	~20°W	1998	Apr-May	ITS90	P133
Fourex	41.5°N	1997	Aug-Sep	ITS90	P128, P130, P131, P132

Table 3.1 *Details for each cruise including nominal latitude / longitude of ship's track, year and month of survey and temperature scale and IAPSO Standard Seawater batch used.*

Salinity is determined using the Practical Salinity Scale 1978 (PSS78), a usage that has been mandatory since January 1, 1982 (Culkin and Ridout, 1989). Since the PSS78 algorithms were adjusted to eliminate the ppt (parts per thousand) and 10^{-3} used in previous scales salinity is a dimensionless quantity. As such, salinity in this work is expressed by a dimensionless number; for example "S = 35.022", or "the salinity is 35.022". It should be noted, however, that salt transport is reported using the units Sv psu in order to clearly distinguish it from volume transport, which is given in Sv.

By definition, a seawater of practical salinity 35 has a conductivity ratio of unity at 15°C with a potassium chloride (KCl) solution containing 32.4356 grams KCl per kilogram of solution (Culkin and Ridout, 1989). In practice, in the laboratory, salinity is calculated by comparing the electrical

conductivity of the sample with that of a standard of known salinity at the same temperature. The measured conductivity ratio is then converted to salinity by means of the equations in the PSS78. Temperatures used in the PSS78 are measured according to the IPTS68. The equation is valid in the temperature range –2°C to +35°C and salinity range 21 to 42.

IAPSO Standard Seawater is the only internationally recommended standard for salinity determinations. Standard Seawater is natural North Atlantic surface water, purified by filtration through activated carbon cartridge filters and irradiation with UV light. The water is thoroughly mixed in a large tank, distilled water is added to provide the required salinity, and 'standard seawater' is finally sealed in glass ampoules. Selected ampoules from each batch are then calibrated using the defined standard potassium chloride solution.

The IAPSO Standard Seawater service originally operated from a laboratory in Copenhagen until 1975 when responsibility for its operation was taken over first by the IOS in Wormley, and then in April 1989 by Ocean Scientific International Ltd., Surrey. The use of a single standard for all salinity determinations helps ensure uniformity in salinity measurements throughout the oceanographic community. The standard seawater batches used in each cruise are detailed in Table 3.1.

3.4.3 Salinity Biases

When combining data from different sources, there is always the possibility of a mismatch in water properties due either to changes in the water column or to systematic sampling errors. In the calculation of geostrophic velocities, systematic differences in salinity or temperature can result in unrealistically large velocities at the intersection of different data sets, particularly noticeable in the deep water.

The uniformity of the θ/S relationship of water below 3000 m in the Northeast Atlantic has been well documented (Saunders, 1986). Small systematic differences in salinity measurements between cruises are believed to be due to variations in standard seawater (Saunders, 1986; Mantyla 1994a, 1994b). To check for systematic differences between data sets used in this work, the deep water θ/S relationships were compared. Figure 3.6a shows this relationship for the southwest corner of Med Box 88; the Hesperides salinity is 0.005 saltier than the Oceanus. This difference induced a substantial (2 Sv) transport in the deep water at the corner where the sections meet. By adjusting the salinity of all Hesperides stations used here by 0.005, the transport at the corner was reduced to a more realistic value (Figure 3.6b).

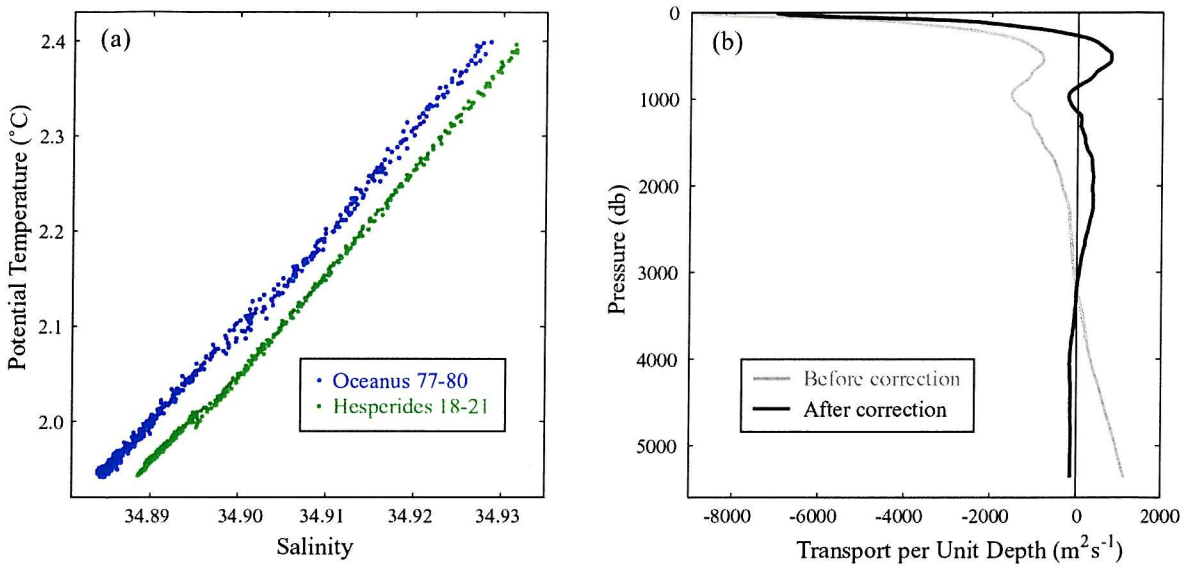

Figure 3.6 *The southwest corner of Med Box 88; (a) deep θ/S plot of stations close to the corner, and (b) geostrophic transport per unit depth profiles referenced to 3200 db before (grey) and after (black) the salinity adjustment of the Hesperides data (by 0.005).*

To calculate the salinity difference between Oceanus and CHAOS data, a regression line was calculated for each data set. The CHAOS salinity was found to be 0.003 saltier than the Oceanus. To determine whether there is a systematic difference with latitude, the data were separated into 5° latitudinal bands. The differences (shown in Table 3.2) do not vary significantly with latitude, and therefore 0.003 in salinity was subtracted from all CHAOS data to bring it in line with Oceanus. Oceanus data is taken as the standard here following Mantyla (1994b) who used the Oceanus 20°W transect as a baseline to adjust all Atlantic sections in order to eliminate biases.

Latitude range (degrees)	CHAOS salinity – Oceanus salinity
20-25	0.00244
25-30	0.00411
30-35	0.00314
35-40	0.00270
40-45	0.00287
45-50	0.00284
20-50	0.00297

Table 3.2
Salinity difference between CHAOS and Oceanus data below 4000 m depth in discreet latitude ranges.

The greatest salinity difference between Discovery 230 and Oceanus data was 0.001. This was deemed to be insignificant given the limits of measurement accuracy and therefore no adjustment was made to the Discovery data. The Discovery 189 data, however, had to be adjusted by subtraction of 0.003 in salinity. The same adjustment (-0.003) was applied to the Ronald H Brown salinities to bring them in line with Oceanus data.

3.4.4 Note on Deep Water Potential Density

During an investigation of deep water properties an interesting feature was discovered. The profiles of σ_3 (potential density referenced to 3000 db) for Med Box 88 appeared to separate into two distinct curves below 4000 m (Figure 3.7). Although not detailed here, this phenomena is also apparent in Med Box 98. Possible causes of the separation are: (1) it is an artefact due to the use of data from different cruises and as such showing some bias between data sets; or (2) it is due to the modulation of deep water as it progresses northwards.

Figure 3.7a shows that it is not due to a bias between data sets as all Hesperides (southern section) data is on the denser curve, Discovery (northern section) data is on the less dense curve, and Oceanus (western section) data is split across the two. Further study (Figure 3.7b) shows that the division occurs at around 37°N, with denser deep water at stations south of this latitude. The profiles between the two distinct curves (highlighted in green in Figure 3.7b) are from Oceanus stations 56 at 37.5°N and 55 at 38.0°N.

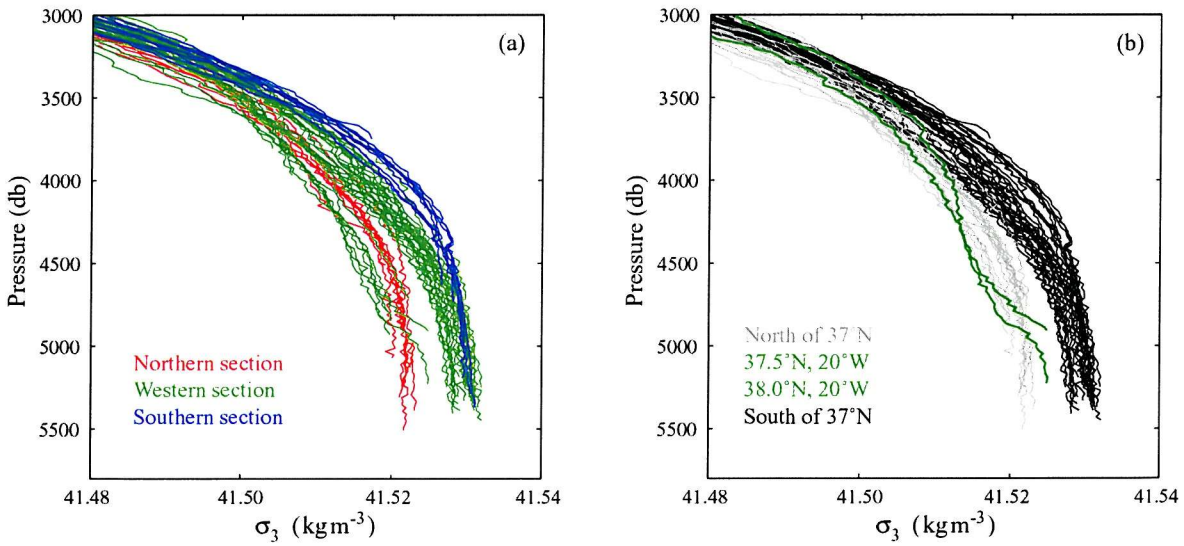

Figure 3.7 *Med Box 88 profiles of σ_3 below 3000 db showing (a) southern section (Hesperides) data in blue, western section (Oceanus) data in green and northern section (Discovery 189) data in red, (b) profiles south of 37°N in black, north of 37°N in grey, and Oceanus stations 55 at 38°N and 56 at 37.5°N in green.*

A ridge associated with the East Azores Fracture Zone runs along 37°N, with its crest at 4000 to 4500 m (discussed in Chapter 2). The ridge restricts the northward progression of deep and bottom water, which piles up against the bathymetry (as shown by Saunders, 1987). The flow is thus channelled and intensified through gaps in the ridge at 16°W (Discovery Gap) and 19.5°W. Mixing occurs at channels such as the Vema and Romanche fracture zones (Bryden and Nurser, 2002), which diffuses heat downwards from above, warming the water and making it less dense. This

explains the north-south divide in deep density. At the latitude of the ridge and the gap, property profiles lie between the two distinct values, showing mixing in progress. A jump in salinity, temperature and σ_3 properties at 4700 m in the vicinity of the ridge is apparent in the Oceanus data, as shown in Figure 3.8.

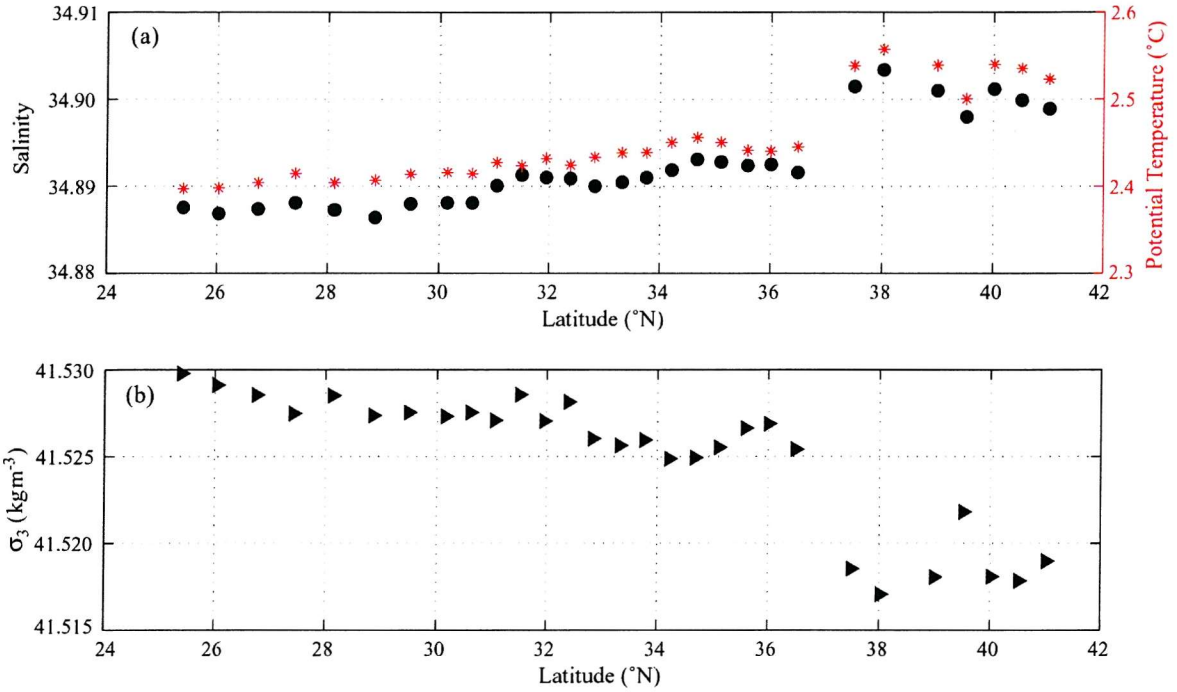

Figure 3.8 *Variation of properties at 4700 m depth along the Oceanus section (western edge of Med Box 88); (a) salinity (black circles) and potential temperature (red stars), and (b) σ_3 (kgm^{-3}).*

3.4.5 WOCE Section AR16

An additional dataset, ideal for the purposes of this work, can be found in the WOCE data archives. The repeat section AR16 was undertaken in 1991 by E. Hagen on board *R/V A. V. Humboldt*. The cruise surveyed a four-sided box, closing off the Strait of Gibraltar with its eastern leg (Figure 3.9a). Detailed study of the deep θ/S data showed large differences in salinity (of order 0.05) compared to other data in this region (Figure 3.9b).

There is a depth-dependent offset between the AR16 and Oceanus data indicating that the data have not been calibrated taking pressure into account. This is also shown by the offset of the CTD and bottle data. Communication with the cruise Principal Scientist, E. Hagen, explained that major problems were encountered on the cruise with the CTD so that the reserve unit equipped with sensors of 'second quality' was used. Due to a loss of man power, the final calibration was not completed before submitting the dataset to WOCE (Hagen, pers. comm.). Hagen noted that the

conductivity sensor used showed a response to changes in both temperature and pressure, indicating sensor problems, and making high quality data unrecoverable from this cruise. WOCE AR16 data was therefore not used in this study.

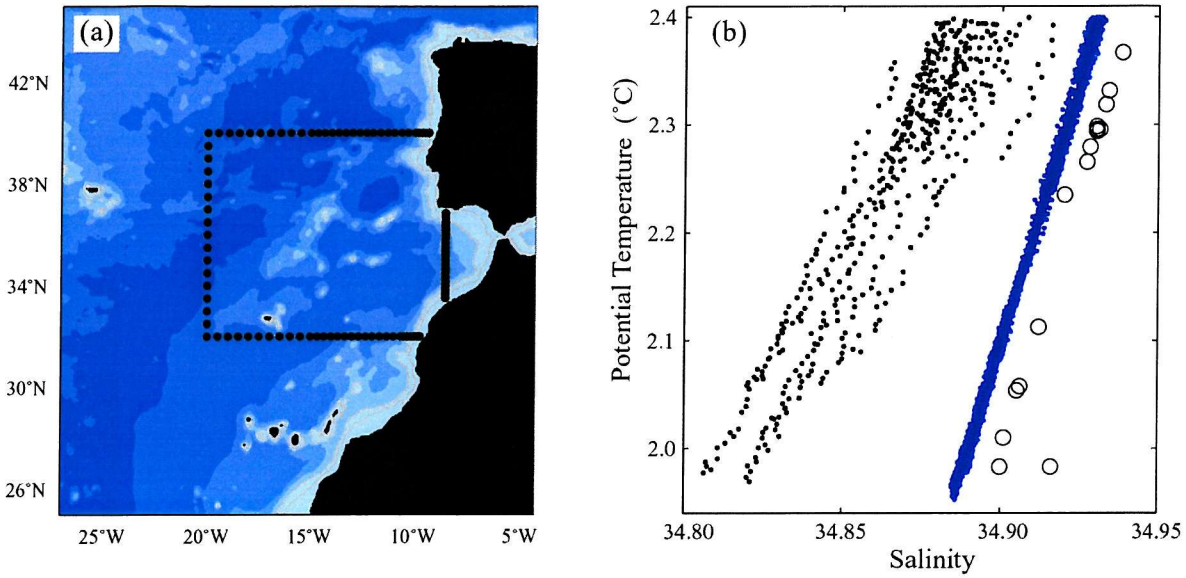

Figure 3.9 *WOCE cruise AR16. (a) Cruise stations, and (b) deep θ/S plot of AR16 data in black (CTD data denoted by dots and bottle data denoted by circles) and Oceanus data in blue.*

3.5 LEVITUS CLIMATOLOGY

The World Ocean Atlas (WOA), commonly known as the Levitus Climatology (or simply Levitus data) after its creator Sydney Levitus, is an ocean climatology based on data held by the National Oceanographic Data Centre (NODC). The original dataset is the *Climatological Atlas of the World Ocean*, published by Levitus (1982). This Atlas was the result of a project to objectively analyse (and quality control) data held by the NODC, producing a global, smoothed climatology of various parameters. WOA 94 represents an extension and continuation of this Atlas, using all data found in the NODC archives up to the first quarter of 1993. There have since been further improvements to the Levitus Climatology, incorporating recent data, resulting in the WOA 98 (Levitus et al., 1998).

The Levitus Climatology is a one-degree latitude-longitude data set of in-situ ocean parameters, such as salinity and temperature. To create such a global data set, strict quality control procedures were necessary. Data which appeared to be unrepresentative of the actual parameter fields in an area of the ocean were termed outliers, and deemed to have occurred either due to instrumentation problems, recording errors, or sampling of temporally and spatially unrepresentative oceanographic features, such as eddies and fronts (Boyer and Levitus, 1994). Outliers were flagged and removed

from the data set before creating the climatology, which is therefore a long term average view of the ocean representing a climatic mean field.

In this study, data from the WOA 98 is used, and is referred to throughout the remainder of this thesis as 'the Levitus data'. As the dataset has already been smoothed and averaged, the Levitus Med Box is created by taking individual stations (at 1° separation) along 24.5°N, 20°W and 41.5°N, without horizontal averaging onto the hydrographic station positions. There are 33 levels in the vertical, ranging from 10 m thickness near the surface to 500 m in the deep ocean. A piecewise cubic Hermite interpolant[3] was used to grid the data onto a 20 db grid for ease of comparison with the hydrographic Med Box data. This interpolation creates a curve which passes through all the points in a profile, and which can then be used to evaluate the property at any depth. Averaged bathymetry data from ETOPO5[4] was used to determine the maximum depth at each grid position, and where this exceeded the maximum depth of the Levitus data, the last known value was extrapolated to the sea bed.

3.6 OCCAM DATA

The Ocean Circulation and Climate Advanced Modelling Project was set up by the UK Natural Environment Research Council, with a core team at Southampton Oceanography Centre directed by Dr David Webb. The principal aim of the project was to develop a high resolution global ocean model to improve our understanding of ocean circulation and the interpretation of WOCE data (Webb et al., 1998). The resulting OCCAM Global Ocean Model is an eddy resolving primitive equation[5] model based on the Bryan-Cox-Semtner ocean general circulation model.

The model is run on a Cray-T3D at the Edinburgh Parallel Computing Centre. It was initialised with Levitus 82 annual average temperature and salinity fields and spun up for a period of 4 years, relaxing towards the Levitus values to ensure that the model did not drift too far during this period. Once the Levitus 94 data sets became available (day 181 of the model run), the model was relaxed towards the annual mean of these values. After the initial spin up, only the surface layer was

---

[3] Numerical Algorithms Group Ltd., UK, 1999: Fortran 77 Lib Mark 19 Manual, Numerical Algorithms Group Ltd., Oxford, UK.

[4] ETOPO5 (Earth Topography - 5 Minute) is digital average land and sea floor elevation data assembled from several uniformly gridded data bases into a worldwide gridded data set with a grid spacing of 5 minutes of latitude by 5 minutes of longitude (http://edc.usgs.gov/glis/hyper/guide/etopo5, 19 Jan. 2003).

[5] A primitive equation model is one in which approximations are made, such as assuming that the ocean is incompressible, the vertical velocity is small, and small changes in density can be neglected except where they affect the horizontal pressure gradient.

relaxed, representing surface heat and freshwater fluxes. The monthly average ECMWF[6] wind stress climatology was used for the wind forcing, the full strength of which was built up over a two month period to avoid the model being given too much of an initial shock. The first main run of the model finished after 25 years.

An additional experiment was undertaken with the Strait of Gibraltar closed, giving a unique method of defining and investigating MW in the North Atlantic. The model grid in the North Atlantic is at an angle to lines of latitude-longitude, and the OCCAM Med Box formed is the closest possible to the hydrographic Med Boxes given the constraints of the rotated grid (refer to Figure 3.1). A full description of the model setup, including details of the forcing mechanisms and grid configuration, is given in Chapter 6.

[6] European Centre for Medium-Range Weather Forecasts

Chapter Four

Methods

4.1	INTRODUCTION	44
4.2	DATA MANIPULATION	44
4.3	JOINING SECTIONS	45
4.4	EKMAN TRANSPORT	52
4.5	BOTTOM TRIANGLES	53
4.6	HEAT & SALT FLUX CALCULATIONS	54
4.7	NET EVAPORATION	55
4.8	THE BOX INVERSE METHOD	57

4.1 INTRODUCTION

There are many problems to be addressed when dealing with hydrographic data. Initially, a decision has to be made on how to grid the data and how to treat data from different sources. Ekman and geostrophic transports must be computed, the latter needing an initial reference level to determine the absolute velocities. For the resulting flow to satisfy a set of constraints, a correction must be applied to the data. This can be computed using inverse techniques. There is also the problem of bottom triangles, areas below the deepest common level of two adjacent stations, for which the geostrophic velocity is not known. These issues and methods for dealing with them are discussed in this chapter.

The data analysis was accomplished using Pstar (the main data analysis tool used aboard UK research vessels) and Matlab. Pstar is a suite of Fortran programs written by physical oceanographers specifically for handling hydrographic data, and therefore has the advantage of containing programs for calculating oceanographic variables (such as geostrophic velocity and potential temperature).

4.2 DATA MANIPULATION

The 2 db hydrographic CTD data were gridded onto a constant pressure interval grid, from 10 to 5500 db, every 20 db. This is a useful grid to use because most CTD casts are taken to approximately 10 db above the bottom. The individual sections were gridded separately, to enable analysis of north, south and west properties and transports. They were then joined together to form the Med Box, to calculate total volume and salt transports. To keep the notation consistent from the perspective of the Med Box, the data has been gridded in such a way that positive velocities denote transport into, and negative velocities denote transport out of, the Med Box (Figure 4.1). It should be noted that this is contrary to the normal convention for the northern section (41.5°N) where positive velocities usually denote northward transport.

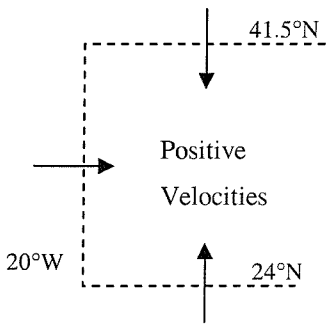

Figure 4.1
Med Box schematic illustrating that positive velocities denote transport into the box.

The calculation of property fluxes, such as the salt flux across a section, requires the use of both salinity and velocity. However, salinity is measured at station positions whereas velocity is calculated between stations. For transport calculations, properties such as salinity have therefore been linearly interpolated onto the velocity positions.

4.3 JOINING SECTIONS

The hydrographic Med Boxes are created using data from three separate sections and thus the issue of crossovers or corner stations must be considered. Unless the sections were sampled concurrently, there is the possibility that the water properties at that location may have changed. How to deal with joining data from different sections is therefore a difficult problem, with authors favouring a variety of methods. The methods range from "allowances were made in contouring" (Wyrtki 1971) to using least squares techniques (Gouretski and Jancke 1999, 2001). Johnson et al. (2001) made linear fits of properties on potential temperature surfaces against distance along the cruise track from the crossover. Their method adjusts the measurements to give internal consistency. It is possible to integrate up to the corner along each section separately, but this would result in a jump in dynamic height and is therefore unsuitable for this study as a dynamically consistent solution is required.

The method used for this thesis is as follows. The deep θ/S properties of the sections were checked to ensure that no systematic errors exist between cruise data sets (described in Chapter 3). The stations closest to each corner were then examined to ensure that they were not sampling an eddy which would bias the result. The two stations at the corner position (one from each section) and four stations close to that position were then used to create a new corner station. Each individual corner (crossover) requires careful consideration. Figure 4.2 shows hydrographic station positions close to the north and south corners (upper and lower rows respectively) of the two hydrographic Med Boxes. In each plot, stations from the zonal section are denoted by dots and those from the meridional section by crosses. The corner station is represented by a white star and the stations used in its creation are circled (listed in Table 4.1).

The section crossovers at the northern corners occur at a seamount, 41.5°N 20°W; a station was made at that position on all four cruises. Defining the Med Box corner stations at this position would create very large bottom triangles. It was therefore decided to move the north-west corners just off this high bathymetry, displacing them 22 km to the east. For both Med Boxes the six stations circled in the upper plots in Figure 4.2 were used rather than those closest to the corner (the initial intention). The close stations to the north and west (oc47 and di11978, fx36 and ch13460)

are in shallower water, so the circled stations were considered to be more representative of waters at the newly defined deeper corner stations. The station in Med Box 88 at 26°W 25.5°N (oc79) was excluded from the creation of the south-west corner station as it sampled a meddy. The station at 26°N (oc78) had similar properties to stations nearer to 24.5°N and so was included in the creation of the corner station despite its distance.

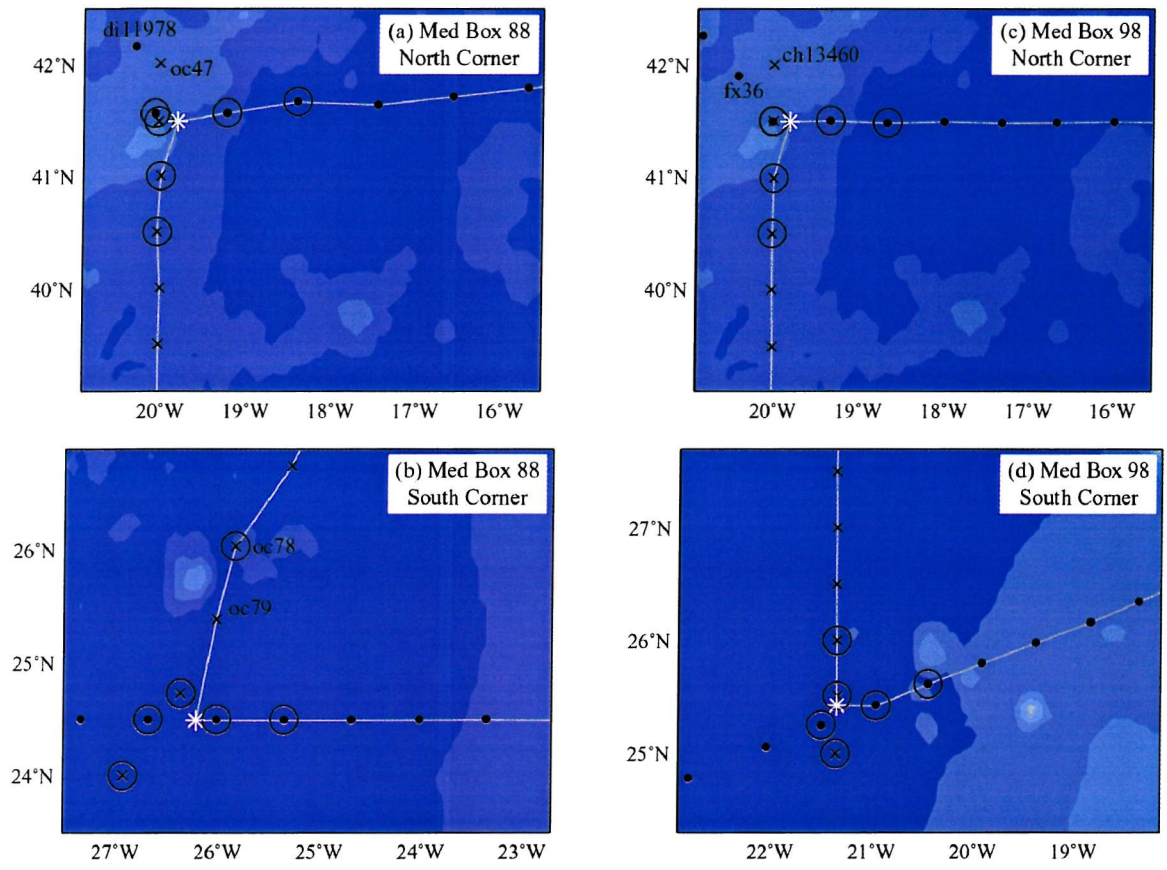

Figure 4.2 *Positions of stations near the corners of Med Box 88 (left) and Med Box 98 (right). Stations from the zonal sections are denoted by dots, and from the meridional sections by crosses. The new corner station is indicated by a white star, and those used to create it are circled. (di = Discovery 189, oc = Oceanus, ch = CHAOS, fx = Fourex)*

The position of each hydrographic Med Box corner and the stations used to create them are detailed in Table 4.1. Isobaric averaging using linear regression was employed to create the corner stations. This method smoothes the transition between the data sets but does not significantly change the actual data. The model was used to calculate properties at the position of each individual station used in the analysis, and the errors were estimated by the rms (root mean square) difference between these modelled values and the original data. The rms differences are detailed in the final columns of Table 4.1, and profiles of the differences are shown in Figure 4.3.

Note that for both boxes, the differences are smaller at the southern corner than the northern corner, possibly due to lower variability. The temperature and salinity differences have similar profiles, but in the north the surface temperature difference is comparatively larger than the salinity

difference. The larger rms differences at mid-depths at the northern corners are due to the influence of MW at some stations and not others. The method can be considered reliable since the magnitude of the errors are typically less than half of the actual differences between adjacent stations. Figure 4.4 shows the geographical positions of the station pairs for each Med Box, and Tables 4.2 and 4.3 detail the station pair positions and the stations making up each pair for the hydrographic and Levitus boxes.

Med Box	Corner	Position	Stations used	rms difference of fit to stations	
				Temperature (°C)	Salinity
88	south	26.20°W 24.50°N	He 20, 21, 22 Oc 78, 80, 81	0.044	0.007
	north	19.80°W 41.50°N	Oc 48, 49, 50 Di 11975-7	0.198	0.032
98	south	21.33°W 25.43°N	Ba 17, 18, 19 Ch 13426-8	0.070	0.014
	north	19.80°W 41.50°N	Ch 13457-9 Fx 33, 34, 35	0.156	0.022

Table 4.1 *Position of each corner station and details of the hydrographic stations used in the model to create the new stations. Also given, for both salinity and temperature, are the mean differences and mean percentage errors between observed and modelled properties for all stations used to create the corner.*

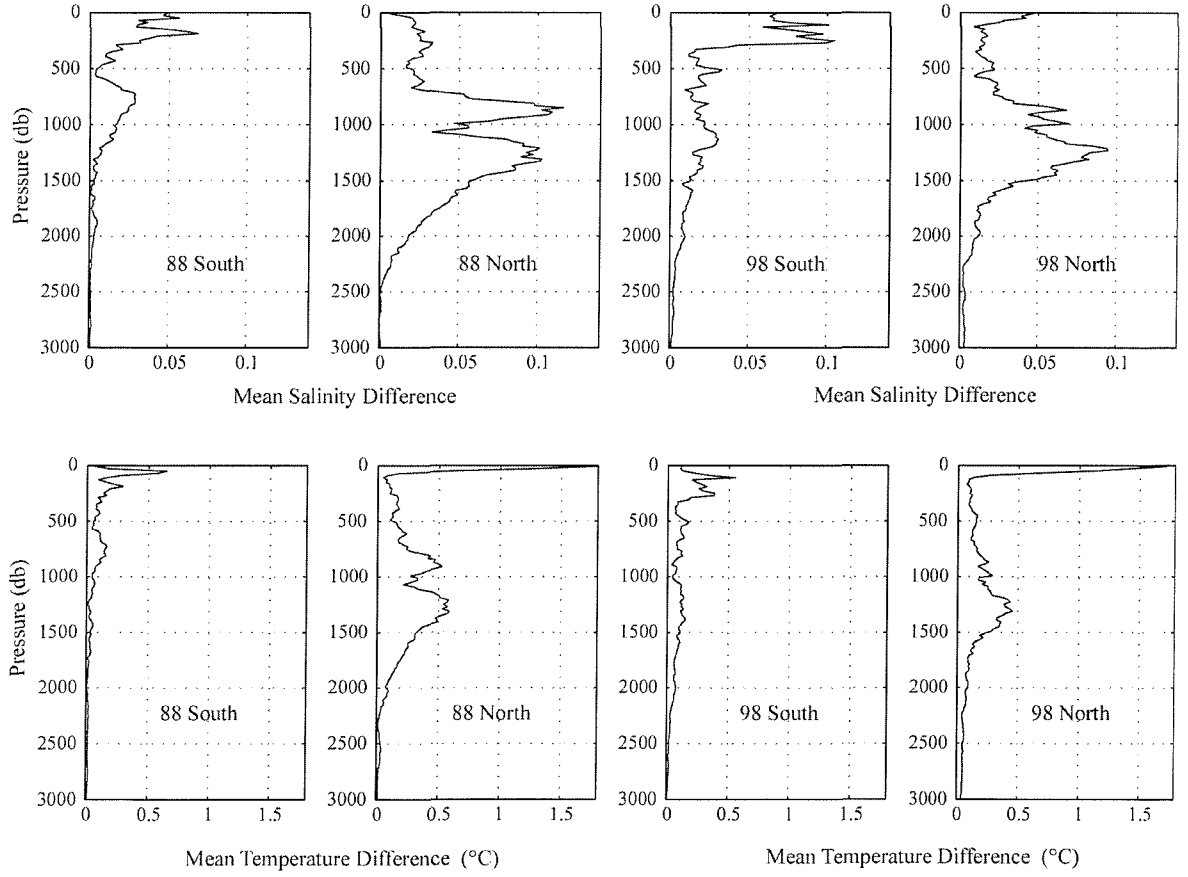

Figure 4.3 *Profiles of mean rms differences between the observed and modelled properties (for all stations used to create the corner station).*

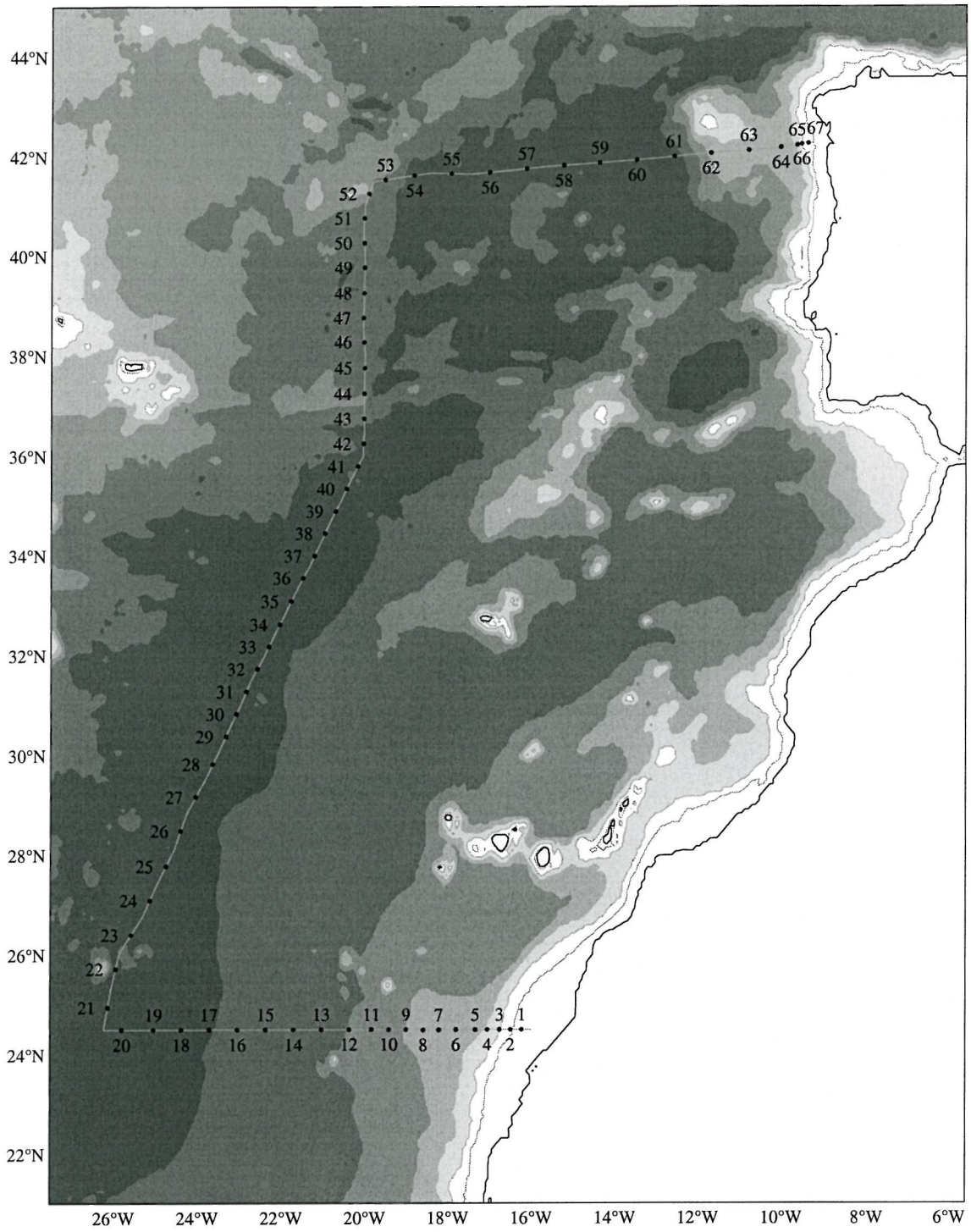

Figure 4.4a Map showing Med Box 88 with superimposed station-pair positions.

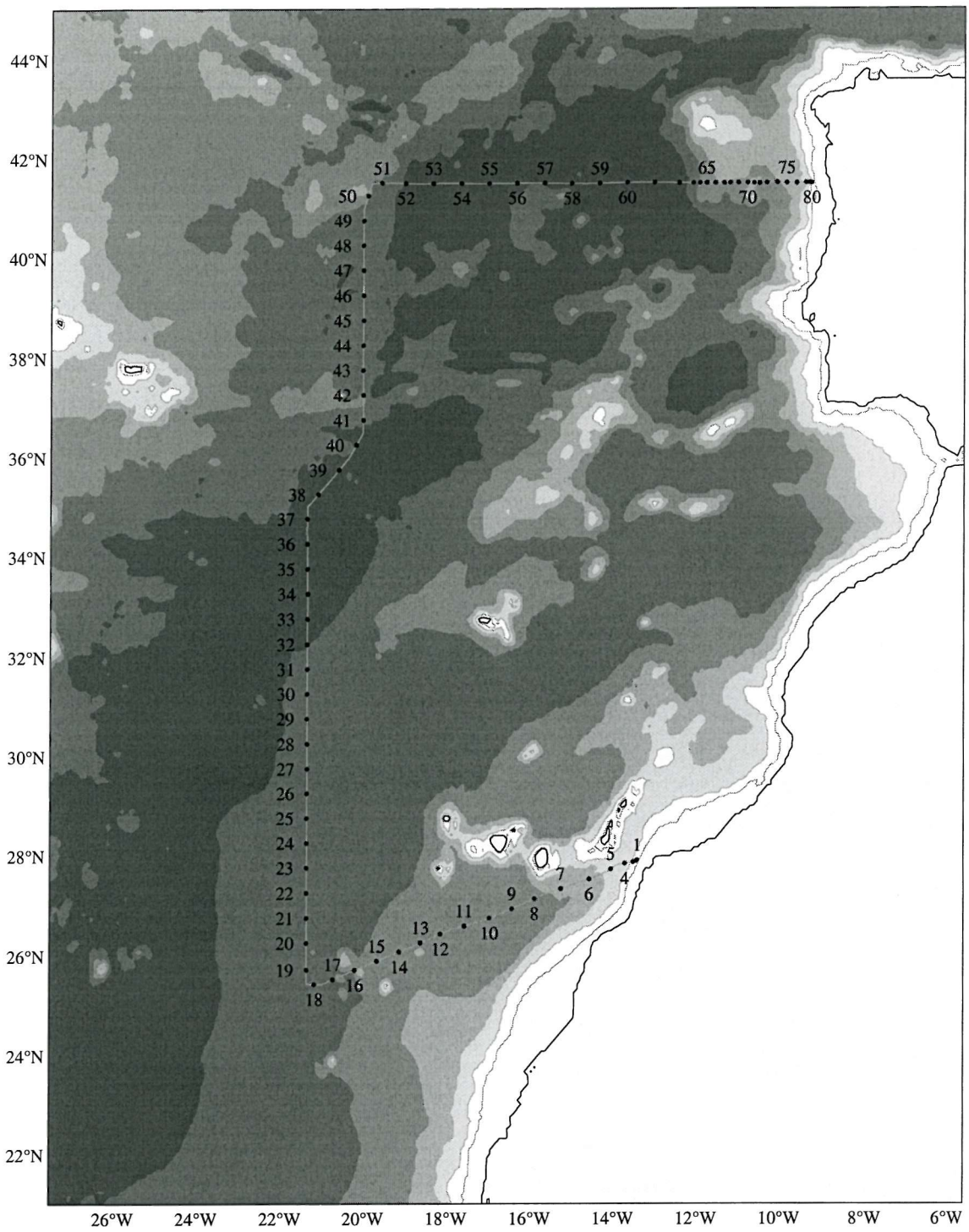

Figure 4.4b Map showing Med Box 98 with superimposed station-pair positions.

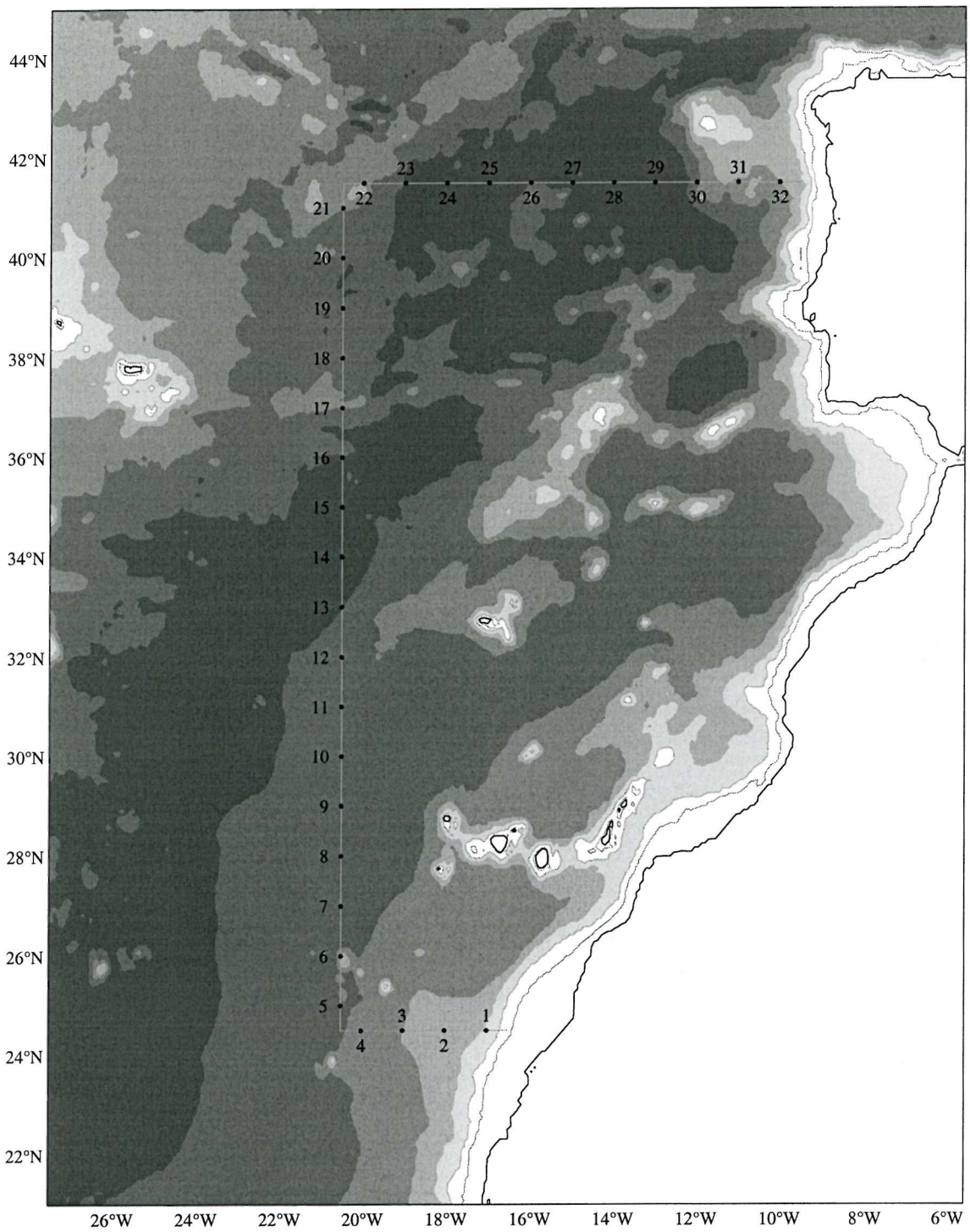

Figure 4.4c Map showing Levitus Med Box with superimposed station-pair positions.

South Section					West Section					North Section				
#	Lon °E	Lat °N	Station Pair		#	Lon °E	Lat °N	Station Pair		#	Lon °E	Lat °N	Station Pair	
1	-16.19	24.50	he001	he002	21	-26.10	24.94	corner1	oc079	53	-19.51	41.54	corner2	di11976
2	-16.45	24.50	he002	he003	22	-25.91	25.71	oc079	oc078	54	-18.81	41.63	di11976	di11975
3	-16.72	24.50	he003	he004	23	-25.55	26.39	oc078	oc077	55	-17.92	41.66	di11975	di11974
4	-17.01	24.50	he004	he005	24	-25.10	27.08	oc077	oc076	56	-17.00	41.69	di11974	di11973
5	-17.30	24.50	he005	he006	25	-24.72	27.77	oc076	oc075	57	-16.12	41.76	di11973	di11972
6	-17.76	24.50	he006	he007	26	-24.36	28.48	oc075	oc074	58	-15.23	41.82	di11972	di11971
7	-18.17	24.49	he007	he008	27	-24.01	29.16	oc074	oc073	59	-14.37	41.88	di11971	di11970
8	-18.54	24.49	he008	he009	28	-23.61	29.82	oc073	oc072	60	-13.48	41.93	di11970	di11969
9	-18.96	24.50	he009	he010	29	-23.29	30.38	oc072	oc071	61	-12.56	42.00	di11969	di11968
10	-19.37	24.50	he010	he011	30	-23.04	30.83	oc071	oc070	62	-11.68	42.07	di11968	di11967
11	-19.79	24.50	he011	he012	31	-22.80	31.27	oc070	oc069	63	-10.78	42.12	di11967	di11966
12	-20.33	24.50	he012	he013	32	-22.55	31.72	oc069	oc068	64	-10.01	42.19	di11966	di11965
13	-21.00	24.50	he013	he014	33	-22.27	32.17	oc068	oc067	65	-9.61	42.23	di11965	di11964
14	-21.66	24.50	he014	he015	34	-22.01	32.61	oc067	oc066	66	-9.50	42.25	di11964	di11963
15	-22.33	24.50	he015	he016	35	-21.74	33.08	oc066	oc065	67	-9.35	42.26	di11963	di11962
16	-23.00	24.50	he016	he017	36	-21.46	33.54	oc065	oc064					
17	-23.67	24.50	he017	he018	37	-21.19	33.99	oc064	oc063					
18	-24.33	24.50	he018	he019	38	-20.94	34.44	oc063	oc062					
19	-25.00	24.50	he019	he020	39	-20.68	34.89	oc062	oc061					
20	-25.77	24.50	he020	corner1	40	-20.42	35.34	oc061	oc060					
					41	-20.15	35.79	oc060	oc059					
					42	-20.01	36.25	oc059	oc058					
					43	-20.01	36.75	oc058	oc057					
					44	-20.01	37.25	oc057	oc056					
					45	-19.99	37.76	oc056	oc055					
					46	-20.01	38.27	oc055	oc054					
					47	-20.03	38.76	oc054	oc053					
					48	-20.01	39.25	oc053	oc052					
					49	-20.00	39.77	oc052	oc051					
					50	-20.01	40.27	oc051	oc050					
					51	-20.01	40.76	oc050	oc049					
					52	-19.90	41.26	oc049	corner2					

South Section					West Section					North Section				
#	Lon °E	Lat °N	Station Pair		#	Lon °E	Lat °N	Station Pair		#	Lon °E	Lat °N	Station Pair	
1	-13.39	27.91	ba001	ba002	19	-21.33	25.72	corner1	ch13428	51	-19.56	41.50	corner2	fx034
2	-13.41	27.89	ba002	ba003	20	-21.33	26.25	ch13428	ch13429	52	-18.99	41.50	fx034	fx033
3	-13.48	27.87	ba003	ba004	21	-21.34	26.75	ch13429	ch13430	53	-18.33	41.49	fx033	fx032
4	-13.68	27.84	ba004	ba005	22	-21.34	27.25	ch13430	ch13431	54	-17.65	41.49	fx032	fx031
5	-14.02	27.73	ba005	ba006	23	-21.34	27.75	ch13431	ch13432	55	-16.99	41.49	fx031	fx030
6	-14.54	27.53	ba006	ba007	24	-21.33	28.25	ch13432	ch13433	56	-16.33	41.50	fx030	fx029
7	-15.22	27.33	ba007	ba008	25	-21.34	28.75	ch13433	ch13434	57	-15.66	41.50	fx029	fx028
8	-15.85	27.13	ba008	ba009	26	-21.33	29.25	ch13434	ch13435	58	-15.01	41.49	fx028	fx027
9	-16.39	26.93	ba009	ba010	27	-21.33	29.74	ch13435	ch13436	59	-14.34	41.49	fx027	fx026
10	-16.93	26.75	ba010	ba011	28	-21.33	30.25	ch13436	ch13437	60	-13.67	41.50	fx026	fx025
11	-17.53	26.59	ba011	ba012	29	-21.34	30.75	ch13437	ch13438	61	-13.01	41.51	fx025	fx024
12	-18.10	26.43	ba012	ba013	30	-21.33	31.25	ch13438	ch13439	62	-12.41	41.50	fx024	fx021
13	-18.57	26.26	ba013	ba014	31	-21.33	31.75	ch13439	ch13440	63	-12.07	41.50	fx021	fx020
14	-19.09	26.07	ba014	ba015	32	-21.33	32.25	ch13440	ch13441	64	-11.91	41.50	fx020	fx019
15	-19.63	25.89	ba015	ba016	33	-21.33	32.75	ch13441	ch13442	65	-11.75	41.50	fx019	fx018
16	-20.17	25.71	ba016	ba017	34	-21.32	33.26	ch13442	ch13443	66	-11.54	41.49	fx018	fx017
17	-20.69	25.52	ba017	ba018	35	-21.33	33.75	ch13443	ch13444	67	-11.33	41.49	fx017	fx016
18	-21.14	25.43	ba018	corner1	36	-21.34	34.26	ch13444	ch13445	68	-11.18	41.50	fx016	fx015
					37	-21.34	34.76	ch13445	ch13446	69	-10.99	41.50	fx015	fx014
					38	-21.08	35.25	ch13446	ch13447	70	-10.77	41.50	fx014	fx013
					39	-20.58	35.75	ch13447	ch13448	71	-10.61	41.50	fx013	fx012
					40	-20.16	36.25	ch13448	ch13449	72	-10.48	41.49	fx012	fx011
					41	-19.99	36.75	ch13449	ch13450	73	-10.31	41.50	fx011	fx010
					42	-20.00	37.26	ch13450	ch13451	74	-10.05	41.50	fx010	fx009
					43	-20.01	37.75	ch13451	ch13452	75	-9.83	41.50	fx009	fx008
					44	-20.00	38.25	ch13452	ch13453	76	-9.59	41.50	fx008	fx007
					45	-20.00	38.75	ch13453	ch13454	77	-9.36	41.50	fx007	fx006
					46	-20.00	39.25	ch13454	ch13455	78	-9.28	41.50	fx006	fx005
					47	-20.00	39.75	ch13455	ch13456	79	-9.25	41.50	fx005	fx004
					48	-20.00	40.25	ch13456	ch13457	80	-9.23	41.50	fx004	fx003
					49	-20.00	40.75	ch13457	ch13458					
					50	-19.90	41.25	ch13458	corner2					

Table 4.2 *Station-pair positions for Med Box 88 (upper table) and Med Box 98 (lower table). Also listed are the stations making up each pair. (he = Hesperides, oc = Oceanus, di = Discovery189, ba = Ronald H. Brown, ch = CHAOS, fx = Fourex).*

South Section			West Section			North Section		
#	Lon °E	Lat °N	#	Lon °E	Lat °N	#	Lon °E	Lat °N
1	-17.0	24.5	5	-20.5	25.0	22	-20.0	41.5
2	-18.0	24.5	6	-20.5	26.0	23	-19.0	41.5
3	-19.0	24.5	7	-20.5	27.0	24	-18.0	41.5
4	-20.0	24.5	8	-20.5	28.0	25	-17.0	41.5
			9	-20.5	29.0	26	-16.0	41.5
			10	-20.5	30.0	27	-15.0	41.5
			11	-20.5	31.0	28	-14.0	41.5
			12	-20.5	32.0	29	-13.0	41.5
			13	-20.5	33.0	30	-12.0	41.5
			14	-20.5	34.0	31	-11.0	41.5
			15	-20.5	35.0	32	-10.0	41.5
			16	-20.5	36.0			
			17	-20.5	37.0			
			18	-20.5	38.0			
			19	-20.5	39.0			
			20	-20.5	40.0			
			21	-20.5	41.0			

Table 4.3
Station-pair positions for the Levitus Med Boxes.

4.4 EKMAN TRANSPORT

A significant contribution to the general ocean circulation is provided by wind driven currents. In this thesis, Ekman transport is estimated using climatological wind stress fields from the SOC global Air-Sea Heat and Momentum Flux Climatology (as reported in Josey et al., 1998):

$$\text{Ekman transport} = -\frac{\tau^x \Delta x}{\rho f}$$

where τ^x is the wind stress along the section, Δx is the distance between stations, f is the Coriolis parameter ($= 2\Omega\sin\phi$) and ρ is density. The wind stress values were projected onto station pair positions to allow the cross-track component of the Ekman transport to be calculated at those positions. The Ekman transport estimates can then be combined with property measurements in order to calculate property fluxes;

$$\text{Ekman salt flux} = \left(-\frac{\tau^x \Delta x}{\rho f}\right) S \qquad \text{Ekman heat flux} = \left(-\frac{\tau^x \Delta x}{\rho f}\right) \theta \rho C_p$$

using the average potential temperature (θ), salinity (S), and density (ρ) over the surface 50 m. The annual average wind stress field was used to calculate estimates of the annual average Ekman transport, which for this thesis is a better representation than monthly or seasonal values because the hydrographic data being used is non-synoptic.

4.5 BOTTOM TRIANGLES

Bottom triangles are a notorious problem. Having calculated geostrophic velocities, which only go as deep as the deepest common temperature and salinity measurements for each station pair, how does one treat the area below this deepest common level if one station is deeper than the other?

Initially, the velocity of the bottom triangle was taken to be the deepest calculated geostrophic velocity. However, this method is likely to over-estimate the transport in the bottom triangle, especially where there is a large difference in the depth of adjacent stations. To make a more accurate estimate, it is assumed that the velocity at the sea bed is zero, with a linear gradient to the deepest calculated geostrophic velocity, v, at the top of the triangle (illustrated schematically in Figure 4.5). Salinity and temperature were estimated using a weighted average of the values below the deepest common level. As discussed above, for data other than the bottom triangles, temperature and salinity were averaged onto the geostrophic velocity positions.

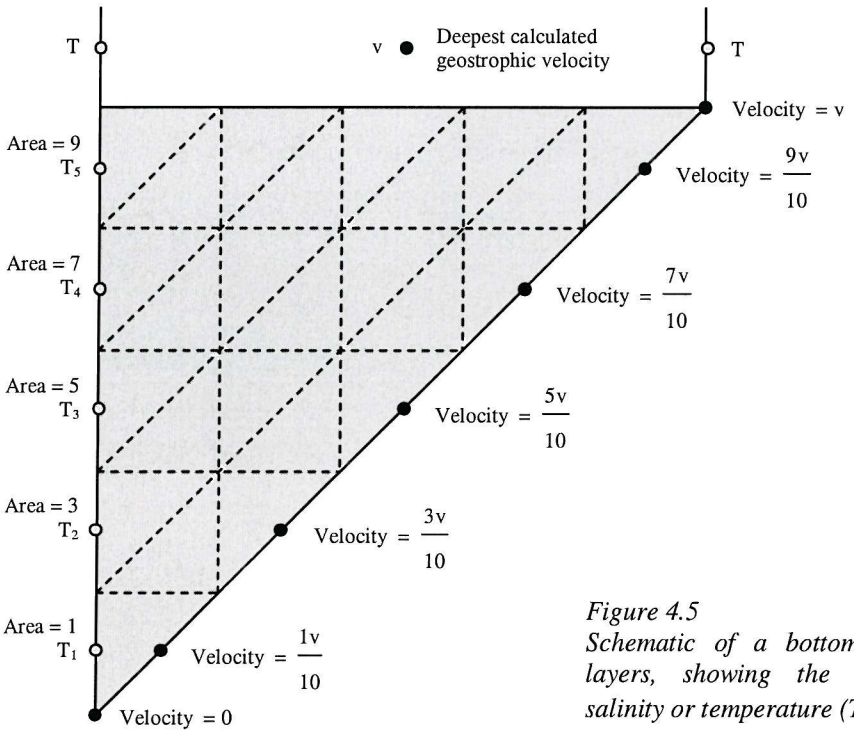

Figure 4.5
Schematic of a bottom triangle with five layers, showing the area, velocity and salinity or temperature (T) for each layer.

Using this scheme, the estimated bottom triangle velocity (v_{bt}) and property (T_{bt}) values are:

$$v_{bt} = \frac{2}{3}v, \qquad T_{bt} = \frac{\sum(\text{Area} \times \text{property})}{\sum \text{Area}}$$

As an example, for the bottom triangle shown in Figure 4.5, the estimated property value is

$$T_{bt} = \frac{(1 \times T_1) + (3 \times T_2) + (5 \times T_3) + (7 \times T_4) + (9 \times T_5)}{(1 + 3 + 5 + 7 + 9)}$$

As the Levitus data has been interpolated onto a 20 db depth grid to match the hydrographic data, this method is also used for the Levitus bottom triangles.

4.6 HEAT & SALT FLUX CALCULATIONS

The heat flux due to ocean currents can strictly only be calculated for an area of ocean where mass is conserved. Since the Med Box encloses an area of the eastern North Atlantic and effectively the entire Mediterranean Sea, mass is conserved and the heat transport out of the box can be calculated by integrating the following equation along the three sides of the Med Box:

$$F_h = \int\int (\rho \, Cp \, \theta \, v) \, dz \, dx$$

where ρ is the density, C_p the specific heat capacity, θ the potential temperature, and v the component of velocity normal to the section. The heat transport out of the Med Box is the result of water flowing out of the box at one temperature and into the box at a lower temperature.

If one wishes to describe the amount of heat transported by a particular current or water mass, for example the Mediterranean Water, then this must be done in terms of temperature fluxes, as mass will not be conserved. Temperature fluxes are the product of the velocity-weighted average temperature and the volume transport, where the velocity-weighted average temperature is calculated by dividing temperature flux by volume transport. It is useful always to give the separate values (temperature and transport) and not just the calculated temperature flux, as this is heavily dependent on the magnitude of the volume transport.

The same is true of salt fluxes. For an area of ocean where mass is conserved, salt flux is given by:

$$F_s = \int\int (S \, v) \, dz \, dx$$

where S is the salinity. Salt fluxes for an area where mass is not conserved are stated as the volume transport for that area multiplied by the velocity-weighted average salinity.

To determine the mechanisms by which heat and salt are being transported across each section, the calculation is broken up into horizontal and vertical components. Velocity, v, potential temperature, θ, and salinity, S, can each be separated into three components:

1.	Section averaged values	$\langle \underline{v} \rangle$	$\langle \underline{\theta} \rangle$	$\langle \underline{S} \rangle$
2.	Horizontally averaged baroclinic values	$\langle v \rangle(z)$	$\langle \theta \rangle(z)$	$\langle S \rangle(z)$
3.	Deviations from horizontal averages	$v'(x,z)$	$\theta'(x,z)$	$S'(x,z)$

where $v = \langle \underline{v} \rangle + \langle v \rangle(z) + v'(x,z)$

$\theta = \langle \underline{\theta} \rangle + \langle \theta \rangle(z) + \theta'(x,z)$

$S = \langle \underline{S} \rangle + \langle S \rangle(z) + S'(x,z)$

The geostrophic heat and salt transport can be split up into 3 corresponding components:

1.	Barotropic salt flux	$\rho \langle \underline{v} \rangle \langle \underline{S} \rangle A$	due to the net transport at the section-averaged salinity or temperature
	Barotropic heat flux	$\rho C_p \langle \underline{v} \rangle \langle \underline{\theta} \rangle A$	
2.	Baroclinic salt flux	$\int \rho \langle v \rangle(z) \langle S \rangle(z) L(z)\, dx$	due to the horizontally averaged overturning circulation[1]
	Baroclinic heat flux	$\int \rho C_p \langle v \rangle(z) \langle \theta \rangle(z) L(z)\, dx$	
3.	Horizontal salt flux	$\iint \rho v' s'\, dx\, dz$	due to the large-scale gyre circulation and smaller scale eddies
	Horizontal heat flux	$\iint \rho C_p v' \theta'\, dx\, dz$	

where L(z) is the width of the section at each depth and A is the total section area. There is no overall mass transport for the baroclinic heat and salt fluxes, and no net mass transport at any depth for the horizontal fluxes. The horizontal fluxes could be separated into a steady time-mean circulation and an eddy contribution if time-series data were available.

4.7 NET EVAPORATION

As the Med Box is not a closed box, but encompasses the Strait of Gibraltar, the net volume flux into the box is not expected to be exactly zero. As discussed in Chapter 2, the Mediterranean Sea is an enclosed Basin, with only the Strait of Gibraltar connecting it to the Atlantic Ocean. There is an excess of evaporation over precipitation and river runoff in the Mediterranean basin, which is

[1] Zonally averaged vertical-meridional circulation for zonal sections, meridionally averaged vertical-zonal circulation for meridional sections.

compensated by a net inflow of water through the Strait (larger Atlantic inflow than Mediterranean outflow) of approximately 0.04 Sv (Bryden et al., 1994). In addition to this, the surface area enclosed by the Med Boxes west of the Strait of Gibraltar is very large, approximately $2x10^6$ km^2, and therefore any net evaporation from this area could contribute a substantial net mass flux into the Med Box.

Precipitation estimates are relatively poor as they rely on subjective observations ('heavy rain', 'fairly light rain' etc.). An empirical formula is then used to convert this into an actual quantity. Satellite measurements of precipitation are also poor. However, in the eastern North Atlantic the evaporation is fairly well known. The precipitation in this region is light due to strong trade winds putting a lid on convection. As precipitation is small compared with evaporation the net evaporation should be a reasonably good estimate.

Two estimates of the annual net evaporation for the Med Box region were made. The first, using maps of evaporation minus precipitation for the North Atlantic constructed by Schmitt, Bogden and Dorman (1989) gives an estimate of 75 $cmyr^{-1}$, which translates to 0.052 and 0.040 Sv for Med Boxes 88 and 98 respectively. The second method uses data from the SOC global Air-Sea Heat and Momentum Flux Climatology (Josey et al., 1998), and gives estimates of 0.051 and 0.036 Sv for Med Boxes 88 and 98 respectively. The expected net mass flux into each Med Box is therefore of the order of 0.09 Sv for Med Box 88 and 0.08 Sv for Med Box 98. These values are shown in Table 4.4.

	Med Box 88	Med Box 98
Area (km^2)	2.2×10^6	1.7×10^6
Net evaporation over Mediterranean Basin (Sv; estimate from Bryden et al.; 1994)	0.04	0.04
Net evaporation over North Atlantic box region (Sv; from 75 cm yr^{-1} estimate from Schmitt, Bogden and Dorman (1989) maps)	0.052	0.040
Net evaporation over North Atlantic box region (Sv; estimate using SOC climatology)	0.051	0.036
Net evaporation (Sv) over region enclosed by Med Box (North Atlantic + Mediterranean Basin) from 2 methods	0.091 to 0.092	0.076 to 0.080

Table 4.4 Net evaporation calculations for the hydrographic Med Boxes.

The salinity of the entire region enclosed by the Med Box is assumed to be constant over time. Therefore the outflow salinity transport must be equal to the inflow salinity transport, and there should be no net salt flux into or out of the Med Box.

4.8 THE BOX INVERSE METHOD

The geostrophic velocity equation gives relative velocities between two levels, so to determine the absolute velocities throughout the water column, the velocity at some level must be known. When no velocity data is available, the classical approach is to assume a level of no motion (a depth where the velocity is zero). If the data spans an ocean basin or is continuous from coast to coast, fluxes can be calculated to check that the resulting flow is reasonable, such that mass, salt and heat are conserved (when appropriate). If for example, the flow does not conserve mass, a correction is needed to satisfy the constraint. The inverse method used here leads to corrections with minimum mean square amplitude (the system departs minimally from the assumed initial state; Bennett, 1992). For the inverse solution to give best results, it is necessary to start close to the true solution.

The absolute geostrophic velocity normal to the line between a station pair is the sum of the geostrophic velocity and the reference level velocity. The box inverse method, pioneered by Wunsch (1978), is a way of finding the unknown reference level velocities. The method uses a set of constraints derived from conservation statements (for either volume or property fluxes) applied to a closed circuit of hydrographic stations.

The problem is set up as a system of linear simultaneous equations

$$\mathbf{E}\,\mathbf{x} = \mathbf{y} \qquad 4.8.1$$

where **E** is an M x N matrix derived from the constraints placed on the system, **x** is the set of unknowns (N x 1), and **-y** is the flux required to ensure conservation (M x 1).

So, for example, if having calculated geostrophic velocity referenced to some arbitrary level, the net mass flux into the box is -2 Sv, then using a single constraint of total mass conservation (for n station pairs):

E is a matrix of areas between each station pair, $[\ A_1\ A_2 \ldots A_n\ ]$

x is the matrix of unknown reference level velocities, $[\ v_1\ v_2 \ldots v_n\ ]'$ and

y = [2]

as Area x velocity = transport. There are often, as in this study, fewer constraints (M) than unknowns (N), so the system is underdetermined. There are an infinite number of solutions which would satisfy the equation, so a solution is chosen which departs minimally from the assumed initial state (**x** is as small as possible). For the present work, the system of constraints were set up

as a matrix equation and solved using the Matlab singular value decomposition (SVD) subroutine. SVD is used as it is ideal for solving linear least-squares problems, especially when they are rank-deficient (Wilkinson and Reinsch, 1971), as this problem is. It allows a solution to be found which has minimum square error and solution length.

The matrix **E** can be decomposed such that

$$\mathbf{E} = \mathbf{U}\mathbf{S}\mathbf{V}^{T} \qquad 4.8.2$$

where **U** (M x q) and **V** (q x N) are orthogonal matrices whose columns are the eigenvectors u_i, v_i (i = 1 to q) and **S** (q x q) is a diagonal matrix whose diagonal elements are the singular values (q is the rank of the matrix).

Re-arranging equations 4.8.1 and 4.8.2 gives

$$\mathbf{x} = \mathbf{E}^{-1}\mathbf{y} \qquad 4.8.3$$

$$\mathbf{E}^{-1} = \mathbf{V}\mathbf{S}^{-1}\mathbf{U}^{T} \qquad 4.8.4$$

The solution vector is therefore given by

$$\mathbf{x} = \mathbf{V}\mathbf{S}^{-1}\mathbf{U}^{T}\mathbf{y} \qquad 4.8.5$$

To avoid each element of the solution vector being scaled by the cross sectional area of its station pair, column weighting is used following Wunsch (1978). Each column of the matrix is normalised by the corresponding station pair area, using $W_{jj}=D_j\Delta x_j$, where D_j is the water depth between station pair j, and Δx_j is the station pair separation.

Equation 4.8.1 is re-written as

$$\mathbf{E}\mathbf{W}^{-1/2}\mathbf{W}^{1/2}\mathbf{x} = \mathbf{y} \quad \text{or} \quad \mathbf{g}\mathbf{m} = \mathbf{y} \qquad 4.8.6$$

where

$$\mathbf{g} = \mathbf{E}\mathbf{W}^{-1/2} \quad \text{and} \qquad 4.8.7$$

$$\mathbf{m} = \mathbf{W}^{1/2}\mathbf{x} \qquad 4.8.8$$

This weighting scheme, if used with net volume flux as the sole constraint, results in the components of **x** being identical. In other words, a uniform velocity correction (equal to the total flux excess divided by total section area) will be applied across the entire box.

Row weighting must also be employed so that each equation is not weighted by the magnitude or range of the property being transported. For example, if mass and salt conservation equations were used, without weighting, the salt conservation could be 35 times more influential on the result than the mass conservation. Row weighting is accomplished by dividing each side of the equation (matrices **E** and **y**) by its row norm, where

$$\text{row norm} = \Sigma_j (e_{ij})^{½} \qquad 4.8.11$$

The problem is better defined the more constraints one can use. The solution will be closer to reality if the problem is more fully determined. The solution vector, which is obtained by the successive addition of eigenvectors, becomes increasingly complex in structure as the smaller singular values are added. There is no objective way of determining the optimum solution. One essentially wishes to choose the solution degree that gives the best compromise between the size of the solution and the size of the residual norm. Details of the exact constraints used for each Med Box along with a discussion of solution degree choice are given in the following chapter.

Chapter Five

Hydrography: Circulation and Fluxes in the Med Box

5.1	INTRODUCTION	61
5.2	DETERMINATION OF THE VELOCITY FIELD	61
	5.2.1 Initial Reference Level	61
	5.2.2 Inverse Model Constraints	62
	5.2.3 Selection of Solution	64
	5.2.4 Assumptions and Limitations	67
5.3	CIRCULATION	68
	5.3.1 Overturning Circulation	68
	5.3.2 Evaporation	70
	5.3.3 The Circulation in Med Box 98	73
	5.3.4 Hydrographic Variability – Med Box 88	77
	5.3.5 Seasonal Variability – Levitus Med Boxes	81
5.4	SALT FLUXES	87
	5.4.1 Med Box Fluxes	87
	5.4.2 Med Water Fluxes	90
5.5	SUMMARY	93

5.1 INTRODUCTION

This chapter describes results from an investigation into circulation and fluxes in the Med Box region. As described in Chapter 3 (Data), there are two hydrographic Med Boxes (88 and 98) and five Levitus Med Boxes (Annual Average, Winter, Spring, Summer and Autumn). Determination of the velocity field using the box inverse method is first described, including the choice of initial reference level, the constraints used in the model, and how the appropriate solution was selected. The circulation of each box is then investigated; the volume transports across each side and the overall overturning of the region. Finally, salt fluxes are calculated, leading onto the results of Mediterranean Water fluxes.

5.2 DETERMINATION OF THE VELOCITY FIELD

5.2.1 Initial Reference Level

The initial reference level used to calculate the absolute geostrophic velocities was $\sigma_3 = 41.49$ kg m^{-3} (where σ_3 is potential density referenced to 3000 db). Where the water column was shallower than this level, the reference velocity was taken to be zero at the bottom. An isopycnic surface was used in preference to an isobaric surface, as most flow in the oceans occurs along isopycnals. The surface chosen was close to a depth of 3200 db (see Figure 5.1) which has been described in the literature as the most reasonable reference level for this region of the North Atlantic. Saunders (1982) stated that for the eastern North Atlantic, 3200 db cannot be distinguished from a shallower reference level given the errors in computing the geostrophic transport. For a number of the Med Boxes, this initial reference level also has the distinct advantage that it results in minimum net volume flux into the box.

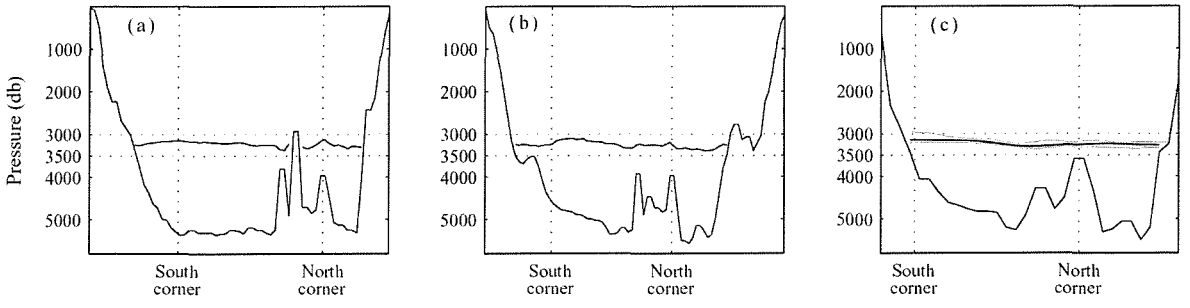

Figure 5.1 *Isopycnal surface $\sigma_3 = 41.49$ kg m^{-3} for (a) Med Box 88, (b) Med Box 98, and (c) Levitus Med Boxes; Annual Average in black, Seasonal in grey.*

5.2.2 Inverse Model Constraints

Having calculated the initial velocities, an inverse model was used to ensure that certain 'known' criteria of the circulation were satisfied. The inverse model uses singular value decomposition to effectively solve an underdetermined linear problem. The formulation of the inverse is described in Chapter 4. The solution is dependent on the starting point, which is why care must be taken in choosing the initial reference level.

The primary model constraint is net mass transport conservation (including Ekman transport), such that there is no net transport into or out of the Med Box. For such mass conservation, there will be a net salt flux across the boundary of the Med Box. This salt flux is related to the amount of net evaporation over the Med Box and Mediterranean Basin, and indeed the amount of net evaporation can be estimated from the net salt flux (evaporation = net salt flux / mean salinity). Alternatively one could use a salt conservation constraint and estimate the net mass transport across the boundaries of the Med Box. This approach has the unfortunate aspect that the net mass transport appears to be a trivially small number. Thus, in this thesis, mass is conserved and salt flux estimated.

For the inverse calculation, the deep water column below 2500 m is divided into six layers separated by appropriate isopycnals, shown in Figure 5.2 and detailed in Table 5.1. One assumption of the model is that there is no mixing across these density surfaces. This assumption is invalid higher in the water column due to the mixing and entrainment of MW within the box boundaries. The six layers were chosen in order to extract as much information as possible from the system. It is recognised that the constraints are approximations with a degree of uncertainty.

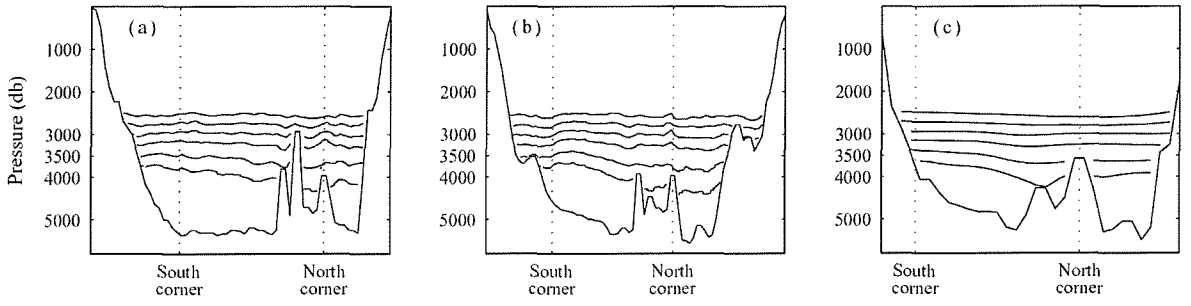

Figure 5.2 *Isopycnal surfaces σ_3 = 41.43 (shallowest), 41.55, 41.475, 41.49, 41.505 and 41.515 (deepest) for Med Boxes (a) 88, (b) 98, and (c) Levitus Annual Average.*

Table 5.1 also shows the number of observations in each layer for each box, the mean layer depth and the mean layer thickness. As the model assumes no diapycnal mixing, Layer 6, the deepest layer, is also the thickest in order to contain any deep mixing in the fracture zones (described in Chapter 3). The mean layer depth only varied by up to 63 m between 1988 and 1998, and the mean

layer thicknesses in layers 1 to 4 are almost identical. Some variability is expected simply due to the different cruise tracks and longer total section length in 1988. The consistency of these results therefore points to a very stable deep water regime. The differences seen in the Levitus data indicate seasonal variability.

Layer	Layer (σ_3) boundaries	Number of Observations		Mean Layer Depth (m)		Mean Layer Thickness (m)	
		88	98	88	98	88	98
1	41.430 - 41.455	576	724	2657	2680	193	193
2	41.455 - 41.475	581	737	2876	2903	199	207
3	41.475 - 41.490	587	720	3110	3135	215	209
4	41.490 - 41.505	917	1092	3425	3462	356	357
5	41.505 - 41.515	890	959	3822	3885	351	329
6	41.515 - bottom	2366	2079	4573	4538	1080	905

Layer	Number of Observations					Mean Layer Depth (m)					Mean Layer Thickness (m)				
	av	win	spr	sum	aut	av	win	spr	sum	aut	av	win	spr	sum	aut
1	301	288	300	323	307	2651	2611	2660	2684	2661	191	182	191	207	196
2	311	287	306	339	309	2870	2814	2875	2920	2883	199	182	195	218	197
3	335	326	328	325	342	3108	3042	3112	3167	3122	224	209	219	217	229
4	440	426	464	425	482	3407	3320	3424	3465	3464	313	291	319	302	410
5	389	321	509	430	485	3763	3592	3883	3867	3910	312	253	415	347	415
6	980	1163	839	878	821	4429	4346	4466	4466	4467	856	1019	842	800	917

Table 5.1 *Details of the layers chosen for the inverse model, along with the number of observations in each layer, the mean layer depth and the mean layer thickness for each of the Hydrographic Med Boxes (upper table) and Levitus Med Boxes (lower table); Annual Average (av), Winter (win), Spring (spr), Summer (sum) and Autumn (aut).*

The model requires volume, salt anomaly and temperature transport conservation in the deep layers, as listed in Table 5.2. Conservation equations are written for salinity anomaly rather then salinity as it has been found that for tracers that have small variations about a large mean value, the use of anomalies reduces the sensitivity of the inversion to errors (McDougall, 1991). McIntosh and Rintoul (1997) found that it is unimportant for the reference salinity to be exactly equal to the mean value of salinity. For this study salinity anomaly was calculated as salinity minus 34.8.

Constraint number	Constraint description
1	Full water column volume flux balance
2 - 7	Layers 1 to 6 volume flux balance
8 - 13	Layers 1 to 6 salt anomaly flux balance
14 - 19	Layers 1 to 6 temperature flux balance

Table 5.2

Details of the constraints used in the inverse model.

As outlined in Chapter 4, the inverse undertakes both column and row weighting of the constraints. The row weighting scales each equation by its row norm, whilst the column weighting scales each element by the square root of the corresponding station pair area. The advantage of this choice of column weighting is that it yields transports that are unaffected by the number or location of stations (Veronis, 1987). It also results in more of the correction occurring in the shallow stations.

5.2.3 Selection of Solution

The inverse is set up as an underdetermined problem with many possible solutions. The method used here chooses a solution with minimum square length. Solving for all the constraints exactly can lead to an unrealistic circulation pattern by magnifying the errors and producing a set of variable and high reference velocities. It is necessary therefore to choose a preferred solution degree. A higher solution degree means that the system is closer to its solution but at the cost of becoming increasingly noisy. It is therefore desirable to truncate the solution to exclude the very noisy highest degrees (for example Joyce et al., 1986; Mercier et al., 1993). There is no objective method of determining the preferred solution degree. Certain tests can, however, be employed to determine the optimum, which balances the requirements of satisfying the constraints as closely as possible whilst introducing as little noise as possible into the solution.

A simple test is to examine the relative magnitude of the eigenvalues and choose a solution degree just before a sharp decrease in their size. An example of this is shown in Figure 5.3a for Med Box 88, and there is an obvious cut-off at solution degree 7, after which the eigenvalues are at least an order of magnitude smaller.

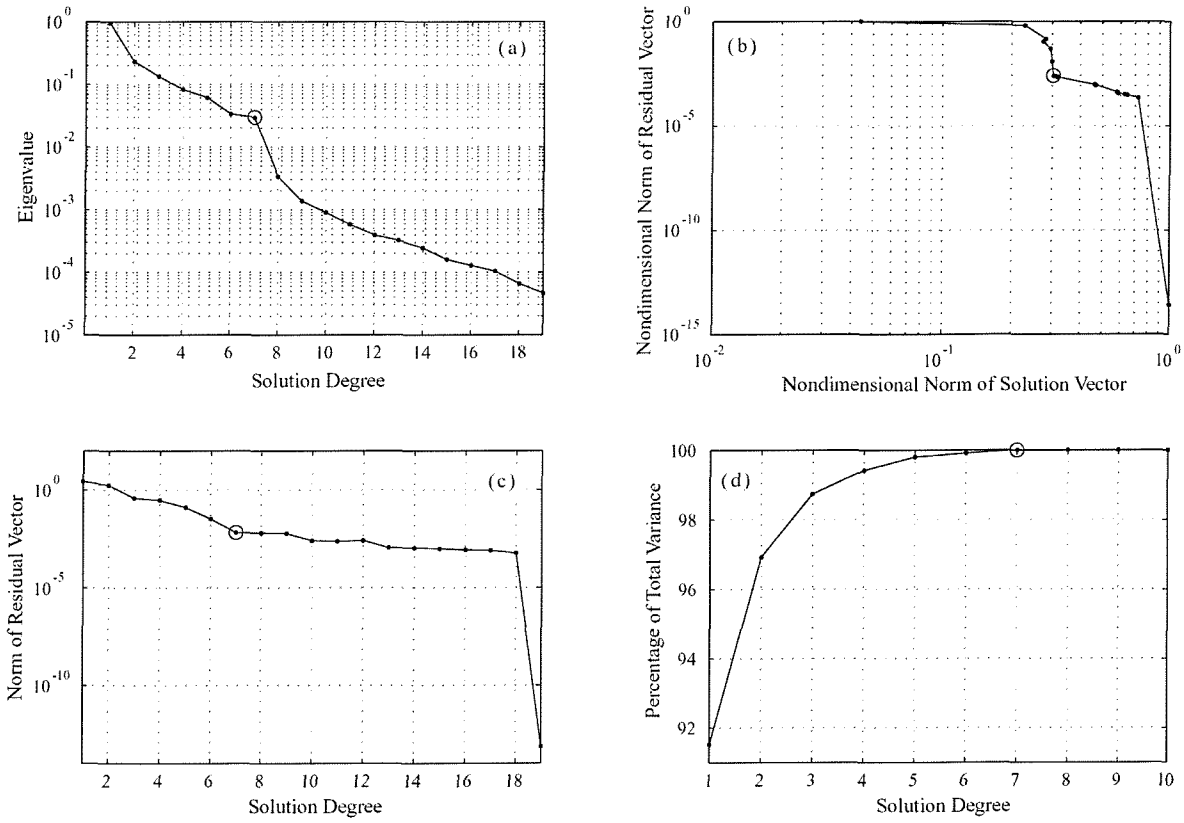

Figure 5.3 *Med Box 88; (a) size of eigenvalue versus solution degree, (b) nondimensional norm of solution vector versus nondimensional norm of residual vector, (c) norm of residual vector versus solution degree, and (d) percentage of total variance versus solution degree*

Another method is the Levenburg - Marquardt analysis (Lawson & Anson, 1974) where solution magnitude is plotted against solution residual magnitude for each solution degree (Figure 5.3b). As more information is added to the system, the solution vector increases, accompanied by a decrease of the residual vector (as the solution satisfies the constraints more closely). The preferred solution degree reaches some acceptable compromise between the magnitude of the residual and solution vectors. For Med Box 88, solution degree 7 occurs after a sharp drop in the residual vector. After solution degree 7 the solution becomes noisier with no significant reduction in residual magnitude.

The norm of the residual vector changes with solution degree (Figure 5.3c). Solution degree 7 can again be highlighted as a turning point between fast and slow decrease of the residual. Another approach is to calculate the contribution of each eigenvector to the answer, revealing how much of the variance is explained by each mode. Plotting the cumulative sum of the percentage of total variance versus solution degree (Figure 5.3d) shows for Med Box 88 that virtually 100% of the total variance is explained by solution degree 7. After this point the eigenvectors add noise and do not contribute significantly to the solution.

These tests indicate solution degree 7 as the optimal choice for Med Box 88. Similar results are found for the other Med Boxes. For each constraint, the residual generally decreases with increasing solution degree (not shown). The first few solution degrees result in some constraints having extremely large residuals. Using solution degree 7 the first constraint (of net volume flux conservation) is satisfied, and most of the other constraints have acceptable residuals, with none exceeding 30% of the required solution. This is true of all the Med Boxes, with the exception that for two of the seasonal Levitus Med Boxes, solution degree 7 resulted in a small net volume flux (~0.0006 Sv). In these cases a small barotropic velocity was added to the entire dataset so that volume flux was conserved. It must be remembered that these tests estimate the agreement of the solution with the basic assumptions, rather than proving the validity of the assumptions themselves.

Figure 5.4 illustrates the difference in magnitude and variability of the barotropic velocities obtained from use of different solution degrees (1, 2, 7 and 19) for the hydrographic and Levitus Annual Average Med Boxes. In all cases, the higher the solution degree, the 'noisier' the resulting velocities (in other words, the structure becomes increasingly complex as smaller eigenvalues are added). The general tendency of the first eigenvector correction (of order -0.01 cm s^{-1}; green line in Figure 5.4) is to spread the total imbalance over all stations. For both Med Boxes 88 and Levitus, solution degree 7 is not significantly noisier than solution degree 2. Solution degree 7 was chosen for all Med Boxes, and the mean values of the final barotropic corrections for each box are given in Table 5.3.

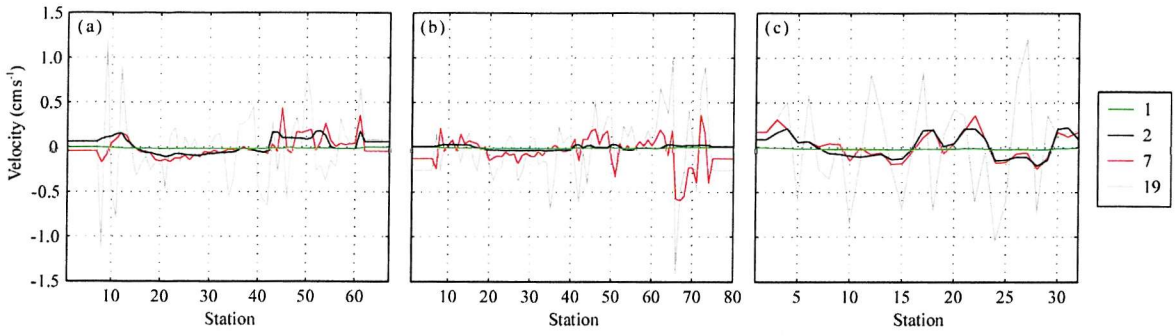

Figure 5.4 *Barotropic corrections (cm s^{-1}) obtained from the inverse model for solution degrees 1 (green), 2 (black), 7 (red; the selected solution) and 19 (thin grey) for (a) Med Box 88, (b) Med Box 98, and (c) the Annual Average Levitus Med Box.*

Med Box	Barotropic Corrections	
	mean (cm s^{-1})	std (cm s^{-1})
88	-0.012	0.115
98	-0.054	0.171
Levitus Ann. Av.	0.027	0.152
Levitus Winter	0.077	0.297
Levitus Spring	0.010	0.174
Levitus Summer	-0.014	0.165
Levitus Autumn	0.035	0.208

Table 5.3

Mean and standard deviation of barotropic corrections (cm s^{-1}) for each Med Box obtained from the inverse model, solution degree 7.

It can be informative to look at how certain results vary with solution degree, and this is how some authors choose which solution to use, or at least to support their choice (for example Tsimplis et al., 1998). Figure 5.5 shows how the net transport into Med Box 98, and across each of its sides individually, varies with the inverse solution degree used. Solution degree 4 conserves transport for the box as a whole, but the net transport across individual sides varies with increasing solution degree, highlighting that the choice of solution degree will affect the circulation results.

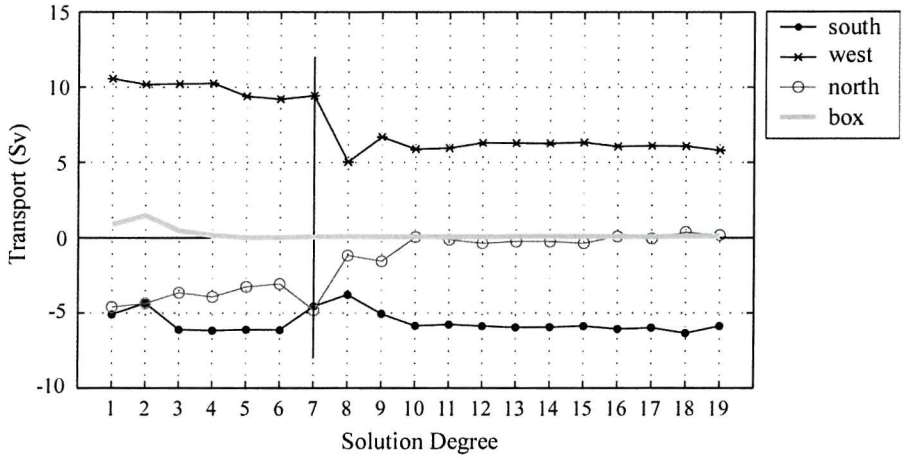

Figure 5.5 *Variability of net transports (Sv) with solution degree for Med Box 98.*

The solution applies a barotropic correction throughout the water column, and its influence can be seen clearly in the net transport profiles resulting from the use of each solution degree (Figure 5.6). The net box profile (Figure 5.6d) varies only slightly, but it can be seen that there are almost two separate sets of solutions for the north and west sides (Figure 5.6b and c). When a solution degree higher than 7 is used, the surface inflow to the box across the west decreases (~1 Sv), the deeper outflow increases (~2 Sv), and to compensate this the deeper inflow from the north also increases (~3 Sv).

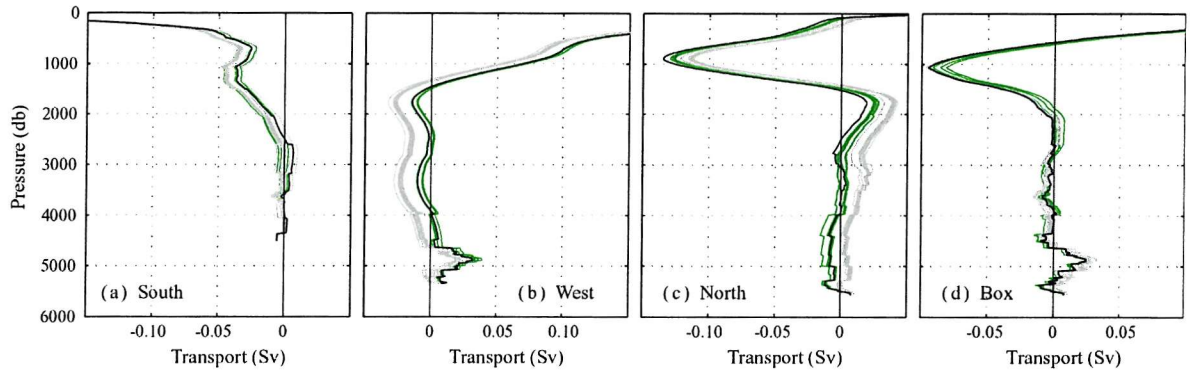

Figure 5.6 *Transport profiles for each side of Med Box 98 and the box as a whole obtained using different solution degrees. Solution degrees 1 to 6 in green, 8 to 19 in light grey and 7 (the chosen solution) in black.*

5.2.4 Assumptions and Limitations

The inverse calculation makes a number of assumptions, which include no significant cross-isopycnal mixing in the deep layers and that the ocean is in geostrophic balance. It is also assumed that instantaneous hydrographic sections represent the long-term mean flows, which, although open to question, allows an investigation of the problem to be made using inverse methods in the absence of truly synoptic measurements.

The use of inverse methods to determine the large scale circulation has a major limitation in regions of strong barotropic flow, for example on the offshore continental slope. The use of direct Acoustic Doppler Current Profiler (ADCP) velocity measurements from detailed near-shore surveys can improve our estimate of the circulation in such regions, however, measurement errors can be of the same order of magnitude as the currents measured.

Inverse methods provide a solution that departs minimally from the initial state; the solution therefore critically depends on a reasonable first guess approximation. This can be hard to achieve without the inclusion of further measurements, for example ADCP or float velocities. Because of the lack of ADCP velocities on most of the cruises used here, it has not been possible to improve the initial guess with direct observations.

5.3 CIRCULATION

5.3.1 Overturning Circulation

The general circulation of this region of the North Atlantic produces an overturning circulation within the Med Box region. Figure 5.7 shows profiles of total transport for each box, and as is immediately obvious, they all have very similar characteristics; water enters the box at the surface and exits at mid-depths. For Med Box 98 for example, there is a 3.6 Sv inflow of surface waters in the top 560 m, whilst the main return flow occurs between 560 and 2000 m.

The overturning circulation is due to water mass conversion resulting from the entrainment of Atlantic waters into the outflowing MW, and also to the fact that surface waters flow into the Mediterranean whilst the outflow is at intermediate depths. The circulation data reveal a new hydrographic estimate of this water mass conversion.

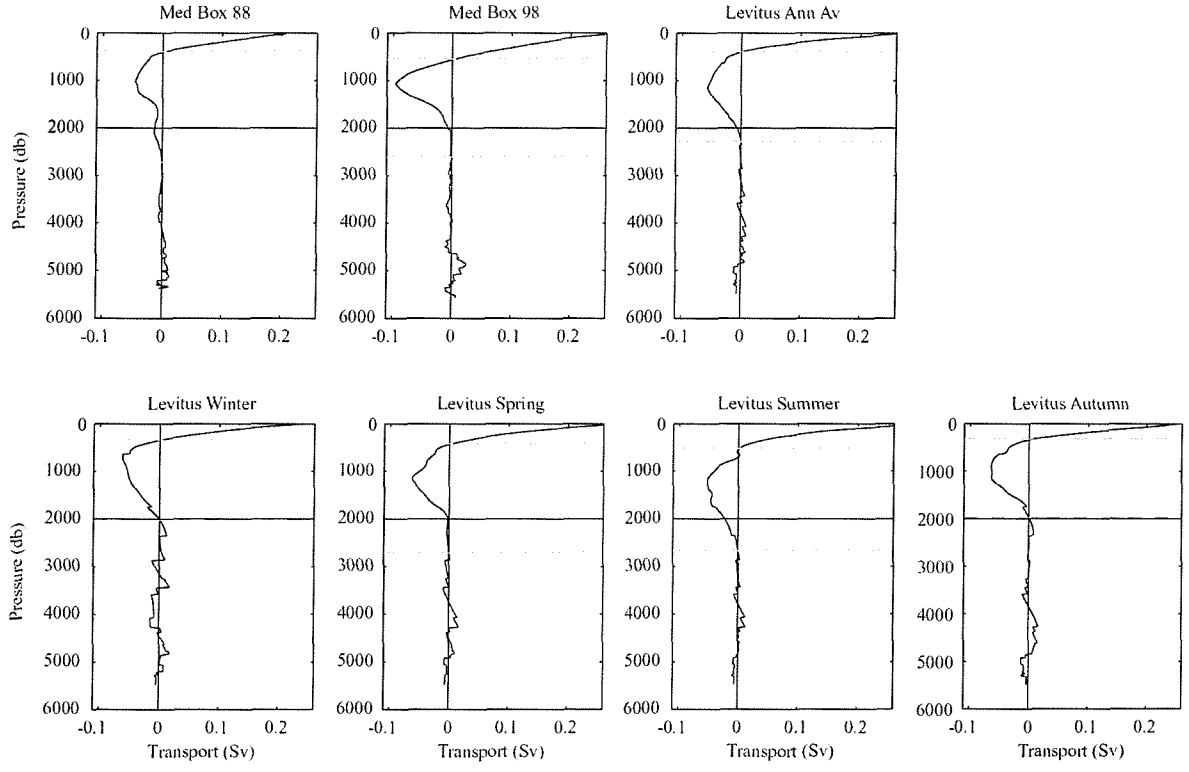

Figure 5.7 *Profiles of total transport for each Med Box. The grey dashed lines indicate the first two zero-crossings (the bottom of the inflowing surface layer and the bottom of the outflowing mid-depth layer). The black line indicates 2000 m. Positive transports represent flux into the box.*

The magnitudes of the surface inflow and mid-depth outflow are given in Table 5.4. The dashed grey lines on each plot in Figure 5.7 indicate the depths of the inflowing surface water and the intermediate outflow, whilst the black line indicates 2000 m. These are the depths listed in

Table 5.4. In two of the Med Boxes (Levitus Winter and Autumn), the base of the outflow is at 2000 m. In the Levitus Annual Average box, it is just below 2000 m at 2277 m (net flow between 2000 and 2277 m is 0.03 Sv which is just 1% of the net outflow). In Med Box 98, the outflow occurs to a depth of 2600 m, but it can be seen that there is very little flow between 2000 and 2600 m (-0.06 Sv; 1.7% of net outflow), and thus it is perfectly reasonable to take 2000 m as the maximum depth of the outflow. The same is true of Levitus Spring, where again the maximum depth of the outflow is 2704 m, but the net transport between 2000 and 2700 is only -0.08 Sv (3% of net outflow). The only two boxes which have significant outflow below 2000 m are Med Boxes 88 and Levitus Summer. These two have outflows to depths of 2700 m (–0.23 Sv; 10% of the net outflow) and 2664 m (–0.3 Sv; 11% of the net outflow) respectively, where the numbers in brackets indicate the net flow between 2000 m and the given depth.

Med Box	Surface Inflow		Mid-depth Outflow to 2000 m		Mid-depth Outflow	
	depth (m)	transport (Sv)	depth (m)	transport (Sv)	depth (m)	transport (Sv)
88	400	2.13	2000	-2.01	2700	-2.24
98	560	3.58	2000	-3.48	2600	-3.54
Levitus Annual Average	413	2.08	2000	-2.76	2277	-2.79
Levitus Winter	353	1.63	2000	-3.08	2013	-3.08
Levitus Spring	433	2.30	2000	-2.69	2704	-2.77
Levitus Summer	534	2.59	2000	-2.48	2664	-2.78
Levitus Autumn	332	1.86	2000	-3.05	1972	-3.05

Table 5.4 *Net transport calculations of the surface inflow (and its depth), and the mid-depth outflow to both 2000 m and its maximum depth for each Med Box. The surface inflow represents the magnitude of the overturning circulation (Sv).*

In general, given all seven Med Boxes, the magnitude of the overturning circulation is 2.3 ± 0.6 Sv (one standard deviation), and the depth of the surface inflow is 432 ± 86 m. The intermediate outflow to 2000 m is –2.8 ± 0.5 Sv, and to the maximum calculated depth is -2.9 ± 0.4 Sv. The maximum depth of the outflow can therefore be taken to be 2000 m. These results show that this is a very robust feature of the circulation.

Transports from Table 5.4 are plotted in Figure 5.8. Both hydrographic Med Boxes have a surface inflow of comparable size to their mid-depth outflow. This is not always the case for the Levitus data, which actually appear to have the relationship that as the inflow increases in size, the outflow decreases. Looking at the Levitus data points in Figure 5.8a, it appears that there may be a seasonal signal in the overturning, with the smallest value occurring in the winter (1.6 Sv), increasing to a maximum in the summer (2.6 Sv). The Med Box 88 value is almost identical to the Annual Average Levitus value, whilst Med Box 98 has an overturning magnitude 1 Sv greater than any of the others.

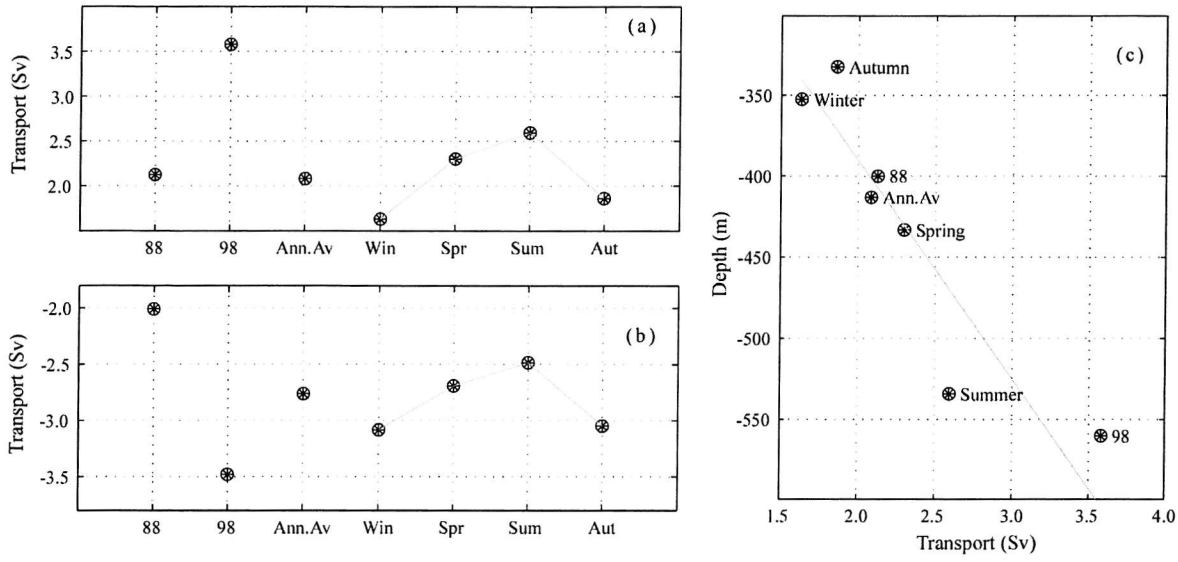

Figure 5.8 *(a) Surface inflow, (b) mid-depth outflow, and (c) surface inflow versus depth of the inflow (regression line plotted in grey; r^2 = 0.83) for each Med Box (Levitus Med Boxes: Ann.Av = Annual Average, Win = Winter, Spr = Spring, Sum = Summer, Aut = Autumn).*

There is a positive correlation ($r^2 = 0.83$) between the strength of the overturning circulation and the depth of the inflowing surface layer (as shown in Figure 5.8c). This coincides with the logical assumption that for the overturning circulation to become stronger, either the flow in the different layers has to increase in speed or the depth of the inflowing layer must increase, or a combination of these.

The following sections investigate the circulation of each individual Med Box to discover how this consistent overturning circulation pattern is formed.

5.3.2 Evaporation

The net evaporation (evaporation minus precipitation) was calculated for the Med Boxes and the Mediterranean Sea using the SOC Global Air-Sea Heat and Momentum Flux Climatology (Josey et al., 1998) as explained in Chapter 4. Figure 5.9(a) to (d) shows the monthly values of each of these fields and their annual averages (dashed lines) for each Med Box. As would be expected, the three Med Boxes have very similar values as they cover much the same area.

The evaporation is much higher than the precipitation for this region of the north east Atlantic, resulting in a positive net evaporation over the area of the box. The annual average net evaporation is 0.051 Sv, 0.036 Sv, and 0.042 Sv for Med Boxes 88, 98 and Levitus respectively. The range over the year is 0.042 - 0.062 Sv, 0.026 - 0.043 Sv, and 0.032 - 0.050 Sv for each box. The difference in values reflects the different Med Box surface areas (2.2×10^6 km^2, 1.7×10^6 km^2, 2.0×10^6 km^2).

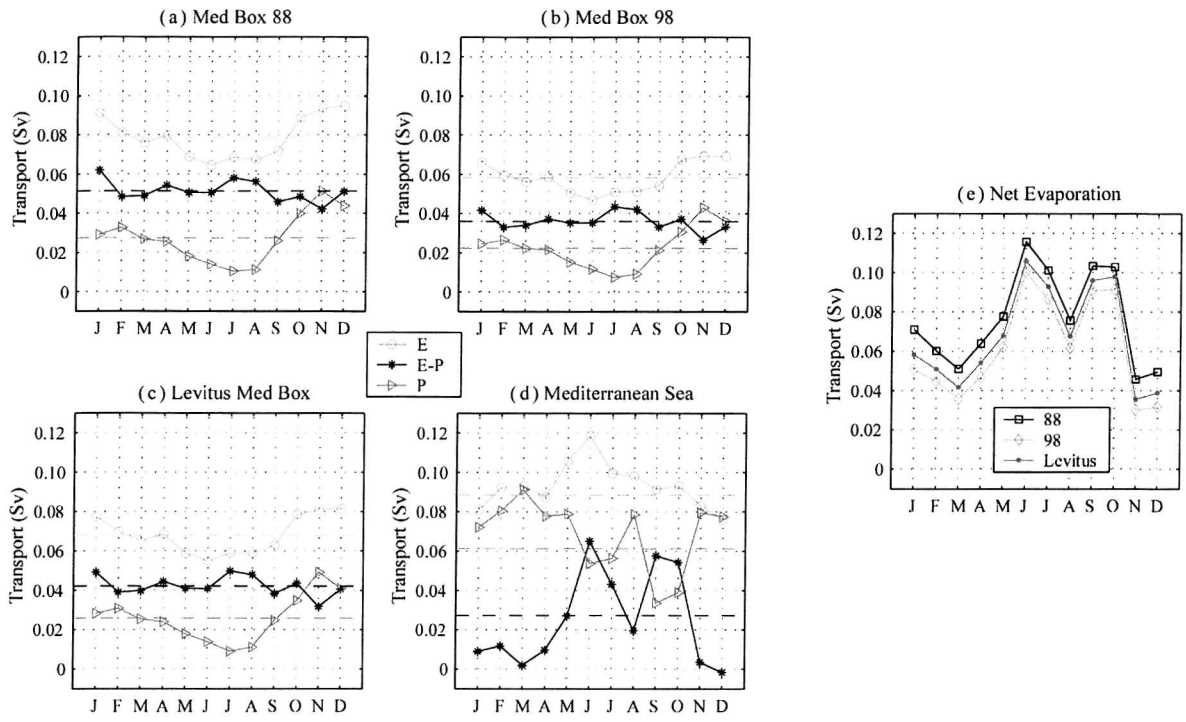

Figure 5.9 *Evaporation (E), precipitation (P) and net evaporation (E-P) calculated using the SOC global Air-Sea Heat and Momentum Flux Climatology (Josey et al., 1998) for (a) Med Box 88, (b) Med Box 98, (c) Levitus Med Box, and (d) the Mediterranean Sea. (e) Net evaporation (over Med Box region + Mediterranean Sea) for the three boxes.*

The values of evaporation and precipitation over the Mediterranean Sea show quite a different pattern to those over the Atlantic Med Box regions (Figure 5.9d). Throughout most of the year there is an excess of evaporation over precipitation, although in December there is actually higher precipitation. Summer has the highest evaporation and lowest precipitation except for an unexpected increase in precipitation in the month of August. This leads to a variable net evaporation with a mean of 0.027 Sv and a range of –0.002 to 0.065 Sv. The annual average value obtained from the SOC climatology compares favourably with the estimate of 0.04 Sv obtained by Bryden et al. (1994).

Given that the Med Boxes effectively enclose the Mediterranean Basin (as the Strait of Gibraltar is open and there is no eastern section to the box), the net evaporation within each box is the sum of the net evaporation over the box surface area and the Mediterranean Sea surface area (shown in Figure 5.9e). This gives mean values of 0.076 Sv, 0.061 Sv, and 0.067 Sv for Med Box 88, 98 and Levitus respectively. These values of net evaporation can be compared with those calculated using the hydrographic data.

There is positive net evaporation over the area encompassed by the Med Box which must be compensated by a net flow into the box. Using the inverse calculation, the net transport into the box was set to zero such that it is possible to use the calculation of the net salt flux out of the box to

estimate an 'effective fresh water transport' (net salt flux divided by mean box salinity). These values are shown in Table 5.5 and Figure 5.10. Each box has a negative salt flux as expected, producing an effective fresh water transport into the box.

Med Box	Salt Flux (Sv psu)	Mean Salinity	Effective Fresh Water Transport (Sv)
88	-2.503	35.218	0.0711
98	-2.241	35.232	0.0636
Levitus Ann Av	-1.512	35.239	0.0429
Levitus Winter	-1.991	35.243	0.0565
Levitus Spring	-0.539	35.237	0.0153
Levitus Summer	-1.060	35.235	0.0301
Levitus Autumn	-2.777	35.241	0.0788

Table 5.5 *Calculation of effective fresh water transport (Sv) for each Med Box, from net salt flux (Sv psu) and mean salinity. These values are shown pictorially in Figure 5.10. Negative salt flux values indicate that the circulation carries saltier water out of the box.*

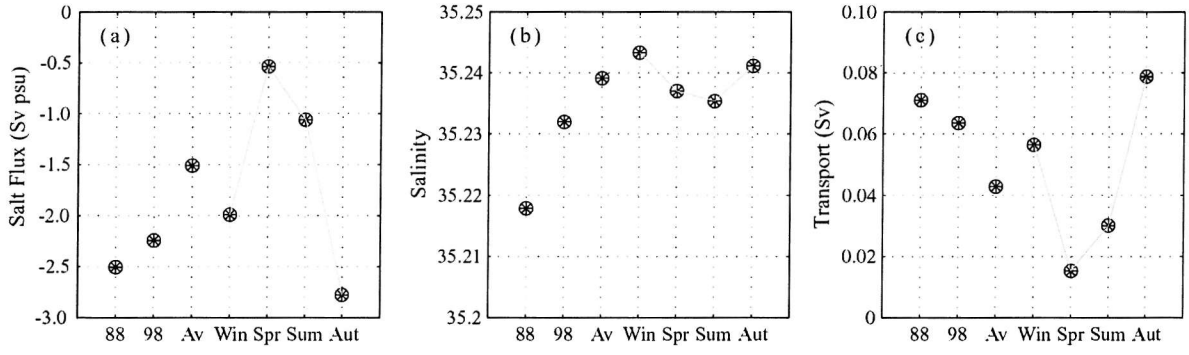

Figure 5.10 *(a) Net salt flux, (b) mean salinity, and (c) effective fresh water transport for each Med Box. (Levitus Med Boxes: Av = Annual Average, Win = Winter, Spr = Spring, Sum = Summer, Aut = Autumn).*

The hydrographic Med Box values for the net freshwater inflow (88: 0.071 Sv, 98: 0.064 Sv) are in remarkably good agreement with the values of net evaporation (88: 0.077 Sv, 98: 0.061 Sv), suggesting that the net circulation regimes and SOC climatology are close to reality. The Levitus values are reasonably close (within ~0.01 Sv) to the net evaporation total of 0.067 Sv for Autumn and Winter (0.078 and 0.057 Sv respectively), but are a little low in Spring and Summer (0.015 and 0.030 Sv). Curiously, the effective fresh water transport into the box is lowest in Spring and Summer, opposite to what would be expected from the seasonal evaporation cycle unless there is a time lag in the response.

5.3.3 The Circulation in Med Box 98

This section considers the circulation in the 90's, using Med Box 98. The following sections will consider the variability of the circulation by analysing the other hydrographic (88) and Levitus Med Boxes (Annual Average and Seasonal). In Section 5.3.1, the overall overturning circulation of the Med Box region was quantified. The next step is to determine the components of this net box circulation by looking at each individual section.

It is advantageous to start any investigation by examining the water properties found in the area of study. The θ/S curve is a useful tool for this purpose, and is shown in Figure 5.11 for Med Box 98, with data from each individual section highlighted. The change in the water properties between sections can be seen clearly. The southern section has a tighter θ/S relationship than the other two sides which contain more water masses. The influence of warm and saline MW is apparent on part of the western section, and on the entire northern section which has the highest salinities and temperatures (for subsurface waters). There is effectively no MW signal on the southern boundary. There is a discontinuity between the west and the north sections for waters above 15°C; the western edge is missing the gradation of salinities towards those values seen in the north. This may be explained by the non-synopticity of the sections, which will have a greater effect on surface waters due to atmospheric influences.

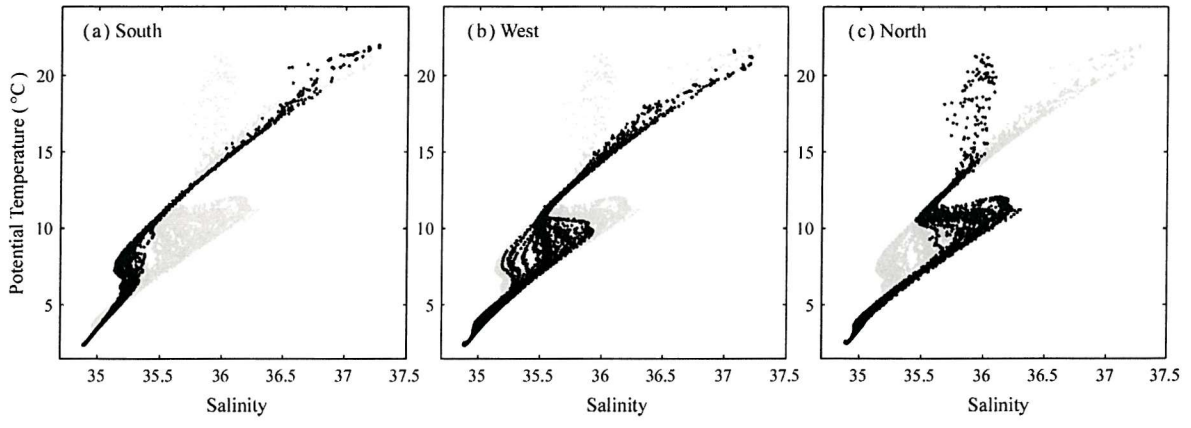

Figure 5.11 θ/S plots for Med Box 98; data for the whole box is shown in each plot in grey, while specific data (as detailed) is shown in black, (a) south, (b) west, and (c) north.

Mean profiles of potential temperature and salinity and profiles of total transport for each section are shown in Figure 5.12 and Figure 5.13. The same profiles are shown in both figures, but Figure 5.12 groups them by section highlighting relationships between different properties at particular depths, whilst Figure 5.13 groups the profiles by type, allowing direct comparison between sections.

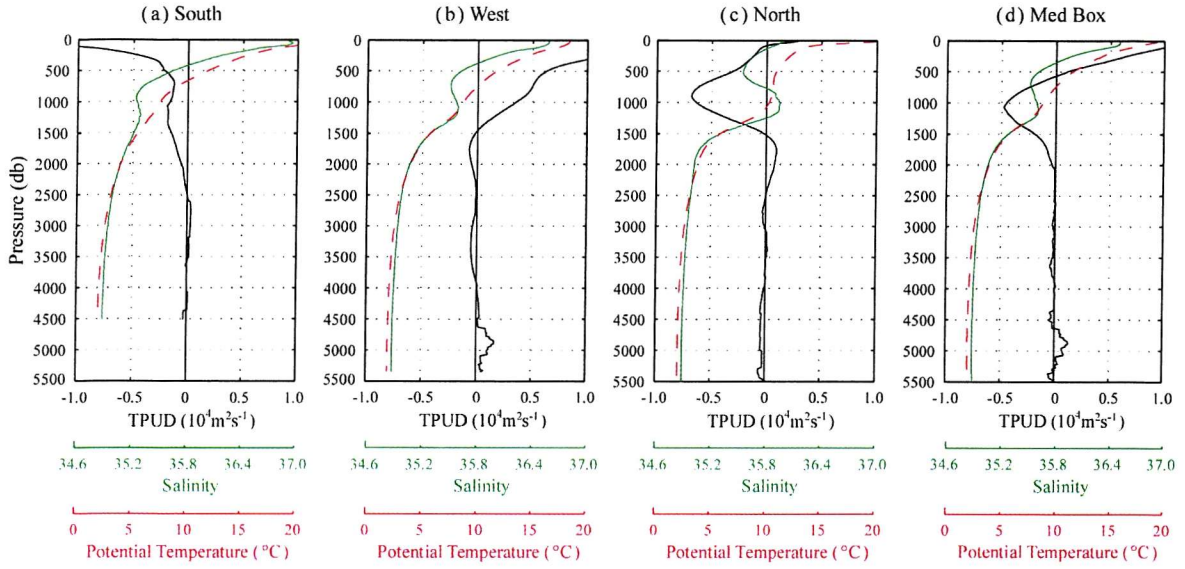

Figure 5.12 *Med Box 98 profiles of transport per unit depth (TPUD; 10^4 m^2 s^{-1}; black), and horizontally averaged salinity (green) and potential temperature (°C; dashed red) for the (a) southern edge, (b) western edge, (c) northern edge, and (d) whole box.*

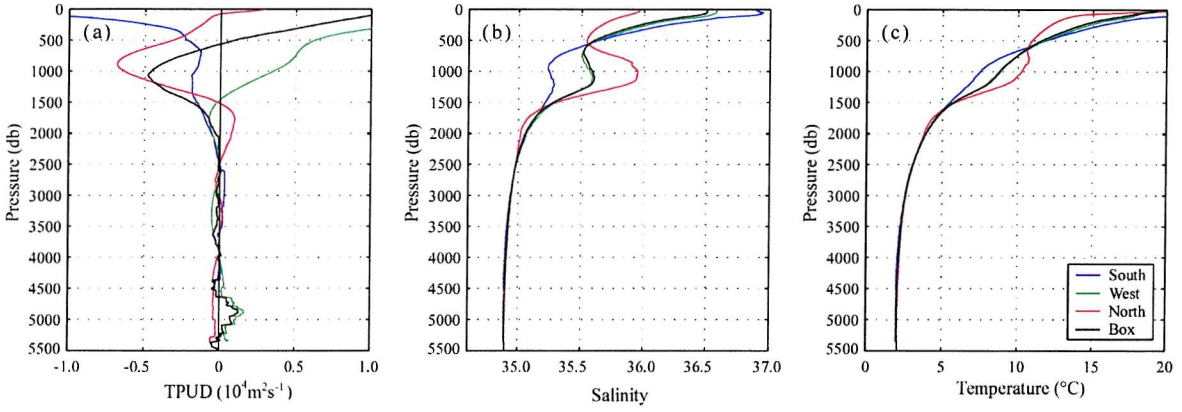

Figure 5.13 *Med Box 98 profiles of (a) transport per unit depth (TPUD; 10^4 m^2 s^{-1}), (b) horizontally averaged salinity and (c) horizontally averaged potential temperature (°C) for the southern edge (blue), western edge (green), northern edge (red) and whole box (black).*

Figure 5.12d shows the net Med Box transport profile that has already been discussed in terms of the net surface inflow (3.6 Sv) and mid-depth outflow (-3.5 Sv). It can be seen how the net outflow coincides with the mid-depth salinity maximum. There is also a slight maximum in the potential temperature, although this is not as well defined. The individual section transport profiles show that waters enter the box mainly from the west and leave to the north and south both at surface and mid-depths. There is, in fact, very little net inflow at all across either the north or south sides of the box. In the top 570 m, there is a 6.7 Sv inflow from the west, and outflows to the north and south of -0.5 Sv and -2.6 Sv respectively. The net box mid-depth outflow comprises a 2.5 Sv inflow from the west, and -4.0 Sv and -2.0 Sv outflows to the north and south (these values are summarized in Table 5.6). The main influences on the net transport profile are obviously the strong surface inflow from the west and mid-depth outflow to the north.

	Depth (m)	Transport (Sv) Box	South	West	North
Surface Inflow	569	3.58	-2.63	6.69	-0.48
Mid-depth outflow	2000	-3.48	-2.03	2.52	-3.96

Table 5.6 *Net transports across each boundary of Med Box 98 in the surface layer (down to 569 m) and at mid-depths (569 to 2000 m). Note that positive transports are into the box. This is a further breakdown of Table 5.4.*

The profiles of salinity and potential temperature show that all the variability occurs in the surface and intermediate waters. The mid-depth salinity and temperature maxima on the northern section are centered at 1000 db, and are coincident with the strong northward flow. There is not such an evident potential temperature maximum on the western edge, although the salinity maximum is clear and centered at ~1200 db, slightly deeper than for the northern profile.

Figure 5.14 shows cumulative transports for the surface layer (0 to 560 db) and the intermediate layer (560 to 2000 db), for which the net transports across each boundary are detailed in Table 5.6. It shows that much of the transport in the two layers is similar. For the southern section there is very little difference at all. It appears that the main differences occur because the inflows are stronger in the surface layer than at depth, and on the northern section, the outflows are stronger at depth.

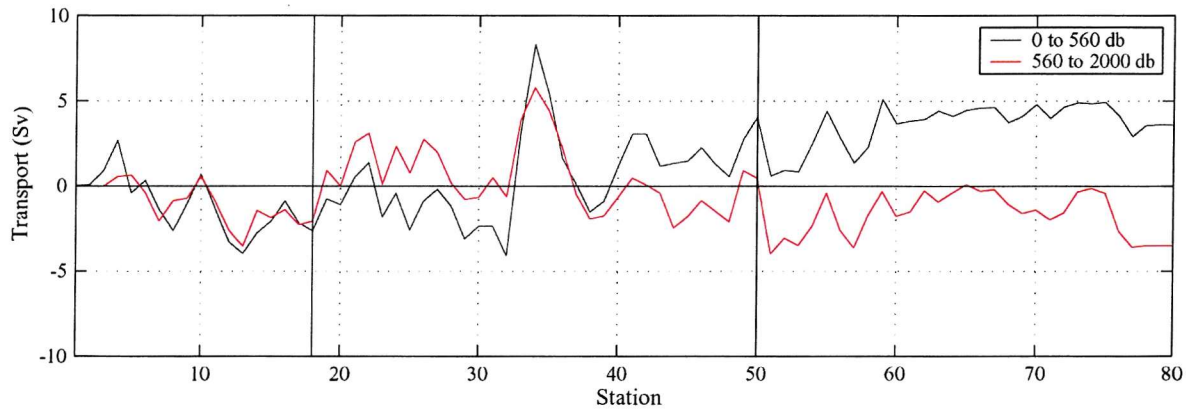

Figure 5.14 *Cumulative transports for Med Box 98 for the net inflowing surface layer (0 to 560 db; black), and the net outflowing intermediate layer (560 to 2000 db; red).*

It is interesting to look in detail at the upper part of the water column (down to 2500 m) for the sections which contain MW. Figures 5.15 and 5.16 show (a) salinity contours with the zero velocity contour overlaid in black, and (b) transport contours for the western and northern sides respectively. The vertical striated transport pattern typical of geostrophic circulation is evident. There are a number of eddies in the top 500 m (Figure 5.15b), and the strong inflow between 32 and 34°N is likely to be the Azores current. The high salinity MW at mid-depths (Figure 5.15a) is mostly flowing westwards out of the box although some is flowing eastwards in small recirculations.

On the northern section (Figure 5.16), the high salinity MW at the eastern edge of the section is all flowing northwards out of the box. The MW signal is seen throughout most of the section at these depths, and whilst the MW between 12°W and 10°W is mainly flowing north, some is advected southwards.

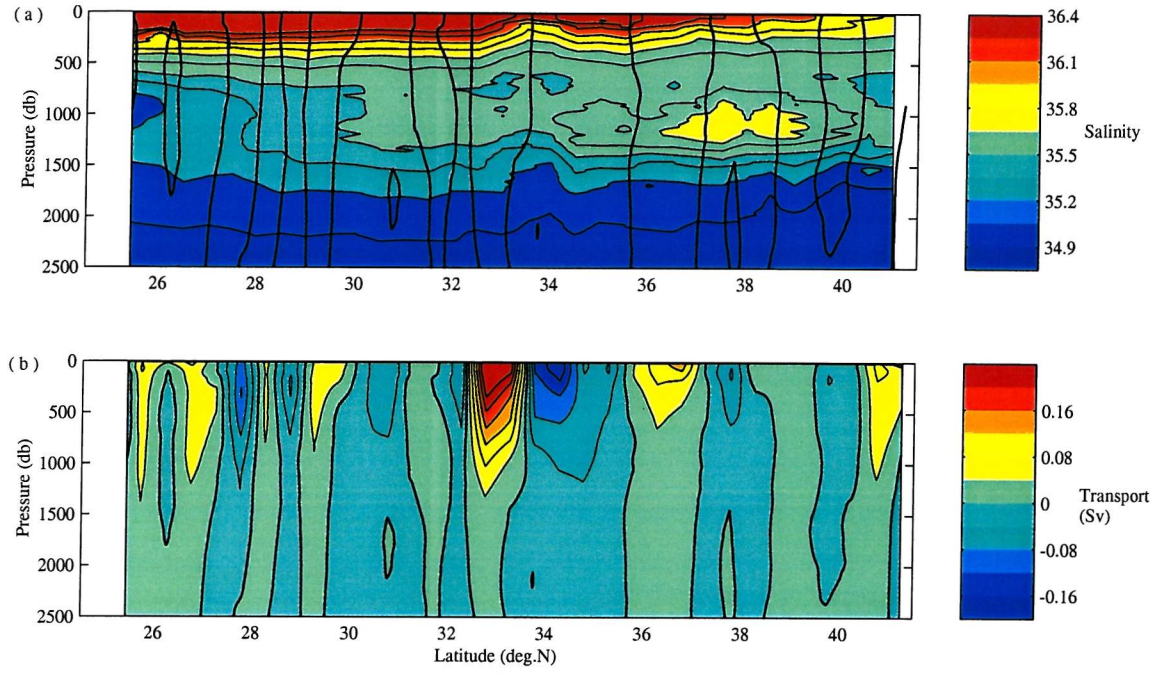

Figure 5.15 Contour plots of (a) salinity, with the zero transport contour overlaid in black, and (b) transport for the western side of Med Box 98. Positive transports represent flow into the box.

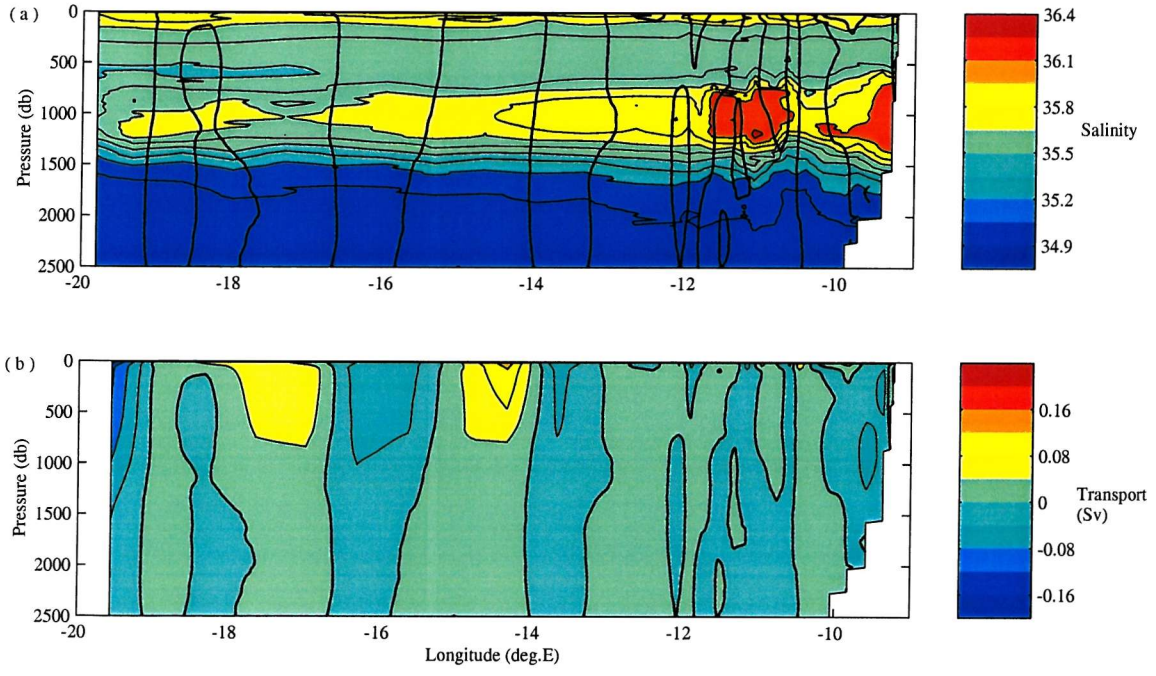

Figure 5.16 Contour plots of (a) salinity, with the zero transport contour overlaid in black, and (b) transport for the northern side of Med Box 98. Positive transports represent flow into the box.

5.3.4 Hydrographic Variability – Med Box 88

After a detailed discussion of the circulation and properties of Med Box 98, this section examines the circulation and properties of Med Box 88, and highlights the main differences. Figure 5.17 shows the θ/S plots for the box, highlighting data from each of its sides individually, and again there is a fairly tight relationship on the southern section, with no sign of any MW on this boundary. MW is evident on part of the western section, with more observations of higher salinities than were observed in 98. As in 98, the influence of MW is seen throughout the northern section, but this time, the highest MW salinities are seen on the west side. In this box, the surface properties on the western edge vary, whilst to the north the surface water is much cooler than it was in 98.

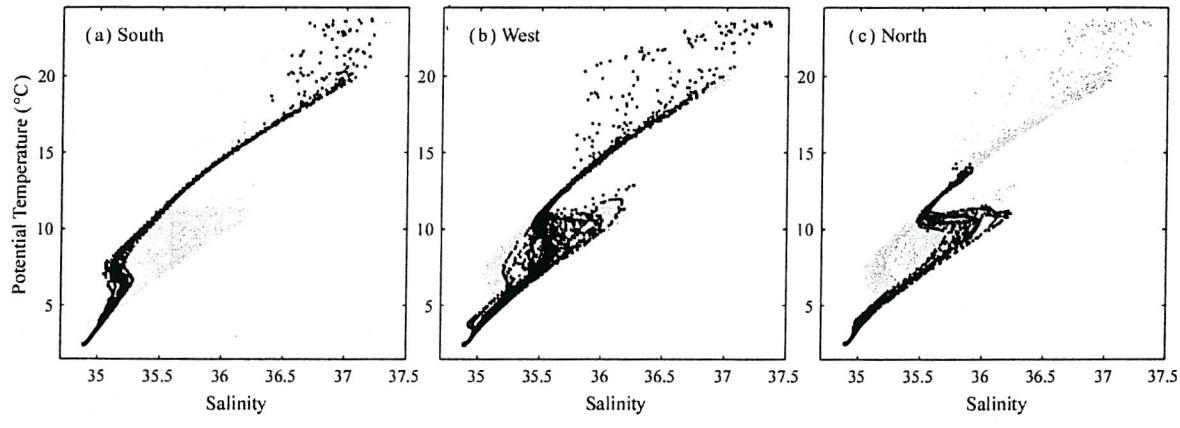

Figure 5.17 θ/S plots for Med Box 88; data for the whole box is shown in each plot in grey, while specific data (as detailed) is shown in black, (a) south, (b) west, and (c) north.

Some of the highest MW salinities of Med Box 88 occur at the southern end of the western section where two meddies were encountered at 25°N and 27°N (maximum salinities of 36.36 and 35.95 respectively). They have high anomalies of salinity and temperature (as was obvious in the θ/S diagrams and can be seen in Figure 5.18) and oxygen compared to the surrounding water and low values of silica, nitrate and phosphate (not shown). From the geostrophic velocity profiles (Figure 5.18c), it can be deduced that the meddies are rotating anticyclonically as expected. They have maximum azimuthal velocities of 6.6 cm s^{-1} at 780 m depth (25°N) and 0.8 cm s^{-1} at 870 m depth (27°N), these depths coinciding with the property maxima at the centre of each feature. From these profiles it also appears that they are lens-shaped, and that the shallower meddy at 25°N has larger property anomalies and greater azimuthal velocities, and may even have a surface signature. The effects of double diffusion can clearly be seen in the property profiles as 'steps' on the underside of each feature.

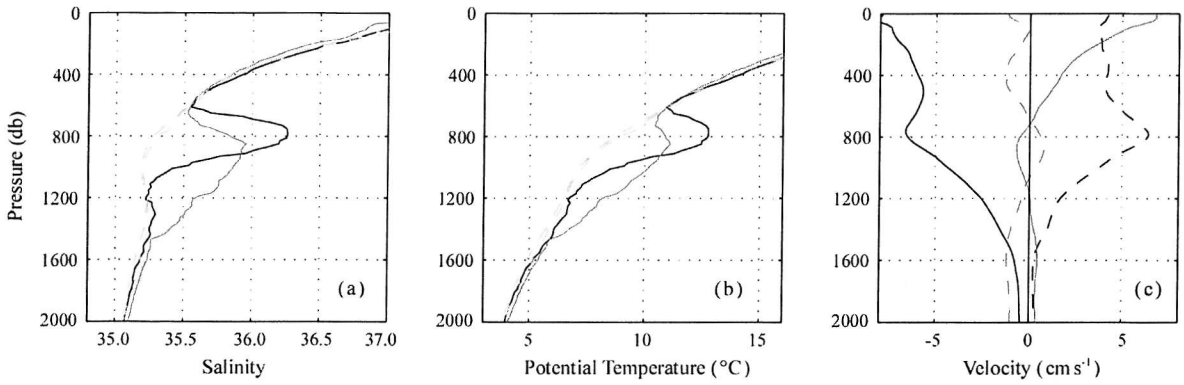

Figure 5.18 Meddies on the Oceanus section (Med Box 88, western side). Profiles of (a) salinity, and (b) potential temperature for stations oc77 to oc80. Stations 79 (black) and 77 (grey) are meddies at 25°N and 27°N respectively, the other two stations (in dashed grey) are outside the meddies. Also shown in (c) are geostrophic velocity profiles at the northern edge (dashed) and southern edge (solid) of the meddies at 25°N (black) and 27°N (grey).

The mean potential temperature and salinity, and total transport profiles for each section are shown in Figures 5.19 and 5.20. The net surface inflow to the box again comes solely from the west, which has net inflow down to 1000 m. As summarized in Table 5.7, in the top 400 m where the net inflow of 2.13 Sv to the box occurs, there is a 5.5 Sv inflow from the west, a -2.71 Sv outflow to the south, and just -0.62 Sv to the north; a similar pattern to that in 98 (although the net inflow layer was deeper in 98).

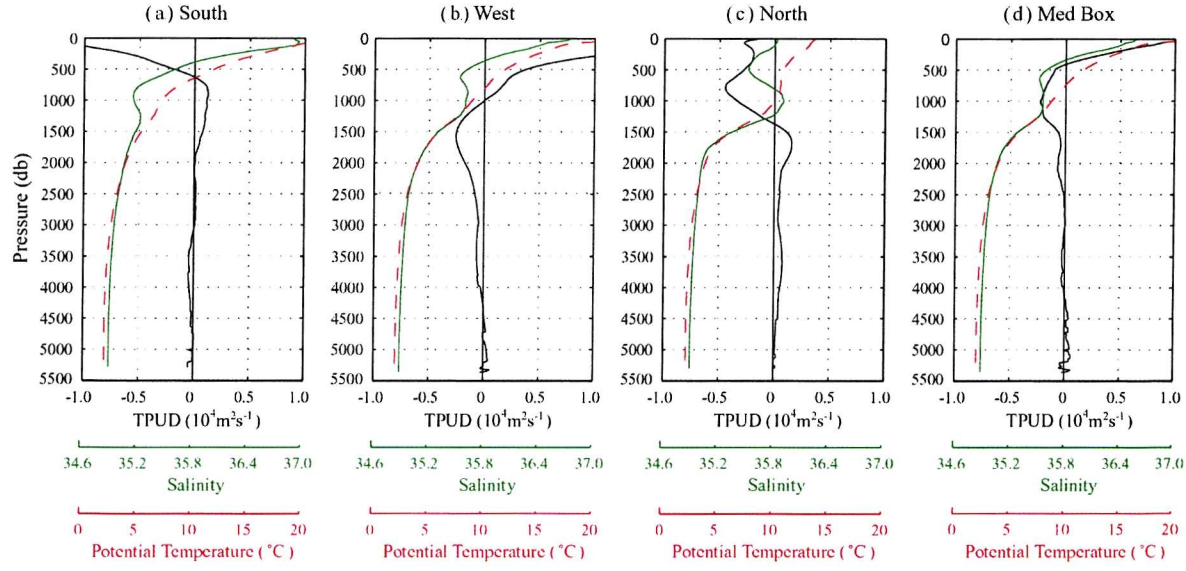

Figure 5.19 Med Box 88 profiles of transport per unit depth (TPUD; 10^4 m^2 s^{-1}; black), horizontally averaged salinity (green) and potential temperature (°C; dashed red) for the (a) southern edge, (b) western edge, (c) northern edge, and (d) whole box.

At intermediate depths, there is more variability between the two boxes. There is a small net inflow from the south (0.63 Sv between 400 and 2000 m), but yet again there is little net flow below 2000 db. There is a net outflow below 1000 db to the west with a maximum at 1500 db, resulting in a net outflow between 400 and 2000 m of –0.6 Sv. At certain depths (1000 to 1500 m) the high salinity MW signal is coincident with a net outflow.

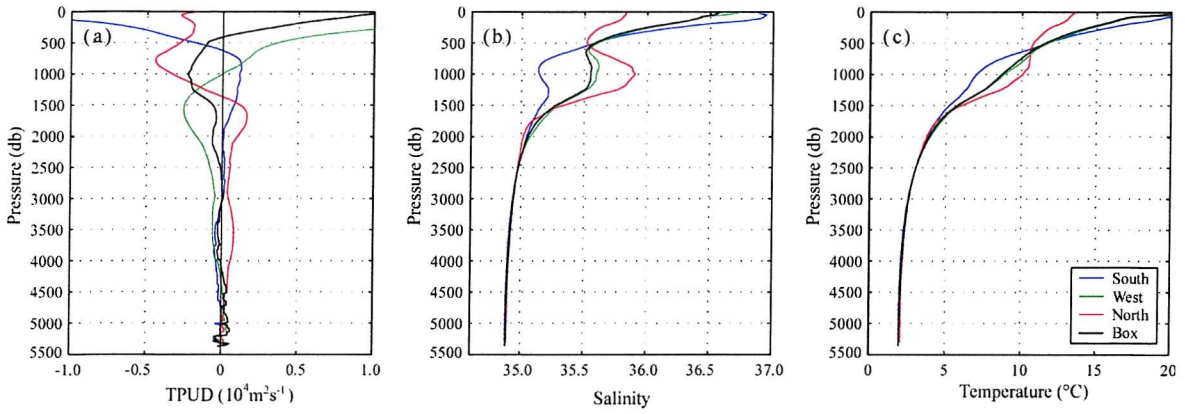

Figure 5.20 Med Box 88 profiles of (a) transport per unit depth (TPUD; 10^4 m^2 s^{-1}), (b) horizontally averaged salinity and (c) horizontally averaged potential temperature (°C) for the southern edge (blue), western edge (green), northern edge (red) and whole box (black)

Although the highest individual MW salinities are found on the western section, the northern section has by far the highest mean mid-depth salinities. There appears to be a double maxima in salinity on the western section, at ~900 db and 1100 db, probably due to the occurrence of the meddies. The influence of MW can also be seen in the mean temperature profiles, which are highest to the north and lowest to the south of the box. On the northern section, the salinity maximum occurs almost totally in the layers occupied by the net outflow.

	Depth (m)	Transport (Sv)			
		Box	South	West	North
Surface Inflow	400	2.13	-2.71	5.45	-0.62
Mid-depth outflow	2000	-2.01	0.63	-0.57	-2.05

Table 5.7 Net transports across each boundary of Med Box 88 in the surface layer (down to 400 m) and at mid-depths (400 to 2000 m). Note that positive transports are into the box. This is a further breakdown of Table 5.4.

Salinity and transport contours for the western and northern sides of Med Box 88 are shown in Figures 5.21 and 5.22 respectively. The two meddies at 25°N and 27°N are clearly visible in the salinity plot, and as already noted from Figure 5.18, the meddies are rotating anticyclonically. The meddy at 25°N has a stronger circulation which reaches the surface, whilst the meddy at 27°N is much weaker and its circulation is distinct from the overlying waters. The main flow of highly saline MW occurs between 35°N and 40°N. The circulation pattern implies that the middle portion centered at 37°N is a meddy because it is rotating anticyclonically, with the vertical axis at the middle of the extremely highly saline core. The core has salinities greater than 36.16, whereas the MW to the north and south of it have maximum salinities of 36.0 and 35.96 respectively. The two maxima centered at 36°N and 39°N are coincident with the westward velocities, and hence are interpreted to be the general background MW flow. Referring back to Figure 5.15, it is clear that in 98, the MW has lower salinities (maximum ~35.92) and is one coherent water mass. To the north

(Figure 5.22) there is far less eddy variability in 88 and the highly saline MW core at the eastern edge of the northern section is flowing northwards, whilst to its west there is a southward return flow of the fresher waters.

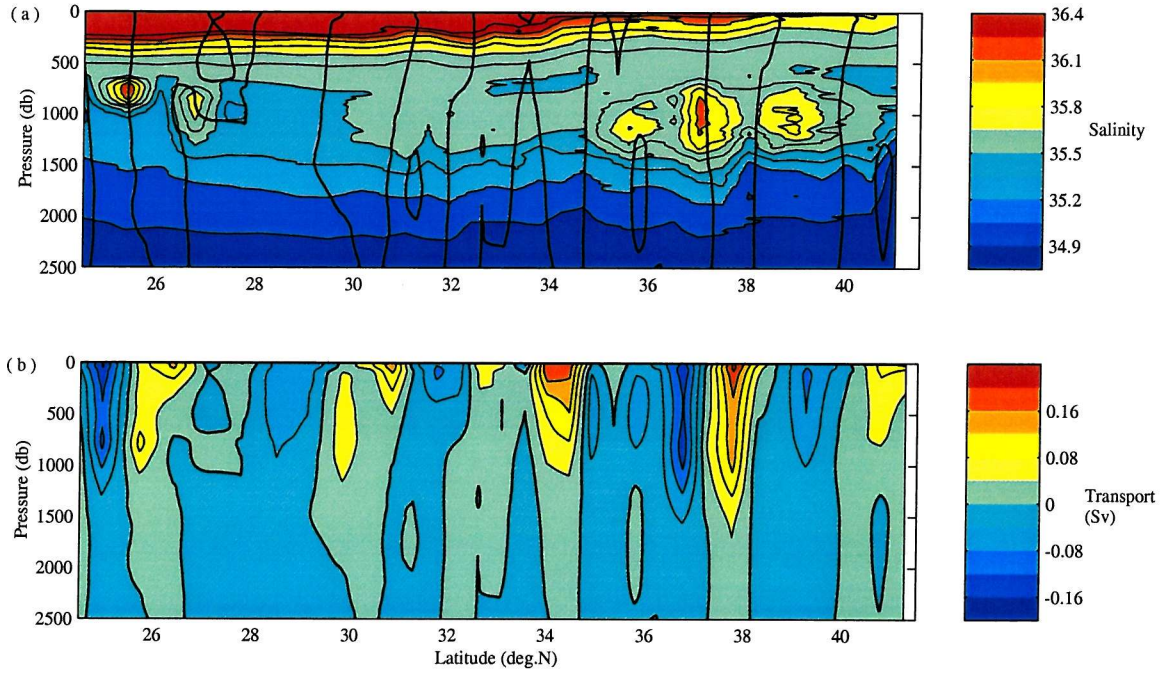

Figure 5.21 *Contour plots of (a) salinity, with the zero transport contour overlaid in black, and (b) transport for the western side of Med Box 88. Positive transports represent flow into the box.*

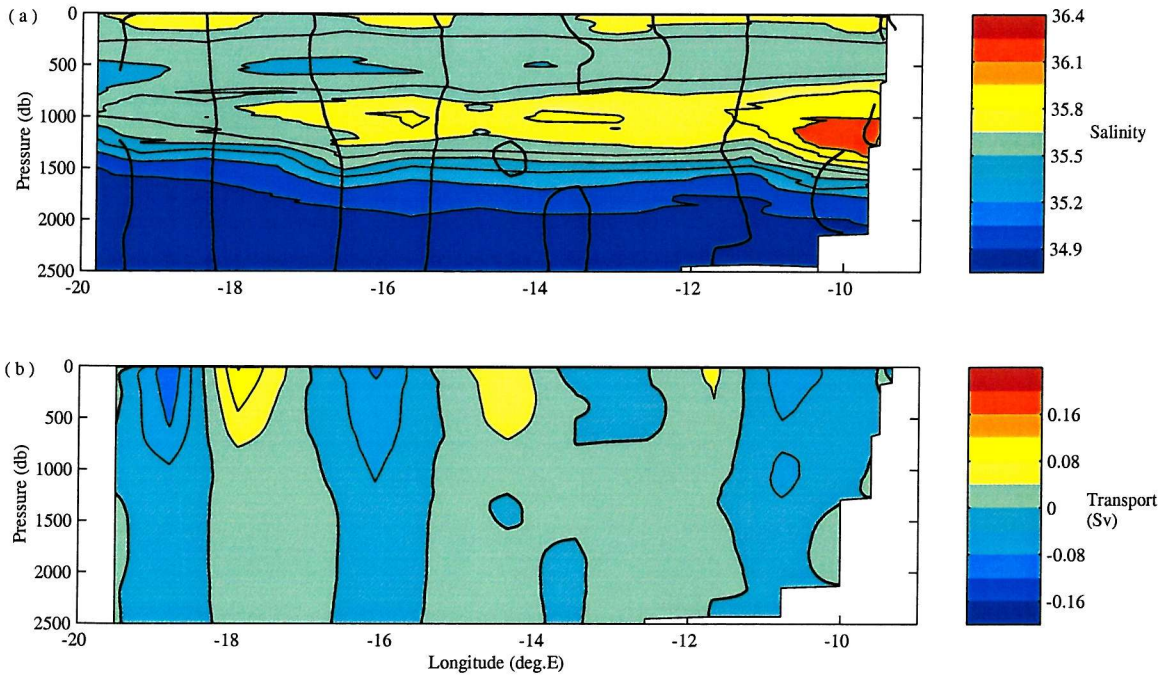

Figure 5.22 *Contour plots of (a) salinity, with the zero transport contour overlaid in black, and (b) transport for the northern side of Med Box 88. Positive transports represent flow into the box.*

Cumulative transports for the surface layer (0 to 560 db) and the intermediate layer (560 to 2000 db) are shown in Figure 5.23 for Med Box 88. The spatial variability due to eddies is evident, and as seen in Med Box 98, much of the transport in the two layers is similar. There is a stronger inflow at mid-depths than in the surface waters on the southern section. The influence of the meddies at mid-depth can also be seen to be stronger in 88 than in 98.

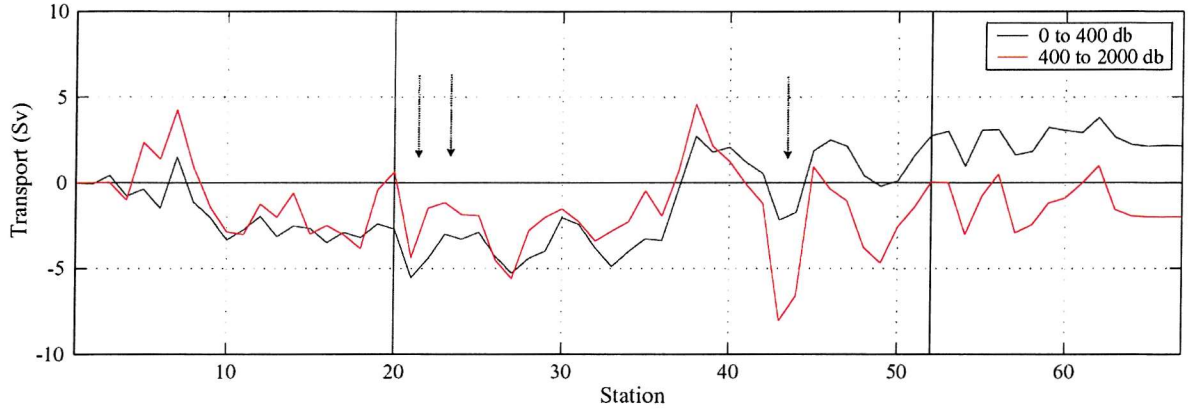

Figure 5.23 Cumulative transports for each side of Med Box 88 for the net inflowing surface layer (0 to 400 db; black) and the net outflowing intermediate layer (400 to 2000 db; red). Arrows indicate meddy positions.

5.3.5 Seasonal Variability – Levitus Med Boxes

The Levitus climatology data is fundamentally a smoothed version of historical hydrographic stations. This can be seen in the θ/S profiles (Figure 5.24), which are all perfect curves with no interesting variability. The southern section (admittedly only 4 stations) has a tight θ/S relationship, with no hint of any high MW salinities. The highest mid-depth (MW) salinities are found on the north section. The maximum salinity is 36.156 compared with maxima of 36.260 and 36.301 in Med Boxes 88 and 98 respectively.

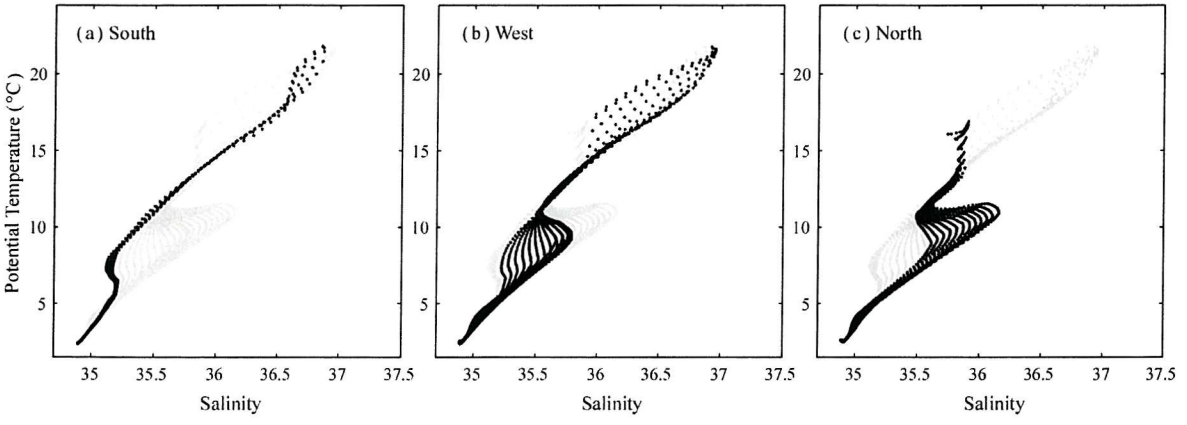

Figure 5.24 θ/S plots for the Annual Average Levitus Med Box; data for the whole box is shown in each plot in grey, while specific data (as detailed) is shown in black.

The mid-depth temperatures are also lower than those in the hydrographic boxes; 11.42°C compared with 12.77°C and 11.98°C. Of course, these are the Annual Average Levitus values; there is small seasonal variability, but the main differences are seen in the surface waters which are warmer in the summer and cooler in the winter (not shown).

The transports across each side of the box vary throughout the year. Figure 5.25 shows profiles of total transport per unit depth for each box and for the individual sides. The total box profiles (Figure 5.25a) are strikingly similar, with perhaps the exception of Summer, which has a deeper mid-depth outflow. The profiles for each side, however, are not so similar. Across the southern section, there is a surface outflow at all times of year, but the transport below ~500 db varies from very little net flow in Spring to a large inflow in the Autumn. It can be seen in Figure 5.26 (Levitus profiles in green, and Med Box 88 and 98 profiles in red and black respectively), that the Annual Average Levitus agrees with Med Box 88 below ~700 db.

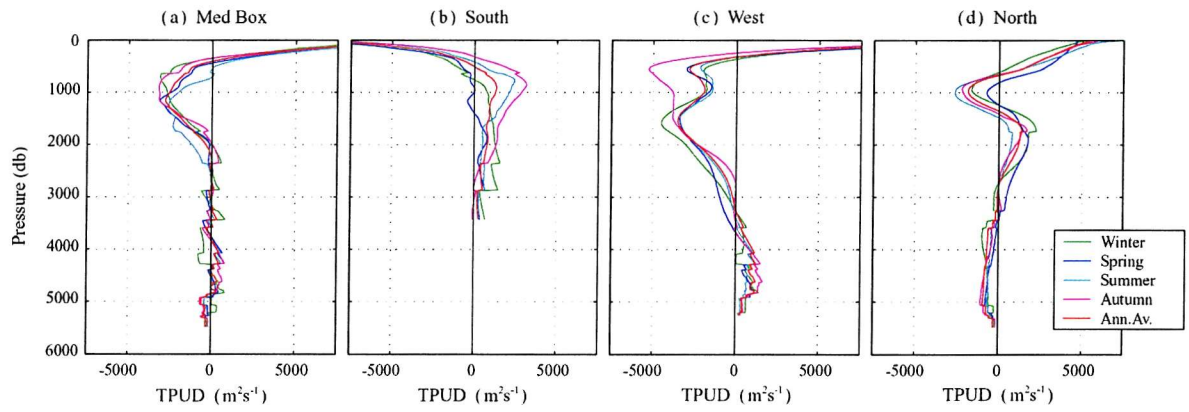

Figure 5.25 Total transport per unit depth profiles for (a) the Med Box, and its individual sides; (b) south, (c) west, and (d) north. Data is shown from Levitus Winter (green), Spring (blue), Summer (cyan), Autumn (magenta), and Annual Average (red).

The transport profiles for the western edge are similar, with the exception of Autumn which has a strong outflow centred on 500 m. All the profiles show a much shallower and smaller net surface inflow than the hydrographic Med Boxes (Figure 5.26c; Table 5.8) and a larger outflow. The Annual Average net surface inflow is just 1.6 Sv, whereas the 88 inflow is 6.7 Sv, and the 98 inflow is 9.5 Sv. There is net outflow below ~300 db in all the Levitus realisations, varying between -5 and -7 Sv, whereas in Med Box 88, the net outflow is deeper than 1000 db, and in 98, deeper than 1500 db, with far smaller magnitudes.

The profiles for the northern section again show marked dissimilarities to the hydrography. In all cases, there is net inflow in the surface layers down to ~700 to 800 db varying between 1.7 and 2.7 Sv, compared with a net outflow in the hydrographic boxes. The mid-depth net outflow is significantly smaller (-0.2 to -1.4 Sv, compared with -3.4 and -5 Sv for the hydrography) and

confined to a thinner layer. The net inflow is largest in Spring and smallest in Winter, whilst the net outflow is largest in Summer and smallest in Spring. All the profiles show a net inflow below ~1500 db, in agreement with the hydrography, and a net outflow below ~3000 db, which is similar to that in 98. On the whole, the net Levitus Med Box circulation is closest to that of Med Box 88, but there are significant differences in the circulation across the western and northern box sides.

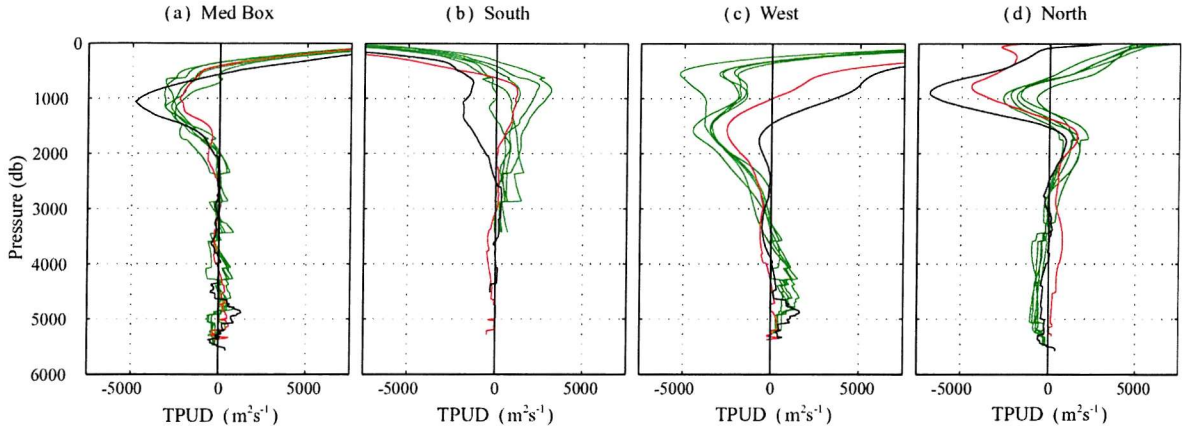

Figure 5.26 *Total transport per unit depth profiles for (a) the Med Box, and its individual sides; (b) south, (c) west, and (d) north. Data is shown from Med Box 88 (red), Med Box 98 (black) and the Levitus Med Boxes (green). Positive transports represent flow into the box.*

		total transport (Sv)	surface inflow / **outflow** depth (m)	transport (Sv)	mid-depth inflow / **outflow** depth (m)	transport (Sv)	other inflow / **outflow** depth (m)	transport (Sv)
South	Winter	1.41	0 - 740	**-1.92**	740 - bottom	3.33		
	Spring	**-0.84**	0 - 900	**-1.71**	900 - bottom	0.87		
	Summer	1.61	0 - 400	**-1.02**	400 - bottom	2.64		
	Autumn	3.21	0 - 300	**-0.85**	300 - bottom	4.06		
	Ann.Av.	0.86	0 - 500	**-1.33**	500 - bottom	2.19		
	88	**-2.50**	0 - 620	**-3.10**	620 - bottom	0.59		
	98	**-4.61**	0 - 620	**-2.76**	620 - bottom	**-1.85**		
West	Winter	**-3.38**	0 - 340	1.72	340 - 3200	**-6.32**		
	Spring	**-2.85**	0 - 320	1.92	320 - 3600	**-6.05**		
	Summer	**-2.27**	0 - 320	1.47	320 - 3320	**-5.02**		
	Autumn	**-4.41**	0 - 240	1.11	240 - 3400	**-7.20**		
	Ann.Av.	**-2.11**	0 - 300	1.61	300 - 3180	**-5.33**		
	88	3.60	0 - 980	6.75	980 - 4300	**-3.36**		
	98	9.45	0 - 1440	9.49	1440 - 3880	**-0.84**		
North	Winter	1.97	0 - 580	1.67	580 - 1220	**-0.67**	1220 - 2680	1.89
	Spring	3.69	0 - 780	2.69	780 - 1220	**-0.20**	1220 - 3380	2.01
	Summer	0.66	0 - 640	2.52	640 - 1460	**-1.35**	1460 - 2720	0.58
	Autumn	1.20	0 - 640	2.24	640 - 1400	**-1.09**	1400 - 2640	0.90
	Ann.Av.	1.25	0 - 660	2.20	660 - 1340	**-0.82**	1340 - 2740	1.08
	88	**-1.10**	0 - 0	0.00	0 - 1360	**-3.43**	1360 - 3000	1.30
	98	**-4.84**	0 - 60	0.37	60 - 1500	**-5.15**	1500 - 2480	0.55

Table 5.8 *Net transports in defined layers across each Med Box boundary. Positive transports represent flow into the box.*

The Annual Average Levitus Med Box transport per unit depth and mean property profiles are shown in Figures 5.27 and 5.28. These highlight the relationship between the transports (discussed previously) and the properties. The main points to note are: the shape of the transport profile for the western edge mimics the salinity profile, with a stronger outflow at ~600 db than at the deeper, higher salinity MW level (Figure 5.27b); the salinity maximum on the northern section coincides with the mid-depth net outflow (Figure 5.27c); the net box circulation brings surface water into the box, and exports high salinity water at mid-depths (Figure 5.27d); and the northern section has the highest mean salinities, although the western section mean salinity is higher than the box mean salinity at mid-depths (Figure 5.28b).

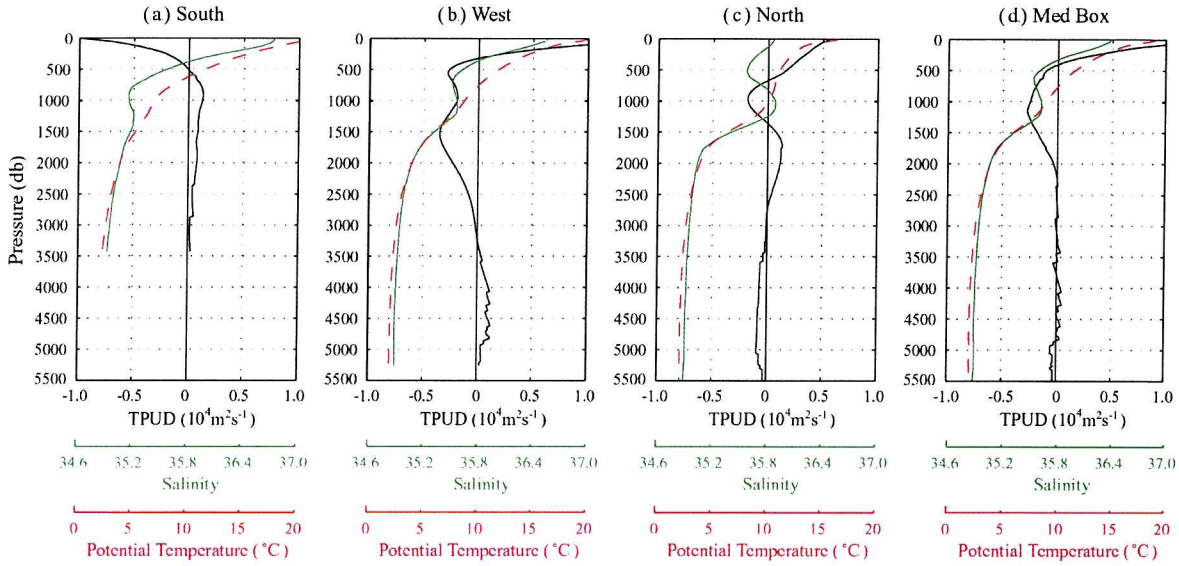

Figure 5.27 Med Box Levitus Annual Average profiles of transport per unit depth (TPUD; 10^4 m^2 s^{-1}; black), horizontally averaged salinity (green) and potential temperature (°C; dashed red) for the (a) southern edge, (b) western edge, (c) northern edge, and (d) whole box.

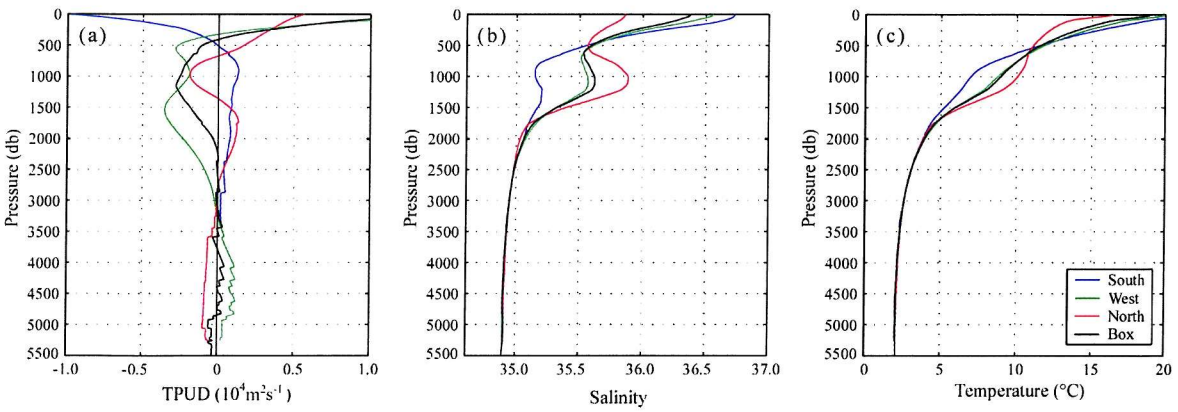

Figure 5.28 Med Box Levitus Annual Average profiles of (a) transport per unit depth (TPUD; 10^4 m^2 s^{-1}), (b) horizontally averaged salinity and (c) horizontally averaged potential temperature (°C) for the southern edge (blue), western edge (green), northern edge (red) and whole box (black).

It is interesting to look at contour plots of variables such as salinity and velocity as shown in Figure 5.29 for the upper 2500 m of each Med Box. This emphasises the difference between a climatology and a hydrographic section (compare with Figure 5.22, page 80 for example). There are no eddies in the data; the ultra-smoothed properties have produced a smooth flow. The highest salinities that are found in meddies or restricted currents in the real world are lost. This also results in much smaller velocities and transports. The highest velocity in any of the Levitus Med Boxes is 3.3 cm s^{-1}, compared with maxima of 26.1 and 72.3 cm s^{-1} in Med Boxes 88 and 98 respectively. This prompts the question, "Can this smoothed data tell us anything useful about the real ocean?"

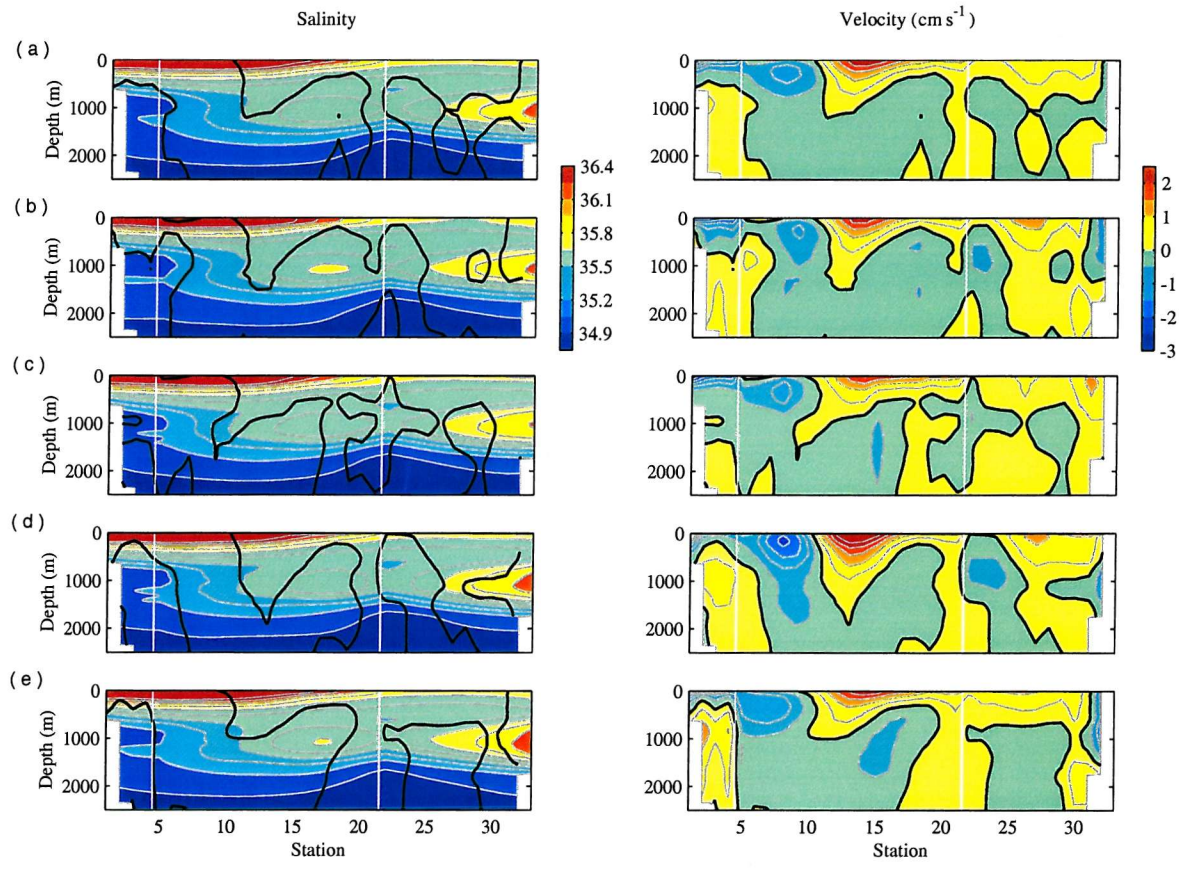

Figure 5.29 Contour plots of salinity and velocity (cm s^{-1}) for each of the Levitus Med Boxes; (a) Annual Average, (b) Winter, (c) Spring, (d) Summer, and (e) Autumn. The salinity contour plots have the zero velocity contour overlaid in black. Positive transports represent flow into the box. The vertical white lines indicate the box corners.

In all seasons apart from Spring, the highest salinity MW on the northern section up against the eastern boundary is flowing northwards. On the western boundary, the majority of the higher salinity MW is flowing westwards. There is some variability in the MW properties, but it is mostly a trend in the salinity signal rather than mesoscale variability.

Figure 5.30 showing cumulative transports for the surface (0 to 413 db; upper plot) and intermediate (413 to 2013 db; lower plot) layers highlights the smooth nature of the circulation in the Levitus Med Boxes. There is very little difference in the upper layer transports throughout the year, although in Summer the westward flow between stations 5 and 10 (25°N and 30°N) and the eastwards flow further north are slightly stronger (also seen in Figure 5.29d). Transport in the intermediate water exhibits more variability. The major difference is seen in the Spring, when there is no net flow across the southern boundary, and a southwards flow at the eastern edge of the northern boundary.

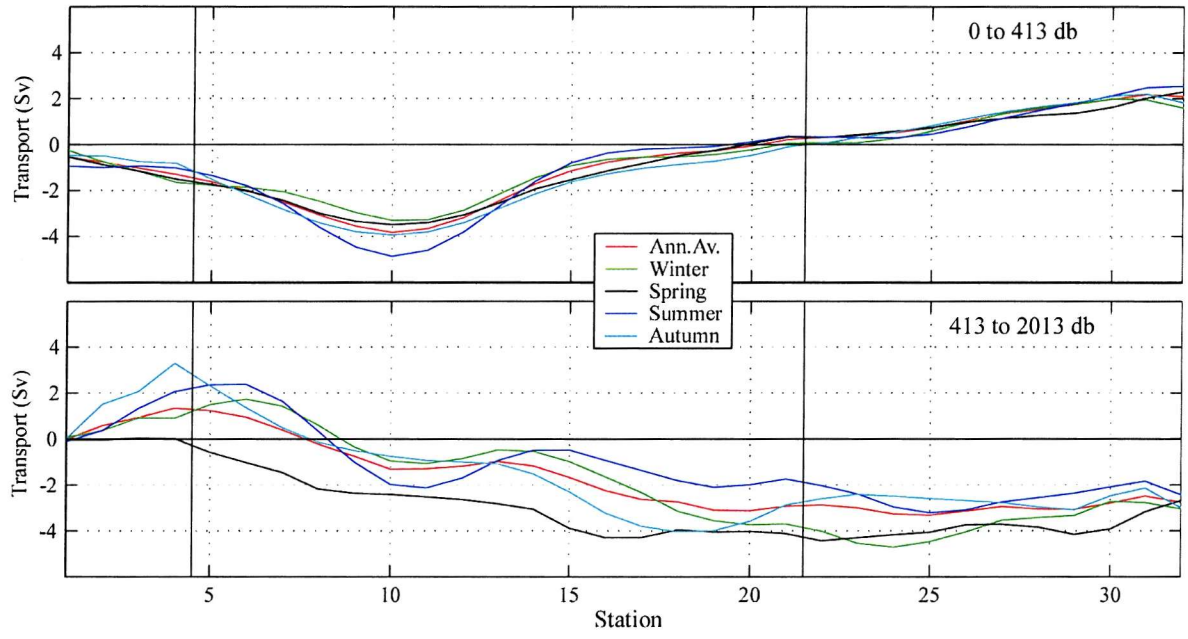

Figure 5.30 Cumulative transports for the Levitus Med Boxes for the net inflowing surface layer (0 to 413 db; upper plot) and the net outflowing intermediate layer (413 to 2013 db; lower plot).

In summary, the Levitus data exhibit some variability throughout the year, but without the small scale variability inherent in oceanic sections. Properties and flows are smoothed giving, perhaps, a distorted picture of the ocean. It will be interesting to see the difference between the data sets when examining salt fluxes in the following section.

5.4 SALT FLUXES

5.4.1 Med Box Fluxes

Due to the fact that there is an overturning circulation whereby surface waters are entering and saltier intermediate waters are leaving the Med Box, for zero mass transport there is a net salt flux out of the box. The net salt fluxes were calculated in Section 5.3.2 and are given in Table 5.5 (page 72). The hydrographic boxes have net salt fluxes of -2.5 Sv psu and -2.2 Sv psu (Med Boxes 88 and 98 respectively) and the Levitus box net salt fluxes vary between -0.5 in Spring and -2.8 in Summer, with an Annual Average of -1.5 Sv psu.

The salt fluxes are divided into baroclinic and horizontal components as detailed in Chapter 4 to aid in understanding the transport methods. Horizontal transports show correlations between high salinity and high velocity, and therefore reveal the depths at which salt anomalies are transported throughout the water column due to the large scale gyre circulation and the smaller scale eddies. Baroclinic transports are due to the overturning circulation and are defined such that there is no net volume transport across the boundary in question.

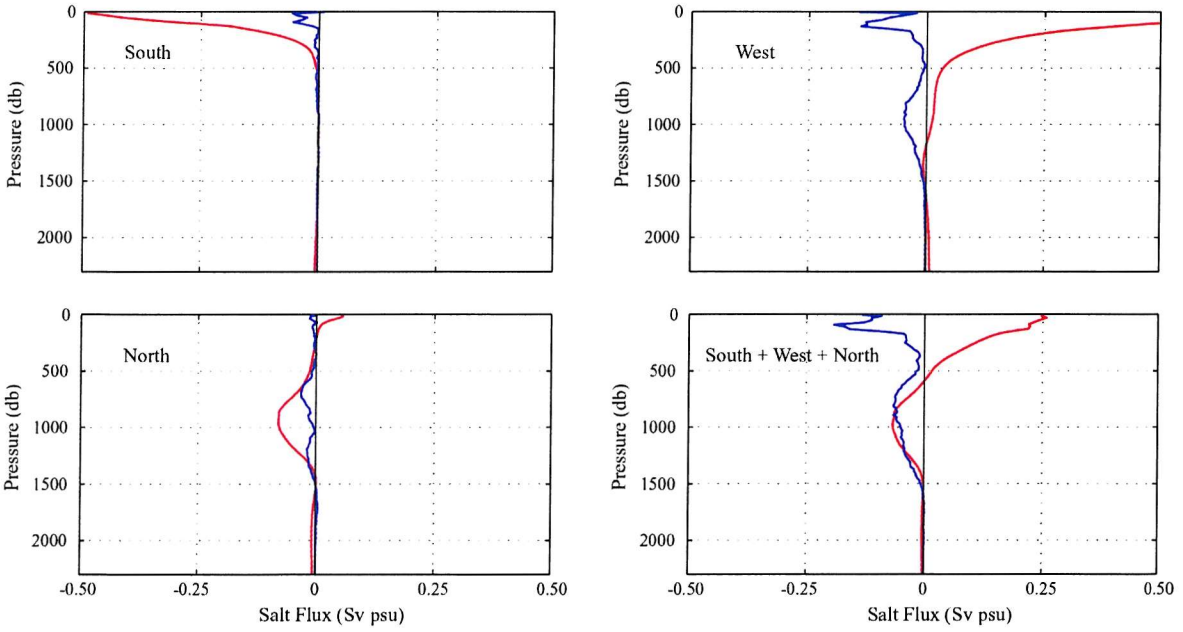

Figure 5.31 Baroclinic (red) and horizontal (blue) salt flux profiles for Med Box 98. Profiles are shown for each individual side and the sum of the three sides.

The baroclinic and horizontal salt flux profiles for Med Box 98 are shown in Figure 5.31. The x-axis is chosen to contain the entire profile, thus demonstrating the magnitude of the surface effects with relation to the subsurface fluxes. At this scale, Med Box 88 salt fluxes show similar variability, and fluxes below 2000 db are insignificant. The transports can be divided into two

components: the surface fluxes above ~500 db, and the mid-depth fluxes between ~500 and 1500 db. It is apparent from this figure that there are insignificant baroclinic salt fluxes and no horizontal salt fluxes below approximately 1500 db. At this scale, the profiles are very similar in both Med Boxes. The baroclinic circulation (shown in red) is acting to bring salt into the box in the surface, due to a much larger inflow from the west than outflow to the south, and remove salt from the box at mid-depths, mostly to the north. The horizontal fluxes (shown in blue), however, are negative at all depths, indicating that the higher salinities are being transported out of the box.

Figure 5.32 shows the same salt flux profiles, but focuses on the depths influenced by the MW (400 to 1600 db). A larger mid-depth salt exodus in Med Box 98 than in Med Box 88 is revealed, due primarily to the differences in the northern section. In comparison with the other sections, the southern section has insignificant salt fluxes at these depths, supporting the earlier statement that there is very little MW crossing this southern boundary.

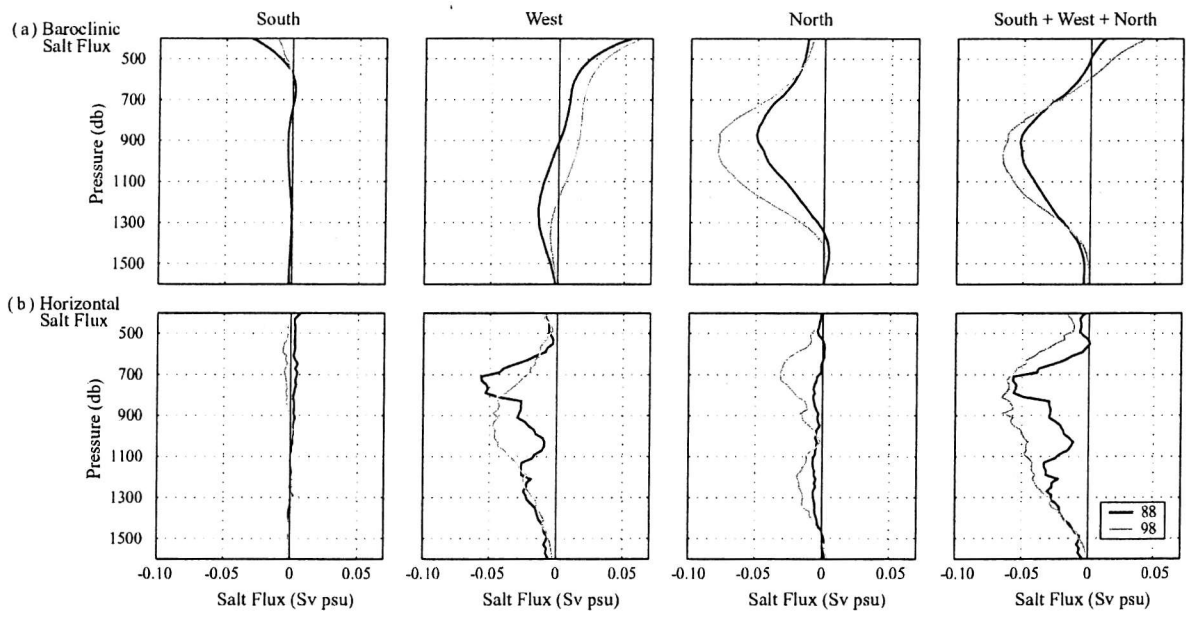

Figure 5.32 (a) Baroclinic and (b) horizontal salt flux profiles for Med Boxes 88 (black) and 98 (grey) between 400 and 1600 db. Profiles are shown for each individual side and the sum of the three sides.

The 98 north section has two very distinct cores in horizontal salt flux, with the upper core transporting higher salinity anomaly than the lower. These cores are at depths of 500 to 1000 m and 1000 to 1500 m and are taking salt northwards, out of the Med Box. An analysis of graphs of v', S' and θ' (not shown here) show that the shape of these profiles (the two cores) is due to the S' and θ' terms and not the v' term. It should also be noted that most of this flux occurs at the eastern side of the section, east of 13°W, which coincides with observations of the MW flowing poleward in an eastern boundary undercurrent (Zenk and Armi, 1990). The horizontal fluxes to the north in Med Box 88 are far smaller, due to lower salinity variability within the MW layers at the time the section was surveyed.

The western section also shows transport of salinity anomalies out of the Med Boxes in the depth range 500 to 1500 m. On this section, two distinct cores are seen in Med Box 88, centred at 750 and 1200 m, again with more anomalous salt flow in the upper 500 m of this range than the lower. The majority of this flux occurs between 33 and 40°N, which coincides with the position of the main core of MW that can be seen on the contour plots (Figure 5.15a and Figure 5.21a). There is almost no horizontal salt flux at 25 to 27°N in Med Box 88 - the southern meddy locations. This is surprising considering their anomalous signatures, but is due to the geostrophic velocity calculations which reveal circulating flow with little overall average.

As far as the horizontal fluxes are concerned, the primary source appears to be the MW exiting the box at intermediate depths across the northern and western boundaries. The profiles highlight how nearly all of the subsurface salt flux occurs at the same depths, revealing the range occupied by the MW; 500 to 1500 m. The corresponding calculations of MW fluxes will be undertaken after a brief look at how the Levitus salt fluxes differ from the hydrography.

The Levitus Annual Average horizontal salt fluxes are shown in Figure 5.33. Only the Annual Average data is shown for two reasons: firstly because the seasonal profiles are reasonably similar, and secondly because the primary reason for showing this figure is to highlight the differences between the Levitus data and the hydrography (shown in Figure 5.31 and Figure 5.32). The comparison of the Levitus horizontal fluxes with hydrography is very striking, and the main difference is immediately obvious; there are no mid-depth horizontal fluxes in the Levitus data (across individual sections). This is due to the smooth nature of the data and highlights the fact that there is no eddy variability. Although there is little variability on each individual box edge, taking the box as a whole (final plot in Figure 5.33), there is evidently horizontal variability, which shows up as a horizontal salt flux and reveals the levels occupied by the MW, 600 to 1500 db. This salt flux is due mainly to outflowing intermediate water of higher salinity on the western edge.

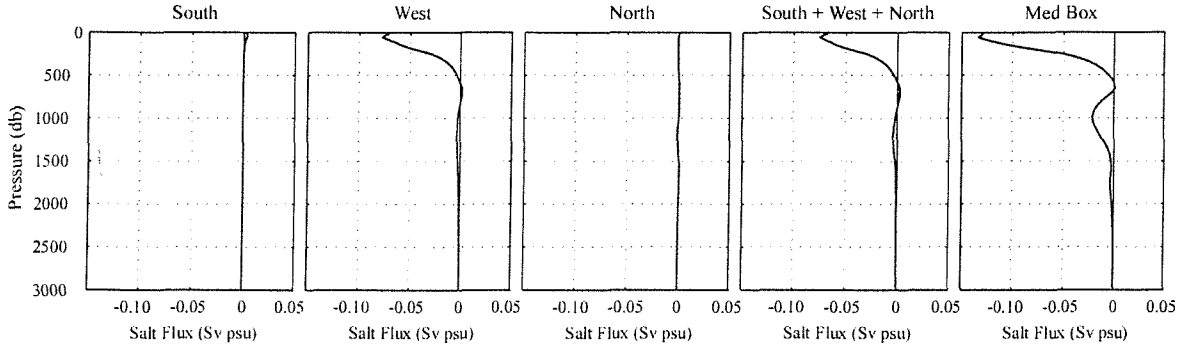

Figure 5.33 Horizontal salt flux profiles for the Levitus Annual Average Med Box. Profiles are shown for each individual side, the sum of the three sides and the box as a whole.

A comparison of whole box baroclinic and horizontal salt flux profiles for the hydrographic and annual average Levitus Med Boxes is shown in Figure 5.34 with the net fluxes detailed in Table 5.9. The under-representation of the horizontal fluxes in the Levitus data is evident, with the main difference seen at mid-depths. The baroclinic salt fluxes in Levitus are more comparable with the Hydrography, although the total (1.12 Sv psu) is lower than either Med Box 88 or 98. The baroclinic salt flux is positive in all Med Boxes due to higher salinity surface waters entering the region and lower salinity intermediate waters leaving.

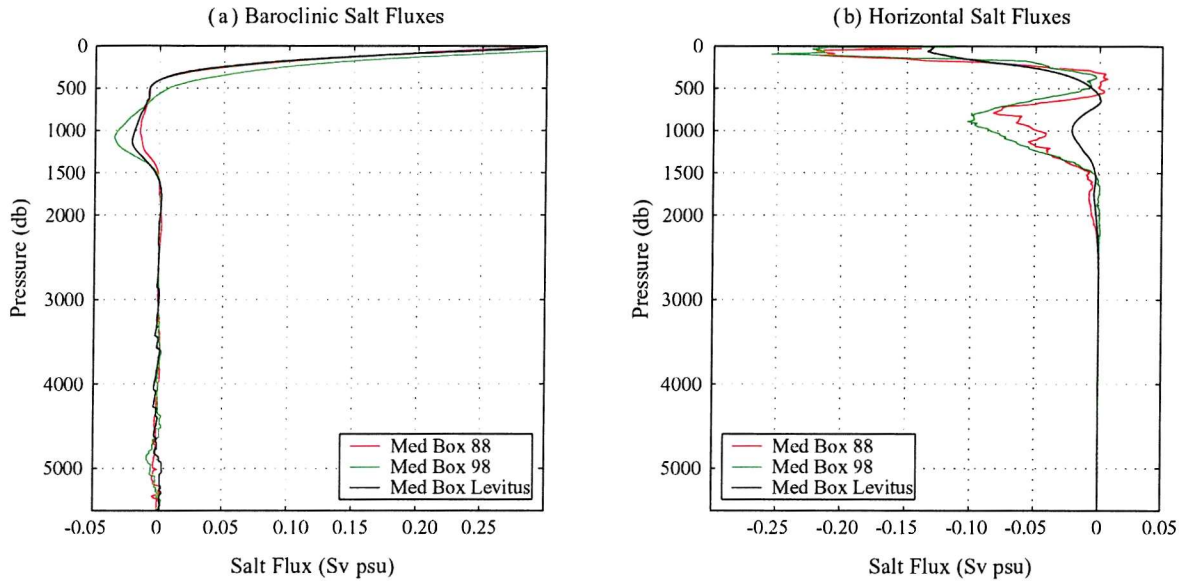

Figure 5.34 *(a) Baroclinic and (b) horizontal salt flux profiles for Med Box 88 (red), Med Box 98 (green) and Annual Average Levitus Med Box (black).*

Med Box	Baroclinic Salt Flux (Sv psu)	Horizontal Salt Flux (Sv psu)	Total Salt Flux (Sv psu)
88	1.88	-4.38	-2.50
98	2.62	-4.86	-2.24
Levitus Annual Average	1.12	-2.63	-1.51

Table 5.9 *Net baroclinic and horizontal salt fluxes (Sv psu) in the hydrographic and Annual Average Levitus Med Boxes.*

5.4.2 Med Water Fluxes

The MW layers are defined using the horizontal salt flux profiles as explained in the previous section; and are 500 to 1500 db for the hydrographic Med Boxes and 600 to 1500 db for the Levitus Med Boxes. The choice of these layers is confirmed by the mean profiles of the positive salinity anomaly for each box (Figure 5.35b), which is calculated relative to the box average

salinity (Figure 5.35a). These profiles highlight the relatively low salinity anomalies in Levitus compared with the hydrography, especially in view of the fact that the mean salinities are very similar.

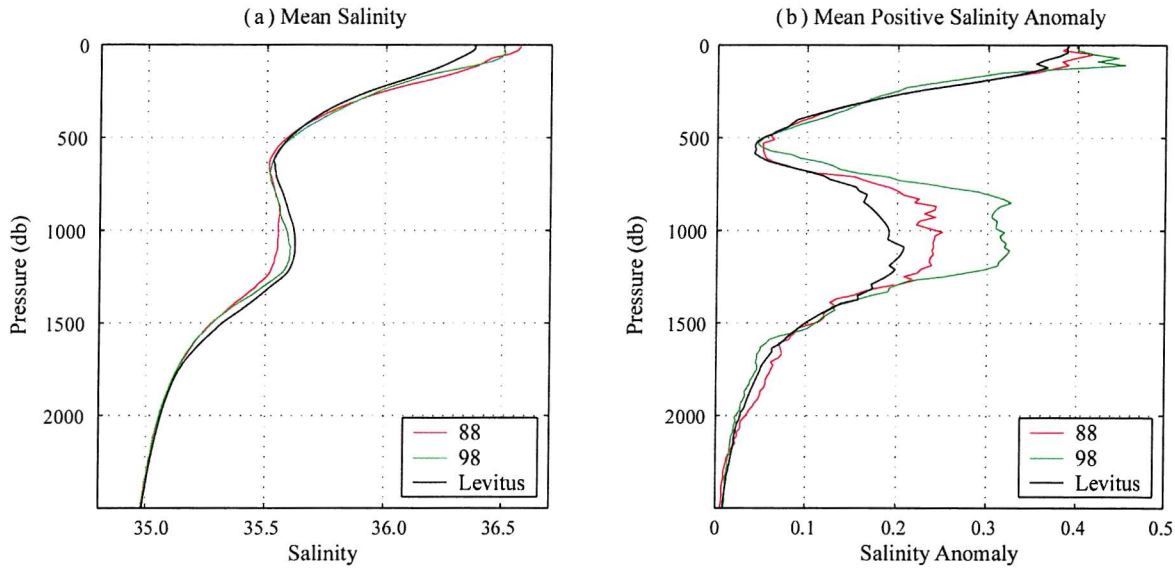

Figure 5.35 (a) Mean salinity and (b) mean positive salinity anomaly profiles relative to box mean salinity for Med Box 88 (red), Med Box 98 (green) and the Annual Average Levitus Med Box (black).

The mean salinity in the MW layers for the hydrographic and annual average Levitus Med Boxes is detailed in Table 5.10. Surprisingly, the Levitus Med Box has the same mean salinity as Med Box 98, which is 0.02 higher than in 88. Transport weighted salinities were calculated for the inflowing and outflowing water separately for the west and north sections, and the anomaly given relative to the box mean salinity (Table 5.10). These very clearly show that, apart from the western Levitus section, the outflow salinity is higher than the inflow salinity at MW depths. Also highlighted in this table is the fact that the salinities on the northern section are higher than those on the west. From these values, it seems that there is a higher transport of MW salt to the north than to the west.

Med Box	MW depths (m)	Box mean salinity	section	Inflowing water		Outflowing water	
				TWS	anomaly	TWS	anomaly
88	500 - 1500	35.5019	west	35.5730	0.071	35.6160	0.114
			north	35.6777	0.176	35.7331	0.231
98	500 - 1500	35.5238	west	35.4795	-0.044	35.5320	0.008
			north	35.7178	0.194	35.7887	0.265
Levitus	600 - 1500	35.5237	west	35.5478	0.024	35.5180	-0.006
			north	35.5667	0.043	35.7736	0.250

Table 5.10 Mediterranean Water depths for Med Boxes 88, 98 and Levitus Annual Average, with the mean box salinity, and transport weighted salinity (TWS) and its anomaly (relative to box mean salinity) for the inflowing and outflowing water, for the western and northern sections.

Calculations of the total salt fluxes within the MW layers associated with both the flow due to the overturning circulation (baroclinic salt flux) and that due to the gyre circulation and eddies (horizontal salt flux) were calculated and are shown in Table 5.11. Calculating the amount of salt flux crossing each boundary as a percentage of the total gives an estimate of the percentage of MW crossing that boundary. These calculation results are given in Table 5.12. The final two columns in Table 5.12 show the percentages of MW crossing the west and north boundaries assuming that none of the salt flux across the southern boundary is due to MW transport. This is a fair assumption having looked carefully at the section properties (θ/S plots for example) and the horizontal salt flux profiles.

Med Box	Depths (m)		Transport (Sv)			Horizontal Salt Flux (Sv psu)			Baroclinic Salt Flux (Sv psu)		
	upper	lower	south	west	north	south	west	north	south	west	north
88	500	1500	0.684	0.167	-2.533	0.077	-1.135	-0.197	-0.052	-0.158	-1.20
98	500	1500	-1.683	3.302	-4.560	-0.065	-1.311	-0.715	-0.005	0.459	-2.09
Levitus Ann.Av	600	1500	0.948	-2.221	-0.699	-0.003	-0.068	0.010	-0.138	-0.541	-0.55
Levitus Winter	600	1500	0.529	-2.214	-0.354	-0.002	-0.341	0.073	-0.083	-0.502	-0.45
Levitus Spring	600	1500	-0.138	-2.089	0.190	0.000	0.059	0.172	-0.037	-0.446	-0.34
Levitus Summer	600	1500	1.675	-1.910	-1.324	0.002	0.045	0.114	-0.214	-0.395	-0.81
Levitus Autumn	600	1500	2.274	-3.604	-1.009	-0.004	0.058	-0.213	-0.218	-0.850	-0.69

Table 5.11 Net transports and salt fluxes (horizontal and baroclinic) across each Med Box section within the MW layers, defined to be 500 to 1500 m for the hydrographic Med Boxes and 600 to 1500 m for the Levitus Med Boxes as indicated.

Med Box	Depths (m)		Percentage[1]			Percentage[2]	
	upper	lower	south	west	north	west	north
88	500	1500	-0.8	48.4	52.4	48.0	52.0
98	500	1500	4.8	23.1	72.1	23.3	76.7
Levitus Ann.Av	600	1500	10.1	47.7	42.2	53.1	46.9
Levitus Winter	600	1500	5.5	65.0	29.5	68.9	31.1
Levitus Spring	600	1500	12.9	60.0	27.1	69.3	30.7
Levitus Summer	600	1500	13.4	28.5	58.0	33.3	66.7
Levitus Autumn	600	1500	7.0	43.1	50.0	46.6	53.4

Table 5.12 Percentages of MW crossing each Med Box boundary.
([1] including every section, [2] ignoring the southern section)

Looking at the hydrographic results, the salt fluxes across the south side of both boxes are very small, and contribute a maximum of 5% of the total (Med Box 98). This can either be included or excluded from the MW calculation (as just explained), and for the hydrographic boxes makes very little difference. In Med Box 88 the horizontal salt fluxes dominate to the west, and the baroclinic to the north, but the net result is that roughly half of the MW is calculated to be going west (48%) and half north (52%). In Med Box 98 the horizontal salt flux to the west is twice that to the north,

but the baroclinic salt flux to the north dominates (-2.1 Sv psu) due to the large northward volume transport (-4.6 Sv) and the fact that the MW is present across most of the section. The net transport into the box from the west results in a positive baroclinic salt flux (0.46 Sv psu), and the consequence of these transports is that 77% of the MW is calculated to be flowing northwards across the northern boundary.

As discussed earlier, the horizontal salt fluxes in the Levitus Boxes are very small due to the smoothed nature of the data. There is almost none across the southern boundary, and the maximum to the west and north are -0.34 (Winter) and -0.21 (Autumn) respectively, although these are much larger than the mean values. It is notable that the baroclinic salt fluxes are always negative (transporting salt out of the box), regardless of whether the net transports in the MW layers are positive or negative. There is significant variability in the percentages of MW crossing each boundary in the seasonal Levitus data, ranging from 31% flowing northwards in Winter and Spring to a maximum of 67% flowing northwards in the summer. The Levitus Med Boxes all exhibit strong outflow to the west at MW depths, whereas the hydrographic boxes suggest a net inflow of intermediate waters across the west section carrying relatively saline waters back into the box.

The choice of MW layers may be questioned, but fears can be dispelled by a simple sensitivity study. In the hydrographic Med Boxes, moving the upper MW boundary by ±100 m changes the calculated percentages of MW crossing each boundary by ±4%, whilst moving the lower boundary by ±100 m changes the percentages by just ±2% for Med Box 88 and ±1% for Med Box 98. In the Levitus boxes, the percentage of MW crossing each boundary is more sensitive to the definition of the MW upper depth levels, although moving that boundary by ±100 m only changes the percentages by ±6.3% (for the Annual Average box). A high degree of confidence can therefore be placed in these MW transport percentage values.

5.5 SUMMARY

The principal aim of the thesis, to determine the transport of MW in the eastern North Atlantic and particularly to assess the northwards and westwards transport of MW, was accomplished using hydrographic data and the climatological Levitus dataset. These datasets were used to create 'Med Boxes' enclosing an area east of 20°W, bounded roughly by 24°N and 41°N, and thus encompassing the Strait of Gibraltar and Mediterranean Outflow. Two hydrographic realisations of the Med Box were made, Med Boxes 88 and 98, using data from six sections. The method used to join the hydrographic sections to ensure a dynamically consistent solution was reviewed in Chapter 4. Five Levitus Med Boxes were constructed; an Annual Average and one for each season.

A box inverse method following Wunsch (1996) was used to determine the full set of reference velocities, having chosen the initial reference level as the $\sigma_3 = 41.49$ kg m^{-3} isopycnal. This level is close to 3200 m, a depth favoured for this region of the eastern North Atlantic (for example Saunders, 1982). The choice of initial reference level did not, in fact, significantly affect the solution in this analysis. The inverse was used to constrain volume, salinity anomaly and heat fluxes within defined layers, and the solution degree was chosen using the Levenburg - Marquardt analysis (Lawson & Anson, 1974).

The inverse model constrained the net volume transport into the box to be zero. The resulting salt flux was then used to give an estimate of the net evaporation over the enclosed region (which includes the Mediterranean Basin) of 0.071 Sv (0.068 Sv) in Med Box 88 (98). This compares very favourably with the evaporation estimate from the SOC Global Air-Sea Heat and Momentum Flux Climatology of 0.077 Sv (0.064 Sv) for Med Box 88 (98), and suggests that the net Med Box circulation regimes and SOC climatology are close to reality.

A principal result of the analysis is a quantification of the magnitude of the overturning circulation within the box boundaries. This circulation involves a surface inflow to the box and a mid-depth outflow, and is due to two factors: (1) the exchange at the Strait of Gibraltar, whereby surface waters enter the Mediterranean and the outflow from the Mediterranean occurs at intermediate depths, and (2) to the water mass transformation associated with the entrainment of surface waters into the Mediterranean outflow. From seven Med Box realisations (two hydrographic and five Levitus), the overturning is found to be a very robust feature, and is calculated to be 2.3 ± 0.6 Sv. The surface inflow occurs to depths of 432 ± 86 m, and the mid-depth outflow to 2000 m. Given that the inflow to the Mediterranean has a magnitude of ~0.7 Sv (Bryden et al., 1994), the calculated overturning circulation gives a value for the entrainment of NACW into the outflowing MW of 1.6 ± 0.6 Sv. Baringer and Price (1997a) estimated that 1.2 Sv of entrainment occurred by Cape St Vincent, meaning that up to 1 Sv of entrainment occurs between Cape St Vincent and the Med Box boundaries.

The main features of the Med Box 98 circulation are a net surface inflow from the west and a strong mid-depth outflow to the north centred at 1000 m; the position of the salinity maximum. This outflow therefore advects the highly saline MW polewards in an eastern boundary undercurrent as observed by numerous studies (for example Reid, 1994; Zenk and Armi, 1990). Although the meridionally averaged zonal transport across 20°W is found to be eastward down to 1500 m, a significant portion of the high salinity MW is within westward flow and points to an advective pathway for MW westwards, in agreement with other observations (Reid, 1994; Daniault et al., 1994).

The main difference in Med Box 88 is that the surface eastward flow across 20°W extends to just 1000 m, with net westward flow below this depth. Three meddies are observed along this boundary at latitudes 25°N, 27°N and 37°N. In Med Box 98, two stacked cores of MW were observed on the northern section in the poleward undercurrent, in agreement with other observations (Zenk and Armi, 1990). They were not observed in Med Box 88 however, indicating interannual variability. A shallow core of MW observed at depths between 400 and 600 m off western Portugal by Ambar (1983) was not observed in either hydrographic Med Box, leading to the same conclusion as reached by Fiuza et al. (1998), that it is probably restricted to the region south of 40°N.

The Levitus data show variability across the seasons, and whilst closest in circulation patterns to Med Box 88, exhibit significant differences from the hydrography in the top 1000 m of the water column. The data is very smooth, lacking the extremes in both property (salinity and temperature) and velocity values that are found in the real ocean. This casts doubt on its usefulness in studying water masses such as MW, with its narrow boundary current and high salinity anomalies that are lost by the averaging process in creating the climatology.

An investigation into Med Box salt fluxes reveals some interesting features. In the hydrographic Med Boxes, whilst the overturning circulation results in positive net baroclinic salt fluxes into the box, the horizontal variability (mainly due to the MW) results in larger negative eddy salt fluxes indicating that the higher salinities are being transported out of the box. The subsurface horizontal salt fluxes all occur within the depth range, 500 to 1500 m, revealing the depths occupied by the MW, the primary source of this flux.

Striking differences between the Levitus and hydrographic data are seen in the horizontal salt fluxes, which are nearly non-existent in the Levitus Med Boxes due to the lack of horizontal variability. To reveal the MW depths in the Levitus data it was necessary to look at the horizontal fluxes for the entire box, as only then was the variability significant. The baroclinic salt fluxes are also lower in the Levitus data, mainly due to the lower salinity values found in the climatology.

Using the salt flux calculations, the percentages of MW crossing each boundary are calculated. In Med Box 98 approximately 75% of the MW flows northwards across 41°N, whereas only 50% crosses the northern boundary in Med Box 88. The difference is due principally to the larger northward mid-depth transports and smaller net westward transports in 98. The salt fluxes across the southern section at MW depths are small, emphasising the fact that there is insignificant MW transport across the southern Med Box boundary.

Chapter Six

OCCAM: Analysis of a Global Ocean Model

6.1 INTRODUCTION 97

6.2 OCCAM DATA 97
- 6.2.1 Model Experiments 97
- 6.2.2 Model Set-up 98
  - *i Forcing* 98
  - *ii Horizontal Grid Configuration* 99
  - *iii Vertical Grid Configuration* 102
  - *iv Strait of Gibraltar* 103
  - *v Model Data Used in the Analysis* 103

6.3 DEFINING MEDITERRANEAN WATER 104

6.4 THE MEDITERRANEAN OUTFLOW 106
- 6.4.1 Exchange at the Strait of Gibraltar 106
- 6.4.2 Model Stability 108

6.5 CIRCULATION 112
- 6.5.1 Initial Mediterranean Water Spreading 112
- 6.5.2 Annual Average Med Box Circulation 114
- 6.5.3 Variability of the Circulation 115
  - *i Annual Variability* 115
  - *ii Seasonal Variability* 116
- 6.5.4 Effects of the Mediterranean Outflow 122
  - *i Med Box Transports* 122
  - *ii North East Atlantic Circulation* 124
- 6.5.5 Extent of the Mediterranean Water in OCCAM 129

6.6 MED BOX FLUXES 131
- 6.6.1 Net Fluxes and Evaporation 131
- 6.6.2 Mediterranean Water Fluxes 134

6.7 SUMMARY 139

6.1 INTRODUCTION

Analysis of hydrographic data gives an instantaneous snapshot of the state of the ocean at the time the data were collected but has a number of inherent problems, some of which have already been highlighted and discussed in this thesis. Two major problems are those of temporal and spatial coverage of the data. Ocean models with continuous temporal and spatial domains can be used to help us understand the limitations of the data coverage.

The model used in this work is OCCAM, the Ocean Circulation and Climate Advanced Modelling Project global ocean model (Webb et al., 1998; described in Chapter 3.6). OCCAM has a 0.25° latitude-longitude grid, and data are available as annual means and as snapshots every 30 days. OCCAM has great potential as a tool for exploring questions of spatial and temporal variability with its global, full-depth coverage and an integration length of 25 years, and to 'fill in the gaps' of our hydrographic data sets and knowledge.

The purpose of this section of work is therefore two-fold. Firstly, the model data set will be fully reviewed and aspects of time variability considered, both on a short (monthly) and seasonal time-scale. Secondly, with the hydrographic results of Chapter 5 still in mind, the scientific questions relating to the transport of Mediterranean Water in the northeast Atlantic will be investigated. Before describing the results, an overview of the model is given including the experiments and the set-up, and the definition of MW in OCCAM is outlined. The exchange at the Strait of Gibraltar and the stability of the model in the final years of integration are then examined. Discussion of the model circulation covers the initial spreading of the MW, the circulation variability, the effects of the Mediterranean Outflow on the North Atlantic, and the extent of the MW in the North Atlantic. Finally, fluxes in the Med Box itself, including calculations of MW transport are discussed.

6.2 OCCAM DATA

6.2.1 Model Experiments

A number of numerical experiments have been run using the OCCAM global ocean model, with horizontal resolutions of 1°, ¼° and 1/12°. The 1° model is fairly coarse and does not produce a realistic outflow or spreading of the MW in the North Atlantic. The 1/12° model has only been run for two years so far, and although interesting small-scale variability can be seen, more years are needed before stability is reached. For these reasons data from the ¼° model is used in this work.

In addition to the main ¼° run, a second experiment was undertaken with the Strait of Gibraltar closed and started from day 3000 of the main run (end of year 8). Both experiments have an integration time of 17 years if the start is taken to be day 3000.

The closed-Strait run is a unique modeling experiment allowing a totally new approach to the investigation of MW transport in the North Atlantic and the effects of the MW outflow on the circulation. It gives a means of identifying MW in the open-Strait run, and can be used as a control in the Med Box studies. The last few years of the model runs are used (detailed in Table 6.1) as it takes time for the high salinity from the Mediterranean to leave the study region. The monthly sampling rate of the model snapshots means that spatial variability might be expected in the annual mean. A higher sampling rate would possibly give a more stable mean picture, but only the 30-day snapshots have been saved.

6.2.2 Model Set-up

i *Forcing*

The ocean is driven by the upper surface boundary conditions, including wind stress (from the 1986-1988 ECMWF monthly climatology) and heat and fresh water fluxes across the air-sea interface. Bottom friction is also applied, determined by the current adjacent to that boundary. The model is forced with same wind field each year so there is no interannual variability in the forcing. The model run therefore does not have a calendar year associated with it, just a model year and month (see Table 6.1).

Model Day	Model Date dd mm yy	Model Day	Model Date dd mm yy	Model Day	Model Date dd mm yy	Model Day	Model Date dd mm yy	Model Day	Model Date dd mm yy
7500	14 Jul 20	7860	09 Jul 21	8220	04 Jul 22	8610	29 Jul 23	8970	23 Jul 24
7530	13 Aug 20	7890	08 Aug 21	8250	03 Aug 22	8640	28 Aug 23	9000	22 Aug 24
7560	12 Sep 20	7920	07 Sep 21	8280	02 Sep 22	8670	27 Sep 23	9030	21 Sep 24
7590	12 Oct 20	7950	07 Oct 21	8310	02 Oct 22	8700	27 Oct 23	9060	21 Oct 24
7620	11 Nov 20	7980	06 Nov 21	8340	01 Nov 22	8730	26 Nov 23	9090	20 Nov 24
7650	11 Dec 20	8010	06 Dec 21	8370	01 Dec 22	8760	26 Dec 23	9120	20 Dec 24
7680	10 Jan 21	8040	05 Jan 22	8400	31 Dec 22	8790	25 Jan 24	9150	19 Jan 25
7710	09 Feb 21	8070	05 Feb 22	8430	30 Jan 23	8820	24 Feb 24	9180	18 Feb 25
7740	11 Mar 21	8100	06 Mar 22	8460	01 Mar 23	8850	25 Mar 24	9210	20 Mar 25
7770	10 Apr 21	8130	05 Apr 22	8490	31 Mar 23	8880	24 Apr 24	9240	19 Apr 25
7800	10 May 21	8160	05 May 22	8520	30 Apr 23	8910	24 May 24	9270	19 May 25
7830	09 Jun 21	8190	04 Jun 22	8550	30 May 23	8940	23 Jun 24	9300	18 Jun 25
				8580	29 Jun 23			9330	18 Jul 25

Table 6.1 *Model dates of snapshot data for the last 5 years of the experiment. The dates are separated to show which data were used to compute each annual mean.*

ii Horizontal Grid Configuration

An Arakawa-B grid is used for the horizontal configuration, with tracers (potential temperature and salinity) defined at the box centres, and velocities (meridional and zonal components) defined at box corners (Figure 6.1). Velocity is set to zero on all solid boundaries and tracer data to null.

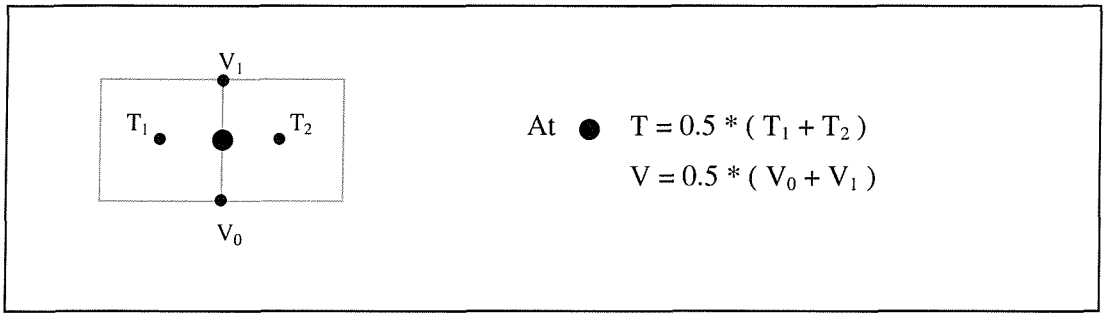

Figure 6.1 Horizontal grid configuration. Tracers are defined at box centres, and velocities at the corners. T_1 and V_1 are corresponding grid cell properties.

To allow for increased accuracy, salinity is stored as a modified variable;

$$\text{salinity}_{(\text{occam})} = \frac{(\text{salinity}_{(\text{PSS78})} - 35)}{1000}$$

and must therefore be converted before use.

To overcome the computational difficulties that arise at the convergence of the meridians in the Arctic, two separate model grids were developed. Model 1 covers the Indian, Pacific and South Atlantic Oceans with a standard latitude-longitude grid. Overlying this is Model 2 which covers the North Atlantic and Arctic Oceans and the Mediterranean Sea and uses a grid rotated through 90° such that the grid poles lie on the geographical equator (shown in Figure 6.2). These two grids communicate very effectively at the Atlantic equator and Bering Straits (as shown by Coward et al., 1994).

The rotated coordinates of Model 2 are converted to normal latitude-longitude coordinates for plotting and discussion. The velocities are also rotated such that meridional and zonal refer to the real world rather than the rotated model grid. However, for calculation purposes (transports), cross-track velocities normal to the grid lines are used.

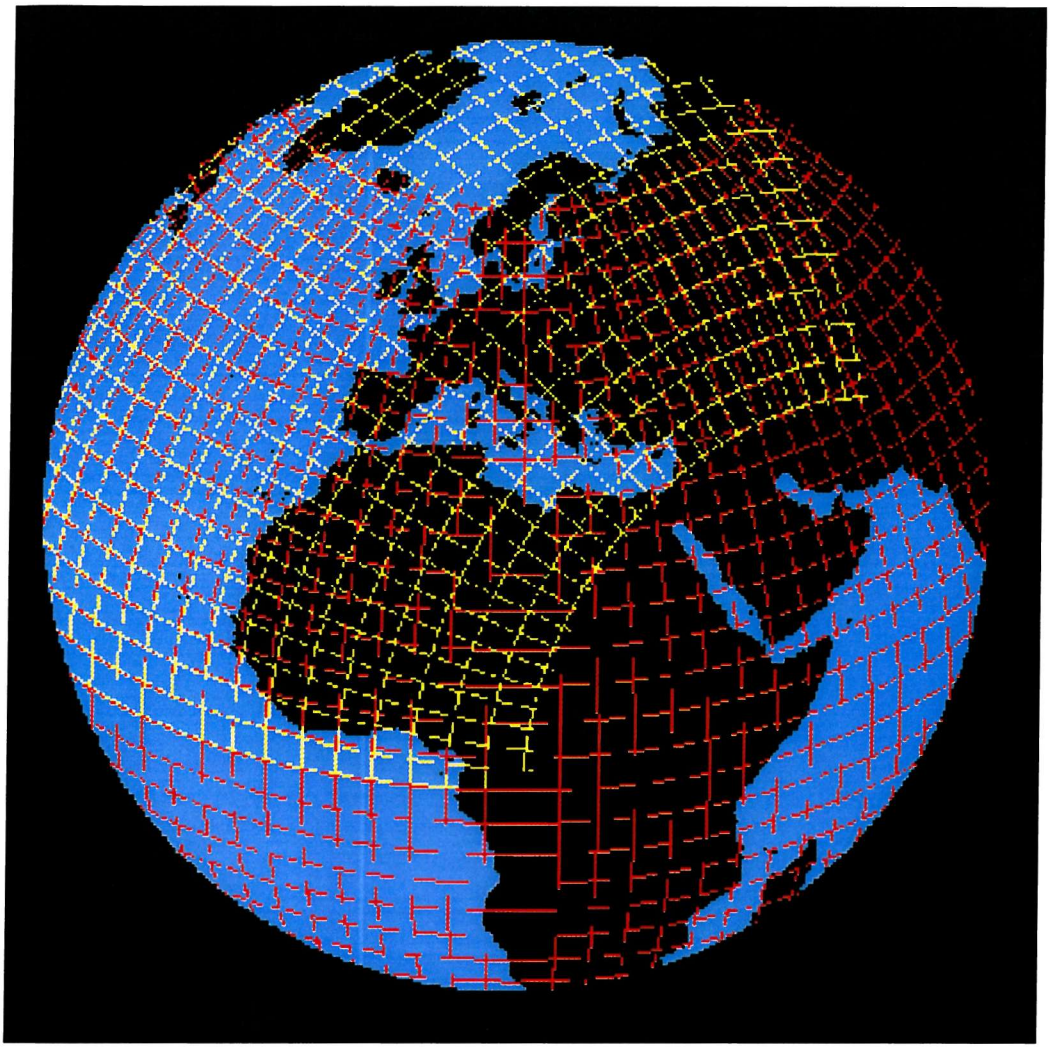

Figure 6.2 *OCCAM model grids, showing real world latitude-longitude lines in red, and the rotated model grid in yellow.*

The formally correct approach to properly conserve quantities and not introduce spurious errors, is to take data along actual model grid lines. These are at an angle to lines of latitude-longitude as can be seen in Figure 6.2. The OCCAM Med Box formed is the closest possible to the hydrographic Med Boxes, given the constraints of the rotated grid. The (I, J) coordinates of the four corners are 102, 137 (southeast), 102, 159 (southwest), 176, 159 (northwest), and 176, 131 (northeast). To create the box, tracer and velocity data are averaged onto the mid-velocity positions. Figure 6.3 shows the positions of the OCCAM Med Box stations, also listed in Table 6.2.

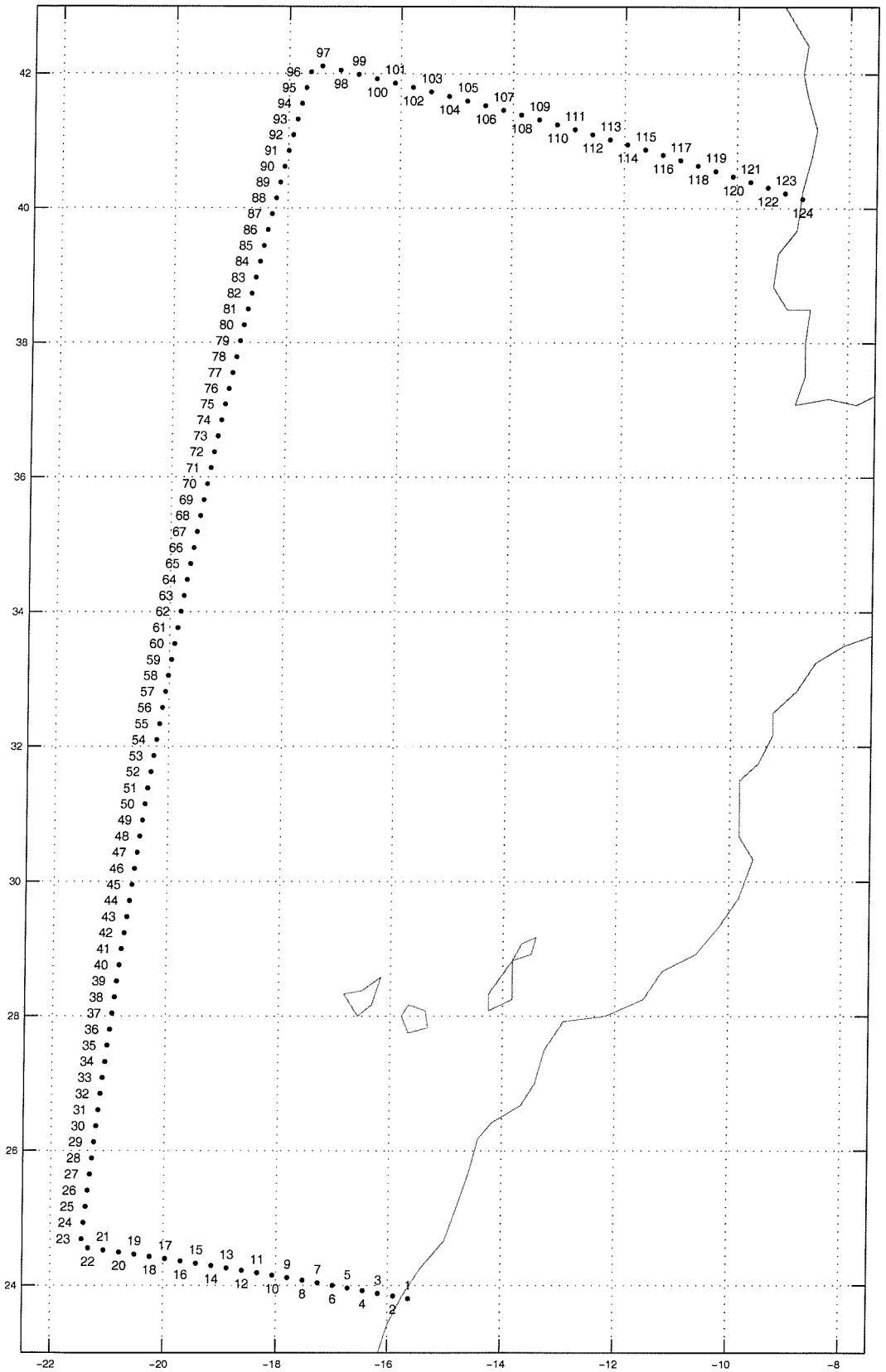

Figure 6.3 *OCCAM Med Box station positions.*

Southern Edge			Western Edge						Northern Edge		
#	lon	lat	#	lon	lat	#	lon	lat	#	lon	lat
1	-15.63	23.80	23	-21.45	24.69	60	-19.91	33.53	97	-17.41	42.11
2	-15.90	23.84	24	-21.42	24.93	61	-19.86	33.76	98	-17.08	42.05
3	-16.17	23.88	25	-21.38	25.17	62	-19.81	34.00	99	-16.75	41.99
4	-16.44	23.92	26	-21.35	25.41	63	-19.76	34.24	100	-16.43	41.93
5	-16.71	23.96	27	-21.31	25.65	64	-19.70	34.48	101	-16.10	41.86
6	-16.98	24.00	28	-21.28	25.89	65	-19.65	34.71	102	-15.78	41.80
7	-17.25	24.04	29	-21.24	26.13	66	-19.59	34.95	103	-15.46	41.73
8	-17.52	24.08	30	-21.21	26.37	67	-19.54	35.19	104	-15.13	41.66
9	-17.80	24.11	31	-21.17	26.61	68	-19.48	35.42	105	-14.81	41.59
10	-18.07	24.15	32	-21.14	26.85	69	-19.42	35.66	106	-14.49	41.53
11	-18.34	24.19	33	-21.10	27.09	70	-19.37	35.90	107	-14.17	41.46
12	-18.61	24.22	34	-21.06	27.33	71	-19.31	36.13	108	-13.85	41.39
13	-18.88	24.26	35	-21.02	27.56	72	-19.25	36.37	109	-13.53	41.31
14	-19.15	24.29	36	-20.99	27.80	73	-19.19	36.61	110	-13.21	41.24
15	-19.42	24.33	37	-20.95	28.04	74	-19.13	36.85	111	-12.90	41.17
16	-19.70	24.36	38	-20.91	28.28	75	-19.07	37.08	112	-12.58	41.09
17	-19.97	24.40	39	-20.87	28.52	76	-19.01	37.32	113	-12.26	41.02
18	-20.24	24.43	40	-20.83	28.76	77	-18.95	37.55	114	-11.95	40.94
19	-20.51	24.46	41	-20.79	29.00	78	-18.88	37.79	115	-11.63	40.87
20	-20.78	24.49	42	-20.75	29.24	79	-18.82	38.03	116	-11.32	40.79
21	-21.06	24.53	43	-20.70	29.48	80	-18.75	38.26	117	-11.00	40.71
22	-21.33	24.56	44	-20.66	29.71	81	-18.69	38.50	118	-10.69	40.63
			45	-20.62	29.95	82	-18.62	38.73	119	-10.38	40.55
			46	-20.58	30.19	83	-18.56	38.97	120	-10.07	40.47
			47	-20.53	30.43	84	-18.49	39.21	121	-9.76	40.39
			48	-20.49	30.67	85	-18.42	39.44	122	-9.45	40.31
			49	-20.44	30.91	86	-18.35	39.68	123	-9.14	40.22
			50	-20.4	31.15	87	-18.28	39.91	124	-8.83	40.14
			51	-20.35	31.38	88	-18.21	40.15			
			52	-20.31	31.62	89	-18.14	40.38			
			53	-20.26	31.86	90	-18.06	40.62			
			54	-20.21	32.1	91	-17.99	40.85			
			55	-20.16	32.34	92	-17.92	41.09			
			56	-20.11	32.57	93	-17.84	41.32			
			57	-20.06	32.81	94	-17.76	41.56			
			58	-20.01	33.05	95	-17.69	41.79			
			59	-19.96	33.29	96	-17.61	42.03			

Table 6.2 OCCAM Med Box station coordinates.

iii Vertical Grid Configuration

OCCAM is a level model with 36 levels in the vertical, ranging from 20 m thickness near the surface to 255 m at 5500 m depth (detailed in Table 6.3). These layers were chosen to best represent the mixed layer, the thermocline, and the topography of the deep ocean. The top layer includes the Ekman transport, and due to the model configuration bottom triangles do not need to be considered.

The model has a free surface, with the sea surface height defined at each position by a variable. This must be allowed for in any calculations involving area or depth. Two additional variables, kmt and kmu, indicate the deepest layer containing data for tracers and velocities respectively at each grid position. A kmt value of 6 would indicate that the top 6 layers are within the water column, while layers 7 to 36 below the sea bed should contain null data. These variables are necessary to distinguish real data from the zeros used to indicate null data.

Level	Tracer point depth* (m)	Tracer box thickness (m)	Level	Tracer point depth* (m)	Tracer box thickness (m)
1	9.87	20.00	19	1326.01	183.09
2	30.43	21.20	20	1515.91	196.29
3	52.35	22.75	21	1718.17	207.81
4	76.05	24.77	22	1931.09	217.60
5	102.04	27.37	23	2152.96	225.75
6	130.97	30.70	24	2382.21	232.40
7	163.67	34.94	25	2617.43	237.74
8	201.13	40.28	26	2857.42	241.99
9	244.55	46.92	27	3101.18	245.33
10	295.34	55.05	28	3347.89	247.93
11	355.07	64.84	29	3596.89	249.95
12	425.44	76.35	30	3847.67	251.51
13	508.18	89.53	31	4099.82	252.71
14	604.87	104.18	32	4353.01	253.63
15	716.83	119.95	33	4607.02	254.33
16	844.91	136.30	34	4861.63	254.87
17	989.43	152.66	35	5116.72	255.28
18	1150.09	168.43	36	5372.17	255.59

Table 6.3

OCCAM vertical grid settings

iv Strait of Gibraltar

In the main run of OCCAM, the Strait of Gibraltar is open and there is no forcing or relaxing of the Mediterranean Outflow. It is controlled, as in reality, by the differences between the water properties of the Atlantic Ocean and Mediterranean Sea. However, as one would expect, there are some significant differences between the real and model Straits of Gibraltar. Unlike in reality, the narrowest and shallowest parts of the Strait are at the same location in the model. The Tarifa Narrows have a real width of 14 km; however, within the model this narrow point can be represented only by a region two grid cells wide (such that there is one velocity point), which is approximately 50 km in the $\frac{1}{4}^{\circ}$ grid. These differences may result in discrepancies between the real and model Outflows and their subsequent spreading in the North Atlantic.

v Model Data Used in the Analysis

Annual averages of each of the last five years of the model runs and 'snapshot' data every 30 days are available. The snapshot data is a glimpse of the model at that particular time, and not an average for the day, week, or month from which it is taken. Unless stated otherwise the 'annual average' used here is the average of the final year (twelve 30-day snapshots) of the model experiment. Snapshot data from the final year are used to investigate variability. This data is referred to by season rather than the particular day, the snapshot used being representative of that season. The data used are day 9240 (19 April 25; Spring), day 9330 (18 July 25; Summer), day 9060 (21 October 24; Autumn), and day 9150 (19 Jan 25; Winter).

6.3 DEFINING MEDITERRANEAN WATER

The great advantage of the closed-Strait run is that it provides a means of identifying MW in the open-Strait run. The method used is to calculate the salinity difference, saldiff (where saldiff = $\text{salinity}_{\text{openStrait}} - \text{salinity}_{\text{closedStrait}}$), between the two experiments, and define MW to have a saldiff value greater than a certain limit. This method is chosen because the only difference between the two experiments is the lack of the Mediterranean Outflow in the closed-Strait run.

The saldiff contours for the Med Box using averaged data from the last year of the model runs are shown in Figure 6.4. Station number is given on the x-axis, where station 1 is the southwest corner, and station 124 is the northwest corner (Figure 6.3). The vertical lines show the positions of the corners. These figures can be interpreted by considering a perspective from within the box, looking first to the south, then to the west and then to the north.

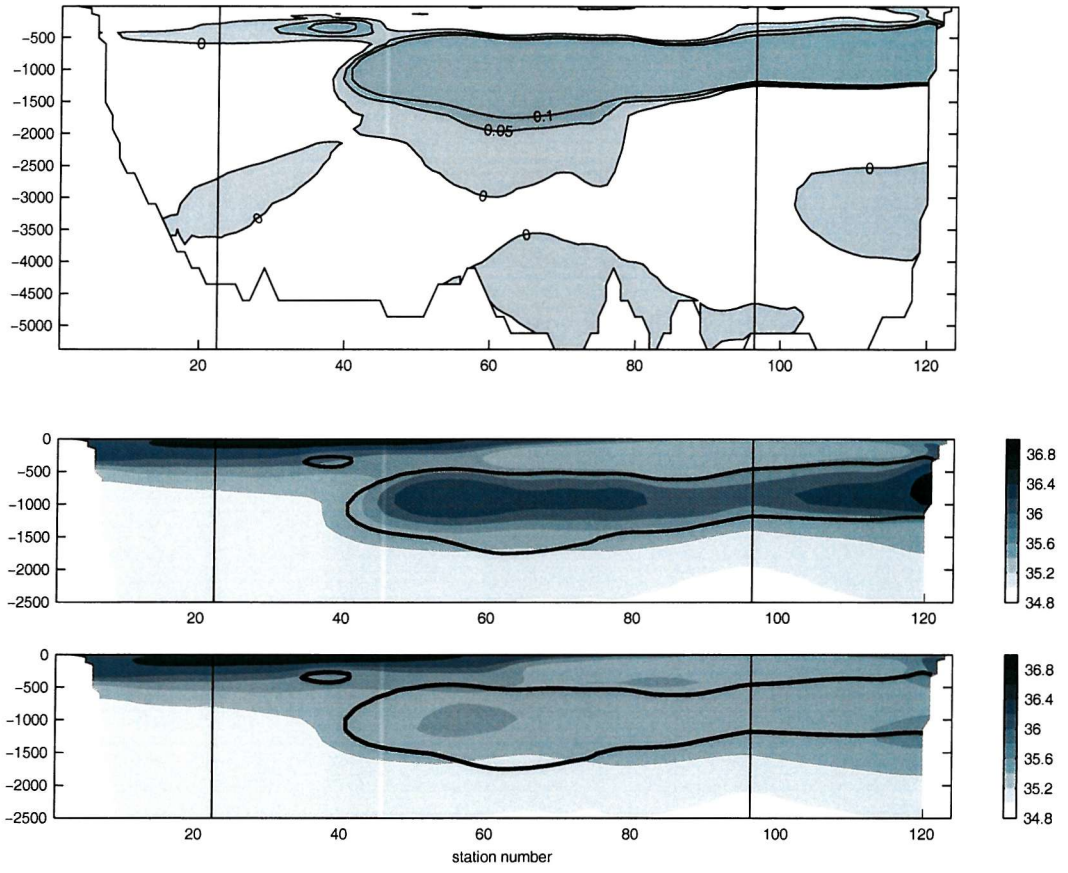

Figure 6.4 *Definition of Mediterranean Water (OCCAM Annual Average Med Box) using saldiff, the salinity difference between the main run and the closed-Strait run. (a) salinity difference (saldiff = open Strait salinity – closed Strait salinity), (b) salinity (open Strait run), and (c) salinity (closed Strait run), both with the 0.1 saldiff contour shown in black.*

The limit to define MW was taken to be 0.1. A MW definition based on the zero saldiff contour would not be robust because small differences between the two model experiments (outside of the MW) will arise purely due to variability between model runs. For this reason, the zero contour encompasses a larger area than could be defined to be MW (Figure 6.4a). The use of saldiffs larger than 0.1 ensures that the salinity differences considered are those due to the MW.

The two lower plots in Figure 6.4 show salinity contours for the main run and the closed-Strait run respectively, with the threshold saldiff contour overlaid. These plots highlight the difference between the two model experiments and also the remnants of high salinity MW in the closed-Strait run (Figure 6.4c).

The salinity profiles and θ/S plots for the Med Box and each of its sides individually (with MW highlighted; Figure 6.5) illustrates how the MW definition could have been made using a θ/S curve, a popular way of defining water masses. There is no MW on the southern boundary, or on the western boundary south of station 40 at 29°N. North of this latitude however, MW exclusively occupies the mid-depths of the water column. There is an interesting feature between 260 and 420 m depth, stations 35 to 41 (27.6°N to 29°N), on the western edge of the box, which is highlighted in black in Figure 6.5. There must be a link between this water and the Mediterranean Outflow but it is assumed this is not MW for the purpose of calculating fluxes of MW across each boundary.

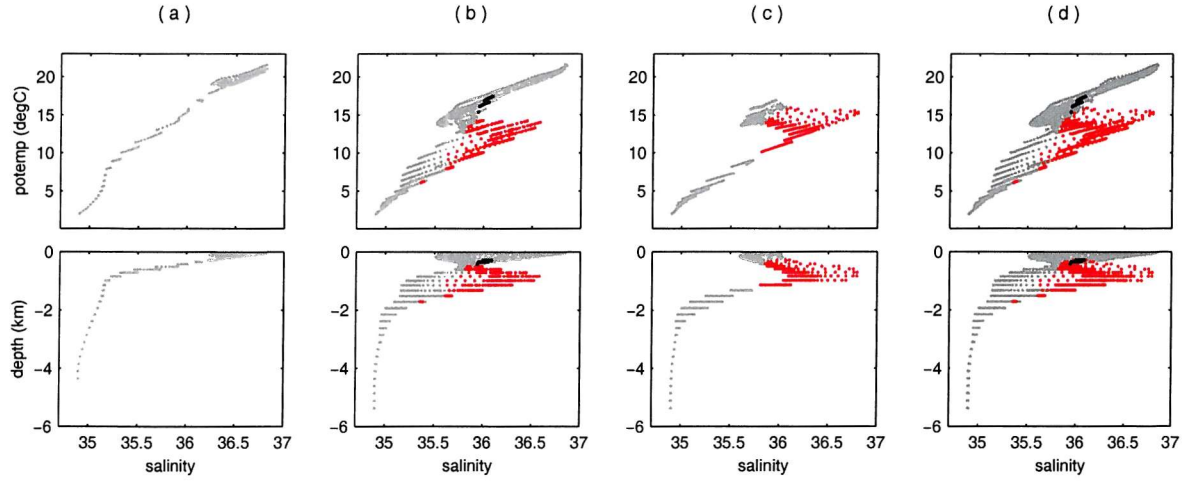

Figure 6.5 *θ/S plots (top row) and salinity profiles (bottom row) for the OCCAM Annual Average Med Box: (a) southern side; (b) western side; (c) northern side; and (d) whole box. Red shows water defined as Mediterranean Water using the 0.1 saldiff limit.*

6.4 THE MEDITERRANEAN OUTFLOW

6.4.1 Exchange at the Strait of Gibraltar

Hydrographic observations show that the exchange can be approximated by a two-layer flow. North Atlantic Central Water flows into the Mediterranean above outflowing denser and more saline Mediterranean Water. As reviewed in Chapter 2, the net flow into the Mediterranean has been calculated to be approximately 0.04 Sv (Bryden et al., 1994), which is the sum of the net evaporation and river run off over the Mediterranean Basin. The overturning is just under 1 Sv (0.76 Sv of inflowing Atlantic Water and 0.72 Sv of outflowing MW).

In OCCAM, the Strait of Gibraltar at its narrowest is two grid cells wide and 324 m deep (10 layers). The top 7 layers are always inflowing Atlantic Water, and layers 8, 9 and 10 are always outflowing MW. Figure 6.6 shows velocity and property profiles at the Strait of both annual average data from the last year (year 24 to 25) of the model run (black), and data from day 9000 (August, year 24; grey). It can be seen that the overturning circulation is just over 1 Sv, slightly higher than would be expected in the real world. The high salinity and temperature of the outflowing MW is evident, and the interface between the two water masses is well defined by a density of approximately 27.3 Kg m^{-3}. The snapshot data is very slightly different from the annual average case, indicating that there is variability in the outflow.

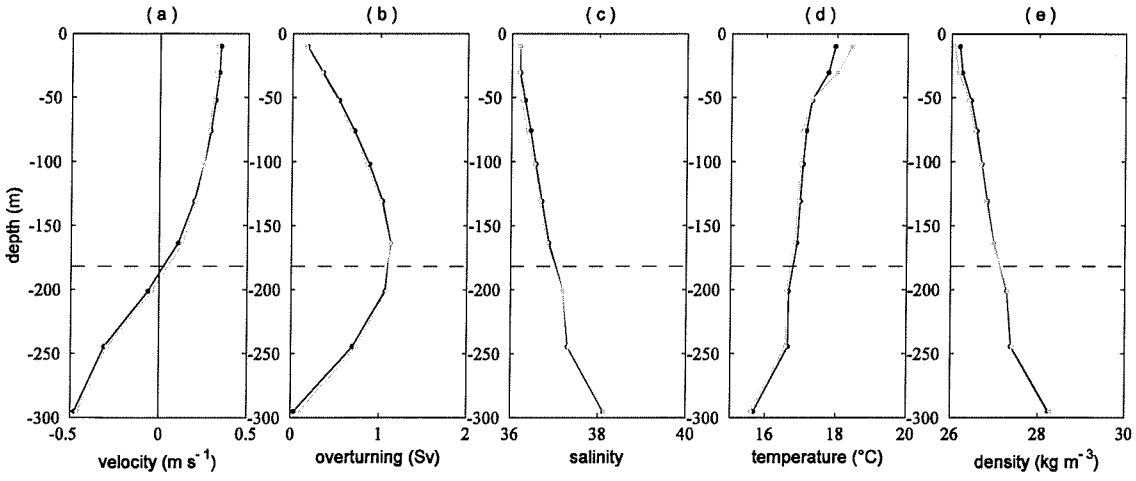

Figure 6.6 *Annual average profiles at the Strait of Gibraltar from the last year of the model run (black) and day 9000 (grey) of: (a) eastward along-Strait velocity, (b) overturning, (c) salinity, (d) potential temperature, and (e) potential density. The dashed line represents the interface between inflowing Atlantic Water and outflowing Mediterranean Water at the bottom of layer 7.*

The variability of the exchange, along with the outflowing MW properties are shown in Figure 6.7. There is evidence of a strong annual cycle in all transports and water properties, indicating that the wind field is a dominant forcing mechanism in the model. The Mediterranean Outflow transport varies by 0.4 Sv, being weakest in August (~1 Sv) and strongest around January (~1.4 Sv). To balance this, the Atlantic Water inflow is also strongest in winter and weakest in summer. The net flow into the Mediterranean through the Strait varies between 0.13 and –0.03 Sv, with annual means in the last 5 years of 0.036, 0.034, 0.035, 0.035, and 0.035 Sv. These mean values compare very favourably with the estimate of 0.04 Sv (Bryden et al., 1994). This seasonal variability in Outflow transport may result in a variability in the MW transport across specific lines of latitude and longitude in the North Atlantic, discussed later.

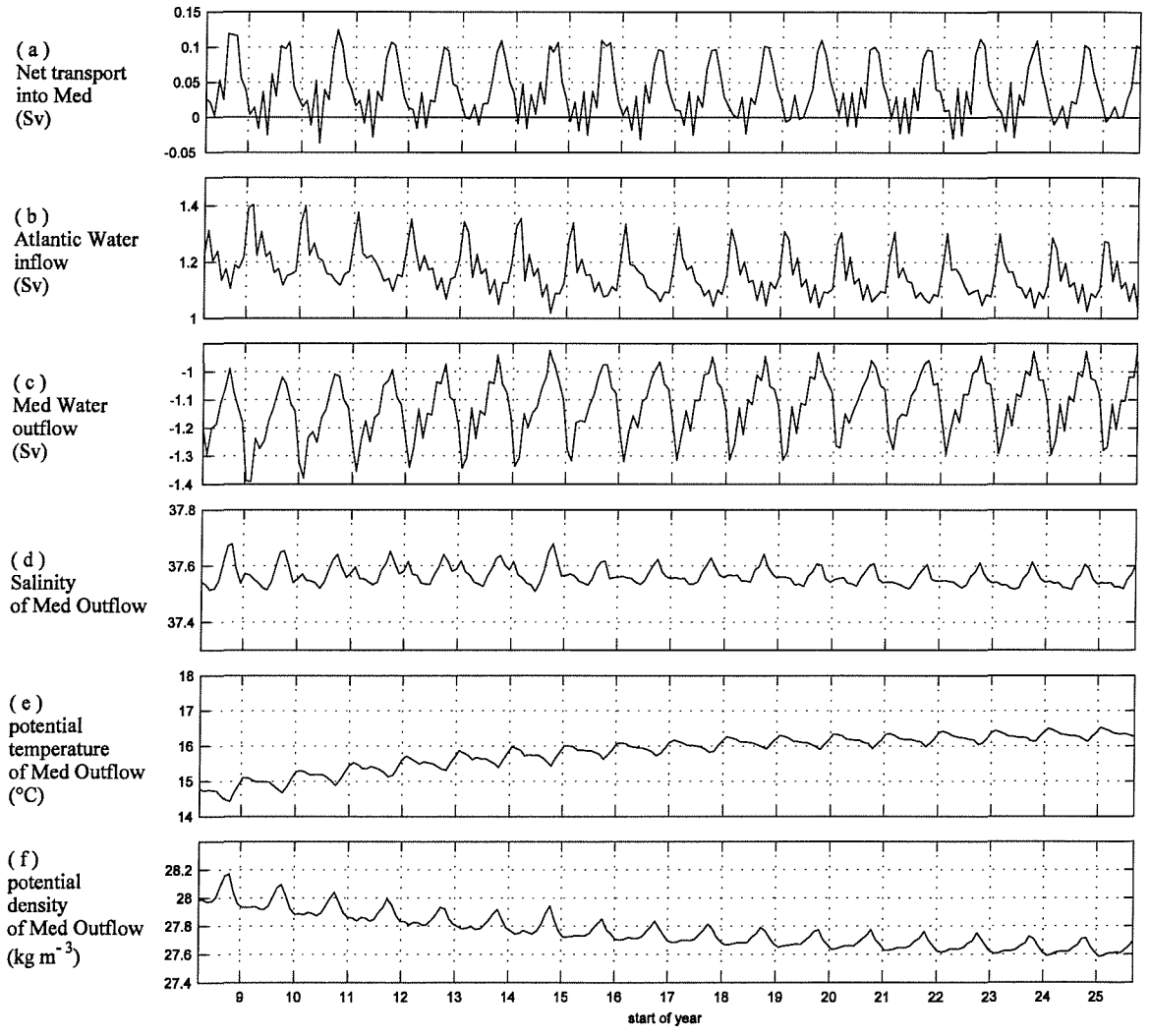

Figure 6.7 *Time series at the Strait of Gibraltar of (a) net transport into the Mediterranean, (b) Atlantic Water inflow, (c) Mediterranean Water outflow, (d) salinity* of the Mediterranean Outflow, (e) potential temperature* of the Mediterranean Outflow, and (f) density* of the Mediterranean Outflow. (* mean properties; area averaged).*

6.4.2 Model Stability

An obvious feature of Figure 6.7 is the increase in temperature of the outflow over time, leading to a decrease in density. This is due to model drift, and results in the MW in the North Atlantic becoming shallower over time. Figure 6.8 demonstrates this effect, showing a snapshot of a section at approximately 41°N, from 17°W into the coast of Portugal, every 3 months from day 3000. The main core of MW, with salinities greater than 36.4, is initially centered just below 1000 m, and rises to stabilize at a depth of 750 m after approximately six years. The maximum salinity increased from below 36.4 to above 36.4 from day 3000 to day 5520.

Figure 6.9 shows the same time series, but for the closed-Strait run of the model. The first subplot is identical to that in Figure 6.8 since the Strait was closed on day 3000. The MW tongue does not get shallower, instead it becomes weaker over time. Evidence of the higher salinity water of Mediterranean origin is still apparent after 7 years. This is probably due to a change in the circulation after the Strait was closed such that MW remnants are only slowly being eroded away.

The question of 'stability' should be considered when looking at models. Looking at salinity at a few different places (Figure 6.10) can give an indication of whether the model has attained a stable state. Within the core of the MW, at positions 1, 2 and 3, although seasonal variability in the salinity is seen, there is no change in the annual mean value within the last eight years. The seasonal variability at position 3 is very high (~0.4 in salinity), which must be due to variability in the position of the flow. At these 3 positions, in the closed-Strait run, the salinity is slowly but steadily decreasing over time (by ~0.01 per year). At position 4, there is only a very minor seasonal signal, and the high salinity here is possibly due to diffusion rather than direct advection. The closed-Strait run salinity is still decreasing at a rate of ~0.03 per year at the end of the model run. The salinity in the main run at position 5 is increasing by ~0.07 per year, whereas in the closed-Strait run it has been stable for the last 7 years. Position 6 is obviously well outside any influence of MW, the salinity is stable and the same in both model experiments.

In general, these results seem to show that the main run of the model has reached a stable state within the area of the Med Box, although there may be one or two exceptions (such as position 5). The closed-Strait run, however, is not yet in steady state, with remnants of MW slowly decreasing in salinity within the Med Box.

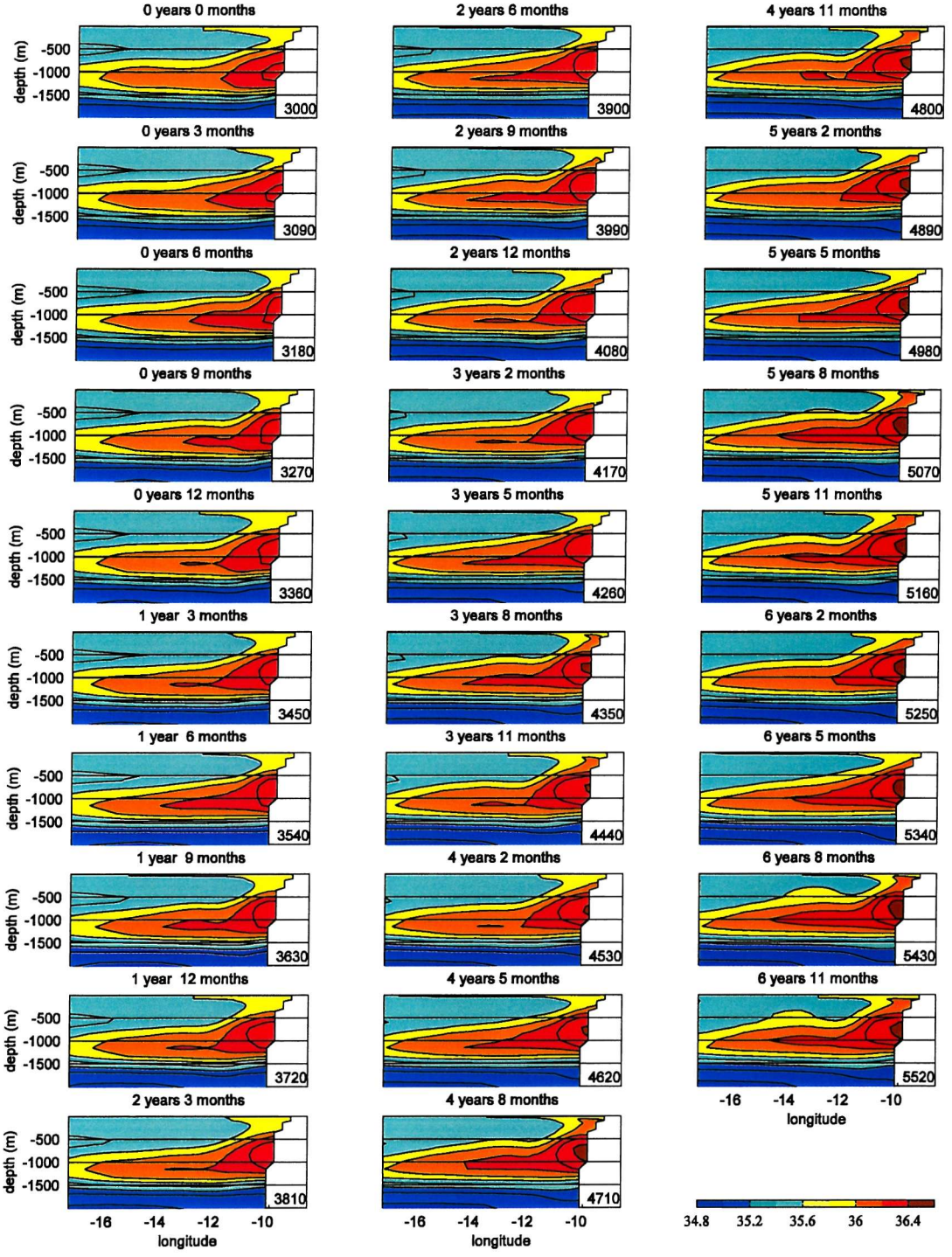

Figure 6.8 *Time series of salinity contours in the upper 2000 m of the main OCCAM run on a section at ~41°N, from 17°W into the coast of Portugal. Data are from snapshots on the days indicated in the bottom right of each plot, with time in years and months since day 3000 shown above.*

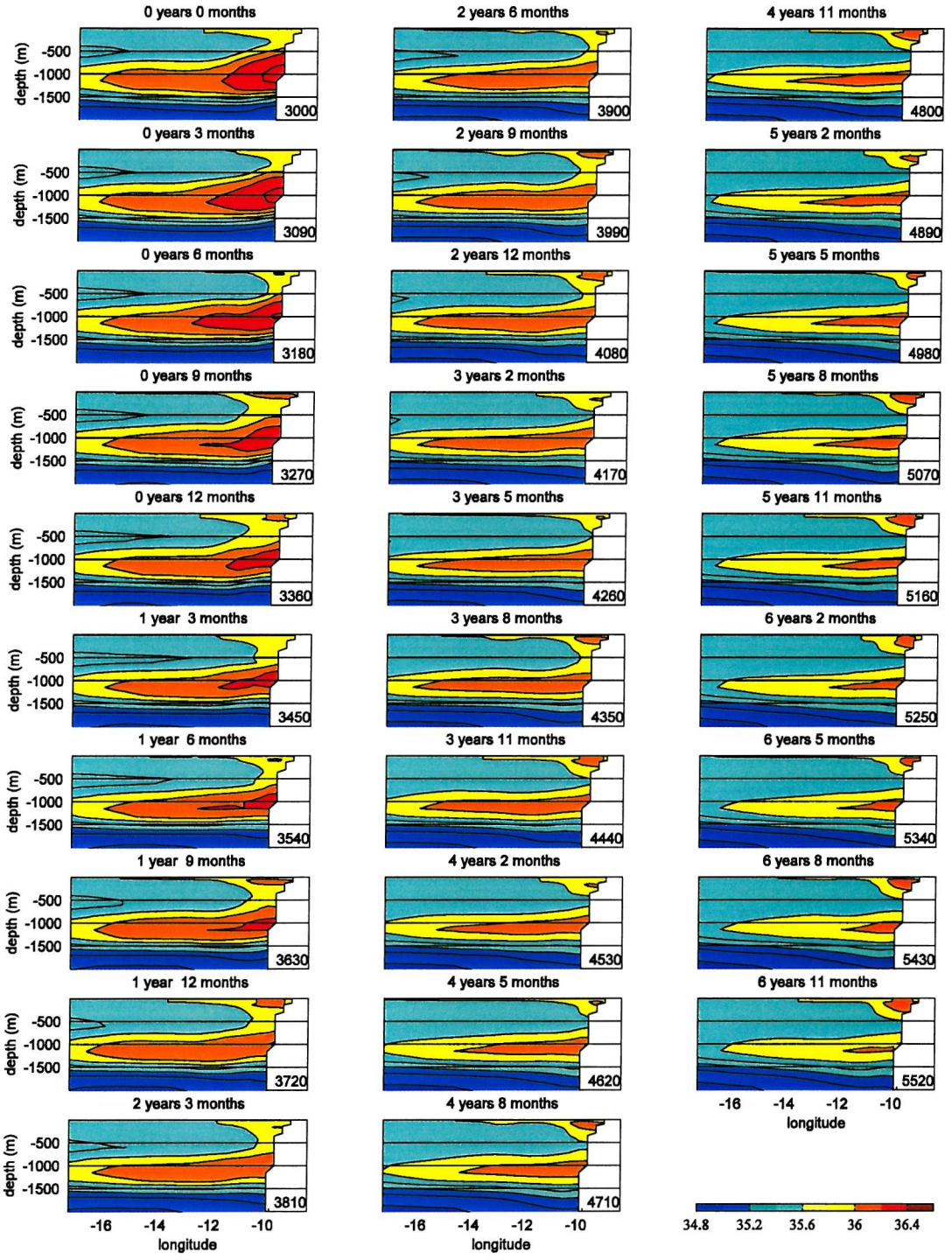

Figure 6.9 *Time series of salinity contours in the upper 2000 m of the OCCAM run with Strait of Gibraltar closed on a section at ~41°N, from 17°W into the coast of Portugal. Data are from snapshots on the days indicated in the bottom right of each plot, with time in years and months since day 3000 shown above.*

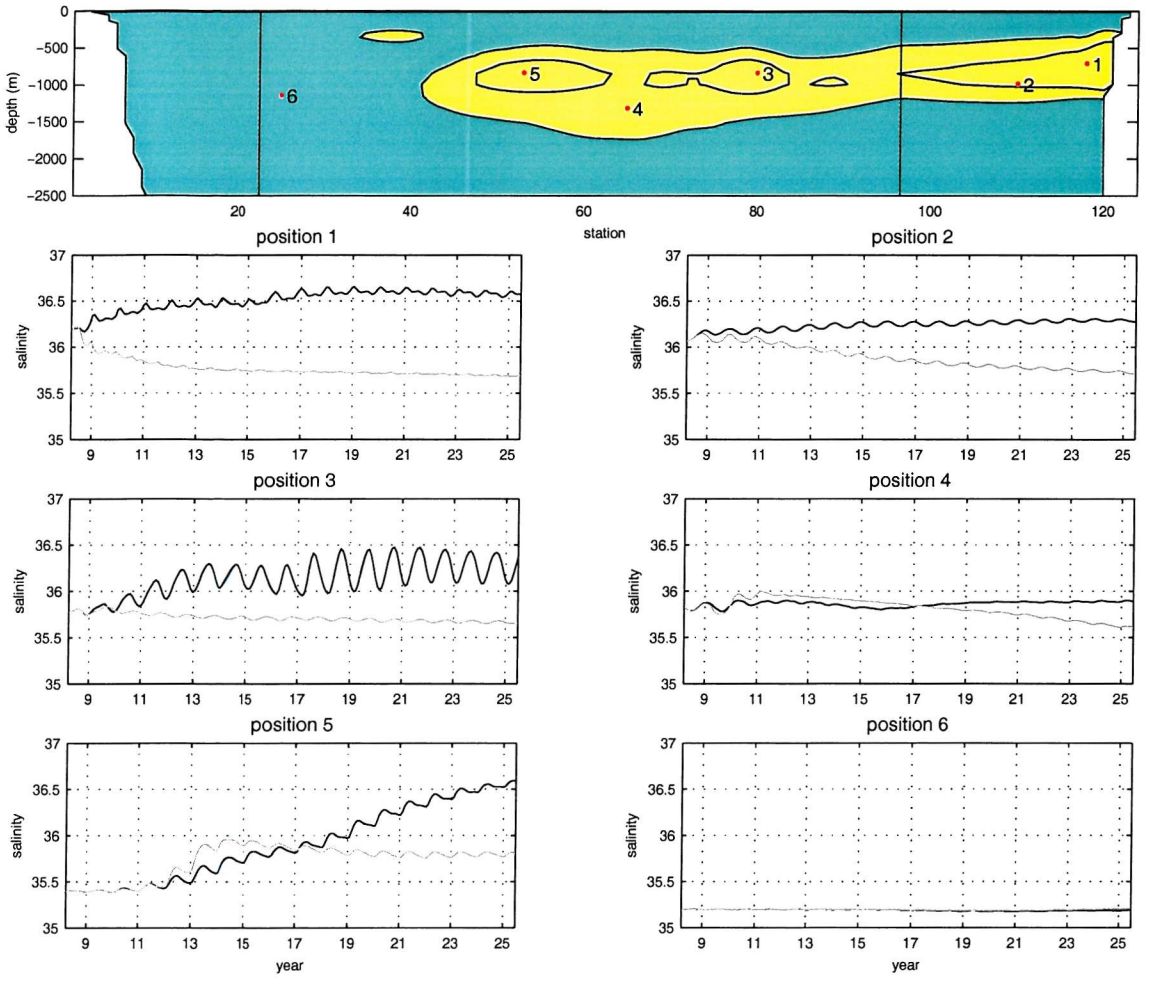

Figure 6.10 *Salinity change over time at different positions around the Med Box. Black is main OCCAM run, grey is closed-Strait run. Top plot shows positions used.*

6.5 CIRCULATION

6.5.1 Initial Mediterranean Water Spreading

The outflowing MW mixes intensely with the North Atlantic Water in the Gulf of Cadiz, and descends to depth in the eastern North Atlantic, centred on model level 16 at 845 m. This can be seen in Figure 6.11 which shows data in the top 2000 m of the water column along a section at roughly 20°W, shown in red on the map. Both salinity (6.11a) and saldiff (6.11b) contours are shown, highlighting the fact that this is MW as the higher salinities have positive saldiff values, and hence are not present in the closed-Strait run. The profiles in Figures 6.11c and 6.11d show the mean saldiff for this section versus depth and model level respectively. The positive saldiff values are seen lying between 500 and 1600 m, model levels 13 to 20, with the largest anomalies centred at about 900 m, levels 16 and 17.

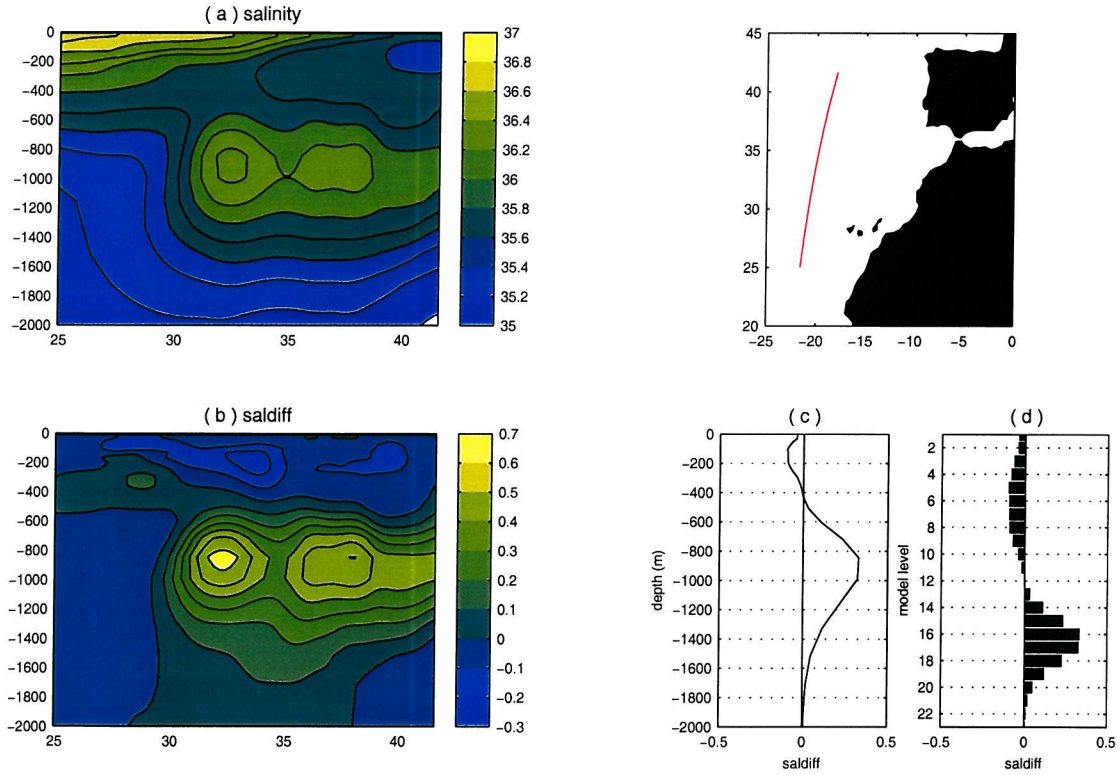

Figure 6.11 *Annual average data from a quasi-meridional section along ~20°W (shown in the map). (a) salinity and (b) saldiff contours in the upper 2000 m of the section. Also shown is the mean saldiff profile versus (c) depth and (d) model level.*

This westward route is just one of the pathways the MW takes as it leaves the Gulf of Cadiz. Figure 6.12 shows annual average salinity and saldiff contours as well as velocity vectors at model level 16 (845 m). Water flows mainly westward out of the Strait of Gibraltar along the northern

boundary of the Gulf of Cadiz as far as Cape St Vincent. The velocities decrease markedly at this point and the flow divides, some to flow northwards along the Portuguese coast, and the remainder flowing due west. Part of this westward flow recirculates back into the Gulf of Cadiz and then flows to the southwest joining a direct southwestward flow from the Strait. From velocity data (Figure 6.12a) the initial southwestward flow, which turns towards the west at about 15°W, appears to be the main pathway of the MW. However, it is apparent from the salinity and saldiff contours (6.12b and c) that the routes to the north and west are at least equally as important. In fact, the saldiff contours suggest that these two routes carry most of the salinity signature from the Mediterranean. As far as the velocities are concerned, there would appear to be a need to examine the pathways at different times of year, which will be undertaken in section 6.5.3.

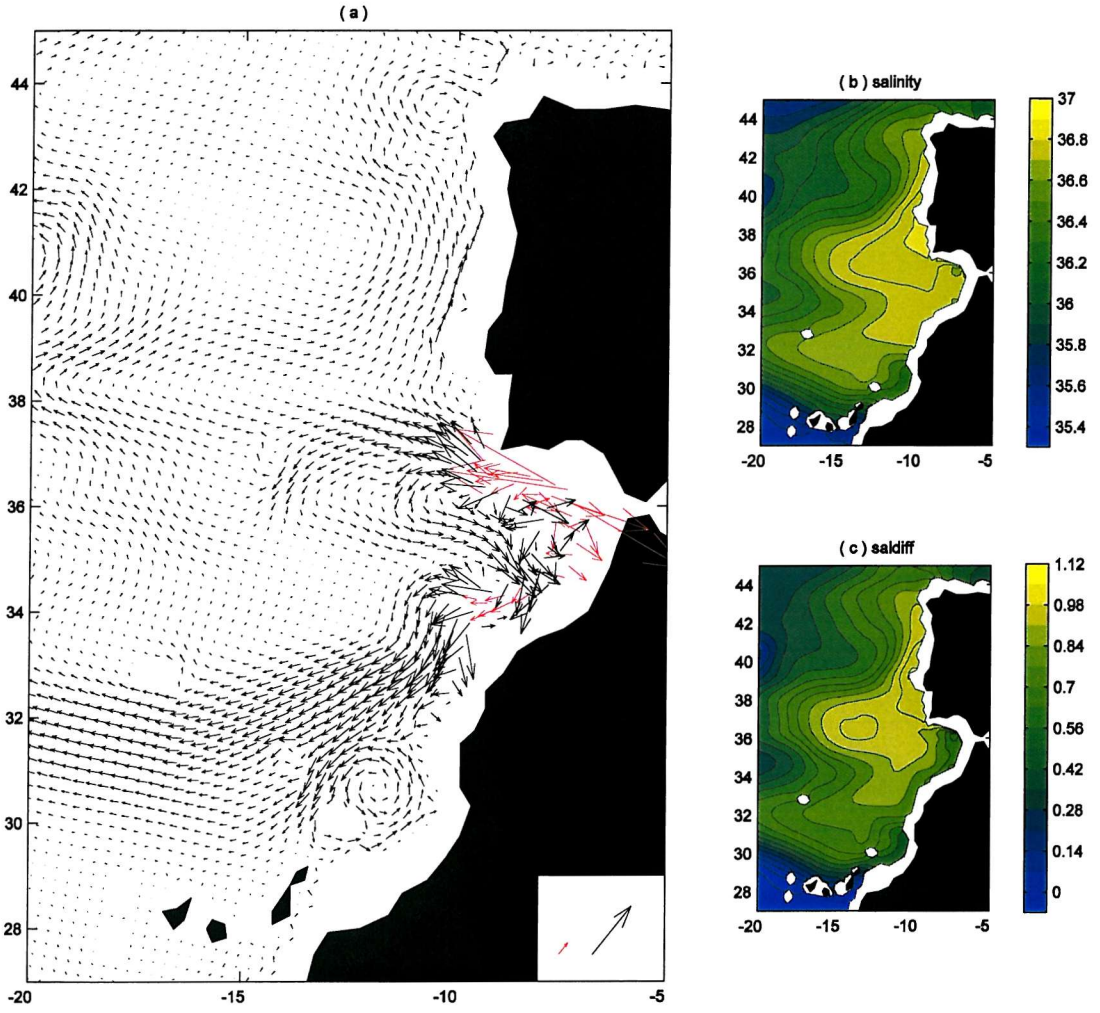

Figure 6.12 *Initial pathways the MW takes as it leaves the Gulf of Cadiz, shown by (a) velocity vectors, where the arrows in the key are 4 cm s^{-1}, (b) salinity contours and (c) saldiff contours. Data shown is the average from last 5 years of the model runs, level 16 (845 m).*

6.5.2 Annual Average Med Box Circulation

Before investigating the variability of the circulation, it is sensible to look at the annual average case. Figure 6.13 shows transport profiles for the whole Med Box (6.13d) and each side individually; (a) southern edge, (b) western edge, and (c) northern edge. It must be noted that the y-axis gives model level not depth, and remembered that positive values indicate transports into the box. The profile for the whole box shows that there is a net inflow in the surface layers of 2.64 Sv, and a net outflow at mid-depths, layers 11 to 18 (~300 to 1200 m). This overturning circulation is, as discussed in the hydrography chapter, due in part to the inflow of surface waters to the Mediterranean and the outflow of MW at mid-depths, and in part to the transformation of surface waters to intermediate waters in the Gulf of Cadiz when the Atlantic waters are mixing with and being entrained by the Mediterranean Outflow (Jia, 2000).

The profiles for each side of the Med Box show that effectively all of the surface input to the box is across the western edge. Most of the mid-depth exodus is also across the western edge, between 465 and 1600 m (levels 13 to 20). On the southern section there is surface outflow down to 660 m, with little happening below this level. There is also surface outflow to the north down to 324 m (level 11), inflow in the 3 layers below this, and outflow again between 555 and 915 m (levels 14 to 16; -0.36 Sv), but these are all relatively small. There is also a net inflow across the northern section between 915 and 1616 m (levels 17 to 20) of 0.89 Sv.

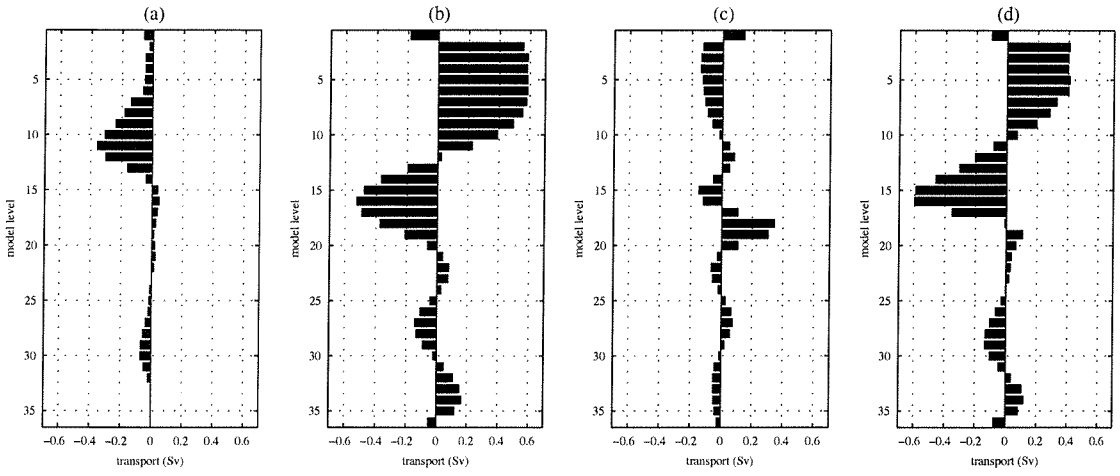

Figure 6.13 *OCCAM Annual Average Med Box transport profiles for the main run. (a) south, (b) west, (c) north, and (d) whole box.*

6.5.3 Variability of the Circulation

The question to ask of this annual average picture of the circulation is how representative is it of the norm? In other words, how much variability is there in the model? This section starts off by looking at the inter-annual variability (using annual averages) and then moves to shorter time scales to examine the seasonal variability (using snapshot data from different months as detailed in §6.2.2) to decide whether or not there is a clear seasonal cycle.

i Annual Variability

To look at the inter-annual variability in the model, Med Box transports are chosen. Figure 6.14 shows contour plots of annual average transport in the top 3000 m of the Med Box for the last 5 years of the model run, with each sub-plot being a different year. What is immediately obvious is that the main features of the circulation remain the same each year, and that there is really very little variability in either the spatial sense or the magnitude of the transports. This is to be expected because as mentioned earlier (section 6.2.2), the model is forced with winds from the 1986-1988 ECMWF monthly climatology (the same wind field each year). So as stated, there is no true inter-annual variability in the system, and this is upheld by Figure 6.14.

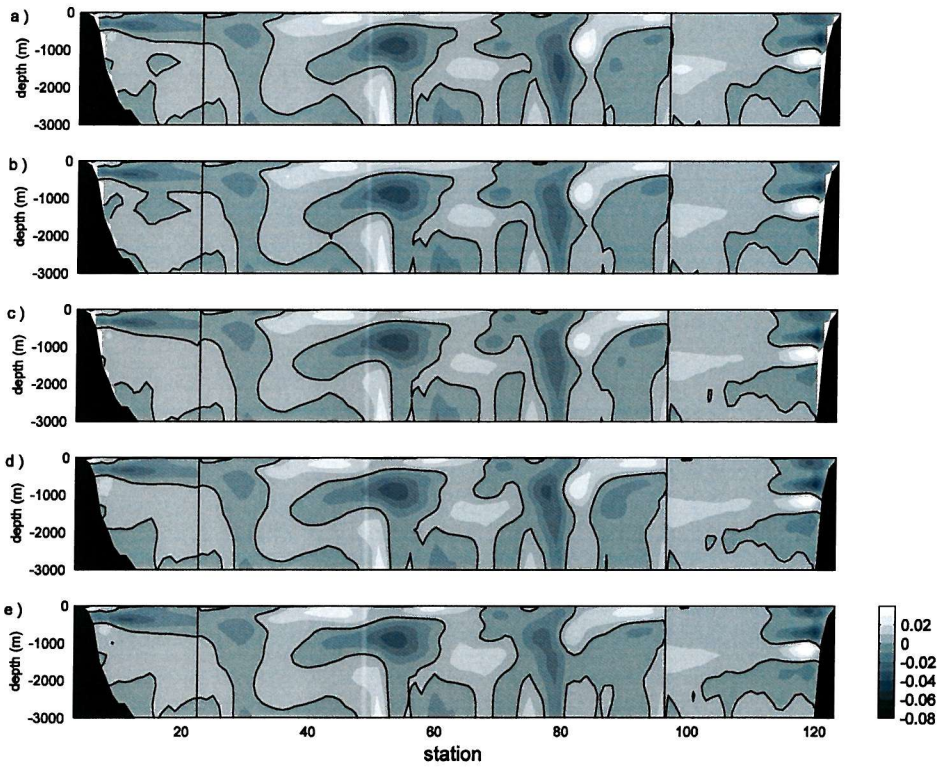

Figure 6.14 *OCCAM Med Box transport in the upper 3000 m for the annual average of each of the last five years of the open-Strait experiment; (a) July 20 – June 21, (b) July 21 – June 22, (c) July 22 – June 23, (d) July 23 – June 24, and (e) July 24 – July 25.*

ii Seasonal Variability

An investigation into seasonal variability commences with a look at the circulation at model level 16 (845 m depth) during each season. Figure 6.15 shows velocity vectors overlying salinity contours for a) Spring, b) Summer, c) Autumn, and d) Winter. These snapshot views of the circulation can be compared with the annual average shown in Figure 6.12.

At all times of year, the southwestward pathway of MW can be seen, although it varies slightly in position by a degree or so. Throughout most of the year there is a cyclonic recirculation which splits off from this southwestward flow at 31°N 12.5°W against the coast, which is also shown by the salinity contours. It is only in winter when the recirculation is not present, because part of the flow remains against the coast.

In none of the figures does a direct westward pathway from Cape St Vincent appear obvious, rather the high salinity signal is advected westward by an indirect route which includes a number of recirculations. These recirculations are certainly too large to be called eddies. In Spring (Figure 6.15a) there is a strong anticyclonic flow or recirculation centered at 22°W, 37.5°N. This flow is positioned at an extrusion of the high salinity and is following the salinity contours. There is probably a feedback process occurring here, where the anticylconic flow is enhanced due to the 'bulging' of the salinity contours, which in turn enhances the extrusion of the high salinity northwestwards. This occurrence of the flow following the isohalines can also be seen slightly further north. The number of these large recirculations and their exact locality varies slightly throughout the year. Although there is no obvious westward pathway at any particular time, the recirculations within the model are obviously playing an effective role in transferring the high salinity MW to the west between ~35 and 40°N.

The northward flow along the Portuguese continental slope at 845 m depth exhibits some surprising properties. In the Spring (Figure 6.15a) the flow is very narrow and is right up against the slope. There is also a slightly weaker but wider return flow to its west. In Summer (6.15b) the northward flow is stronger and wider, still pressed up against the slope, and with a stronger return flow. The northward flow does not appear to extend beyond ~44°N at this depth. In Autumn (6.15c) the strongest part of the northward flow has started to move away from the slope, has strengthened considerably and is over three degrees in width. The flow now appears to be rounding Cape Finisterre and at least some of it follows the northern coast of Spain towards the east. The southward return flow is very weak, and is centred now at 15°W.

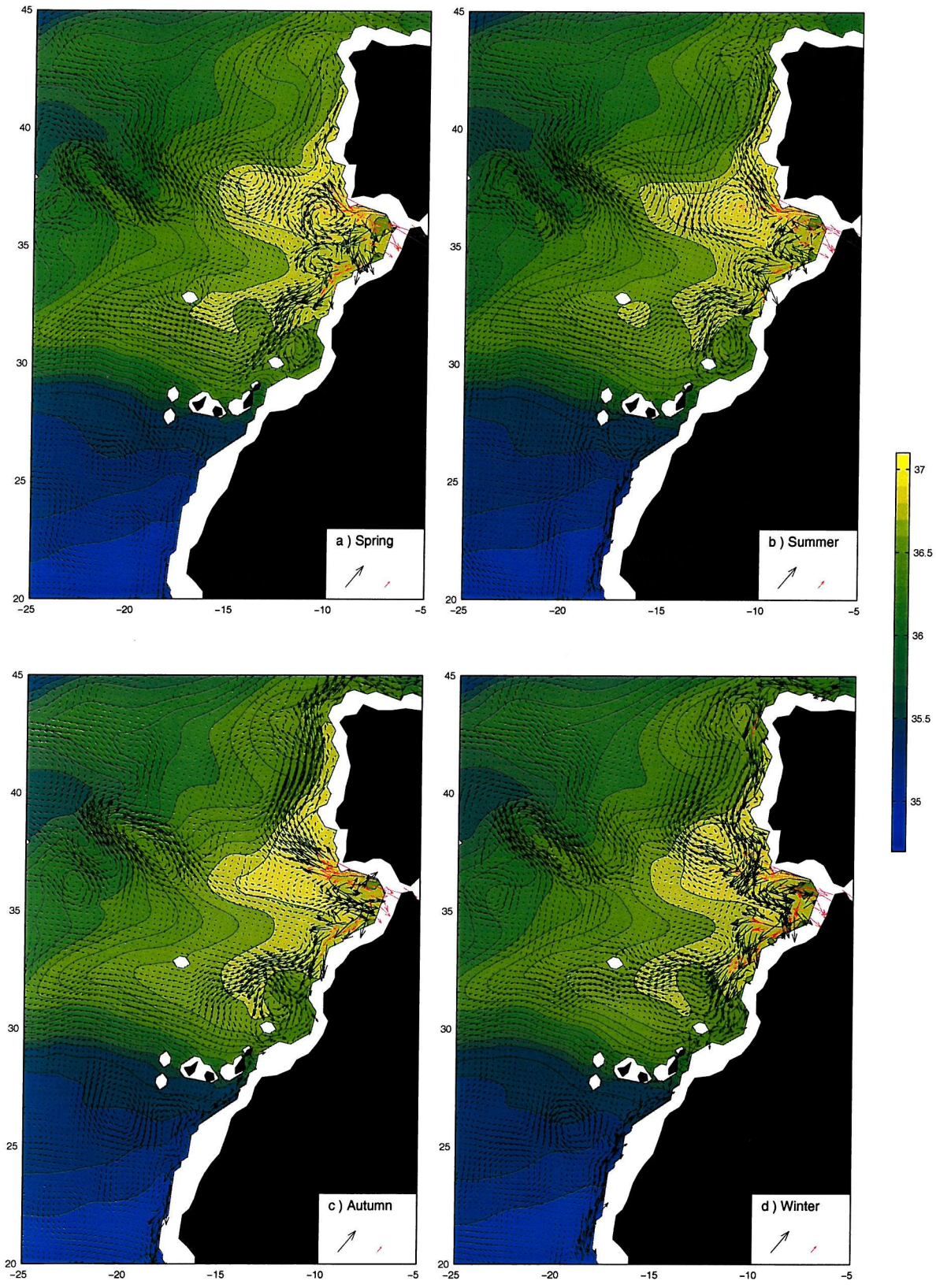

Figure 6.15 *OCCAM velocity vectors overlying salinity contours at level 16 (845 m) in the open-Strait experiment. (a) Spring, (b) Summer, (c) Autumn, and (d) Winter. Keys show arrows of 4 cm s^{-1}.*

The main surprise comes in the winter (6.15d) when the flow appears to reverse completely. There is now a strong southward flow against the slope and the northward flow is right offshore. This leads to a bulging of the isohalines towards the north between about 12°W and 14°W. Throughout the year, until the winter season, the high salinity isohalines against the continental slope can be seen extending further northwards with the increasing northward flow, however, in the Winter they retract southwards in response to the southward flow of lower salinity waters from the north.

The question now is, how far throughout the water column does this circulation pattern extend? Figure 6.16 shows velocity contours in the upper 2000 m along a section at approximately 42°N (shown in red on the map). Data from the annual average as well as each season are shown. As is immediately obvious, the flows extend most of the way throughout the top 2000 m. It is possible to see how the northward flow that is against the slope and relatively narrow in the Spring, strengthens and becomes wider in the Summer, and extends throughout the top 2000 m. In the Autumn, the core of the flow has moved offshore and again there is an increase in its width. Its core speed has also increased to 2.8 cm s^{-1}. By mid-Winter, the northward flow has decreased in strength and moved offshore, displaced by the strong southward flow against the slope which reaches from 300 m downwards, and has speeds up to -4.0 cm s^{-1} at its core. So it does appear that in OCCAM, in the winter, there is a complete reversal of the along-slope flow below 300 m, and that the velocity field at 845 m depth (shown in Figure 6.15) is representative of this part of the water column.

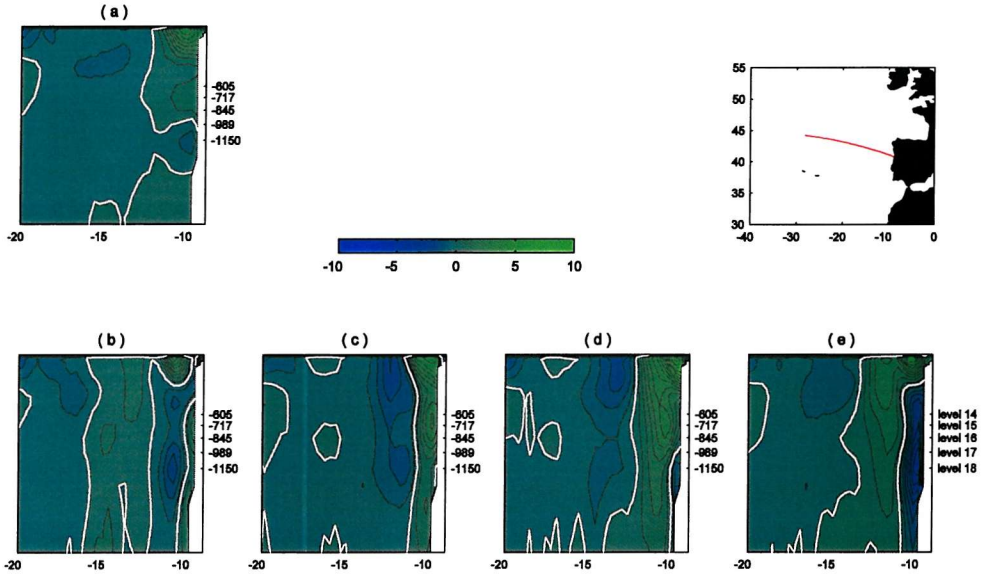

Figure 6.16 *Northward velocity in the upper 2000 m along a section at approximately 42N (shown on the map) for (a) Annual Average, (b) Spring, (c) Summer, (d) Autumn, and (e) Winter. The zero contour is highlighted in white, and then every 0.5 cm s^{-1}s are contoured. The depth of layers most relevant to MW transport at this location are labeled.*

It is interesting to see the pattern of velocities and their variability around the box at a specific depth. Figure 6.17 shows velocities at 717 m (level 15) from every snapshot (once every 30 days) in the final 3 years of the model run. The top figure shows all the data together, with each year in a different colour. It is obvious that the majority of the variability occurs in 3 places; against the African continental slope (station 8) and against the Portuguese continental slope (station 120), where in both places the velocities switch from positive to negative over the course of the year, and between stations 68 and 90 (which are between 35 and 40°N on the western side). The sub-plots below show the data split up by month. Within each of these sub-plots, in other words during each month, the data are very similar, further supporting the fact that there is almost no inter-annual variability in the model.

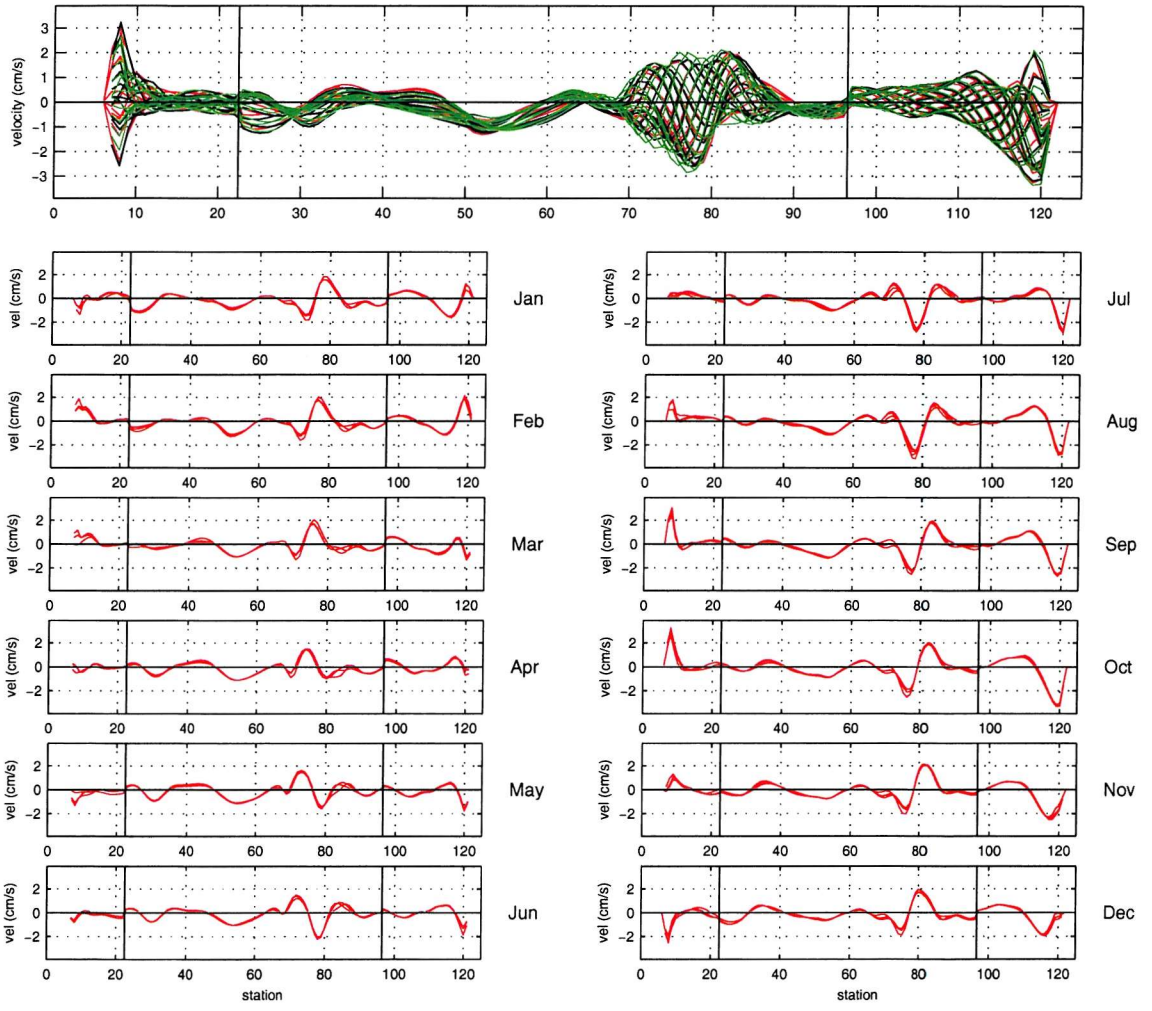

Figure 6.17 *OCCAM Med Box velocities at level 15 (717 m), monthly snapshot data from the last 3 years of the open-Strait run, with each year shown in a different colour. (a) all data, (b) data split up by month. (p.229 & 230) Positive values represent flow into the Med Box.*

Velocities from the northern edge (stations 97 to 124) show the pattern that is seen in Figure 6.16. However, the progression of northward flow becomes clear as the monthly data is considered. Starting in March, there is a narrow flow with velocities greatest near the boundary. The width and strength of the flow increases with time, with the peak of the flow moving further from the boundary. Maximum strength is attained in October, but the flow moves further west until it is cut off from the boundary by the southward flow in January and February. For most of the year (83%) a northward boundary flow is seen. In March, the northward flow continues to move westward and decrease in intensity as the southward flow moves away from the boundary, until it disappears completely by about July.

The position of the outflowing water across the western edge also appears to vary throughout the year. From May, the peak of the outflow can be followed from station 79 southwards (to lower station number). Flow intensity increases until August and then the velocities decrease until there is no flow left the following May, and the cycle starts again. These effects are very much wave-like in appearance, but are due to the variability of the large recirculations seen in Figure 6.15.

Having determined that there is variability in the velocities, it is useful to examine the change in transport profiles throughout the seasons. These are shown in Figure 6.18, with the Annual Average profiles shown in the left hand column for comparison. Again, it should be noted that the y-axes give model level, not depth, and that positive transports are into the box. For the whole box (top row of figures) there is always net inflow in the surface layers (although of varying magnitude and maximum) and net outflow at mid-depths. The southern section always has outflowing water in the top 15 layers (down to 780 m), below which the circulation is variable. The circulation of the western section down to ~layer 20 is very consistent, with net inflow in the top 11 or 12 layers, and net outflow below, with the greatest transport always in layer 16 (779 to 915 m). Transports below layer 20 show considerable variability. The northern section clearly shows variability in the net transports at each level. There is no distinct, consistent outflow at MW depths as on the western section, and this is due to the occurrence of both northward and southward flows at these depths, as shown in Figure 6.16.

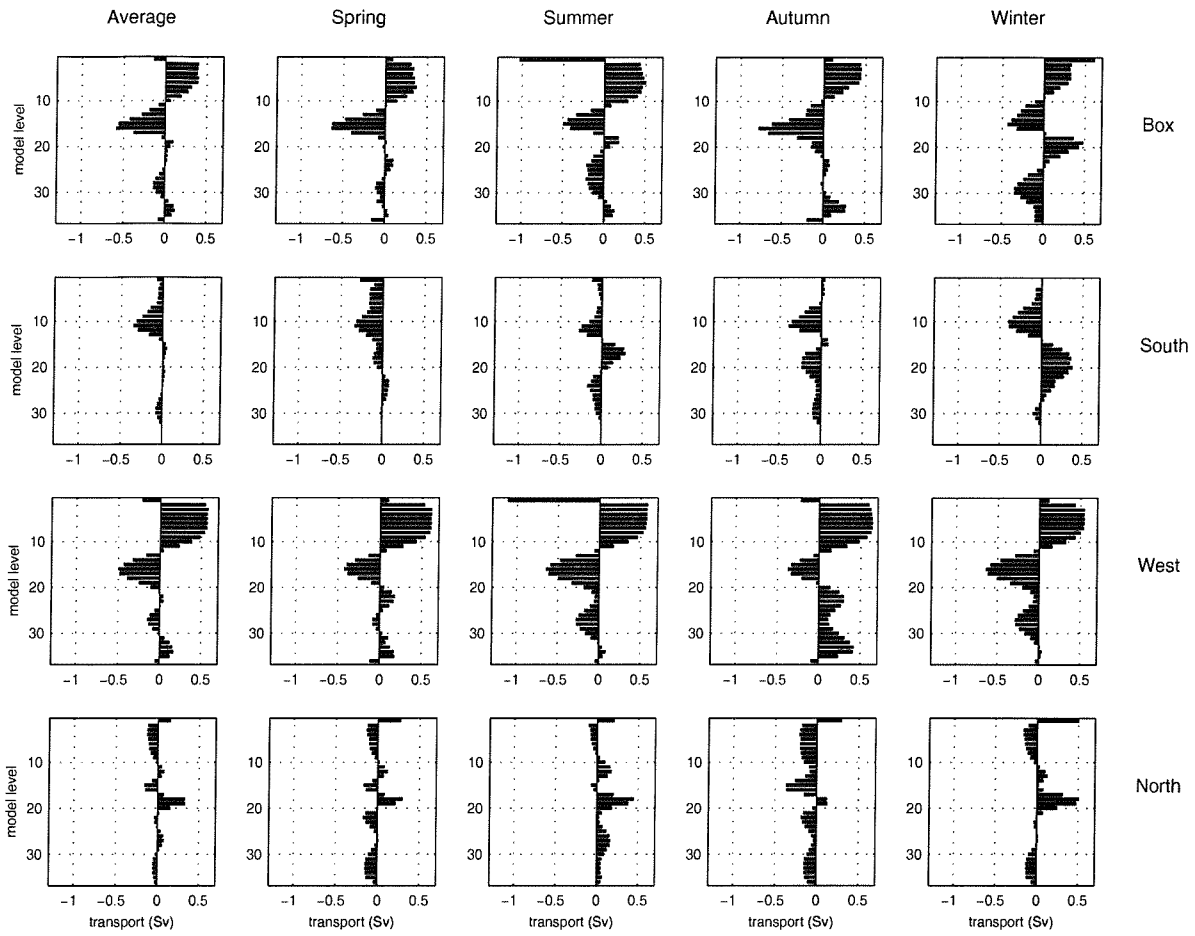

Figure 6.18 *OCCAM Med Box transport profiles for the Open-Strait experiment. The top row of figures are total transports for the whole box, the second row show transports across the southern boundary, the third row show transports across the western boundary, and the bottom row show transports across the northern boundary, with positive transports being into the box. The five columns each show data from a different time; (a) Annual Average, (b) Spring, (c) Summer, (d) Autumn and (e) Winter.*

6.5.4 Effects of the Mediterranean Outflow

An interesting question to address with OCCAM model data is how the presence of the Mediterranean Outflow affects the circulation. This section first considers the Med Box in isolation, and then the effects further afield in the northeast Atlantic.

i Med Box Transports

The effect of the Mediterranean Outflow on transports into and out of the Med Box is shown in Figure 6.19. Profiles of total transport across each side of the box, and the whole box, are shown for both the open-Strait (black) and closed-Strait (red) experiments. A summary of the differences is shown in Figure 6.19e. It is immediately apparent that there is very little difference on the southern section. The western side of the box has a strong inflow in the surface layers in the open-Strait run and a reduced inflow when the Strait is closed. There is considerable difference between levels 14 and 20 (555 to 1616 m); once the Strait is closed, the strong outflow at these depths is significantly reduced, resulting in a net inflow between levels 17 and 20. There is little difference to the net surface transports across the northern box edge, but below level 12 it is a different story. Instead of a net outflow at levels 14 to 16, there is a net inflow when there is no Gibraltar source of MW, and the stronger net inflow below (levels 17 to 20) becomes a weaker net outflow. The overall circulation for the box has weaker inflow in the surface layers (down to ~250 m) and weaker outflow at mid-depths. The explanation for these differences is that once the Strait is closed, there is no inflow of surface waters to the Mediterranean and no input of Mediterranean Waters at mid-depths to the box, and therefore no transformation of surface waters to intermediate waters within the box. In other words, the overturning circulation is greatly reduced when the Strait is closed.

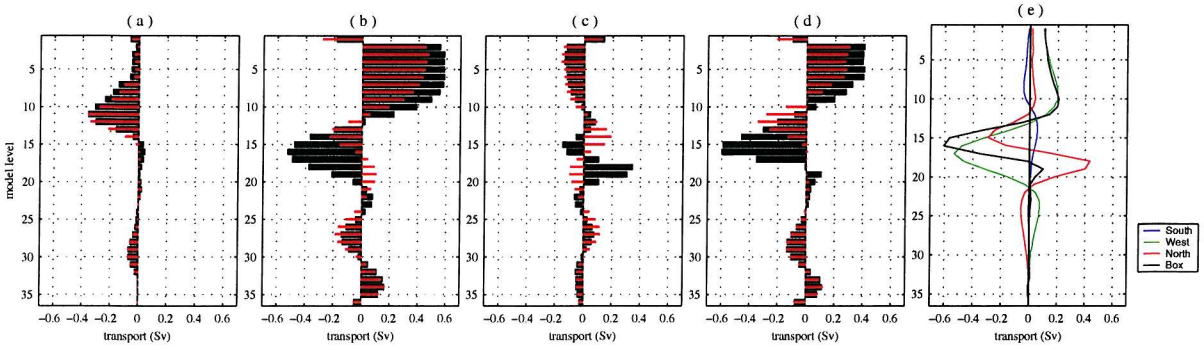

Figure 6.19 *OCCAM Annual Average Med Box transport profiles for both the open- (black) and closed-Strait (red) runs. (a) south, (b) west, (c) north, and (d) whole box. (e) Transport differences (Strait-open minus Strait-closed).*

The reduced overturning circulation in the closed-Strait experiment is also seen in Figure 6.20a, a time series of its magnitude over the final five years of the model experiments. The red line is the open-Strait run, the green is the closed-Strait run, and the annual average of each is shown in black. The magnitude of the surface inflow (or the magnitude of the overturning) is approximately 2.6 Sv in the open-Strait run and 1.4 Sv in the closed-Strait run. The annual average graphs suggest that on average the magnitude is slowly increasing; in the open-Strait run by ~0.048 Sv yr^{-1} (a 2% increase), and in the closed-Strait run by ~0.042 Sv yr^{-1} (a 3% increase).

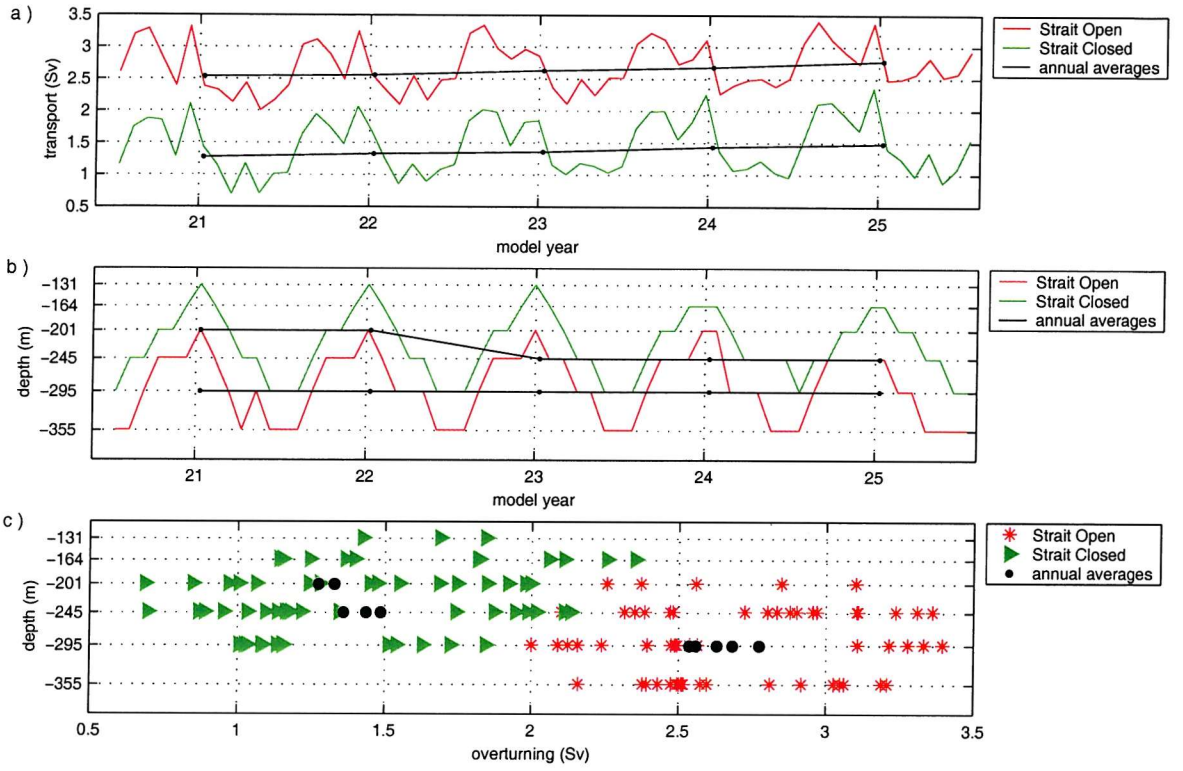

Figure 6.20 *Net surface inflow in the OCCAM Med Box. (a) Time series of the magnitude of the net inflow for the last five years of both the open-Strait (red) and closed-Strait (green) runs. (b) Time series of the maximum depth of the inflow for the last five years of both the open-Strait (red) and closed-Strait (green) runs. (c) Relationship between the magnitude of the net inflow and its depth. Annual averages are shown in black.*

The magnitude of the net surface inflow varies seasonally, with the largest flows occurring in the latter half of each year. The largest inflow coincides with the smallest exchanges at the Strait of Gibraltar (Figure 6.8). In the absence of the closed-Strait run comparison, it could be concluded either that there is a 6-month lag between the increased flow through the Strait and the increased inflows of surface water into the box (due to their distance apart), or that a slower Mediterranean Outflow entrains more surface waters. The seasonal pattern, however, is the same for both experiments, leading to the conclusion that the net surface inflow is wind-driven and not influenced by variability in the Mediterranean Outflow.

Figure 6.20b shows how the maximum depth of the surface inflow changes throughout the year (and over the last 5 years of the experiments). It increases by one level in the closed-Strait experiment, but otherwise hardly changed from the open-Strait run. There does not seem to be a very good correlation between the depth and magnitude of the inflow (Figure 6.20c), although in the closed-Strait run, the magnitude of the overturning is smaller and the depth of the inflow is shallower than in the main run.

ii North East Atlantic Circulation

As it was shown earlier that level 16 is representative of the MW depths, this level can be used to look at the circulation differences between the open- and closed-Strait experiments in the northeast Atlantic. Figure 6.21 gives velocity vectors for this level, showing the open-Strait data on the left, and the closed-Strait data on the right for (a) Spring, (b) Summer, (c) Autumn, (d) Winter, and (e) the Annual Average.

An immediately apparent difference at all times of year, is the absence in the closed-Strait run of the very high velocities denoted by the red arrows that are present only in the main run. This is exactly as expected, because the high velocities in the open-Strait run are within the Mediterranean Outflow. There is also much less variability, or eddying, in the Gulf of Cadiz and to its south when the Strait is closed, again due to the absence of the Mediterranean Outflow.

In the Spring, the northward flow against the Portuguese continental slope is actually a southward flow in the closed-Strait run. In Summer and Autumn, the northward flow (which is stronger than during the Spring) remains northward in the closed-Strait run, but is considerably weaker. In the Winter, however, as previously noted, there is southward flow against this boundary, which is faster when the Strait is closed. The presence of the Mediterranean Outflow therefore does have an effect on the boundary flow at all times of year, it increases the flow to the north (which in the case of the Winter circulation pattern, means that the southward flow is decreased). This is upheld by the Annual Average case (6.21e) which shows a relatively slow southward flow when the Strait is closed, but a northward flow when the Strait is open.

Looking further north at the Bay of Biscay, in Autumn and Winter (6.21c and 6.21d) there is a curious circulation pattern in the closed-Strait experiment. There is a strong boundary flow which switches direction over the course of the three months, such that in the Autumn, there is a continuous flow from Cape St Vincent all the way northwards and then around the Bay of Biscay, and in the Winter, it is continuous in the other direction, even continuing around the Gulf of Cadiz and further south to the Canary Islands. The pattern is very similar in the open-Strait run, although modulated by the Med Outflow.

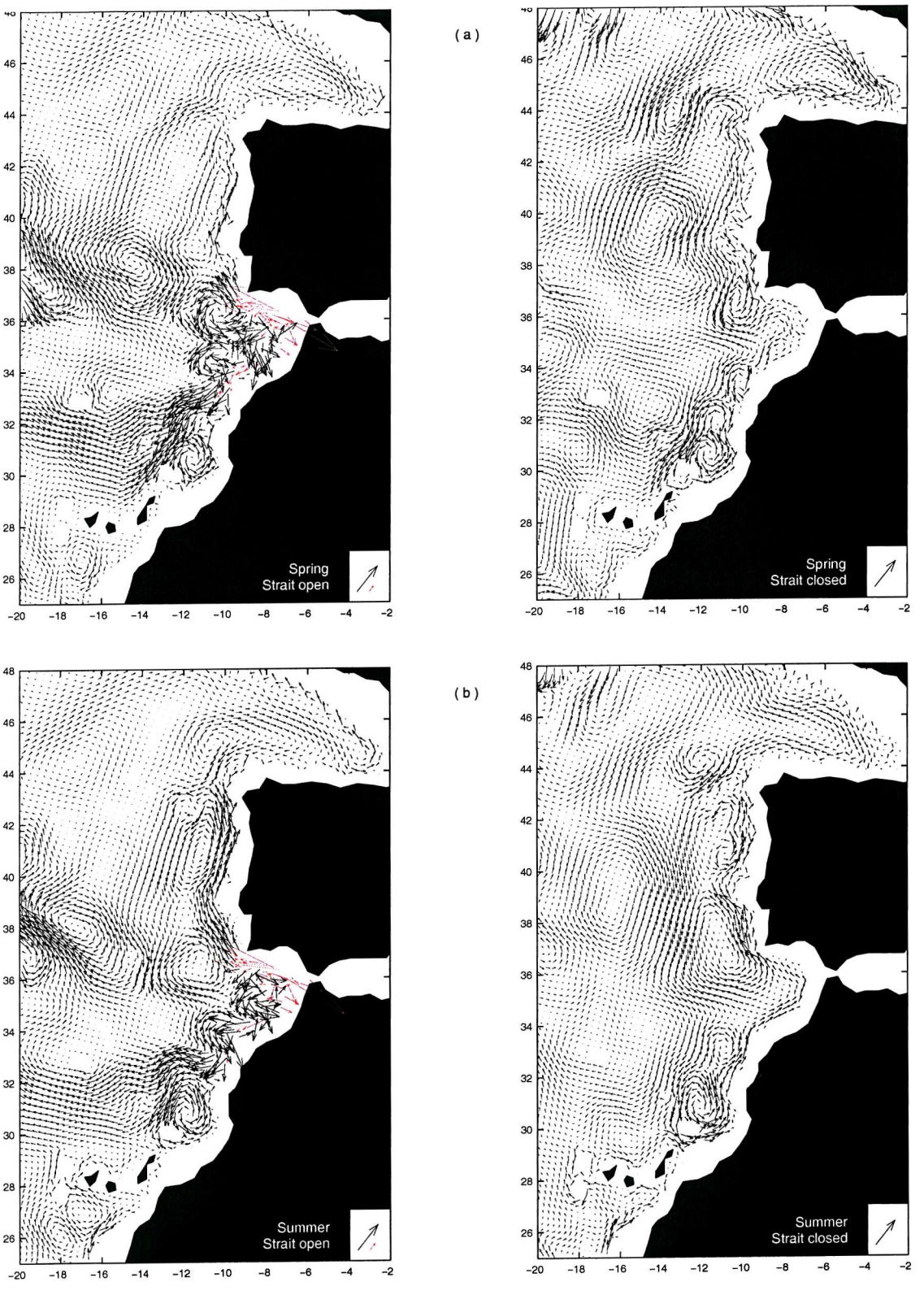

Figure 6.21 *OCCAM velocity vectors at level 16 (845 m) for both the open-Strait experiment (shown on the left) and closed-Strait experiment (on the right) for (a) Spring, (b) Summer, (c) Autumn, (d) Winter, and (e) Annual Average. The keys show vectors of 4 cm s^{-1}.*
Continued for (c), (d) and (e) on following pages...

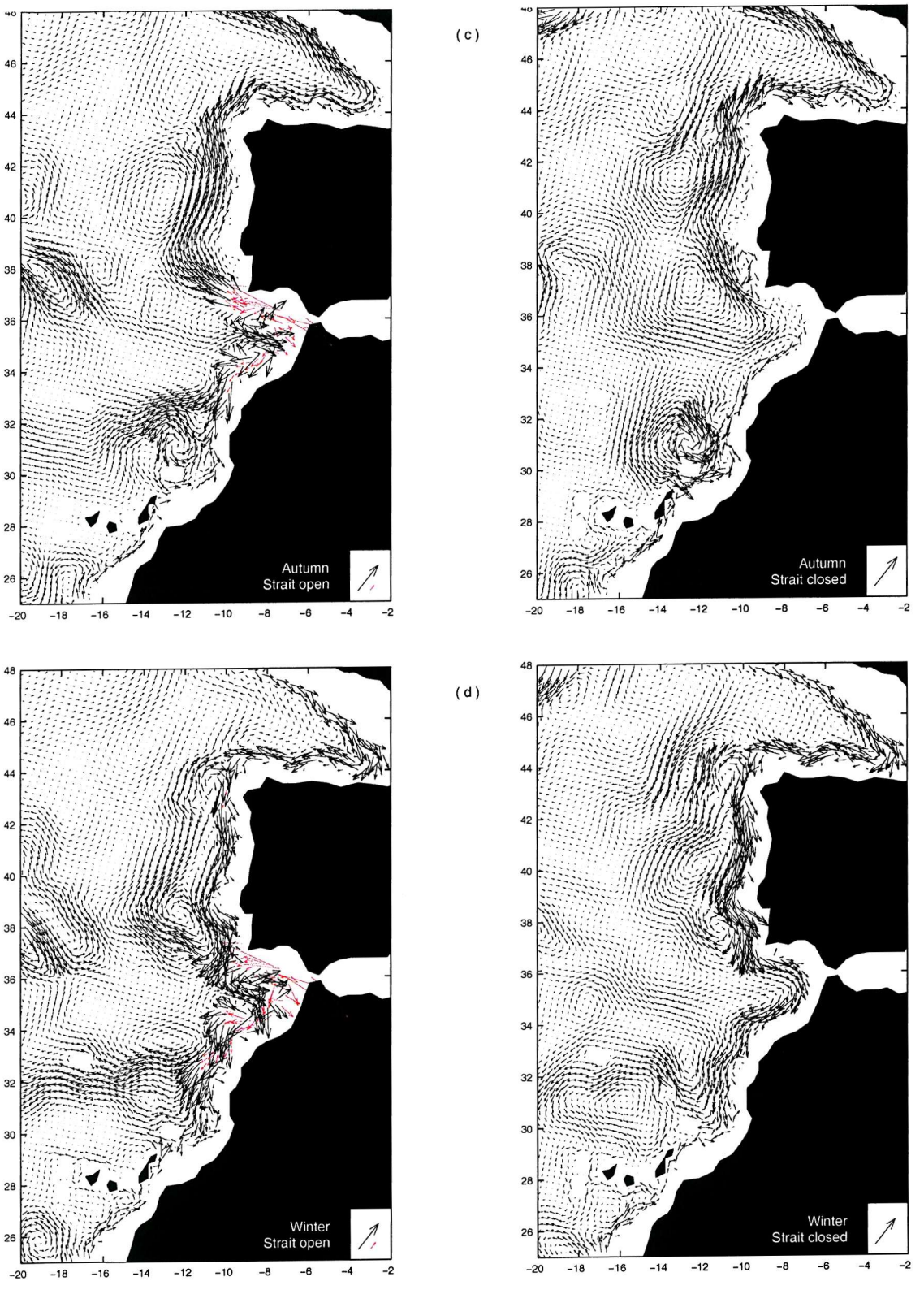

Figure 6.21 *contd... (c) Autumn, (d) Winter*
Continued for (e) on following page...

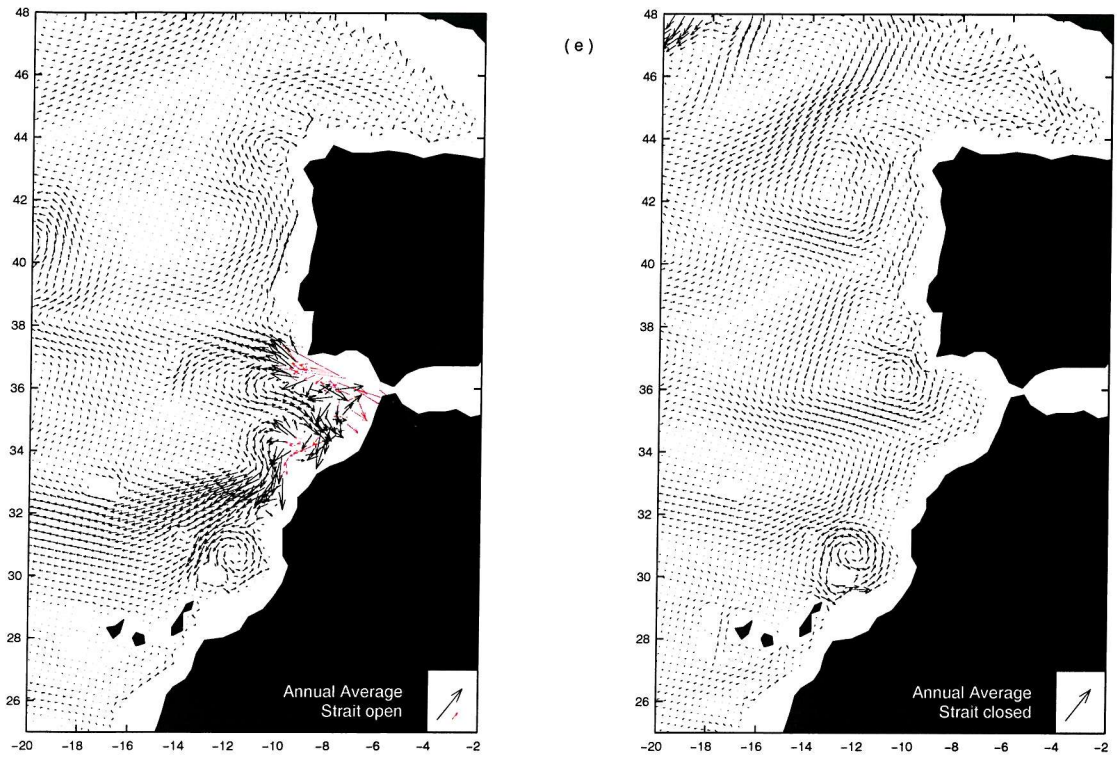

Figure 6.21 contd... (e) Annual Average

Other differences of note are that the strong recirculations between ~36 and 40°N to the west of 18°W are very much reduced, or even absent in the closed-Strait run, and that the southwestward pathway from the Gulf of Cadiz is similarly much reduced or absent.

Another method for examining the effect of the Med Outflow in the model is to look at the distribution of high salinity waters that are present in the open-Strait experiment and not in the closed-Strait experiment. MW has been defined for the Med Box as water that has a saldiff greater than 0.1; Figure 6.22 therefore shows saldiff contours greater than 0.1 for levels 1, 6, and 12 to 21. The depth range of each layer is given in brackets next to the level number.

There is an important differentiation to make between certain water masses that show up in these figures. The saldiff contours which originate from the Strait of Gibraltar (have highest values next to the Strait) denote the actual MW. These contours help elucidate the direct pathways and spreading of the MW as has been previously discussed.

The water mass that is seen in the top 12 levels (between the surface and 465 m) between 20 and 30°N, was mentioned when discussing the definition of MW in section 6.3 because the easternmost extension of the saldiff tongue crosses the western boundary of the Med Box at certain depths. As was pointed out then this is not MW, although there must be a link between this water mass and the

Med Outflow probably due to vertical mixing as the salinity here is lower when the Strait is closed. This link, however, is not immediately apparent.

Further north, between approximately 40 and 50°N, another area with higher salinities in the open-Strait run can be seen between the surface and 1000 m. This is the pathway of the North Atlantic Current (NAC), and the patchy appearance of this flow is probably due to the non-steadiness of the NAC, with its eddies and meanders, and variability of the sub-polar front over time. The NAC is obviously present in both model experiments, but is saltier when the Strait of Gibraltar is open. This indicates that the high salinities from the Med Outflow reach across the North Atlantic, which can actually be seen in levels 16 to 20 where a filament of the MW extends westwards at ~40 to 42°N. The NAC picks up the high salinity and carries it northeastwards back across the Atlantic. In other words, this is an indirect effect of the Mediterranean Outflow, rather than the direct effect seen around the Gulf of Cadiz.

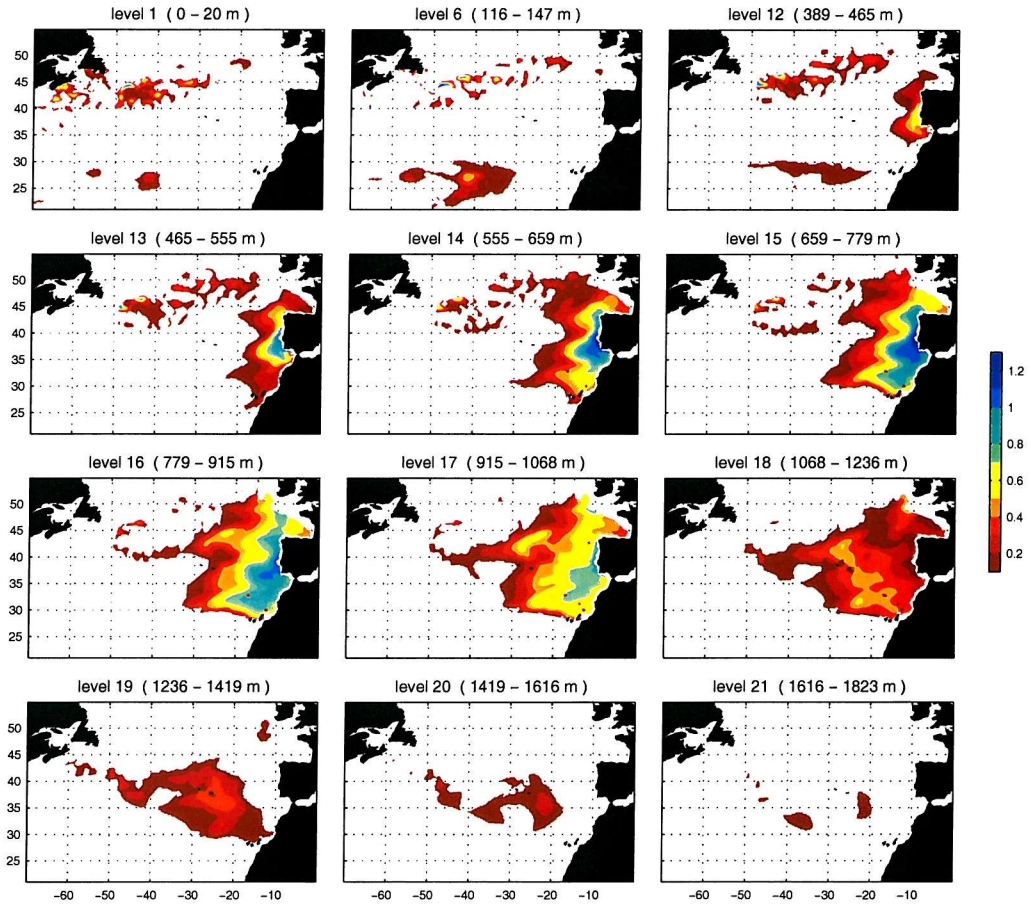

Figure 6.22 *Effect and extent of the Med Water in OCCAM shown by saldiff contours (> 0.1) for levels 1, 6, and 12 to 21, Annual Average data.*

6.5.5 Extent of the Mediterranean Water in OCCAM

Visually, Figure 6.22 gives the best idea of the extent of the MW in OCCAM. The water mass dominates the eastern North Atlantic north of ~30°N at depths between 500 and 1400 m. Its southern boundary below 660 m is a remarkably distinct line, stretching from the Canary Islands, almost due west. At model levels 13 and 14 (465 to 659 m), a narrow branch of the MW extends just to the south of the Canary Islands, but does not reach further south than 26°N. The greatest westward extent of the MW is seen below 780 m (model level 16), where it spreads beyond 30°W. Indeed, a thin filament reaches across the North Atlantic to as far as ~50°W at certain latitudes. In the surface layers the effects of the MW can be seen as far north as 52°N, the high salinity signal being carried eastwards in the NAC as discussed in the previous section. The direct MW flow also reaches 52°N in levels 14 to 18 (555 to 1236 m). There is, however, no evidence that any MW reaches the Rockall Trough or beyond, either directly or indirectly in OCCAM.

This direct northward spreading of the MW is shown in Figure 6.23 by salinity contours of a number of quasi-zonal sections (which are detailed on the map). The highest salinities are seen up against the boundary all the way along the Portuguese continental slope. The flow remains a boundary current as it rounds the corner at Cape Finisterre and proceeds northwards across the Bay of Biscay. This is also shown in Figure 6.22, levels 15 to 18. The last vestiges of the MW are seen in the trough between the Goban Spur and Porcupine Bank.

In order to ascertain any differences in the MW spreading at different depths, Figure 6.22 is summarised by Figure 6.24, which shows the lateral extent of the MW (from saldiff contour 0.1) at levels 10 to 17. There are two main observations to be made from this figure. First, the greater the depth, the greater the extent of MW influence. Second, the upper layers appear to undergo mainly northward spreading of MW. There is only northward spreading at 295 m (level 10). At layer 13 (508 m depth) the MW reaches further to the north than to the west. By level 14 (600 m depth), the MW reaches slightly further west, and this trend of a more westward extent of the MW continues at deeper levels.

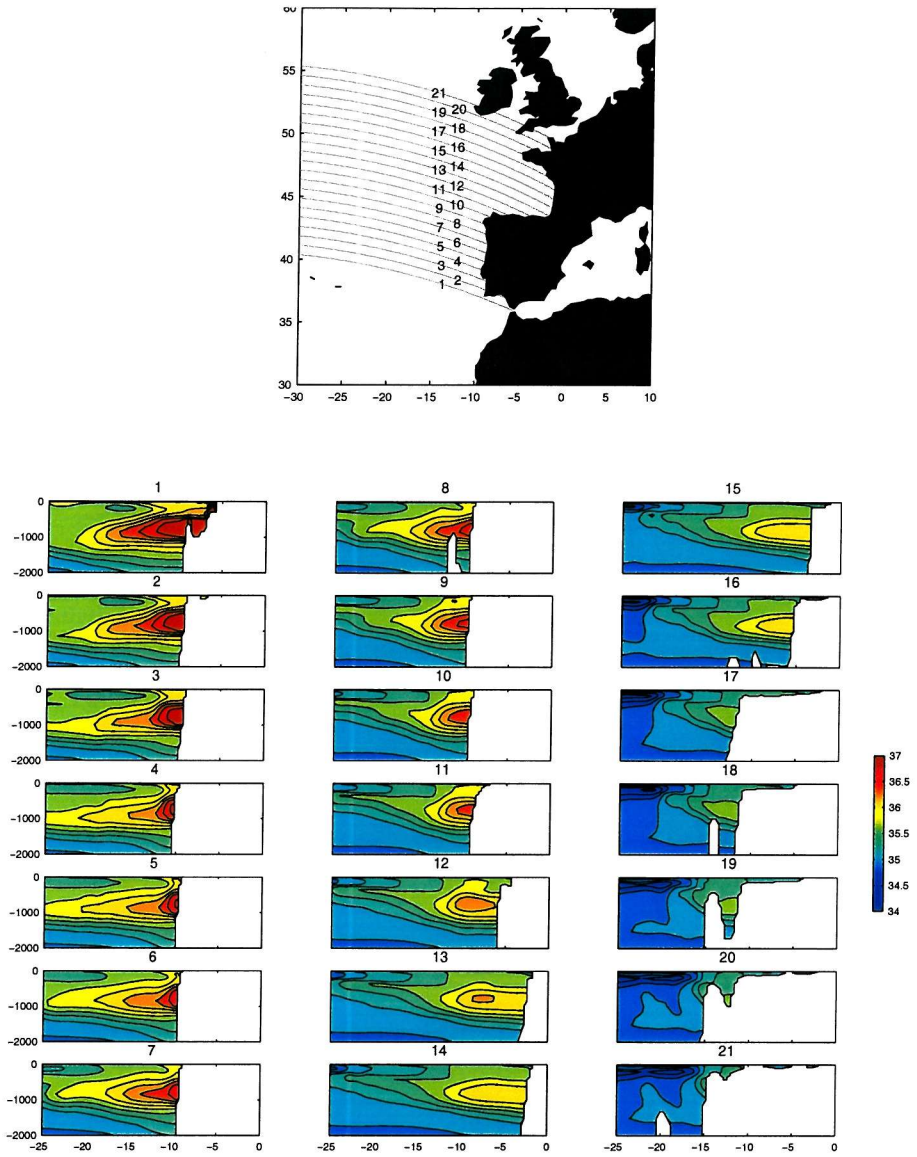

Figure 6.23 *Northward spread of 'MW', shown by salinity contours in the upper 2000 m along different sections (shown in the map).*

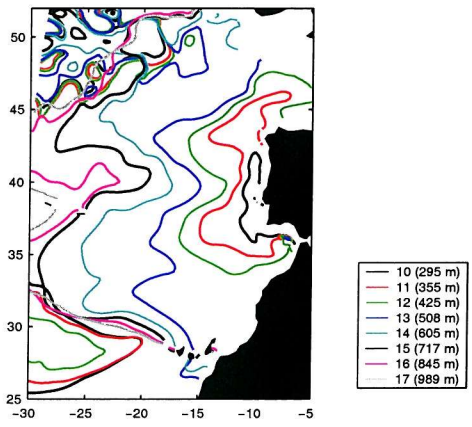

Figure 6.24
Spread of 'MW' (defined by the saldiff contour 0.1) at different levels in OCCAM.

6.6 MED BOX FLUXES

6.6.1 Net Fluxes and Evaporation

Using the same method as for the hydrography, it is possible to calculate the expected net evaporation over the area of the OCCAM Med Box (not including the Mediterranean Basin). Figure 6.25 shows the results of this calculation, which is done using data from the SOC global Air-Sea Heat and Momentum Flux Climatology (Josey et al., 1998). The left hand figure shows the position of the Med Box and coastline, with the one degree climatology grid shown as dots, and those denoted as being 'inside' the Med Box and therefore used for the calculation in black. The right hand figure shows the total evaporation (E), precipitation (P) and net evaporation (E-P) throughout the year, as well as the Annual Averages (dashed lines). The evaporation is much higher than the precipitation for this area of the north east Atlantic, resulting in a positive net evaporation over the area of the box. The Annual Average net evaporation is 0.04 Sv, and the range over the year is 0.03 to 0.05 Sv.

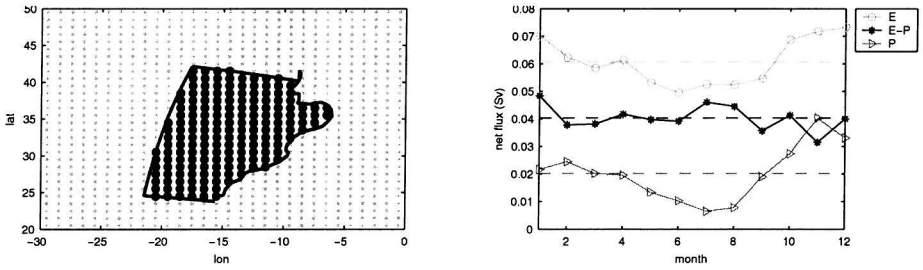

Figure 6.25 *Net evaporation calculation for the OCCAM Med Box, using the SOC global Air-Sea Heat and Momentum Flux Climatology (Josey et al., 1998). The figure on the left shows the OCCAM Med Box and adjoining coastline, black circles show grid points denoted as 'inside' the box and therefore used in the calculation. The right-hand figure shows evaporation (E), precipitation (P) and net evaporation (E-P) for the OCCAM Med Box throughout the year.*

These values of net evaporation can be compared with those calculated using the model data. A net transport into the Med Box can be viewed as a net evaporation over the area enclosed by the box, which includes the Mediterranean Basin for the open-Strait experiment. Note however, that this is only sensible for the annual average values because at any particular instant in time sea level can change and fluxes would not balance for such a large area. Figure 6.26a shows the time series of net transport into the OCCAM Med Box for the open-Strait run (in black) and closed-Strait run (in red) for the last five years of each experiment. There is a distinct seasonal signal, with maximum values occurring in the summer or autumn, as might be expected. The annual average values are detailed in Table 6.4, and show that the averages for the final five years are 0.054 Sv and 0.010 Sv

for the open- and closed-Strait runs respectively. The net transport into the Box is much lower in the closed-Strait run because it is a much smaller area over which evaporation is occurring. There is a reasonably good agreement between the net evaporation calculated using the SOC climatology and OCCAM's net effective evaporation.

It is shown in Figure 6.26b and Table 6.4 that there is variability in the net salt flux, with a mean of 0.538 Sv psu in the open-Strait run. Having a positive salt flux into the box implies (as total transport is also positive) that the salinity in the box (and / or Mediterranean) is increasing. The closed-Strait net salt flux is much lower than the open-Strait run and the mean is nearer zero, suggesting that it is the salinity of the Mediterranean that is increasing. There does not appear to be a change in salinity of the Med Outflow, which is quite steady over the final six years of the experiment (refer back to Figure 6.8), however, if there is a net increase in the salinity of the Med, it could take a long time before that increase is reflected in the outflow salinity.

Plotting the time series of the mean salinity for the box (Figure 6.26c) shows this suggested increase. The rates of increase of salinity per year are 0.00312 and 0.00084 for the open- and closed-Strait experiments respectively. The much slower rate of increase in the closed-Strait experiment reflects the lower net salt flux into the box.

The final graph in Figure 6.26 shows the absolute transport weighted salinity for the OCCAM Med Box, given by

$$\text{Absolute transport weighted salinity} = \frac{\int\int |\,\text{salt flux}\,| \,dx\,dz}{\int\int |\,\text{transport}\,| \,dx\,dz}$$

This value is, as its name suggests, an average value of the salinity, weighted by transport rather than area as is the normal method of calculating means. It is used to elucidate any relationship between the transport of a particular water mass and its salinity. The absolute values are used because it is a non-unidirectional flow and the net transports are tiny. The variability seen is a reflection of the variability in the transport. The difference between the open- and closed-Strait experiments is 0.075, which is exactly twice the difference between their mean salinities, reflecting the transport difference between the two experiments. On average, the transport weighted salinities are at least 0.426 higher than the mean salinities, which means that the higher salinities are in the faster flowing water.

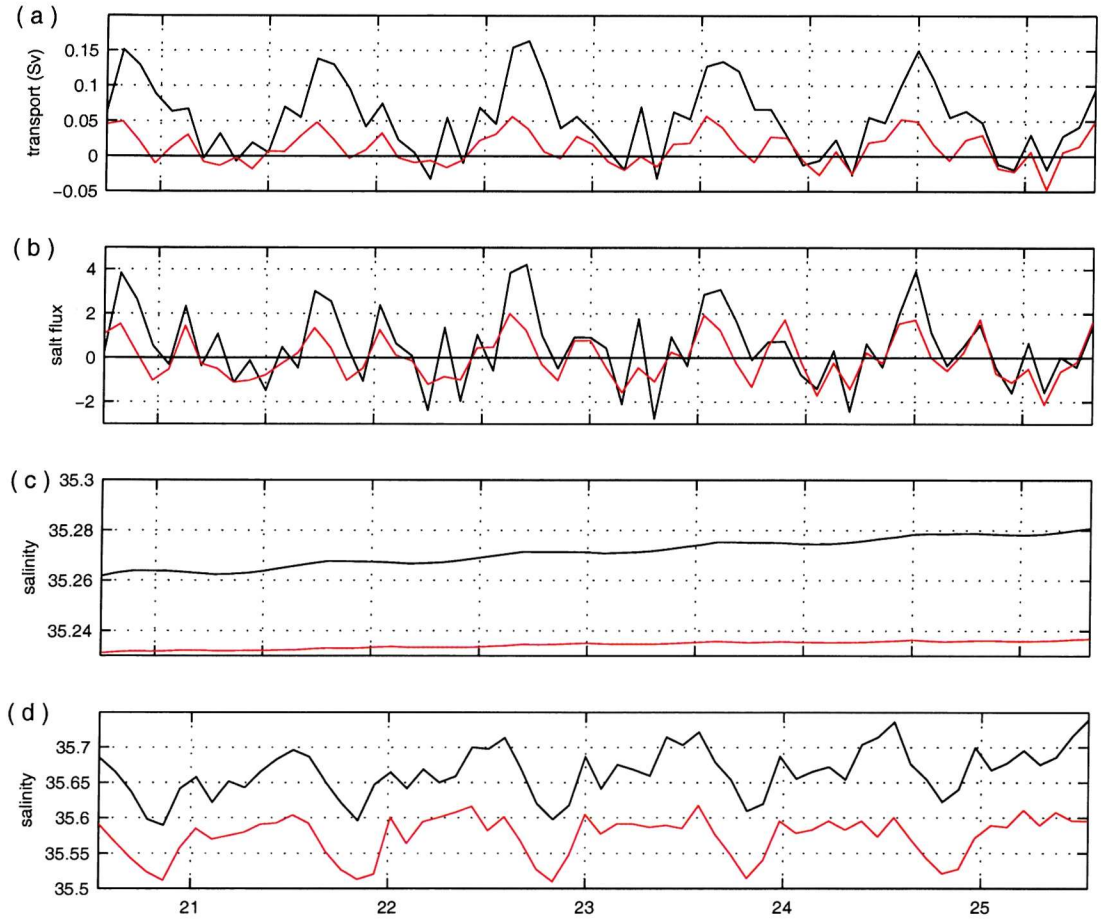

Figure 6.26 *Time series of (a) total transport, (b) net salt flux, (c) mean salinity, and (d) absolute transport-weighted salinity for OCCAM Med Boxes, open-Strait data in black and closed-Strait in red.*

Year	Net transport (Sv)		Net Salt Flux (Sv psu)		Mean Salinity		Abs TW Salinity	
	with MW	no MW	with MW	no MW	with MW	no MW	with MW	no MW
21	0.056	0.009	0.647	-0.105	35.2633	35.2318	35.700	35.641
22	0.053	0.009	0.478	-0.072	35.2673	35.2331	35.721	35.660
23	0.057	0.012	0.588	0.040	35.2714	35.2345	35.737	35.661
24	0.055	0.014	0.526	0.139	35.2753	35.2354	35.750	35.666
25	0.047	0.007	0.411	-0.045	35.2789	35.2360	35.757	35.666
21-25	0.054	0.010	0.538	-0.009	35.2713	35.2342	35.734	35.660

Table 6.4 *OCCAM Med Box Annual Average (years 21 to 25, and the mean for all five years) values of net transport, net salt flux, mean salinity and absolute transport weighted salinity (Abs TW Salinity), for both the open-Strait (with MW) and closed-Strait (no MW) experiments.*

6.6.2 Mediterranean Water Fluxes

Having discussed the net fluxes and circulation for the Med Box as a whole, it is now fitting to look at the MW itself. The best way to commence this, however, is to look at mean salinity profiles for the Med Box. Figure 6.27a shows profiles of mean salinity for the box and each of its sides for both the open- and closed-Strait experiments (denoted by solid and dashed lines respectively). Figures 6.27b and 6.27c show the difference between the open- and closed-Strait profiles versus depth and model level respectively. On the west and north sides, the mid-depths are much more saline in the open-Strait run, revealing the presence of the MW, and its core depth at about 850 m (model level 16). The salinity on the southern section is almost exactly the same in both runs, confirming that little MW crosses this southern boundary.

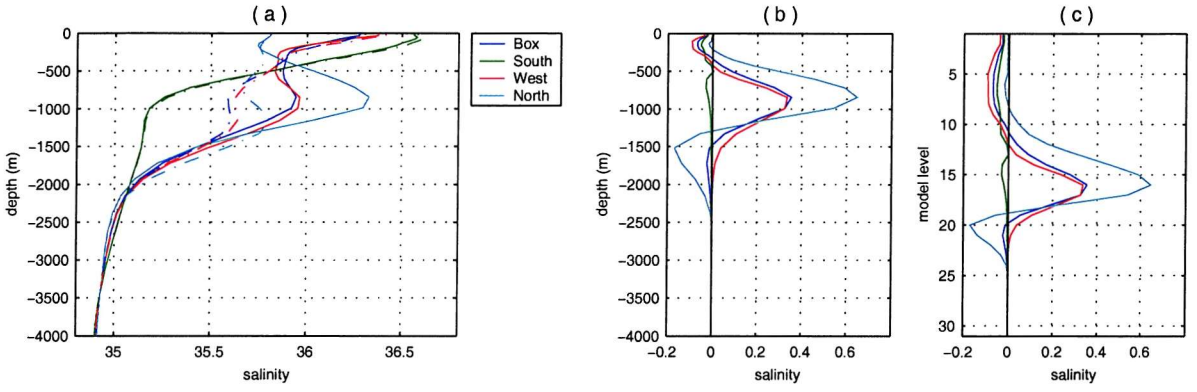

Figure 6.27 *OCCAM Med Box (average of the last 5 years) profiles of (a) mean salinity for the whole box and each side, for both the open-Strait (solid) and closed-Strait (dashed) runs, (b) difference between the mean open- and closed-Strait profiles versus depth, and (c) difference between the mean open- and closed-Strait profiles versus model level.*

The MW is slightly shallower in the water column on the northern section than on the western, as was mentioned earlier. The northern section also has much higher salinities and the largest differences between the two model runs. In the closed-Strait run, the salinities between 1000 and 1500 m are still high on the northern edge, not because of a large reduction in velocities at MW levels as was expected when looking at Figure 6.9 (§6.4.2), but because of the seasonal change in direction of the flow, preventing all the water of Mediterranean origin from being advected away to the north (as discovered in Figure 6.15, §6.1.3). There is also the likelihood that some of the high salinities below the main MW core depth in the main run (on both sides of the box) are there due to diffusion and will take a long time to be eroded away.

To start looking specifically at the MW itself, the MW definition was used to isolate that water mass. Figure 6.28 shows the total MW transport and its mean salinity at every station around the Med Box for the Annual Average case (6.28a and 6.28b respectively), and also the seasonal mean salinity (6.28c). A number of observations can be made from this figure. There is no MW between stations 1 and 43, which is south of 29.5°N, and north of this latitude, MW is both entering and leaving the Med Box. The main outflow locations on the western edge are between stations 44 and 60 (29.5°N and 33.5°N; 1.64 Sv), and 74 and 80 (36.8°N and 38.3°N; 0.67 Sv), and on the northern edge between stations 113 and 121 (12.3°W and 9.8°W; 0.56 Sv). This is as expected from the figure of velocity vectors at level 16 (Figure 6.12). What becomes clear from this figure, however, is the magnitude of and difference between the transports across each boundary. The red bars show the transports from the closed-Strait run, and highlight how the outflow decreases once the Strait of Gibraltar is shut.

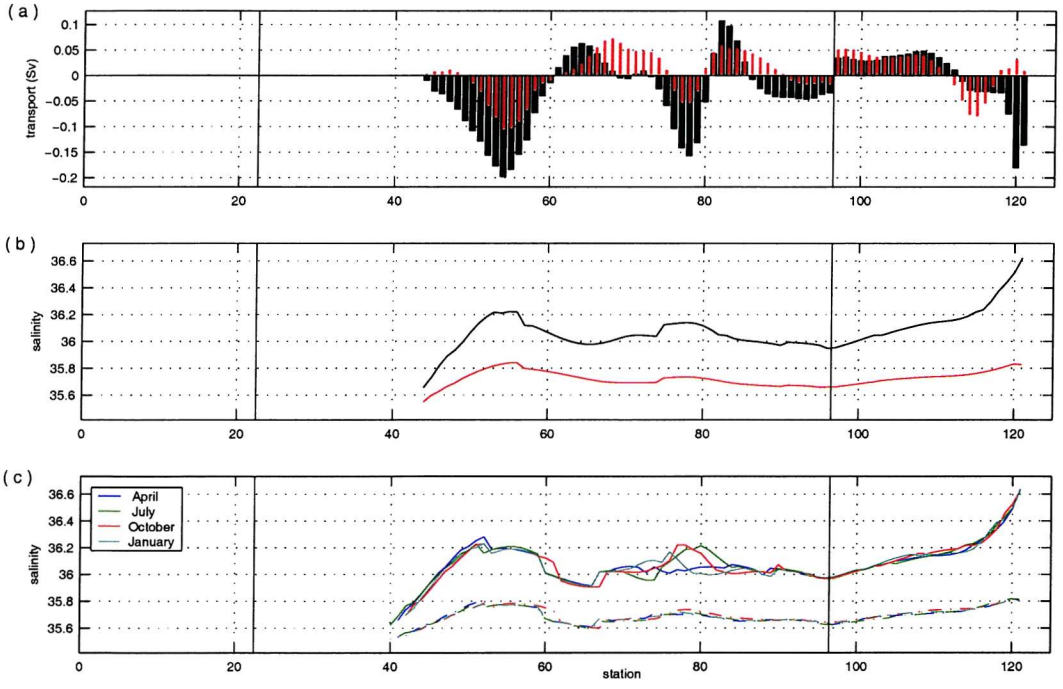

Figure 6.28 *OCCAM Med Box total transport and mean salinity within the MW layer at each station for both the Open- (black) and Closed-Strait (red) runs. Whilst the upper two plots show data from the annual average, the bottom plot shows the mean salinity from snapshot data in April, July, October and January, with the open-Strait run in solid lines and the closed-Strait run in dashed lines.*

The mean MW salinity for each run (Figure 6.28b), shows that where there is net outflow, the salinities are higher than locations of net inflow. This points to the outflowing water coming more directly from the Strait, whereas the inflowing water has recirculated and is 'older'. The salinity is highest on the northern edge of the box, and increases towards the coast, which suggests that there

has been less mixing of the water mass along this pathway. In general, as higher salinities are being transported out of the box and lower salinities into it, the implication is that there is a salt flux out of the box in the MW layers, as would be expected!

The closed-Strait run has much lower salinities, but the same pattern can still just be seen, indicating that the high salinity from the outflow has not been completely eroded. The seasonal salinities vary very slightly on the western edge of the box only, although not at all in the closed-Strait run.

Having looked at the annual average picture of the transport, the seasonal variations can be investigated. Figure 6.29 shows the net transport at each station for the MW layer, for both the open- and closed-Strait experiments (in black and red respectively). The annual average is shown again in 6.29a for comparison, and all plots have the same scales. At any given instant (one of the seasonal snapshots in b to e) the net transports for an inflow or outflow are generally larger than in the mean, and this is because of the variability of the circulation.

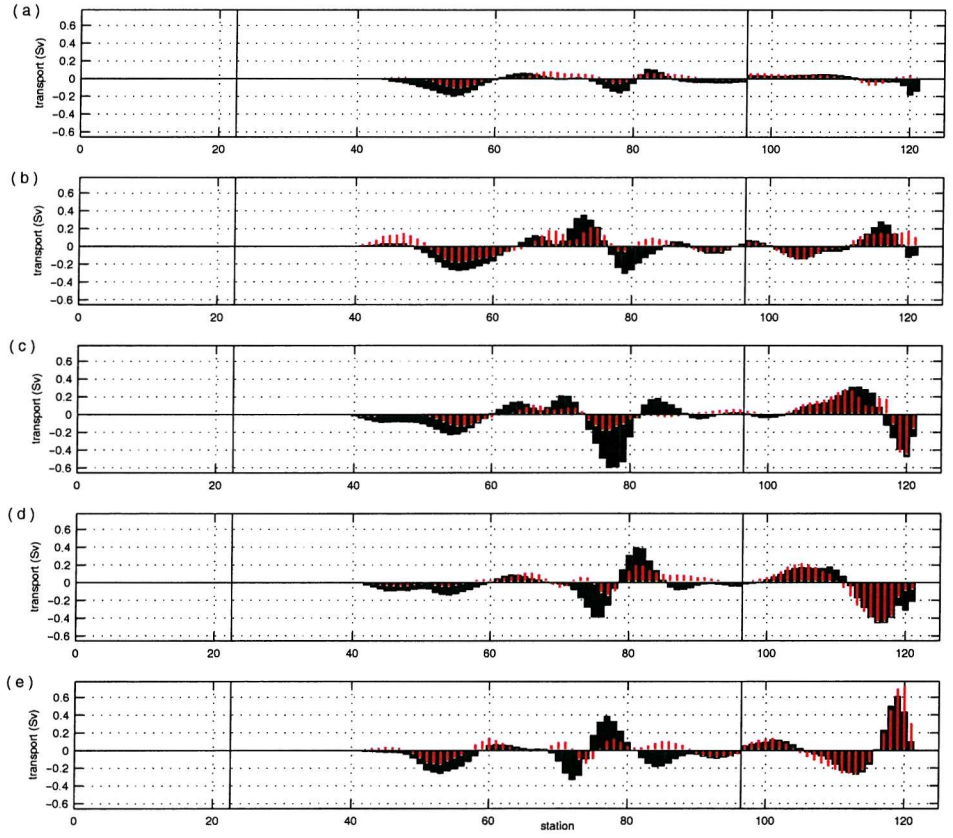

Figure 6.29 *MW transport at each station (i): OCCAM Med Box total transport within the MW layer at each station for both the Open- (black) and Closed-Strait (red) runs, showing data from the annual average as well as one snapshot from each season*

The differences between the open- and closed-Strait transports are much larger on the western edge than the northern edge. To the west, there is a marked decrease in the strength of the horizontal circulation when the Strait is closed, whereas to the north there is a surprisingly small change. The reason for this, however, has already been discovered (Figure 6.21): the boundary flows are present even when there is no Mediterranean Outflow, so in the open-Strait run the outflow just increases the flux to the north (which is negative on the northern edge), or in the case when the boundary flow was southwards (6.29e), acts to decrease the strength of the southward flow.

The two regions of outflow on the western side of the box have different characteristics. The outflow between stations 40 and 60 is reasonably constant, but the outflow between stations 60 and 90 is very variable. The effect of the transport variability can be seen in the saldiff, shown for level 15 in Figure 6.30. Data from every monthly snaphot in the last 3 years of the experiments is plotted, with each year a different colour. The main features of this figure are the two maxima, one smooth and one 'hashed', on the western edge of the box. These show the positions of the outflowing MW, and the hashed region highlights where there is lateral variability in the position (as seen in Figure 6.29).

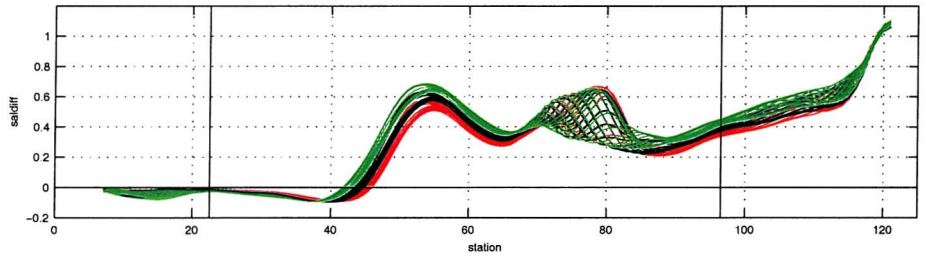

Figure 6.30 *OCCAM Med Box saldiff at level 15 (717 m), monthly snapshot data from the last 3 years of the open-Strait run, with each year shown in a different colour (red, black, green for years 23, 24, 25).*

There is always a net transport out of the box within the MW layers in the open-Strait run. This is shown in the time series in Figure 6.31a, along with the net transport across each side of the box. Results from the closed-Strait run are shown as dashed lines. The transport is strongest in the Autumn, when it has a large northward component. At this time, the westward component of the transport actually decreases. For a large part of the year the net transport across the northern boundary in the MW layers is into the box (southwards). This is due to the underlying equatorward boundary flow (as seen in Figures 6.15 and 6.21) and not a lack of northward MW transport.

When the Strait is closed, the net transport in the MW layers varies between positive and negative with a very similar pattern to the open-Strait run. The difference, of between 2 and 3 Sv, gives the actual transport of the MW. Most of this difference is due to the flow across the western edge of

the box (Figure 6.31b). The actual quantities of MW flowing across each boundary (calculated using these differences) are shown in Figure 6.32a. As just suggested, more MW crosses the western than the northern boundary, and there is an inverse relationship between the two, such that when the flow to the north increases, the flow to the west decreases, and vice versa.

Although there is less MW crossing the northern boundary, it has a higher mean absolute transport weighted salinity (shown in Figure 6.31c). The result of this is that the salt fluxes across each boundary due to the MW alone (Figure 6.32b) are much closer in magnitude than the MW transports. Using these salt fluxes, the proportion of MW crossing each boundary has been calculated and is shown in Figure 6.32c. Averaged over the final five years of the model experiments (shown as dashed lines), 61.4% of the MW flows across the western boundary of the Med Box, and 38.6% of the MW flows northwards. There is quite a lot of variability in these figures, with the amount of MW flowing westwards varying between 43% and 77%, and the amount flowing northwards varying between 23% and 57%.

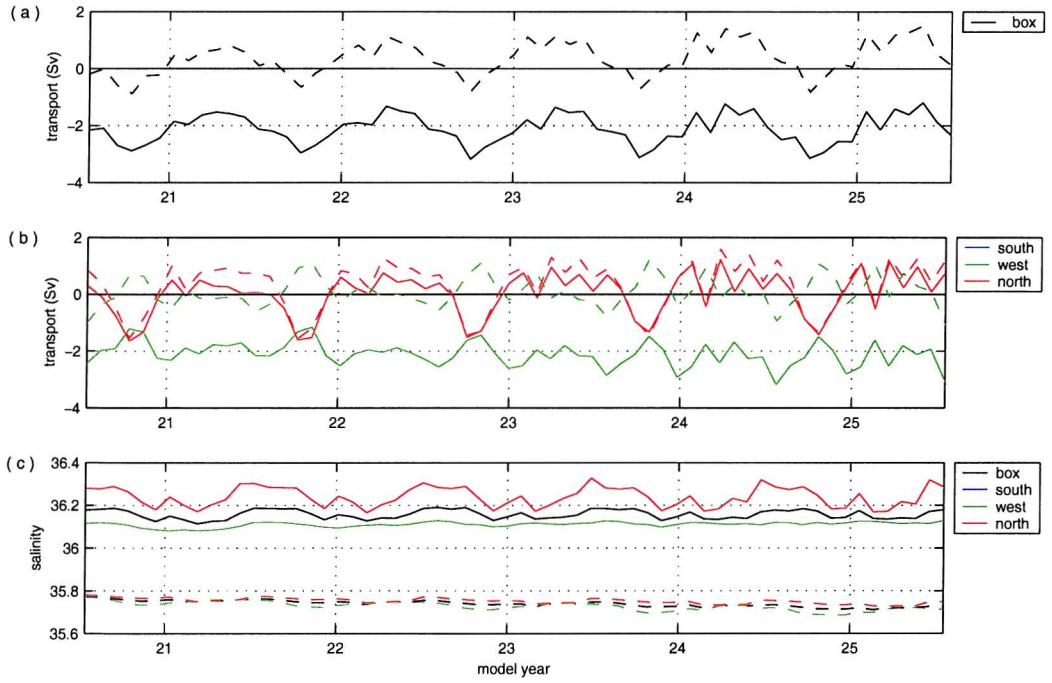

Figure 6.31 *Time series of total transport in the Med Box MW layers for both the open-Strait (solid) and closed-Strait (dashed) runs, with positive transports being into the box. (a) Whole box, (b) transport across the southern section in blue, across the west in green and across the north in red. (c) Corresponding time series of mean absolute transport weighted salinity.*

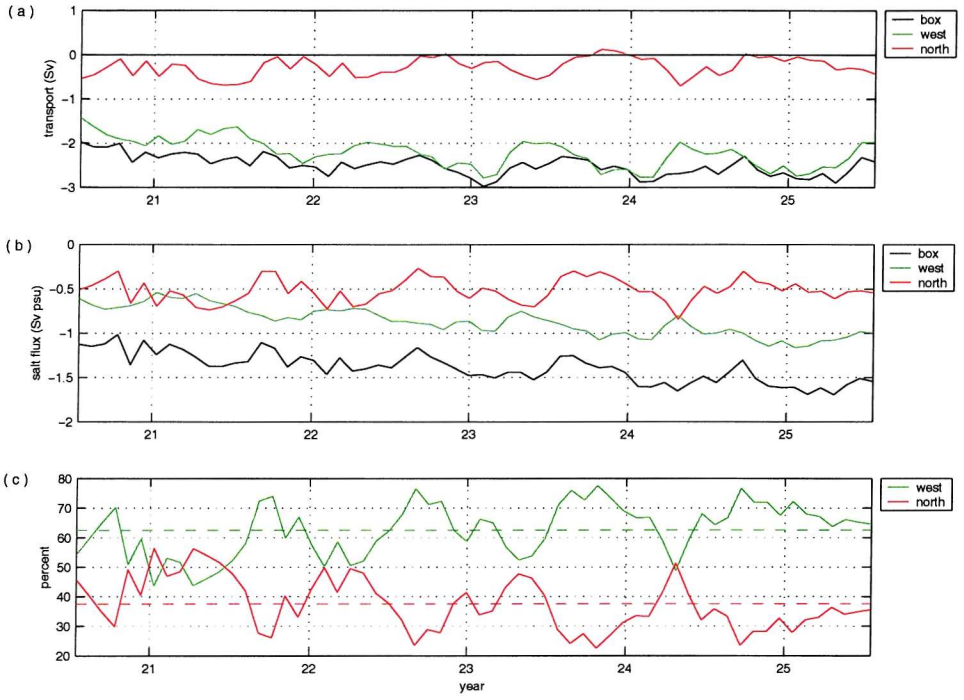

Figure 6.32 *Med Box time series of (a) MW transport, (b) MW salt flux, and (c) percentage of MW crossing each boundary with the 5-year means plotted as dashed lines. Fluxes are calculated using the difference between the open- and closed-Strait experiments.*

6.7 SUMMARY

Data from OCCAM (the Ocean Circulation and Climate Advanced Modelling Project Global Ocean Model) is used to address temporal and spatial variability of the circulation and fluxes in the eastern North Atlantic. The 0.25° latitude-longitude grid model was run for 25 years in total, with the final 17 years being re-run with the Strait of Gibraltar closed. The model uses a rotated grid in the North Atlantic to overcome the computational problems of a convergence of the meridians at the North Pole. The OCCAM Med Box is formed by taking data along the model grid lines, which are at an angle to normal lines of latitude and longitude.

The only difference between the two model experiments is the status of the Strait of Gibraltar, giving a unique dataset for investigating the transport of MW in the North Atlantic and the effects of the MW outflow on the circulation. For this study, MW was defined as waters with salinities 0.1 higher than those in the closed-Strait run. The closed-Strait run has not yet reached steady state, with remnants of MW still observed.

The circulation in the Med Box is such that there is inflow in the surface layers and outflow at mid-depths. The principal reason for this overturning circulation is the exchange at the Strait of Gibraltar and associated water mass transformation (due to entrainment) of North Atlantic Central Water. This is reflected in the closed-Strait run, when both the Med Box surface inflow and mid-depth outflow are much reduced. The greatest differences are seen on the western section, consistent with the hypothesis of Jia (2000) that the Mediterranean Outflow induces the Azores Current. The magnitude of the net surface inflow in OCCAM (2.64 Sv) is comparable with the hydrographic values (2.13 and 3.58 Sv for Med Boxes 88 and 98 respectively). The magnitude of the model overturning implies an entrainment value of 1.2 Sv (the difference between the net surface inflow in the open- and closed-Strait runs), consistent with the hydrographic estimate of 1.6 ± 0.6 Sv.

Another difference between the two OCCAM experiments is seen in the circulation in the Gulf of Cadiz. With the Strait open there is variability in the circulation with high velocities at the depth of the Mediterranean Outflow. In contrast, with the Strait closed there is a smooth boundary flow and no extreme velocities are observed.

Flux calculations show that, as expected, there is a net volume transport into the Med Box (0.054 Sv and 0.010 Sv for the open- and closed-Strait runs respectively), which is equivalent to the net evaporation over the area enclosed by the box. The SOC climatology estimates a net evaporation for the region enclosed by the OCCAM Med Box of 0.067 Sv (0.04 Sv over the Atlantic Med Box region plus 0.027 Sv over the Mediterranean Basin). The hydrographic estimate of net evaporation agrees remarkably well with the SOC climatology estimate, suggesting that both are close to reality. OCCAM therefore seems to underestimate the net evaporation over the region enclosed by the Med Box, primarily due to the evaporation over the Atlantic region being a factor of 3 smaller. Surprisingly, the net salt flux into the OCCAM Med Box is positive. The explanation for this is that the salinity within the Med Box is increasing.

There is little interannual variability in the model as it is forced with winds from the 1986-1988 ECMWF monthly climatology. There is, however, significant seasonal variability, particularly to the west of Iberia. At MW depths, for most of the year the boundary flow is northwards but varying in size and intensity. In Winter the northward boundary current moves offshore and is replaced by a southward flow. Regardless of the direction of the current, the highest salinities on the northern side of the Med Box are found against the continental slope, consistent with the hydrographic observations (Chapter 5).

The reversal of the eastern boundary flow is not consistent with the hydrographic Med Boxes, which reveal strong northward flow at mid-depth. These Med Boxes, however, provide a picture of the mean circulation, whereas the current reversal in the model is transitory. Current meter measurements on the continental slope at 40°N reveal an apparent persistent northward flow at 1000 m depth at 9.5°W, but with brief periods of southward flow at 10°W. (Daniault et al., 1994). The observational evidence does not support the complete reversal of the flow in OCCAM extending to 12°W.

There are three pathways taken by the MW in the model North Atlantic: to the north along the Iberian continental slope; to the west from Cape St Vincent; and to the southwest as far as the Canary Islands and then westward. Flow to the southwest is a direct current, whereas the flux of MW due west from Cape St Vincent occurs via a number of large eddies or recirculations. In the hydrographic Med Boxes (Chapter 5) a similar northward pathway for MW is seen, however, only one advective westward pathway between 35 and 40°N is observed. MW only appeared at the western boundary south of ~35°N in meddies (Med Box 88), which are not resolved in the OCCAM ¼° model. There is no observational evidence for an advective southwestward pathway in historical hydrographic data as represented by the Levitus data set.

Using the difference between the two OCCAM experiments to calculate the transport of MW and its associated salt flux, both a net transport and a net salt flux out of the box were found in the open-Strait run. On average, over the final 5 years of the experiment, 61% of the MW was seen to flow westwards across the western boundary of the Med Box, and 39% of the MW flow northwards. These proportions vary by ±17%. The percentages of MW flowing across the northern boundaries of Med Boxes 88 and 98 are approximately 50% and 75% respectively. Although the seasonal variability of the OCCAM MW flow encompasses the hydrographic estimates, on average a higher proportion of MW crosses the western boundary in the model. The disparity between the model and observations is due to the difference in the modes of transport. The strong advective southwestward MW pathway in the model does not occur in the hydrography, and the substantial northward mid-depth flow observed in the hydrography is much weaker and more variable in the model.

It appears that MW in the upper model layers (10 to 12) spreads mainly northward, whilst the deeper MW spreads further westward. This is also the general consensus of observational studies (Zenk and Armi, 1990). The farthest south that any MW reaches in OCCAM is 26°N. This is in agreement with the hydrographic Med Boxes, which have no MW crossing their southern boundaries at 24°N.

In the model, high salinities from the Mediterranean Outflow reach as far north as 52°N, both directly in a northward flow from the Gulf of Cadiz, and indirectly via a westward pathway across the North Atlantic at ~35°N which is then upwelled into the North Atlantic Current flowing eastwards towards Ireland. This is inconsistent with Reid's (1994) hypothesis that MW reaches the Nordic Seas directly via an eastern boundary undercurrent, which has also been contradicted by modeling studies (New et al., 2001) and climatological studies (Iorga and Lozer, 1999a, 1999b) that confirm the presence of MW only as far as the Rockall Trough and 50.3°N respectively. It does, however, support the observational analysis of McCartney and Mauritzen (2001) who describe the origin of the high salinities in the Nordic Seas as a shallow, northward branch of the NAC (of which MW is a constituent) which flows through the Rockall Trough. It is known that MW influences the central waters of the North Atlantic (Worthington, 1976; Mauritzen et al., 2001), however, the direct westward pathway observed in OCCAM has not been seen in observational data

In general, the OCCAM model appears to be a reasonable representation of the eastern North Atlantic circulation. However, differences between the model and hydrographic observations should be considered in further model analysis.

Chapter Seven

Conclusions

7.1	INTRODUCTION	144
7.2	DATA AND METHODS	145
7.3	HYDROGRAPHIC DATA ANALYSIS	145
7.4	RESULTS FROM A GLOBAL OCEAN MODEL	146
7.5	SUMMARY	147
7.6	FUTURE WORK	148

One never notices what has been done;
one can only see what remains to be done ...

Marie Curie 1867-1934

7.1 INTRODUCTION

The principal endeavour of this thesis is to investigate the transport of Mediterranean Water (MW) in the North Atlantic Ocean, and specifically to determine how much of the MW flows northwards and how much flows westwards from its source in the Gulf of Cadiz. This chapter presents the main conclusions from this work, highlighting the most significant findings and making recommendations for further study.

Chapter 2 set this work in the wider context of Atlantic Ocean circulation and climate and provided a detailed review of the present understanding of MW circulation in the North Atlantic. The review established several key elements which were the impetus for this work.

The oceans play a central role in regulating our climate, having considerable capacity to store and transport heat, fresh water and carbon (Clarke et al., 2001). In the Atlantic Ocean, the meridional overturning circulation is responsible for the majority of the heat and property transport (Hall and Bryden, 1982). A principal component of this is the thermohaline circulation which is driven by deep convection at high latitudes.

It has been suggested that MW reaches the Nordic Seas, providing the high salinities required to precondition for deep convection. Although there is general agreement that the influence of MW can be seen at these latitudes, it is controversial whether it arrives there by a direct or an indirect route. Reid (1979, 1994) argued for a direct route via an eastern boundary undercurrent, whilst McCartney and Mauritzen (2001) suggested that MW reaches these latitudes indirectly by supplying the interior Atlantic with high salinity water. Whichever hypothesis is correct, MW is an important water mass in the context of the Atlantic thermohaline circulation and climate.

The Mediterranean Sea is becoming saltier due to the diversion of fresh riverine inputs (Bryden and Boscolo, 2002) which will ultimately affect the outflow salinity. In order to be able to predict the effect of this, knowledge of, among other things, the ultimate pathways of MW in the North Atlantic is needed (Bryden and Webb, 1998). As stated by Candela (2001), we do not yet know how much of the outflow proceeds north along the Iberian continental slope and how much flows or circulates slowly westward from the Strait. Quantifying and understanding these details could provide the key to understanding the exact role this water mass plays in the North Atlantic circulation and ultimately in determining our climate.

7.2 DATA AND METHODS

To investigate the transport of MW in the North Atlantic, both observational and model studies are undertaken. Hydrographic data from six cruises are used to create two 'Med Boxes', enclosing an area of the eastern North Atlantic. Careful analysis and quality control are carried out to ensure uniformity across the datasets. This allows the different sections to be joined and enables a dynamically consistent solution. A box inverse method following Wunsch (1996) is used to determine the reference velocities and ensure conservation constraints are satisfied. An investigation into seasonal variability is undertaken using the Levitus climatology (a historical dataset) after application of the inverse correction.

The model used is OCCAM, from the Ocean Circulation and Climate Advance Modelling Project. It is a $\frac{1}{4}^{\circ}$ level model with an integration length of 25 years, and is driven by the upper surface boundary conditions including wind stress from the 1986-1988 ECMWF monthly climatology. Little interannual variability is therefore seen in the circulation, however, seasonal signals can be quantified. One of the primary reasons for choosing this model is that an experiment has been undertaken with the Strait of Gibraltar closed. This unique modeling experiment enables a totally new approach to the investigation of MW transport in the North Atlantic and also of the effects of the MW outflow on the circulation. Using the salinity difference between the two model experiments gives an excellent means of identifying MW in the open-Strait run and produced some very interesting results.

7.3 HYDROGRAPHIC DATA ANALYSIS

In contrast to the view that might be inferred from maps of the eastern North Atlantic salinity at mid-depth, MW does not simply spread out radially and inhabit all areas at 800 to 1200 m depth, it travels in currents and isolated lenses (meddies).

The hydrographic Med Boxes reveal that the main northward flow of MW occurs east of 12°W, at depths of 500 to 1500 m, and the main westward flow into the ocean interior occurs between 35°N and 40°N at similar depths, in agreement with other studies (for example Arhan et al., 1994; Reid, 1994; Bogden et al., 1993; Zenk and Armi, 1990). Whilst there is a net eastward transport across the western section in the top 1000 m (1500 m) in Med Box 88 (98), there is a net salt flux out of the box at mid-depths due to the horizontally varying salinity transport. Higher salinities (MW) are mainly being advected out of the box north of 35°N, whereas the inflowing water typically has lower salinities.

In addition to the circulation differences between the Med Boxes across the western section, there is variability in the mid-depth northward advection (-4 Sv in 98, -2 Sv in 88). These differences in the circulation patterns, as well as variability in the MW salinities observed on the sections (higher MW salinities on the northern section in 98, higher MW salinities on the western section in 88) result in a higher MW transport to the north in Med Box 98 (75%) than observed in Med Box 88 (50%). These values do not appear to be significantly sensitive to the initial reference level used (for reference levels around 3200 db). The salt fluxes across the southern section (24°N) at MW depths are trivial, confirming that there is insignificant MW transport across the southern Med Box boundary.

The net circulation of the region results in a surface water inflow (to depths of 432 ± 86 m) and a mid-depth outflow (to 2000 m). This overturning circulation is attributed both to the exchange at the Strait of Gibraltar where surface waters enter the Mediterranean and the outflow occurs at intermediate depths, and also to the water mass transformation associated with the entrainment of North Atlantic Central Water (NACW) into the outflowing MW. The magnitude of the overturning is 2.3 ± 0.6 Sv; a very robust feature. Taking 0.7 Sv to be the transport of Atlantic Waters into the Mediterranean (Bryden et al., 1994), an estimate can be made of the total entrainment of NACW into the outflowing MW within the Med Box boundaries of 1.6 ± 0.6 Sv.

The Levitus data, whilst giving a reasonable net circulation pattern in the Med Box, displays some striking differences from the hydrography. Horizontal salt fluxes are severely under-represented due to the smoothed nature of the climatology. Baroclinic fluxes are also lower in Levitus data than in the synoptic hydrography. There is significant variability in the percentages of MW calculated to be crossing the Med Box boundaries, ranging from a minimum northward transport in Spring (31%) to a maximum northward transport in Summer (67%). However, these are not felt to be a reliable depiction of the 'real' MW transport due to the under-estimation of the salt fluxes and the lack of property extrema. Although Levitus data can be used to give a broad overview of the region, it is inappropriate to draw specific conclusions regarding transport of a water mass such as Mediterranean Water.

7.4 Results from a Global Ocean Model

Chapter 6 investigates the transport and fluxes of Mediterranean Water in a global ocean model, OCCAM. The most immediate effect of the Mediterranean Outflow in the North Atlantic is to produce an enhanced overturning circulation within the Gulf of Cadiz due to the entrainment of Atlantic waters into the outflow. This is seen by the difference between the two experiments,

where the net surface inflow and mid-depth outflow are much reduced when the Strait of Gibraltar is closed. A proportion of this reduction is also obviously due to the lack of exchange flow at the Strait when it is closed.

Three MW pathways were identified in the model: to the north along the Iberian continental slope; to the west from Cape St Vincent; and to the south-west as far as the Canary Islands and then westwards. The flow to the south-west is a direct and relatively steady current, whilst the MW flux due west from Cape St Vincent occurs in a number of large eddies or recirculations. Such a strong south-westward pathway has not been reported in the literature. Conversely the northward mid-depth flow along the Iberian continental slope is much weaker and more variable than historical observations indicate.

The extent of MW propagation does not reach the Nordic Seas, contradicting Reid's (1994) hypothesis. High salinities of Mediterranean origin are, however, found as far north as 52°N, being transported both directly in an eastern boundary undercurrent from the Gulf of Cadiz, and indirectly in the North Atlantic Current following a narrow westward pathway across the North Atlantic at ~35°N. This filament of MW stretching across the model Atlantic has not been observed in hydrographic data.

In the model, MW distribution varies with depth, with the upper layers (10 to 12; above approximately 450 m) undergoing mainly northward spreading, whilst the deeper MW spreads further westward. On average over the final five years of the experiment, a higher proportion of MW flows westwards across ~20°W (61%) than northwards across ~41°N (39%). These proportions vary throughout the year. In the Spring, almost equal amounts of MW flow across the western and northern Med Box boundaries, whilst in the Autumn more than 70% flows westwards. The furthest south that any MW reaches in OCCAM is 26°N.

7.5 SUMMARY

Within this thesis both hydrographic and model data have been used to extend our understanding of MW transport in the North Atlantic Ocean. The hydrographic data shows that 50 to 75% of the MW flows northward across 41°N (east of 12°W) at mid-depths, with a weaker advective westward pathway across 20°W (between 35 and 40°N). A total entrainment of NACW into the outflowing MW within the Med Box boundaries is estimated to be 1.6 ± 0.6 Sv. The model data shows a greater proportion of MW flows westward (61%) than northwards (39%), with no evidence that a northward boundary current provides a direct route for Mediterranean salt to reach the Nordic Seas.

The work presented here is a contribution towards an explanation of the mechanisms and pathways of MW transport in the North Atlantic, which is fundamental to understanding the effect that changes in the Mediterranean Outflow may have on circulation and ultimately climate.

7.6 FUTURE WORK

To enhance our understanding of the transport and circulation of MW in the North Atlantic Ocean it would be of great value to extend the work of this thesis to a wider region of the eastern North Atlantic. The study of high quality hydrographic data to the north of the Med Box would complement this work, and provide information on the northern extent of MW influence. The scope for studies further westward are limited, as the next high-quality meridional section is at 52°W and may be beyond the observable (and quantifiable) influence of the Mediterranean Outflow.

Within the framework of this thesis it has not been possible to estimate separately the meddy contribution to MW transport. On the two western hydrographic sections, three meddies were observed on the first, and none on the second. It is open to question how representative either section might be with respect to the occurrence of meddies, and we cannot even be sure at what velocities the observed meddies were crossing the section. Transport of MW by meddies can only really be addressed in the future by combining direct velocity and salinity observations.

References

Ambar I. and M. R. Howe, 1979. Observations of the Mediterranean outflow II. The deep circulation in the vicinity of the Gulf of Cadiz. Deep-Sea Research, 26A, 555-568.

Ambar I., 1983. A shallow core of Mediterranean Water off western Portugal. Deep-Sea Research, 30, 677-680.

Arhan M., A.. Colin de Verdiere and L. Memery, 1994. The eastern boundary of the subtropical North Atlantic. Journal of Physical Oceanography, 24, 1295-1316.

Armi L. and D. Farmer, 1985. The internal hydraulics of the Strait of Gibraltar and associated sills and narrows. Oceanologica Acta, 8 (1), 37-46.

Armi L. and H. Stommel, 1983. Four views of a portion of the North Atlantic Subtropical gyre. Journal of Physical Oceanography, 13, 828-857.

Armi L. and N. A. Bray, 1982. A standard analytic curve of potential temperature versus salinity for the western North Atlantic. Journal of Physical Oceanography, 12, 384-387.

Armi L. and W. Zenk, 1984. Large lenses of highly saline Mediterranean water. Journal of Physical Oceanography, 14, 1560-1567.

Armi L., D. Hebert, N. Oakey, J. Price, P. L. Richardson, T. Rossby and B. Ruddick, 1988. The history and decay of a Mediterranean salt lens. Nature, 333, 649-651.

Armi L., D. Hebert, N. Oakey, J. Price, P. L. Richardson, T. Rossby and B. Ruddick, 1989. Two years in the life of a Mediterranean salt lens. Journal of Physical Oceanography, 19, 354-370.

Bacon S., 1997. Two hydrographic sections across the boundaries of the subpolar gyre: FOUREX. RRS Discovery Cruise 230 Report.

Baringer M. O. and J. F. Price, 1997a. Mixing and spreading of the Mediterranean outflow. Journal of Physical Oceanography, 27, 1654-1677.

Baringer M. O. and J. F. Price, 1997b. Momentum and energy balance of the Mediterranean outflow. Journal of Physical Oceanography, 27, 1678-1692.

Bennet A. F., 1992. Inverse methods in physical oceanography. Cambridge University Press. 346 pp.

Bogden P. S., R. E. Davis and R. Salmon, 1993. The North Atlantic circulation: combining simplified dynamics with hydrographic data. Journal of Marine Research, 51, 1-52.

Bower A. S., 1994. Meddies, eddies, floats and boats: how do Mediterranean and Atlantic waters mix? Oceanus, 37, 12-15.

Bower A.S., L. Armi and I. Ambar, 1997. Lagrangian observations of Meddy formation during a Mediterranean Undercurrent Seeding Experiment. Journal of Physical Oceanography, 27, 2545-2575.

Boyer T. and S. Levitus, 1994. Quality control and processing of historical oceanographic temperature, salinity, and oxygen data. NOAA Technical Report NESDIS 81.

Bryden H. L. and H. Stommel, 1982. Origin of the Mediterranean outflow. Journal of Marine Research, 40, supplement, 55-71.

Bryden H. L. and H. Stommel, 1984. Limiting processes that determine basic features of the circulation in the Mediterranean Sea. Oceanologica Acta, 7 (3), 289-296.

Bryden H. L. and T. H. Kinder, 1986. Gibraltar Experiment, A plan for dynamic and kinematic investigations of Strait mixing, exchange and turbulence. Woods Hole Oceanographic Institution Technical Report WHOI-86-29, 82pp.

Bryden H. L. and T. H. Kinder, 1991a. Recent Progress in Strait Dynamics. Reviews of Geophysics, Supplement, 617-631.

Bryden H. L. and T. H. Kinder, 1991b. Steady two-layer exchange through the Strait of Gibraltar. Deep-Sea Research, 38, Supplement 1, S445-S463.

Bryden H. L. and S. Imawaki, 2001. Ocean heat transport. In *Ocean Circulation and Climate: Observing and Modelling the Global Ocean*, edited by G. Siedler, J. Church and J. Gould, San Francisco, CA: Academic Press, 736pp.

Bryden H. L., E. C. Brady and R. D. Pillsbury, 1989. Flow through the strait of Gibraltar. In Seminario Sobre la Ocedanografia Fisica del Estrecho de Gibraltar, Madrid, 24-28 Octubre 1988. Edited by JL Almazan, H Bryden et al.

Bryden H. L., J. Candela and T. H. Kinder, 1994. Exchange through the Strait of Gibraltar. Progress in Oceanography. 33, 201-248.

Bryden H. L., M. J. Griffiths, A. M. Lavin, R. C. Millard, G. Parrilla and W. M. Smethie, 1996. Decadal changes in water mass characteristics at 24°N in the subtropical North Atlantic Ocean. Journal of Climate, 9 (12), 3162-3186.

Bryden H. L. and D. J. Webb, 1998. A perspective on the need to build a dam across the Strait of Gibraltar. EGS newsletter, 69, 1-3.

Bryden H. L. and G. Nurser, 2002. Effects of strait mixing on ocean stratification. Submitted to Journal of Physical Oceanography.

Bryden H. L. and R. Boscolo, 2002. Why the Mediterranean Sea is becoming saltier. Journal of the Korean Society of Oceanography, 37 (3), 117-124.

Canavate A. R., P. Villanueva Guimerans, F. M. Cantero and H. L. Bryden, 1988. Oceanographic study in four sections of the Strait of Gibraltar. International Hydrographic Review, Monaco, LXV(2), 159-168.

Candela J., C. D. Winant and H. L. Bryden, 1989. Meteorologically forced subinertial flows through the Strait of Gibraltar. Journal of Geophysical Research, 94 (C9), 12667-12679.

Candela J, 2001. Mediterranean Water and global circulation. In *Ocean Circulation and Climate: Observing and Modelling the Global Ocean*, edited by G. Siedler, J. Church and J. Gould, San Francisco, CA: Academic Press, 736pp.

Carpenter W. B. and J. G. Jeffreys, 1870. Report on deep-sea researches carried on during the months of July, August, and September, 1870 in H. M. Surveying-Ship Porcupine. Proceedings of the Royal Society of London, 19, 146-221.

Clarke A., J. Church, and J. Gould, 2001. Ocean processes and climate phenomena. In *Ocean Circulation and Climate: Observing and Modelling the Global Ocean*, edited by G. Siedler, J. Church and J. Gould, San Francisco, CA: Academic Press, 736pp.

Coward A. C., P. D. Killworth and J. R. Blundell, 1994. Tests of a two-grid world ocean model. Journal of Geophysical Research, 99 (c11), 22725-22735.

Culkin F. and P. Ridout, 1989. Salinity: Definitions, determinations, and standards. Sea Technology, October 1989, 47-49.

Daniault N., J. P. Maze and M. Arhan, 1994. Circulation and mixing of Mediterranean Water west of the Iberian Peninsula. Deep-Sea Research, 41, 1685-1714.

Deacon M., 1971. Scientists and the Sea 1650-1900. Academic Press, 445 pp.

Ellett D. J., A. Edwards and R. Bowers, 1986. The hydrography of the Rockall Channel – an overview. Proceedings of the Royal Society of Edinburgh, 88B, 61-81.

Fiuza A. F. G., M. Hamann, I. Ambar, G. D. del Rio, N. Gonzalez and J. M. Cabanas, 1998. Water masses and their circulation off western Iberia during May 1993. Deep-Sea Research, 45, 1127-1160.

Gerdes R., C. Koberle, A. Beckmann, P. Herrmann and J. Willebrand, 1999. Mechanisms for Spreading of Mediterranean Water in Coarse-Resolution Numerical Models. Journal of Physical Oceanography, 29, 1682-1700.

Gouretski V. V. and K. Jancke, 1999. A description and quality assessment of the historical hydrographic data for the South Pacific Ocean. Journal of Atmospheric and Oceanic Technology 16, 1791-1815.

Gouretski V. V. and K. Jancke, 2001. Systematic errors as the cause for an apparent deep water property variability: global analysis of the WOCE and historical hydrographic data. Progress in Oceanography 48, 337-402.

Hall M. M. and H. L. Bryden, 1982. Direct estimates and mechanisms of ocean heat transport. Deep-Sea Research, 29 (3A), 339-359.

Harvey J. and M. Arhan, 1988. The water masses of the central North Atlantic in 1982-84. Journal of Physical Oceanography, 18 (12), 1855-1875.

Huthnance J. M., 1986. The Rockall slope current and shelf edge processes. Proceedings of the Royal Society of Edinburgh, 88B, 83-101.

Iorga M. and M. S. Lozier, 1999a. Signatures of the Mediterranean outflow from a North Atlantic climatology. 1. Salinity and density fields. Journal of Geophysical Research, 104, 25985-26009.

Iorga M. and M. S. Lozier, 1999b. Signatures of the Mediterranean outflow from a North Atlantic climatology. 2. Diagnostic velocity fields. Journal of Geophysical Research, 104, 26011-26029.

Jia Y., 2000. Formation of an Azores current due to Mediterranean overflow in a modelling study of the North Atlantic. Journal of Physical Oceanography, 30 (9), 2342-2358.

Johnson G. C., R. G. Lueck and T. B. Sanford, 1994. Stress on the Mediterranean Outflow Plume: Part 2. Turbulent dissipation and shear measurements. Journal of Physical Oceanography, 24, 2084-2092.

Johnson R. G., 1997. Climate control requires a dam at the Strait of Gibraltar. Eos, 78, 277-281.

Johnson G. C., P. E. Robbins and G. E. Hufford, 2001. Systematic adjustments of hydrographic sections for internal consistency. Journal of Atmospheric and Oceanic Technology 18, 234-1244.

Josey S. A., E. C. Kent and P. K. Taylor, 1998. The Southampton Oceanography Centre (SOC) Ocean – Atmosphere, Heat, Momentum and Freshwater Flux Atlas. Southampton Oceanography Centre Report, No. 6, 30pp.

Joyce T. M., C. Wunsch and S. D. Pierce, 1986. Synoptic Gulf Stream velocity profiles through simultaneous inversion of hydrographic and acoustic Doppler data. Journal of Geophysical Research, 91, 7573-7585.

Kase R. H., A. Beckmann and H.-H. Hinrichsen, 1989. Observational evidence of salt lens formation in the Iberian Basin. Journal of Geophysical Research, 94, 4905-4912.

Kase R. H. and G. Siedler, 1982. Meandering of the subtropical front south-east of the Azores. Nature, 300, 245-246.

Kinder T. H. and G. Parrilla, 1987. Yes, some of the Med outflow does come from great depth! Journal of Geophysical Research, 92, 2901.

King B, 1990. RRS Discovery Cruise 189, 09 Mar-08 Apr 1990. Circulation and structure of the Bay of Biscay and north east Atlantic out to 20°W and 41°N. Institute of Oceanographic Sciences Deacon Laboratory, Cruise Report, No. 225, 45pp.

Lavin A., H. L. Bryden and G. Parrilla, 1998. Meridional transport and heat flux variations in the subtropical North Atlantic. The Global Atmosphere and Ocean System, 6, 269-293.

Lawson C. L. and R. J. Anson, 1974. Solving Least Square Problems. Prentice-Hall, Englewood Cliffs, N. J. 340pp.

Levitus S., 1982. Climatological Atlas of the World Ocean. NOAA Professional Paper 13, 173 pp.

Levitus S., T. P. Boyer, M. E. Conkright, T. O'Brien, J. Antonov, C. Stephens, L. Stathoplos, D. Johnson and R. Gelfeld., 1998. World Ocean Database 1998. Volume I: Introduction. NOAA Atlas NESDIS 18, 346pp.

Mantyla A. W. and J. L. Reid, 1983. Abyssal characteristics of the World Ocean waters. Deep-Sea Research, 30 (8A), 805-833.

Mantyla A. W., 1994a. Standard Seawater comparisons updated. Journal of Physical Oceanography, 17, 543-548.

Mantyla A. W., 1994b. The treatment of inconsistencies in Atlantic deep water salinity data. Deep-Sea Research, 41, 1387-1405.

Marsigli L. F., 1681. Internal observations on the Thracian Bosphorus, or true channel of Constantinople, represented in letters to her majesty Queen Christina of Sweden. In: *Oceanography: Concepts and History*, edited by M. B. Deacon, Hutchinson and Ross, Stroudsburg, Pennsylvania, 33-44.

Mauritzen C., Y. Morel and J. Paillet, 2001. On the influence of Mediterranean water on the central waters of the North Atlantic Ocean. Deep-Sea Research, 48, 347-381.

Maze J. P., M. Arhan and H. Mercier, 1997. Volume budget of the eastern boundary layer off the Iberian Peninsula. Deep-Sea Research, 44, 1543-1574.

McCartney M. S. and C. Mauritzen, 2001. On the origin of the warm inflow to the Nordic Seas. Progress in Oceanography, 51, 125-214.

McCartney M. S. and R. A. Curry, 1993. Transequatorial flow of Antarctic Bottom Water in the western Atlantic ocean: Abyssal geostrophy at the equator. Journal of Physical Oceanography, 23 (6), 1264-1276.

McCartney M. S. and L. D. Talley, 1982. The subpolar mode water of the North Atlantic ocean. Journal of Physical Oceanography, 12, 1169-1188.

McCartney M. S. and L. D. Talley, 1984. Warm-to-cold water conversion in the northern North Atlantic ocean. Journal of Physical Oceanography, 14 (5), 922-935.

McDougall T. J., 1991. Parameterizing mixing in inverse models. Dynamics of Oceanic Internal Gravity Waves, P. Muller and D. Henderson, Eds., 'Aha Hulio'a Winter Workshop, University of Hawaii, 355-386.

McDowell S. E. and H. T. Rossby, 1978. Mediterranean Water: An intense mesoscale eddy off the Bahamas. Science, 202, 1085-1087.

McGee T. D., 1988. Principles and methods of temperature measurement. John Wiley and Sons Inc., 581 pp.

McIntosh P. C. and S. R. Rintoul, 1997. Do box inverse models work? Journal of Physical Oceanography, 27 (2), 291-308.

McTaggart K. E., G. C. Johnson, C. I. Fleurant, and M. O. Baringer, 1999. CTD/O2 measurements collected on a climate and global change cruise along 24°N in the Atlantic Ocean (WOCE Section A6) during January-February 1998. NOAA Data Report.

McWilliams J. C., 1985. Submesoscale, coherent vortices in the ocean. Reviews of Geophysics, 23, 165-182.

Mercier H., M. Ollitrault and P.Y. Le Traon, 1993. Inverse model of the north Atlantic general circulation using lagrangian float data. Journal of Physical Oceanography, 23, 689-715.

Needler G. T. and R. A. Heath, 1975. Diffusion Coefficients Calculated from the Med salinity anomaly in the north Atlantic Ocean. Journal of Physical Oceanography, 5, 173-182.

New A. L., S. Barnard, P. Herrmann and J.-M. Molines, 2001. On the origin and pathway of the saline inflow to the Nordic Seas: insights from models. Progress in Oceanography, 48, 255-287.

Nielson J., 1912. Hydrography of the Mediterranean and adjacent waters. *Report of the Danish Oceanographical Expedition 1908-1910, Copenhagen*, 1, 77-191.

Ochoa J. and N. A. Bray, 1991. Water mass exchange in the Gulf of Cadiz. Deep-Sea Research, 38, 5465-5503.

Paillet J., M. Arhan, M. S. McCartney, 1998. Spreading of Labrador Sea Water in the eastern North Atlantic. Journal of Geophysical Research, 103 (C5), 10223-10239.

Paillet J. and H. Mercier, 1996. An inverse model of the eastern North Atlantic general circulation and thermocline ventilation. Deep-Sea Research, 44, 1293-1328.

Parrilla G., A. Lavin, H. L. Bryden, M. Garcia and R. Millard, 1994a. Rising temperatures in the subtropical North Atlantic Ocean over the past 35 years. Nature, 369, 48-51.

Parrilla G., M. J. Garcia, H. L. Bryden and R. C. Millard, 1994b. Informe Sobre La Campana HE06 (A-5, WOCE, 1992).

Pedlosky J., 1996. Ocean circulation theory. Springer-Verlag, 453 pp.

Pickard G. L. and W. J. Emery, 1990. Descriptive physical oceanography: An Introduction. 5th edition, Oxford: Pergamon Press, 320pp.

Prater M. D. and T. Rossby, 1999. An alternative hypothesis for the origin of the "Mediterranean" salt lens observed off the Bahamas in the Fall of 1976. Journal of Physical Oceanography, 29, 2103-2109.

Price J. F., M. O. Baringer, R. G. Lueck, G. C. Johnson, I. Ambar, G. Parrilla, A. Cantos, M. A. Kennelly, T. B. Sanford, 1993. Mediterranean outflow mixing and dynamics. Science, 259, 1277-1282.

Reid J. L., 1979. On the contribution of the Mediterranean Sea outflow to the Norwegian-Greenland Sea. Deep-Sea Research, 26A, 1199-1223.

Reid J. L., 1994. On the total geostrophic circulation of the North Atlantic Ocean: flow patterns, tracers, and transports. Progress in Oceanography, 33, 1-92.

Rhein M., J. Fischer, W. M. Smethie, D. Smythe-Wright, R. F. Weiss, C. Mertens, D.-H. Min, U. Fleischmann and A. Putzka, 2002. Labrador Sea Water: Pathways, CFC inventory, and formation rates. Journal of Physical Oceanography, 32, 648-665.

Richardson P. L. and K. Mooney, 1975. The Mediterranean Outflow - A simple advection-diffusion model. Journal of Physical Oceanography, 5, 476-482.

Richardson P. L., A. S. Bower and W. Zenk, 2000. A census of Meddies tracked by floats. Progress in Oceanography, 45, 209-250.

Richardson P. L., D. Walsh, L. Armi, M. Schroder and J. F. Price, 1989. Tracking three Meddies with SOFAR floats. Journal of Physical Oceanography, 19, 371-383.

Richardson P. L., M. S. McCartney and C. Maillard, 1991. A search for Meddies in historical data. Dynamics of Atmospheres and Oceans, 15, 241-265.

Sankey T., 1973. The formation of deep water in the north-western Mediterranean. Progress in Oceanography, 6, 159-179.

Saunders P. M., 1982. Circulation in the eastern North Atlantic. Journal of Marine Research, 40, 641-657.

Saunders P. M., 1986. The accuracy of measurement of salinity, oxygen, and temperature in the deep ocean. Journal of Physical Oceanography, 16, 189-195.

Saunders P. M., 1987. Flow through Discovery Gap. Journal of Physical Oceanography, 17, 631-643.

Saunders P.M., 1990. The International temperature scale of 1990, ITS-90. International WOCE Newsletter, No. 10, p.10.

Schmitt R. W., P. S. Bogden and C. E. Dorman, 1989. Evaporation minus precipitation and density fluxes for the North Atlantic. Journal of Physical Oceanography, 19, 1208-1221.

Schmitz W. J. and M. S. McCartney, 1993. On the North Atlantic circulation. Reviews of Geophysics, 31(1), 29-49.

Schultz Tokos K. L., H.-H. Hinrichsen and W. Zenk, 1994. Merging and migration of two meddies. Journal of Physical Oceanography, 24, 2129-2141.

Shapiro G. I. and S. L. Meshchanov, 1996. Spreading pattern and mesoscale structure of Mediterranean outflow in the Iberian basin estimated from historical data. Journal of Marine Systems, 7, 337-348.

Siedler G., J. Church and J. Gould, 2001. *Ocean Circulation and Climate: Observing and Modelling the Global Ocean.* San Francisco, CA: Academic Press, 736pp.

Smythe-Wright D., 1999. A Chemical and Hydrographic Atlantic Ocean Survey: CHAOS. RRS Discovery Cruise 233 Cruise report., Cruise report no 24.

Stephens J. C. and D. P. Marshall, 1999. Dynamics of the Mediterranean Salinity Tongue. Journal of Physical Oceanography, 29, 1425-1441.

Stommel H., A. B. Arons, and A. J. Faller, 1958. Some examples of stationary planetary flow patterns in bounded basins. Tellus, 10, 179-187.

Stommel H., H. L. Bryden and P. Mangelsdorf, 1973. Does some of the Mediterranean Outflow come from great depth? Pure and Applied Geophysics, 105, 879-889.

Talley L. D. and M. S. McCartney, 1982. Distribution and Circulation of Labrador Sea Water. Journal of Physical Oceanography, 12 (11), 1189-1205.

Tsimplis M. N., S. Bacon, and H. L. Bryden, 1998. The circulation of the subtropical south pacific derived from hydrographic data. Journal of Geophysical Research, 103 (C10), 21443-21468.

Tsuchiya M., L. D. Talley and M. S. McCartney, 1992. An eastern Atlantic section from Iceland southward across the equator. Deep-Sea Research 39 (11/12), 1885-1917.

Veronis G., 1987. Inverse methods for ocean circulation. In *General circulation of the ocean.* Ed. by Henry Abarbanel and W Young.

Warren B. A., 1981. Deep Circulation of the World Ocean. In *Evolution of Physical Oceanography*, edited by B. A. Warren and C. Wunsch, 6-41.

Washburn L. and R. H. Kase, 1987. Double diffusion and the distribution of the density ratio in the Mediterranean waterfront south-east of the Azores. Journal of Physical Oceanography, 17, 12-25.

Webb D. J., 1993. A simple model of the effect of the Kerguelen plateau on the strength of the Antarctic Circumpolar Current. Geophysical and Astrophysical Fluid Dynamics, 70, 57-84.

Webb D. J., B. A. de Cuevas and A. C. Coward, 1998. The first main run of the OCCAM global ocean model. Southampton Oceanography Centre Internal document, No. 34, 44pp. (Unpublished manuscript)

Wilkinson, J. H. and C. Reinsch, 1971. Handbook for Automatic Computation, Volume II, Linear Algebra. Springer-Verlag New York, 439 pp.

Worthington L. V., 1976. On the North Atlantic circulation. Johns Hopkins Oceanographic Studies, 6, 1-110.

Worthington L. V., 1981. The water masses of the World Ocean: some results of a fine-scale census. In *Evolution of Physical Oceanography*, edited by B. A. Warren and C. Wunsch, 42-69.

Wunsch C., 1978. The North Atlantic circulation west of 50°W determined by inverse methods. Reviews of Geophysics and Space Physics, 16 (4), 583-620.

Wunsch C., 1996. The Ocean circulation inverse problem. Cambridge University Press. 442pp.

Wyrtki K., 1971. Oceanographic Atlas of the Indian Ocean Expedition. National Science Foundation, 531 pp.

Zenk W. and L. Armi, 1990. The complex spreading pattern of Mediterranean Water off the Portuguese continental slope. Deep-Sea Research, 37 (12), 1805-1823.

But Eeyore was saying to himself, "This writing business. Pencils and what-not.
Over-rated if you ask me. Silly stuff. Nothing in it."

A.A.Milne 1882-1956